Uncertainty Assessment of Hydrological Impacts of Climatic Change in Small Mediterranean Catchments

Haykel Sellami

Thèse présentée en vue de l'obtention du titre de docteur en sciences agronomiques et ingénierie biologique

June 2014

Université Catholique de Louvain
Earth and Life Institute/ Environmental Sciences
Louvain-la-Neuve
Belgique

THESIS EXAMINING BOARD

SUPERVISOR	Prof. M.	Vanclooster	(UCL, Belgium)
CO-SUPERVISORS	Prof. S.	Benabdallah	(CERTE, Tunisia)
	Prof. I.	La Jeunesse	(UT, France)
JURY PRESIDENT	Prof. B.	H. De Frahan	(UCL, Belgium)
JURY MEMBERS	Prof. B.	van Wesemael	(UCL, Belgium)
	Prof. R.	Ludwig	(LMU, Germany)

Acknowledgments

I will forever be thankful to my advisor Prof. Marnik Vanclooster for accepting and providing me with the opportunity to complete my PhD thesis at the GERU laboratory at the Université Catholique de Louvain (UCL). His support and guidance made my thesis work possible. He has been actively interested in my work and has always been available to advise me. He has given me the freedom to pursue various projects without objection. I am very grateful for his patience, motivation, enthusiasm, and immense knowledge. I could not have imagined having a better advisor and mentor for my PhD research.

I especially want to thank my PhD co-advisors Prof. Isabelle La Jeunesse and Prof. Sihem Benabdallah for supporting me during several years. They have been supportive and they have also provided insightful discussions about my research. I could not have succeeded without their invaluable support. Above all, they made me feel a friend, which I appreciate from my heart.

I am also very grateful to Prof. Ralf Ludwig for his scientific advices, suggestions and insightful comments that helped me to improve the quality of this work. I have been very privileged and honored to have him in my PhD jury.

I also have to thank Prof. Bas van Wesemael for his insightful comments and motivating discussions. It has been a great pleasure for me to have him in my PhD committee and jury.

I would like to thank Prof. Bruno Henry de Frahan for accepting to referee my thesis and to chair the PhD jury.

I gratefully acknowledge the funding received towards my PhD from the Islamic Development Bank and the Université Catholique de Louvain. I am also grateful to the financial support received through the CLIMB project for conference participations, meetings, etc.

One of the most interesting and instructive interaction I had was with the members of GERU's research group. I want to thank all GERU members (present and past, academic staff, researchers, students, technical staff, special thanks to Carine) for their support and for providing a pleasant and productive working atmosphere. I will never forget your kindness and support during these years.

Of course no acknowledgments would be complete without giving thanks to my family (Taieb, Zohra, Hela, Haythem and Heni). My parents have taught me about hard work and self-respect, about persistence and about how to be independent. I am grateful for them both and for the 'smart genes' they passed on to me. I dedicate this PhD to my Mom and to the memory of my father.

I must acknowledge with tremendous and deep thanks Haifa Rachid. This thesis would not have happened without her help and "magic power".

Last, but certainly not least, special thanks to my best friend Brahim for encouraging and supporting me for more than 15 years especially the last 4 ones. Thanks, Bra!

Résumé

L'évaluation de l'incertitude des impacts hydrologiques associés au changement climatique est d'une importance fondamentale pour la gestion durable des ressources en eau. Cependant, les modèles hydrologiques et climatiques, souvent utilisés pour évaluer ces impacts, sont sujets à des incertitudes non indépendantes et qui donne naissance à une chaîne complexe d'incertitudes. Quantifier et caractériser ces incertitudes est un vrai défi et ce en particulier pour les bassins versants méditerranéens identifiés comme un *hot spot* d'impact du changement climatique.

Une approche par modélisation basée sur l'utilisation conjointe d'un modèle hydrologique et d'un ensemble de modèles climatiques a été développée pour analyser les incertitudes des projections hydrologiques liées au changement climatique dans deux bassins versant méditerranéens. Les analyses des résultats indiquent que l'incertitude associée aux paramètres du modèle hydrologique est importante et doit systématiquement être considérée dans les études d'impacts liés au changement climatique. Toutefois, le fait que les simulations hydrologiques dépendent des modèles climatiques souligne la nécessité de tenir compte des incertitudes paramétriques associées non seulement aux modèles hydrologiques mais aussi aux modèles climatiques. Aussi, la décomposition de la variance de l'ensemble des incertitudes a révélé que les modèles climatiques représentent la principale source d'erreur pendant la période humide, alors que pendant la période sèche, leur domination diminue et l'incertitude des paramètres hydrologiques devient plus importante. En dépit de ces incertitudes, les projections du changement climatique à l'horizon 2050, sont susceptibles d'induire une diminution des précipitations et une augmentation de la température pour les deux bassins versants étudiés. En outre, les régimes hydrologiques des deux bassins versants sont susceptibles d'être altérés suite à une diminution des eaux de ruissellement, de l'humidité du sol, du débit journalier ainsi que des débits extrêmes. Cela conduira à une réduction générale de la disponibilité en eau douce.

Cependant, d'autres sources d'incertitudes potentiellement importantes n'ont pas été considérées dans cette étude. Par conséquent, les marges d'incertitude estimées dans ce travail sont probablement inférieures à l'incertitude globale associée aux impacts du changement climatique sur l’hydrologie des deux bassins versants étudiés. Une évaluation complète de toutes les sources d'incertitude reste donc à mener pour l’évaluation des impacts hydrologiques des projections du changement climatique dans les bassins versants méditerranéens

Table of contents

Table of contents

List of figures

xxiii

List of tables

List of tables

Acronyms and abbreviations

Abbreviation	**Meaning**
AMU	Average ensemble Modelling Uncertainty
ANN	Artificial Neural network
ASRIL	Average Standardized Relative Interval Length
AWC	Available Water Capacity
CA	Catchment Attribute
CDF	Cumulative Distribution Function
CI	Confidence Interval
CME	Climate Multi-models Ensemble
ETP	Actual Evapotranspiration
FDC	Flow Duration Curve
FF-NN	Feed-Forward Neural Network
GCM	Global circulation Model
GLUE	Generalized Likelihood Uncertainty Estimation
HFD	High Flow Days
LFD	Low Flow Days
Mps	Model parameters
MPU	Model Prediction Uncertainty
NS	Nash and Sutcliffe coefficient
P	Precipitation
ParaSol	Parameter Solution
PDF	Probability Density Function
p-factor	Percentage of observation data bracketed in the uncertainty interval
PI	Prediction Interval
PPU	Parameter Prediction Uncertainty
R	Coefficient of correlation
R^2	Coefficient of determination
RCM	Regional Circulation Model
R-factor	Relative width of the uncertainty interval
RMSE	Root Mean square Error
RUN	Runoff
SA	Sensitivity Analysis
SE	Standard error
SUFI	Sequential Uncertainty Fitting
SWAT	Soil and Water Assessment Tool
SWC	Soil Water Content
UA	Uncertainty Analysis
σ	Standard deviation

CHAPTER I

1 Introduction

1.1 Water resources in the Mediterranean

The Mediterranean region lies in a transition zone between the arid climate of North Africa and the temperate and rainy climate of central Europe. The region is characterized by strong irregularity and variability of precipitation both in time and space. Countries in north Mediterranean receive about 72% of regional precipitation compared to 23% for countries in the east and 5% for countries in the south (Plan Bleu, 2008). Yearly precipitation varies from more than 1000 mm in northern countries to less than 100 mm in southern countries (e.g. South Tunisia).

The climate of the Mediterranean is mild and wet during the winter and hot and dry during the summer. Summer temperature varies between 3 and 15°C but can reach over 40 °C in some countries (e.g. Tunisia, Libya). These adverse climatic conditions in combination with the rapid growth in population, urbanization, industry, irrigated agriculture and tourism has increased pressures on the natural water resources which are already scarce and fragile. Growing water stress may threaten the human livelihoods and the socio-economic development in the countries region. For instance, seven countries (Malta, Libya, Jordan, Israel, Tunisia, Algeria and Egypt) already have a per capita water availability of less than 1000 m^3/year, a common benchmark of water scarcity. However, with the expected increase in the Mediterranean population which is projected to be 550 million by 2025, southern countries are likely to experience a further decline in per capita available water ranging between 25% and 60% (Scoullos et al., 2002). Thus, the number of countries with resources per capita below the critical threshold of 500 m^3/year is expected to increase.

Under the current conditions, the natural resources in the Mediterranean countries are already intensively exploited and mobilized to meet the increasing needs of all water users. For instance, more than 50% of the total average volume of renewable water resources is withdrawn in some countries such as Jordan, Malta, south Spain and Tunisia. This index can reach more than 90% in

Egypt and Libya (Margat and Vallée, 2000). Furthermore, the resources are distributed unevenly within each country. As an example, in Tunisia about 56% of available waters are surface waters against 44% of groundwater (deep and shallow aquifers). In addition, about 80% of surface water of the country is mainly from the north, 12% from the center and 8% from the south (Newbert and Benabdallah, 2003; Louati and Bucknall, 2010). In some Mediterranean countries a non-negligible amount of available water resources are provided by transboundary rivers and/or aquifers. This is the case for the Nile water shared by 9 riparian countries namely Burundi, DR Congo, Egypt, Ethiopia, Kenya, Rwanda, South Sudan, Sudan, Tanzania and Uganda. Another case is the Medjerda river that is shared between Algeria and Tunisia. Therefore, managing these international waters should involve agreements and cooperation between countries. Such cooperation not always easy to establish and a lack of appropriate cooperation can turn to a potential source of conflict.

1.2 Mediterranean climate trend

Since the middle of the 20th century, the number of hydrometeorological observation data in the Mediterranean area has remarkably increased which allows scientists to analyze long-term chronological climate data. Their investigations have shown that the Mediterranean basin has been subject to general increase in temperatures (IPCC, 2007; Giorgi and Lionello, 2008; López-Moreno et al., 2011). Reported temperatures increase over the entire basin in the last 100 years have ranged from 1 to 4.5 °C with more localized warming conditions for the Iberian Peninsula, Italy, the eastern Mediterranean, the central western Mediterranean, and North Africa (Hasanean and Basset, 2006; Vargas-Yáñez et al., 2008; El Kenawy et al., 2009). These studies have also reported that the generalized increase in temperature has been particularly evident in summer. Yet, there is also an increase in the warm events frequency during winter.

For precipitation, a general tendency toward drier climate conditions in the Mediterranean basin over the 20th century has been elucidated by several studies (IPCC, 2007; Goubanova and Li, 2007; Alpert et al., 2008; Giorgi and Lionello, 2008; López-Moreno et al., 2011). However, at more localized scale, the trend of precipitation decrease is affected with large spatial and temporal variability. Hasanean (2004) has found a generalized decrease in precipitation in the south, northeast and slight decrease in the central north, and a winter fall in the central west of the Mediterranean. In assessing the annual and seasonal precipitation patterns over the Iberian Peninsula during the second half of the 20th century, De Luis et al., (2009) found that precipitation has diminished over the entire study area with summer and spring being the most affected season. Conversely, at smaller scale, others findings revealed a slight increase of precipitation in western Italy (Kostopoulou and Jones, 2005), in the north and southern coast of Turkey (Tayanç et al., 2009). There is a general consensus about a generalized trend to less precipitation in the Mediterranean basin over the past century. Besides the reported decrease in precipitation and increase in temperature, the frequency and intensity of the droughts and rainfall extremes have increased in the past century (Luterbacher et al., 2006; Briffa et al., 2009). For instance, Nicault et al. (2008) found that the droughts of the second half of the 20th century were with no precedent in severity since the last 500 years.

There is a general consensus that changes in climate during the past century will amplify in the future and the Mediterranean will be prone to severe climatic changes and variability (IPCC, 2007; Giorgi and Lionello 2008; Ludwig et al., 2011). However, the projected magnitude and the direction of these changes remain uncertain and highly variable over space and time. The projected increase in temperatures is expected to range between 5-7°C in summer and 3-4°C in winter in the Iberian Peninsula while temperatures on the coast are projected to increase by 2°C less than the hinterland (Ludwig et al., 2011). Räisänen et al (2004) have predicted an increase in temperature varying between 4-6°C in summer and 2-4°C in winter for the future time period of 2071-2100. Hertig and Jacobeit (2008) projected an increase in temperature by 4°C by the end of this century for the overall Mediterranean basin. Schneider et al. (2013) found that annual temperatures are likely to increase by an average of 2.3°C. Concerning precipitation, the projected changes are affected by large regional and seasonal disparity. For instance, winter precipitation over the ensemble Mediterranean basin is projected to decrease by a range of -19 to -6.9 % while summer precipitation will diminish by -29.3 to -19% for the future period of 2041-2070, as reported by Schneider et al. (2013). Räisänen et al. (2004) have found that winter precipitation in 2071-2100, is likely to decline by a range -30 to -50% against -50 to -60% for summer months and possibly up to -70% in Southern Europe. A generalized drying condition over the Mediterranean region by the end of this century has been reported by Giorgi and Lionello (2008) in their review of climate change projections based on sets of climate models. These authors highlighted the particular decrease in summer precipitation that exceeds -30%. García-Ruiz et al. (2011) reported that a marked decrease in annual precipitation in the future (2040-2070), in comparison to the baseline period (1960-1990), over the entire Mediterranean basin is evident with the south of Spain, North Africa and the Middle East being the most affected (around − 15%). They also added that a decrease in precipitation (around 10%) is also projected for southern Italy, Greece, and south of Turkey

1.3 Hydrological implications of climate change in Mediterranean

The combined decrease in precipitation and increase in temperature is likely to reduce the amount of water reaching the soil, increase the soil evaporation and plants transpiration (Foley et al., 2005), reduce the soil moisture and decrease the magnitude of river discharge (García-Ruiz et al., 2011). It is further expected that the hydrologic regime alteration will decrease the fresh water availability, increase risks of droughts and floods, with more exacerbated forms of water pollution (Ludwig et al., 2009, 2011). Lespinas et al. (2014) have projected a general water discharge decrease ranging between -26% and -54% in Mediterranean French coastal river basins for 2071-2100 in comparison to 1961-1990. Koutroulis et al. (2013) reported that average water availability is expected to further drop during 2000–2050 to a devastating level of the observed average which is already insufficient to cover current demand in Crete Island (Greece). Schneider et al. (2013) found that simulated discharge of Europe Mediterranean rivers for the future period (2041-2070) is likely to be lower during the entire year in comparison to the reference period (1971-2000). Their results revealed also a substantial decrease in magnitude of monthly flow, maximum and minimum flows which, according to these authors, will lead to more intermittent flow with increasing zero flow events. In assessing the impacts of climate change in southern Italy, Senatore et al. (2011) noted an annual reduction in soil moisture during the whole year. The highest deficits for 2070-2099 are projected during summer (up to −40% compared to the reference period 1961-1990). They also projected a reduction in groundwater storage (−6.5±1.4% and −11.6±1.6%), surface runoff (−25.4±6% and −41.2±5%) and a significant increase in future runoff variability. In their investigation about the impacts of climate change on flow regime of the Merguellil catchment (central Tunisia, North Africa), Abouabdillah et al. (2010) showed that the projected decrease in rainfall and increase in temperature for near 2010-2039 and far 2070-2099 future will lead to a reduction of the total water yield available in the region. They highlighted that future monthly flows will considerably decrease as compared to 1990-2005 conditions with an expected increase in drought duration and a decrease in the magnitude and duration of yearly floods. Fujihara et al. (2008) have estimated that drought return period is expected to decrease from 5.3 year to 2 years and that hydrological drought events in the future are expected to be more frequent in the future for the Sayehan basin (Turkey).

Overall, future climate changes will be expressed through alteration of the hydrologic regime and reduction of the fresh water availability in Mediterranean river basins. Yet, assessing quantitatively the impact of climate change in the region remains uncertain. There is a growing need to better understand and quantify the consequences of climate change on water resources availability, knowing that water is a limiting factor for the economic development of Mediterranean countries.

1.4 Challenges and motivations

While there is a high degree of believe about the likely effect of future climate change on the hydrologic regime and, thus, on water resources availability in Mediterranean region, there is a large uncertainty in the projected magnitude and direction of change from one study to another. Uncertainty in climate change impact studies stems from several sources. Both hydrological and climate models suffer from structural, parametric, inputs and outputs uncertainty. Structural uncertainty is due to the limited knowledge of some real processes (e.g. hydrological and atmospheric processes) and the ability to efficiently translate them into mathematical formulation. Some of these unresolved natural processes are usually simplified or simply ignored in the model design. So, the included and neglected processes and the way they are formulated and parameterized can vary from one model to another depending on the question of interest and the application purpose of the model (Tebaldi and Knutti 2007). Therefore, there is no a single "best" model and the selection of the most appropriate model structure is based on available data and the specific modelling objective. The great statistician George Edward Pelham Box (1919-2013) once said "Essentially, all models are wrong, but some are useful" to emphasize that all models are just a simplification of the reality but they are useful to understand and predict some of part of this reality. However, the problem of identifying the useful model for a given problem and quantifying its structural uncertainty remains challenging.

Hydrological and climate models contain several parameters. Some of them have a process meaning, while others are pure empirical. Generally, process parameters are measurable (e.g. catchment area, CO_2 concentration, etc.) and reflect the properties of the processes included in the model. While effective parameters are those that cannot be measured and their values are usually adjusted in a way that model prediction approximates, as closely and consistently as possible, the observed response of the system. This process is also known as model calibration. There are also some parameters which are difficult to measure in practice but which can be theoretically derived from well understood processes and observations (e.g. hydraulic conductivity, porosity). Thus, it is not surprising that parameter uncertainty is considered one of the most important modelling uncertainty sources and has gained a lot of interest during the last decades (Duan et al., 1992; Beven 2000; Vrugt et al., 2005; Sellami et al., 2013a). Although considerable progress has been made in the development and application of approaches and techniques for parameter uncertainty assessment, the task remains difficult and challenging. This is because of the complex non-linear interactions and interrelations between model parameters.

When it comes to calibrate a model (hydrological or climatic model), historical observation data are needed. However, it is well known that observation data are always affected by uncertainty. This type of uncertainty is commonly referred to as measurement uncertainty. For instance, calibration of hydrological models is usually conducted using observed discharge time series which are derived from a rating curve (stage-discharge relationship). Although it is widely recognized that this relationship (which is actually a model) is affected by errors and, thus, the discharge derived from it is uncertain, it is rarely taken into consideration during the calibration process (Sellami et al., 2013 a).

Another source of uncertainty is related to model input. For instance, in hydrological models input uncertainty can be associated to precipitation, temperature, and GIS data, while in climate models, this type of uncertainty can arise from future emissions of greenhouse gases emission scenario (IPCC, 2001). Input uncertainty is expected to have an impact on the modelling performances and prediction results.

Traditionally, once the hydrological model is calibrated, it is then forced with the climate models outputs for reference and future time periods to assess the impact of climate change on the water resources. However, uncertainty originating from several sources propagates through each step of the climate change impact assessment approach and, consequently, affects the prediction results. Therefore, the need for assessing and quantifying the prediction uncertainty in climate change impact studies is apparent. It is also required to make full benefit of the modelling results not only in practical water resources management and decision making, but also to guide future scientific efforts to improve models and their performances assessment. However, combining several uncertainty sources is not a common practice in climate change impact studies on water resources (Kwon et al., 2012; Bastola et al., 2011). This can be due to the various issues and challenges associated with the application of an integrated uncertainty propagation approach. In fact, the complex interactions and propagations of different errors in climate and hydrological models make the prediction uncertainty assessment challenging. Other technical issues can also be related to the high computational cost of such approach.

The assessment of climate change impacts and their associated uncertainty is more challenging at local scale than at regional level. Several reasons stand behind these challenges. Local climatic and hydrological processes are complex and influenced by a large spatiotemporal variability of climatic conditions and catchment physical properties (soil type, land use, geology, etc.). Further, hydrological models implementation, calibration and validation on local scale can be greatly hindered by limitations in data availability and quality (Koutsouris et al., 2010). For instance, it is common in Mediterranean catchments that no discharge gauging stations are implemented within the catchment and that the available discharge data are often missing making the modelling task tedious. In many climate change impact studies, information about how the climate may change is provided by global climate models (GCMs) on coarse geographical scales (~ 110-180 km) and, thus, cannot be directly linked to local hydrological models (Giorgi and Lionello, 2008). A commonly-used approach is to downscale GCM results, either through statistical or dynamical procedures, to match historical patterns of climate variables at the regional and local scale (Groves et al., 2008). Although these GCMs results are downscaled using regional climate models (RCMs) that consider certain physical processes and produce highly resolved spatial climate information (~ 25-50 km), their simulations do not often agree with local observation variables and remain uncertain. This mismatching in the scale between climate and hydrological models is a real issue not only in climate change impact studies but also for the local water resources management. Indeed, climate change impact studies at regional scale are needed for local water resources management plans. However, trends identified on a local scale may differ significantly from trends based on regional scale data (Pielke et al., 2002; Koutsouris et al., 2010). Therefore, results at the regional level cannot be extended in a straightforward way to the local scale because of the spatial heterogeneity in climate, hydrological processes and catchment properties. For instance, the impact of climate change on some important hydrological features such as low flow which is of a particular interest for the design of hydropower plants and maintaining minimum flow for drinking water, needs to be assessed on the local scale since a river’s low flow regime is influenced by a number of local factors including soil properties, geology, local climatic conditions and hydraulic characteristics of the aquifers. Therefore, it is important to include local effects of climate change in developing practical actions for regional climate change impact adaptation and mitigation (Groves et al., 2008; Tubiello, 2012). However, the number of climatic change impacts on a local scale remains limited particularly in the Mediterranean.

1.5 Objectives

The general objective of this thesis is to assess the uncertainty of the hydrological impacts of climate change in Mediterranean catchments at the local scale. The physically based hydrological model Soil and Water Assessment Tool (SWAT) developed by Arnold et al. (1998) is selected and used to predict the discharge of two small catchments: the Thau catchment in southern France and the Chiba catchment in northeast of Tunisia.

To achieve the above mentioned general objective, several relevant specific scientific questions are addressed:

1) Is the selected hydrological model appropriate for discharge prediction in the selected catchments?
2) How do parameter and discharge uncertainties affect the hydrological model performances and the prediction results?
3) How can discharge be estimated in ungauged or partially gauged catchments within an uncertainty framework?
4) What is the hydrological response of small Mediterranean catchments under climate change projections?
5) How important are different uncertainty sources (hydrological model uncertainty, parameter uncertainty, hydrological data uncertainty, climate model uncertainty) in the total uncertainty of climate change impact assessments?

1.6 Outline of the thesis

To reach the main objective of this research work, the research questions are addressed in 7 specific chapters of this thesis.

In the **first chapter** the general context of the research is presented. The state of the art of climate change and hydrological impact studies for the Mediterranean region is described, and important research questions and research objectives are formulated.

In the **second chapter** the general modelling approach, materials, available data for the Thau and Chiba study sites are presented and described.

The **third chapter** deals with the SWAT model implementation and calibration. In this chapter, parameter sensitivity and uncertainty analysis are presented and discussed. In addition, the performance of the hydrological model is evaluated and the effect of the parameter and discharge uncertainty on the model performance and prediction results are assessed in response to the specific objectives 1 and 2.

The Thau and the Chiba catchments are only partially gauged and lack often observed discharge. Thus, there is a need to estimate the discharge of the entire catchments before assessing the impact of climate change on their respective hydrologic regime. In **chapter four**, a new approach is developed for estimating discharge at the ungauged parts of both study catchments, considering explicitly the estimation uncertainty.

The fourth specific objective related to the impacts of climate change on the hydrologic regime of the Thau and the Chiba catchments is investigated in **chapter five**. The projected changes in some key hydrological indicators are analyzed and uncertainty of ensemble multi-climate models (4 climate scenarios) is assessed.

The last specific question is addressed in **chapter six**. An approach based on artificial intelligence (artificial neural network) is presented to combine and propagate climate models uncertainty into hydrological modelling uncertainty. In this chapter, hydrological prediction uncertainty due to climate change projection is quantified and portioned into uncertainty associated with climatic and hydrological models.

Chapter seven summarizes the main findings of this research work and highlights the perspectives.

CHAPTER II

2 Material and methods

In this chapter the hydrological model, study sites, data available and the general modelling approach are presented.

2.1 Study sites description

The Thau and the Chiba catchments are located on the Mediterranean coast in the south of France (Languedoc-Roussillon) and in the northeast of Tunisia (Cap Bon region), respectively (Figure 2-1).

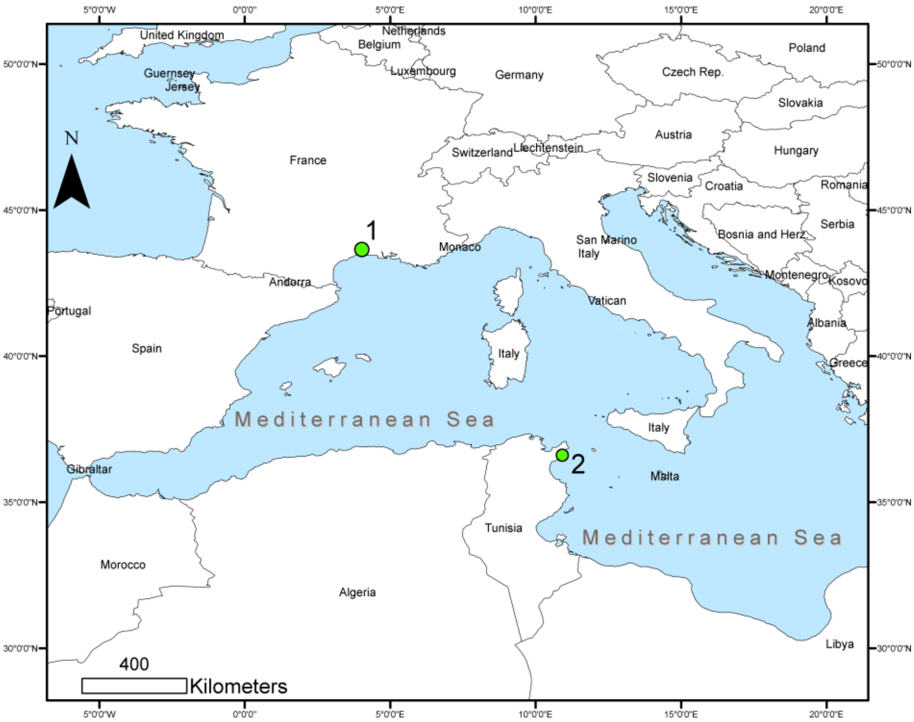

Figure 2-1: Location of the study sites; study site (1) for the Thau catchment and study site (2) for the Chiba catchment

2.1.1 *Description of the Thau catchment*

The Thau catchment is located on the French Mediterranean coast (Languedoc-Rousillon region) and drains an area of approximately 280 km^2. The catchment is drained by ten streams that flow directly into the Thau lagoon (Figure 2-2). The subcatchments sizes vary from

3.42 to 67 km^2 with the biggest one corresponding to the Vène catchment. Other geomorphologic and topographic characteristics of these catchments are given in Table 2-1. Dominant land use types within the study site are vineyards and non-agriculture vegetation (trees, Mediterranean sclerophyllous vegetation). The distribution of the main land use within each subcatchment is given in Table 2-1.

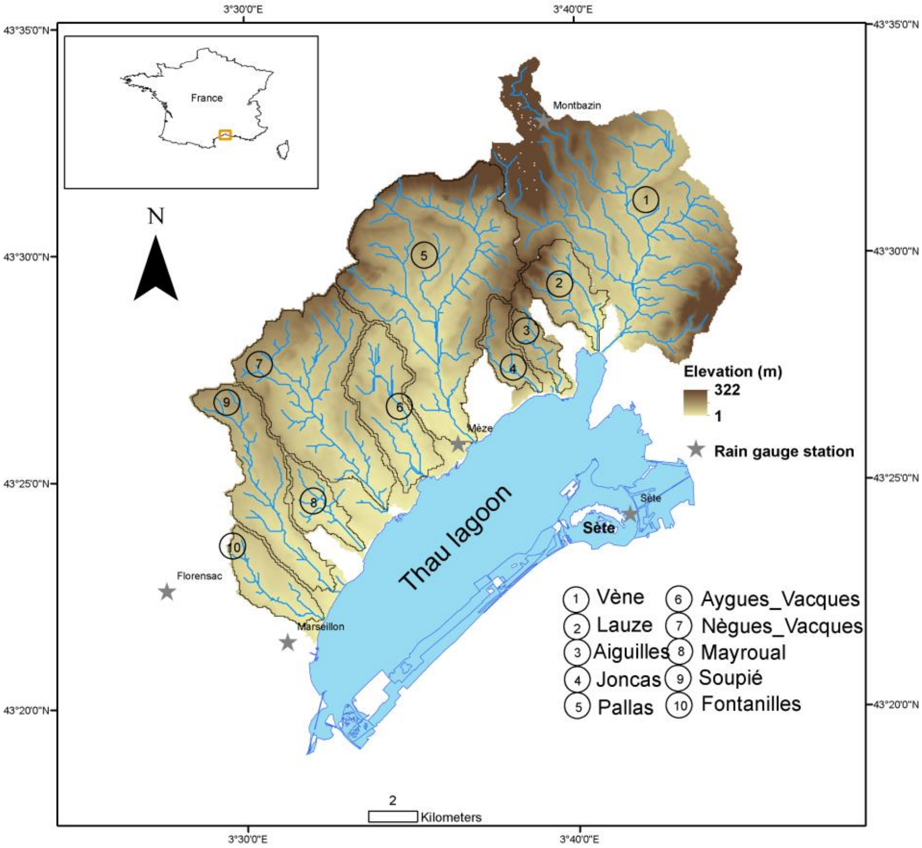

Figure 2-2: Thau catchment

The eastern part of the Thau catchment area is composed of Jurassic limestone overlaid by Miocene marls in its central part, corresponding to 60% of the Vène catchment surface (Figure 2-3).These Jurassic limestone are characterized by the presence of a large karstic aquifer whose limits extend the topographic limits of the catchment and strongly influences the hydrological regime of the Vène catchment (Plus et al., 2006; Chahinian et al., 2011, Sellami et al., 2013a).

Table 2-1: Physical attributes of the Thau subcatchments

Catchment name	Drainage area (km^2)	Mean elevation (m)	Average slope (%)	Vineyards (%)	Non-agr. vegetation (%)	Dominant Soil texture	Geology (surface %)
Vène	67	94.29	8.47	12.3	64	SA-L	JL-MM
Pallas	54	71.33	7	20.35	45.48	S-L	JL-MM
Lauze	9.25	64.22	8.16	8.027	64	S-L	JL-MM
Aiguilles	3.42	60	5.87	0.34	83.27	S-C-L	JL-MM
Joncas	4.14	74.45	6.56	2.5	84.22	S-C-L	JL-MM
Aygues_Vacques	12.34	29.52	3.56	14.4	37.33	S-L	MM
Nègues_Vacques	28.5	53.52	4	29.18	41.32	L	MM
Mayroual	5.1	20.45	2.55	48.63	25.15	L	MM
Soupié	15.82	43.38	3.79	35.88	45	L	MM
Fontanilles	7.4	21.21	2.38	31.39	27.11	L	MM

Note: Soil code: SA-L: sandy loam, S-L: silty loam, S-C-L: silty clayey loam and L: loam.
Geology code: JL, Jurassic Limestone; MM, Miocene Marl

Soils in this part of the Thau catchment are mainly sandy-loam and silty-loam soils, with porosity ranging from 35 to 50 % at 1 m depth of the soil profile. The western part of the Thau catchment is composed of the Eocene marls overlaid mainly by Miocene marls. This region covers the central part of the Pallas, Aygues_Vacques, Nègues_Vacques, Mayroual, Soupié and Fontanilles catchments. Soil textures in this part of the catchment are silty-clayey-loam and loamy, so that runoff generation processes are expected to be different from the eastern part.

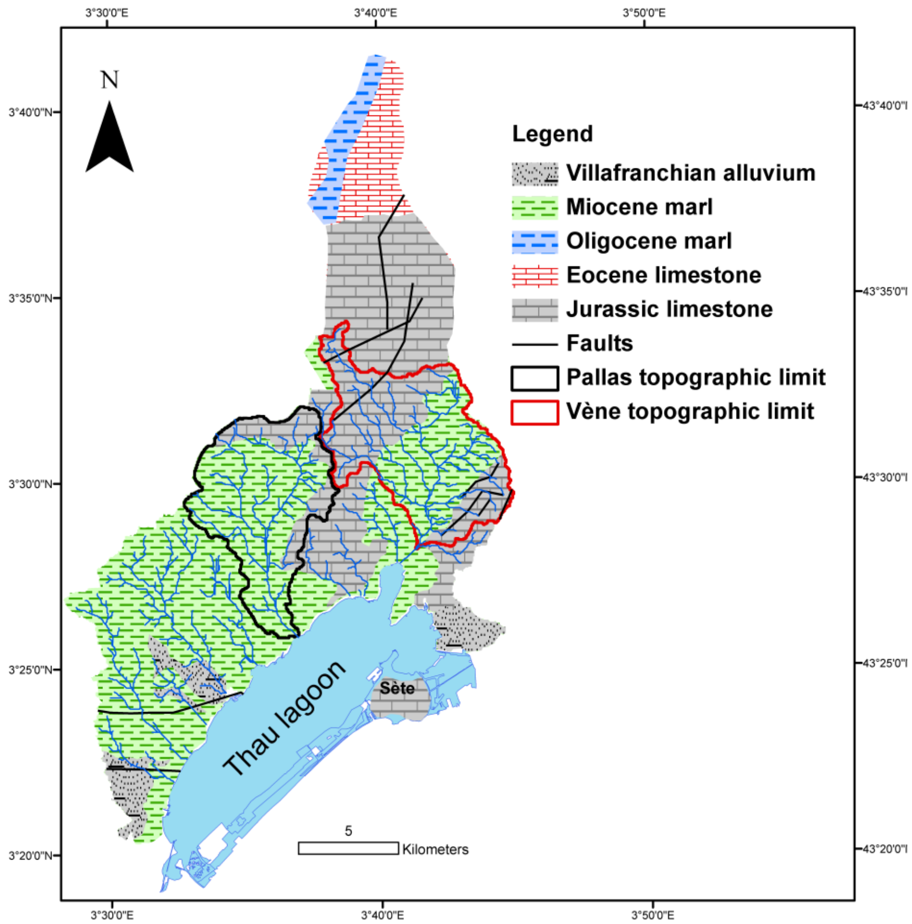

Figure 2-3: Simplified geological map of the Thau catchment and the Vène karstic system (based on France IGN geological map at 1:50000)

The climate is a typical Mediterranean regime characterized by a large seasonal variability of rainfall in time and space, with an annual average value of 600 mm. Precipitation occurs as short intense storms. The hottest months are July and August, where the maximum temperature can exceed 35°C. The coldest months are December and January where daily minimum temperature can reach -5°C.

The Vène and the Pallas are the main subcatchments in the Thau catchment. They cover an area about 67 km^2 and 54 km^2, respectively. Together, they account for more than 50% of the total flow discharging into the Thau lagoon (Plus et al., 2006). The Pallas catchment is intermittent and may cease flowing for several days, weeks or months depending on the severity of the droughts. While the Vène catchment has a perennial flow assured by the contribution of the karstic system (Plus et al., 2006).

2.1.2 *Description of the Chiba catchment*

The Chiba catchment is located in north east Tunisia and drains an area of approximately 200 km^2. It is relatively flat in its central and southern part with an average slope of 3%. The maximum altitude is about 500 m and 40% of the catchment area has an altitude less than 52 m. The catchment is situated in the Mediterranean semi-arid bioclimatic region with an average annual precipitation of 450 mm and average annual temperature of 19 °C. The rainfall is seasonal with high temporal and spatial variability. The wettest months are December and January, while the driest months are July and August. The Chiba catchment is principally drained by the Chiba stream and numerous little streams. The main economic activities within the catchment are related to agriculture where most of the cultivated plots are intended for growing cereals, vegetables and olive groves.

A dam with a retention capacity of about $4x10^6$ m^3 and controlling an area of about 64 km^2 was constructed by the Agriculture Ministry of Tunisia in 1963 in the upstream part of the Chiba catchment. The main function of the Chiba dam is to supply irrigation water to cultivated areas within the catchment.

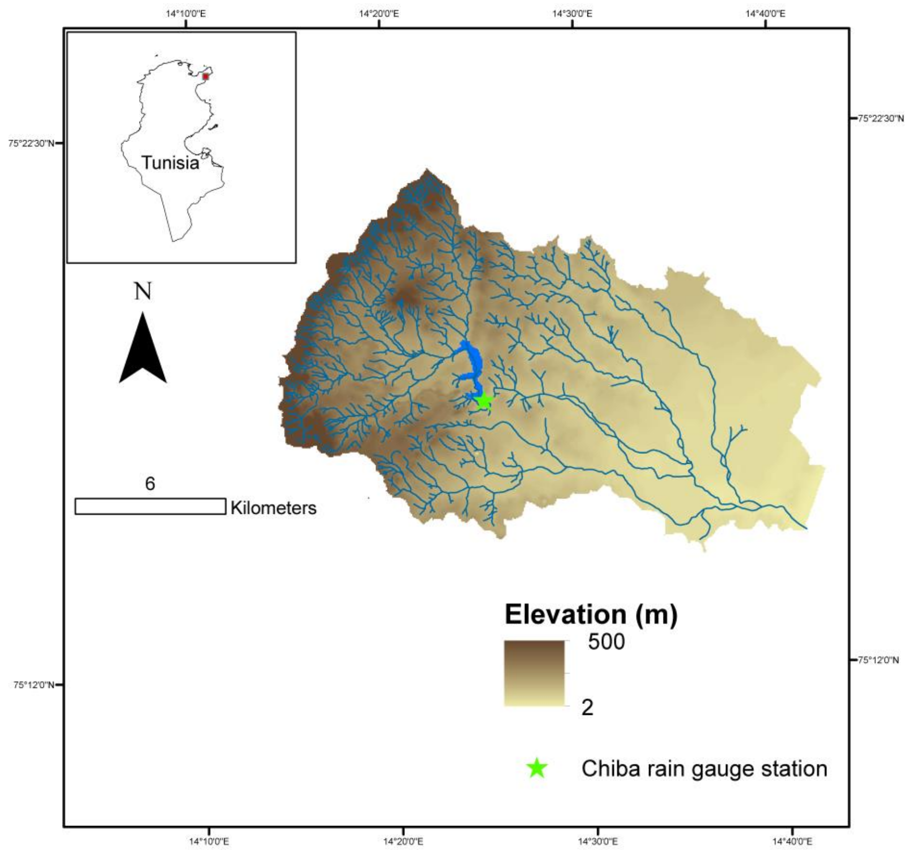

Figure 2-4: Location of the Chiba catchment

The Chiba catchment is a typical case where groundwater depletion and seawater intrusion occur under a semi-arid climate due to the large quantities of water abstracted mainly for agriculture purposes. In order to provide a hydraulic barrier against seawater intrusion, the treated wastewater is infiltrated through ponds and undergoes soil aquifer treatment to improve its quality (Cary et al., 2013).

The geological features of the study site extend from the Middle Miocene made up of sandstones and marls to the recent Holocene deposits made up of alluvium and consolidated sand dunes (Cary et al., 2013). Soils in the Chiba catchment vary from sand to loam with sandy-loam texture being the most frequent one (60% of the catchment area).

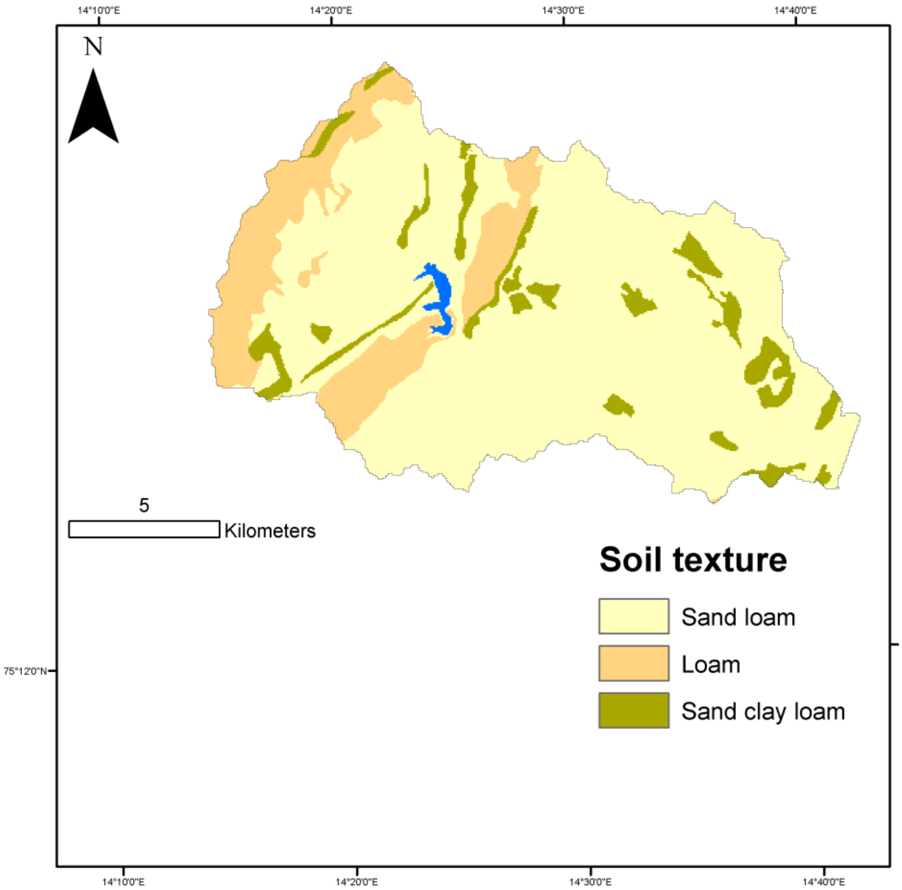

Figure 2-5: Aggregated soil texture distribution within the Chiba catchment

Both Thau and Chiba catchments share a broad set of similarities in climate and in their physical attributes. Table 2-2 gives some similarities and differences between the Thau and the Chiba catchments descriptors. Both catchments discharge into their respective lagoons which are in connection with the Mediterranean Sea and which play an important ecological and economic role in the regions (Table 2-2).

Table 2-2: Physical descriptors of the Thau and the Chiba catchments

Characteristics	Thau	Chiba
Drainage area (Km^2)	280	200
Average elevation (m)	68	89
Maximum elevation (m)	322	500
Average slope (%)	6.26	3
Main land use/ land cover (2010)	Forest and non-agriculture vegetation	Forest and non-agriculture vegetation
Main agriculture activity (2010)	Vineyards	Wheat and olives
Dominant soil texture	Sandy loam (40% of the total area)	Sandy loam (46% of the total area)
Average annual precipitation (mm)	600	450
Average annual temperature (°C)	15	19
Most important river (name)	Vène and Pallas	Oued Chiba
Number of river gauges	2 (Vène and Pallas outlets)	1 (dam location)
Riverflow records (time)	1994-1996	2000-2010 (estimated from the dam balance)
Number of rain gauges within the catchment	2	1
Geology	Jurassic limestone with karstic aquifer in the eastern part.	Plio-quaternary aquifer formed mainly by sand, sandstone and limestone
Lagoon	Thau lagoon (75 km^2)	Korba lagoons and saltmarshes
Lagoon ecologic and economic importance	Breeding and transit zone for fish species. Shellfish cultivation (750 oyster farmers, 2,750 oyster tables and 13,000 tonnes of oysters produced annually). Tourist attraction site (thermal springs).	Abundant birdlife; flamingoes *Phoenicopterus roseus*, spoonbills and avocets are found in the spring, migrants in spring and fall, and ducks during winter time. Classified as among the most important birds site by BirdLife International.

2.2 Selection and description of the hydrological model

Hydrologic models are essential tools to carry out climate change impact studies in the catchment of interest. To date, several models have been used to predict hydrological impacts of climate change all over the world under different climatic conditions. However, in Mediterranean catchments a broad set of requirements is imposed on the selection of the hydrological model. These requirements include the applicability of the model for large and small spatial scales, like river basins, and for long time scales, in view of climate change impact assessment. Furthermore, it should be flexible to deal with poor quantity and quality of data. When the aim of the study is to deliver the modelling results to assist practical implementation of water resources management in the catchment, the hydrological model needs to be able to deal with the spatial heterogeneity of the catchment physiography, represent the physical processes and provide results in a distributed way. The computational cost is also an important factor in the selection of the hydrological model in particular when long-term impact of climate change is to be assessed. The latter requirements call for a physically based and spatially distributed hydrological model. Among the wide existing panoply of physically based and spatially distributed models (MIKE SHE, ModSpa model (Moussa et al., 2007), Wetspa model (Shafii and De Smedt, 2009), the SWAT model (Soil and Water Assessment Tool, (Arnold et al., 1998)) is selected.

2.2.1 Justifications behind selecting the SWAT model

As previously mentioned, the objectives of this research work require a physically distributed model to explicitly account for the spatial and temporal variability in the hydrological processes and climatic conditions at the local scale. Since SWAT is embedded within a GIS environment, physically based inputs both spatially and temporally can be easily incorporated within the model to simulate a set of comprehensive processes such as surface runoff, infiltration, soil percolation, evapotranspiration, groundwater flow, etc. Although SWAT requires large amount of input data, the model has demonstrated good performances in predicting hydrological variables (e.g., discharge) and processes at ungauged catchments and under conditions of limited data availability (Gassman et al., 2007; Mekonnen et al., 2009; Panagopoulos et al., 2011, among others). It should be noted that SWAT was originally developed to operate in ungauged basins with little or no calibration efforts (Arnold et al., 1998). In addition, many SWAT parameters can be estimated automatically using the GIS interface and meteorological information combined with rich soil and land use parameters internal databases. Furthermore, the model parameters are assumed to have physical meaning and, thus, reflect the physical processes occurring within the catchment. These make the SWAT model suitable to address the specific objectives related to the discharge prediction at the ungauged catchments of the Thau and Chiba.

Sensitivity, calibration and uncertainty analyses are among the most important issues in hydrological modelling and are also addressed in this work. Numerous sensitivity analyses have been reported in the SWAT literature (Gassman et al., 2007; Yang et al., 2008; van Griensven et al., 2006), which provide valuable insights regarding which parameters have the greatest impact on SWAT output. As previously discussed, SWAT input parameters are physically based and are allowed to vary within a realistic uncertainty range during model calibration. Various automated sensitivity, calibration and uncertainty analyses approaches and techniques have been developed, improved and incorporated within the SWAT model (Abbaspour et al., 1997; van Griensven et al., 2006). For instance, the SWAT-CUP software (Abbaspour et al., 2008) offers a number of automated calibration/validation and uncertainty analysis techniques including Parameter Solution (ParaSol) procedure (van Griensven and Meixner 2007), the Generalized Likelihood Uncertainty Estimation (GLUE) developed by Beven and Binley (1992), and the Sequential Uncertainty FItting procedure (SUFI-2) technique (Abbaspour et al., 2004).

SWAT has been effectively used for water resources assessment over a wide range of scales and environmental conditions across the globe (Gassman et al. 2007). The design of SWAT makes it useful in simulating the impacts of alternative inputs such as those related to climate change (Neitsch et al., 2005; Arnold et al., 1998). The model has also been successfully applied in Mediterranean catchments for nutrients and discharge simulations. For instance, the model was applied in the Thau catchment to predict discharge and nitrogen yields with acceptable performances (Plus et al. 2006, Chahinian et al. 2011). SWAT applications in Tunisia (Bouraoui et al., 2005; Ouessar et al., 2009; Mosbahi et al., 2011; Aouissi et al., 2012, among others) reported that the model was able to represent the observed hydrological variables (discharge, nutriment, sediment) despite some discrepancy between observations and simulations. The outputs of the model are provided in a distributed format which can be useful for assisting practical water resources management at the local scale.

Other attractive advantages of the SWAT model are related to its continuous version updating and enhancement, its user assisting forums and groups (arcswat google group) and its friendly interface etc. The model can be freely downloaded from the SWAT website (http://swat.tamu.edu/software/swat-model/) where the user can find extensive documentation and user guide. These are the motivations, among others, for selecting the SWAT model in this study.

2.2.2 *Description of the SWAT model*

SWAT is a continuous-time and physically based hydrological model. developed to predict the impact of land management practices on water, sediment and agricultural chemical yields in large complex catchments with different soil, land use and management conditions over long periods of time (Eckhardt et al., 2005). The hydrological model operates by dividing the catchment into subbasins. Each subbasin is further discretized into a series of hydrologic response units (HRUs), which are unique soil-land use combinations. Soil water content, surface runoff, nutrient cycles, sediment yield, crop growth and management practices are simulated for each HRU and then aggregated for the subbasin by a weighted average. The hydrological balance is calculated based on the following equation:

$$\frac{\partial SW}{\partial t} = P_{day} - Q_{surf} - E_a - W_{seep} - Q_{gw} \qquad \text{Equation 2-1}$$

where SW is the soil water content (mm), P_{day} is precipitation rate (mm/day), Q_{surf} is the surface runoff rate (mm/day), E_a is evapotranspiration rate (mm/day), W_{seep} is the water percolation rate from the soil profile (mm/day), and Q_{gw} is the groundwater flow rate (mm/day).

Water in each HRU in SWAT is stored in four storage volumes: snow, soil profile, shallow aquifer, and deep aquifer. Surface runoff from daily rainfall is estimated using the Soil Conservation Service curve number (CN) method (SCS, 1972) which estimates the amount of runoff based on local land use, soil type, and antecedent moisture condition. Calculated flow, sediment yield, and nutrient loading obtained for each subbasin are then routed through the river channel using the variable storage or Muskingum method. The catchment concentration time is estimated using Manning's Kinematic Equation, considering both overland and channel flow.

The soil profile is subdivided into multiple layers that support soil water processes including infiltration, evaporation, plant uptake, lateral flow, and percolation to lower layers. The soil percolation component of SWAT uses a water storage capacity technique to predict flow through each soil layer in the root zone. Downward flow occurs when field capacity of a soil layer is exceeded and the layer below is not saturated. Percolation from the bottom of the soil profile recharges the shallow aquifer. The amount of water entering the shallow aquifer is a function of the total water volume exiting the soil profile and an exponential decay function to account for the recharge time delay. The latter is depending on the overlying geologic formations. If the depth of the shallow aquifer increases above the user defined threshold value, it is assumed that groundwater discharge is occurring and contributing to the reach. Upward flow movement to the overlaying unsaturated soil layers is simulated by routing water from the shallow aquifer storage component to the soil by capillary pressure or by direct absorption by the plant roots.

The model computes evaporation from soils and plants separately. Potential evapotranspiration can be modelled with three options available in SWAT, that is, Penman-Monteith, Priestley–Taylor and Hargreaves methods (Neitsch et al., 2005), depending on data availability. Potential soil water evaporation is estimated as a function of potential ET and leaf area index. Actual soil evaporation is estimated by using exponential functions of soil depth and water content. Plant water evaporation is simulated as a linear function of potential evapotranspiration, leaf area index, and root depth, and can be limited by soil water content. More detailed descriptions of the SWAT model can be found in Neitsch et al., (2005).

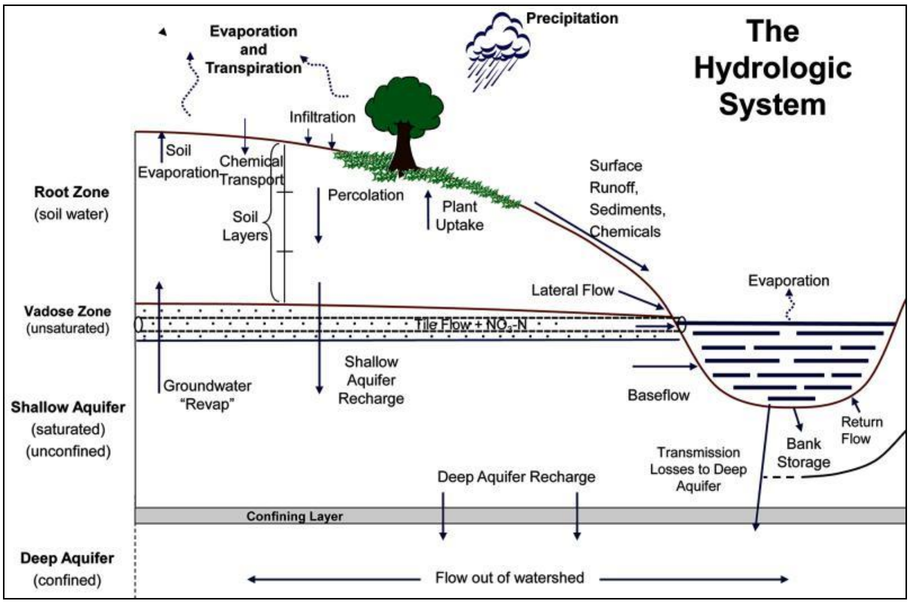

Figure 2-6: Conceptualization of the hydrological cycle in the SWAT model (Source: Soil and Water Assessment Tool, Theoretical documentation, Version 2009. http://twri.tamu.edu/reports/2011/tr406.pdf)

2.2.3 SWAT model data requirement

Two types of data are required for the implementation of the SWAT model; time series climatic data and spatial data. Climatic time series data including precipitation, maximum and minimum temperatures, solar radiation, air relative humidity, and wind speed, are generally required on a daily time step. Air relative humidity is required if the Penman-Monteith or the Priestly- Taylor evapotranspiration routines are selected. Wind speed is only necessary if the Penman-Monteith method is used. Measured or generated sub-daily precipitation inputs are required if the Green and Ampt infiltration method is selected. The maximum and minimum temperatures are used to calculate daily soil and water temperatures. Generated weather inputs are calculated from tables consisting of 13 monthly climatic variables, which are derived from statistics of long-term measured weather records.

The SWAT system is embedded within a Geographic Information System (GIS) that can easily integrate the required spatial data. These data include, digital elevation model (DEM), stream network, soil and land use maps. In addition to maps, a database of several parameters for each soil layer and land use type needs to be linked to their corresponding GIS layer. To allow the spatial variation in climate over the study catchment, climatic data are entered in SWAT as points linked to their corresponding time series data.

2.2.4 SWAT model pre-processing

Several steps are required to implement the SWAT model for the study catchments. The first step is the **catchment delineation** and creation of the subcatchments boundaries based on the DEM. In order to improve hydrographic segmentation and subcatchments boundaries delineation, the network can be encoded and superimposed onto the DEM in cases where the latter does not provide accurate location of the stream network. Based on a user defined threshold value, namely CSTV, the catchment is subdivided into number of subcatchments. The choice of CSTV value is crucial since it will define the size and the number of the subcatchments, the simulation performance and the computational time of the model (FitzHugh and Mackay, 2000; Romanowicz et al., 2005).

The second step in the SWAT pre-processing phase consists of the **HRU definition**. The subcatchments created are further subdivided into unique combination of land use, soil and slope. Here again, the user has the choice to select a threshold value to either consider multiple HRUs, dominant HRUs or a single HRU for the entire subcatchment.

Once the HRUs are defined and the climatic data are assigned to the SWAT project, input files such as .sol, .hru, .rte, .gw, etc., required for the model simulations, are generated. These inputs files include all the necessary model parameters and methods to **run SWAT**.

2.3 SWAT model implementation on the Thau and the Chiba catchments

The available data as well as their providers and resolutions for implementing the SWAT model on the Thau and the Chiba catchments are summarized in Table 2-3. More description about the model discretization and implementation on each catchment is given below.

2.3.1 SWAT on the Thau catchment

Subcatchments delineation

As the Thau catchment is made of ten small subcatchments, SWAT is implemented on each of them using the local data available. Based on the DEM (French Nation Geographic Institute, at 1:50000) and the drainage network, each catchment is subdivided into several subcatchments during the pre-processing phase. The number of subcatchments varies from one catchment to another based on the catchment size and on the CSTV threshold. Romanowicz et al. (2005) showed that a parabolic function characterizes the relationship between the CSTV values and the SWAT model performances. The authors found that the best fit between simulation and observation is obtained when the CSTV suggested by the model is selected. SWAT suggests a CSTV value for each catchment which is actually the optimal compromise between subcatchment aggregation level, model computational cost and performances. Based on this, the CSTV values suggested by SWAT are selected for catchments discretization. For instance, for the Vène and the Pallas catchments 17 and 19 subcatchments are created, respectively.

During the process of intersecting the land use (CLIMB project, at 1:50000), soil data (INRA Montpellier, France) and slope maps, multiple HRUs are created within each subcatchment (Figure 2-7). In order to eliminate minor land uses, soils and slopes, a threshold level of 10% is selected in each subbasin. In other words, if the percentage of soil, land use and slope type is less than 10% of the subbasin area, it is considered negligible and therefore not included in the HRUs generation procedure. For instance, given these thresholds, 111 and 116 HRUs are created for the Vène and the Pallas catchments, respectively. The HRUs consist of homogeneous land use, soil and topographic characteristics. They represent percentages of the subcatchment area and are not identified spatially within a SWAT simulation.

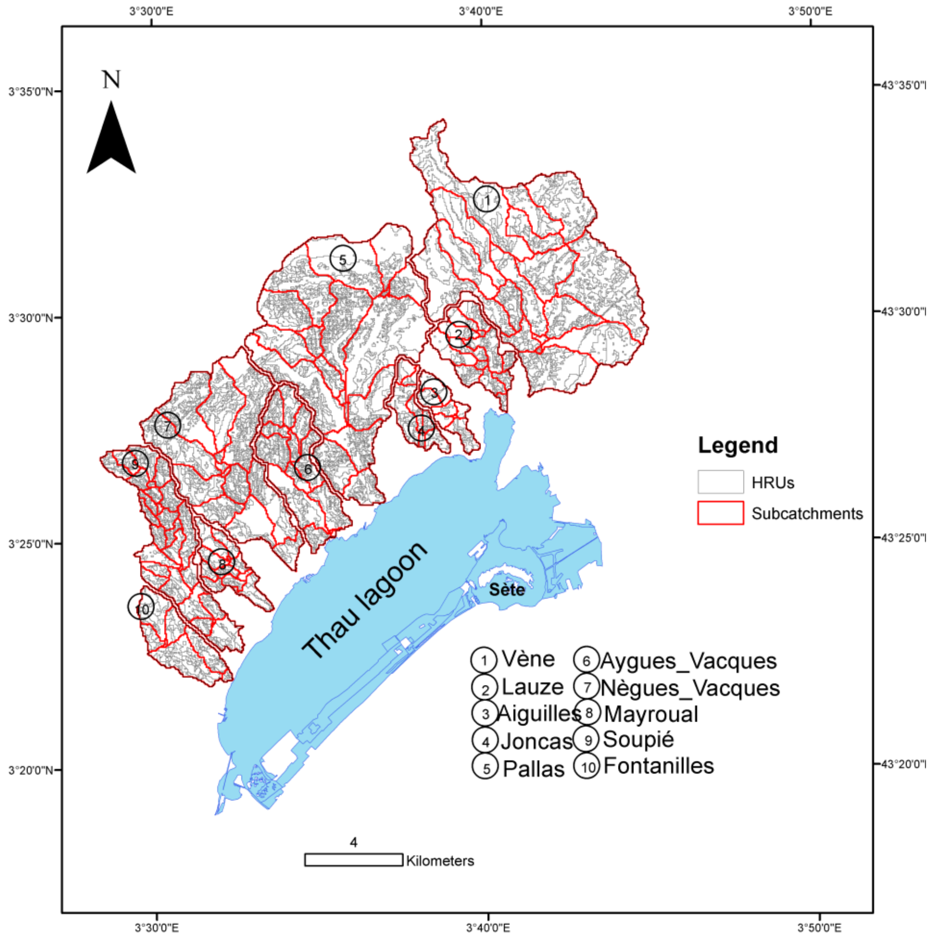

Figure 2-7: Subcatchments and HRUs subdivision of the Thau catchment

Table 2-3: Available data used for SWAT set up on the Thau and the Chiba catchments

SWAT inputs	Resolution		Data provider	
	Thau	Chiba	Thau	Chiba
Precipitation **Temperature** **Humidity** **Solar radiation** **Wind speed**	Daily (1950-2010) Daily (1963-2010) Daily (1990-2010) Daily (1990-2010) Daily (1990-2010)	Daily (1976-2010) Daily (1968-2010) Daily (1989-2010) Daily (1989-2010) Daily (1989-2010)	Climatic station of Sète (Météo France, France), Méze, Montbazin, Marseillon, Florensac and meteorological station of Fréjorgues (France)	Climatic station of the Chiba dam, Lebna, and Korba and meteorological station of Kélibia (Ministry of Agriculture, Tunisia)
Digital Elevation Model (D.E.M)	50m grid	50m grid	French National Geographic Institute	Derived by digitizing the topographic map
Soil map and soil database	1:50 000	1:50 000	INRA-Montpellier, France	Ministry of Agriculture, Tunisia
Land use maps and database	1:50 000 (2010)	1:50 000 (2010)	CLIMB project	CLIMB project
SWAT set up				
Evapotranspiration method	Daily	Daily	Penman-Monteith method	Penman-Monteith method
Surface runoff volume method	Daily	Daily	SCS curve number	SCS curve number
Channel flow routing method	Daily	Daily	variable storage coefficient	variable storage coefficient
Model warming –up period	Daily (4 years)	Daily (2 years)	---	---
Discharge for model calibration	Daily (1994-1996)	Daily (2000-2010)	Vène and Pallas streamflow gauge stations	Estimated from the Chiba dam water balance
SWAT simulation				
Simulation period	Daily (1990-2010)	Daily (1998-2010)	---	---

Soil and land use parameterization

The soil map of the Thau catchment is made of several pedological units each composed of one or more soil types. Each soil type is linked to a detailed soil database (provided by INRA, Montpellier, France) where several measured physico-chemical parameters (depth, organic matter, textural analysis, rock fraction, etc.) for each soil type horizon are available. However, for practical implementation of the SWAT model, the dominant soil type of each pedological unit is considered. Other soil parameters required by the hydrological model to calculate the movement of water in the soil profile are not available and, therefore, are estimated using pedotransfer functions (PTFs). These missing soil parameters include the bulk density (BD), available water capacity (AWC), saturated hydraulic conductivity (*K*s), and soil erodibility factor (USLE K).

$$BD = 1.8 + 1.236 \times \frac{OM}{100} - 2.91 \times \sqrt{\frac{OM}{100}} \,. \qquad \text{Equation 2-2}$$

with OM, the organic matter content expressed in percentage (%) Bollen et al. (1995). According to Van Genuchten (1980),

$$AWC = \frac{\theta_s - \theta_r}{\left[1 + (\alpha_{h50})^n\right]^m} - \frac{\theta_s - \theta_r}{\left[1 + (\alpha_{h15,000})^n\right]^m} \qquad \text{Equation 2-3}$$

and (Wösten et al., 1999)

$$K_S = e^{\left(k_S^*\right)} \qquad \text{Equation 2-4}$$

where θ_s and θ_r are the saturated and residual soil water contents (m^3/m^3), respectively. α and k_S^* are two Mualem, Van Genuchten (1980) parameters (Wösten et al., 1999) expressed in cm^{-1}, h_{50} and $h_{15,000}$ are the pressure head (cm) at the field capacity and the permanent wilting point, respectively. The soil erodibility factor (USLE_K) is calculated according to Williams (1995).

$$USLE\_K = f_{cSA} \times f_{C-S} \times f_{OC} \times f_{hiSA} \qquad \text{Equation 2-5}$$

$$\text{with}\begin{cases} f_{CSA} = 0.2 + 0.3 \times e^{\left(-0.256 \times SA \times \left(1 - \frac{S}{100}\right)\right)} \\ f_{C-S} = \left(\dfrac{S}{C+S}\right)^{0.3} \\ f_{OC} = 1 - \dfrac{0.25 \times OC}{OC + e^{(3.72 - 2.95 \times OC)}}; OC = \dfrac{OM}{1.72} \\ f_{hiSA} = 1 - \dfrac{0.7 \times \left(1 - \dfrac{S}{100}\right)}{1 - \dfrac{S}{100} + e^{\left(-5.5 + 22.9 \times \left(1 - \frac{S}{100}\right)\right)}} \end{cases}$$

where S, SA, C and OC are silt, sand, clay and organic carbon fractions in (%), respectively. f_{cSA} is a factor, that diminishes the erodibility factor in soils with high coarse sand content and increases it for soils with little sand. $f_{C\text{-}S}$ reduces the soil erodibility factor with high clay to silt contents. f_{OC} reduces the K factor for soils with higher organic carbon content and f_{hiSA} lowers the erodibility factor for soils with extremely high sand content.

Besides soil physical and chemical properties, SWAT requires a definition of hydrologic soil group (HSG) for each soil type. Based on the infiltration capacity of soils, the U.S. National Resources Conservation Service (NRCS) classifies soils into four hydrologic groups. According to (NRCS, 2004), soils with similar runoff potential under similar cover conditions belong to the same soil hydrologic group. These are briefly described below.

- Hydrologic soil group A corresponds to soils with low runoff potential where the average permeability of the surface layer is higher than 254 mm/hour. These soils have high infiltration rate even when thoroughly wetted. They chiefly consist of deep, well drained to excessively drained sands or gravels. They have a high rate of water transmission.
- Hydrologic soil group B encompasses soils with moderate infiltration rate with the average permeability of the surface layer ranges between 84 and 254 mm/hour. They chiefly are moderately deep to deep, moderately well-drained to well-drained soils that have moderately fine to moderately coarse textures. They have a moderate rate of water transmission.

- Hydrologic soil group C corresponds to soils with slow infiltration rate with the average permeability of the surface layer ranges between 8.4 and 84 mm/hour. They chiefly have a layer that impedes downward movement of water or have moderately fine to fine texture with a slow rate of water transmission.
- Hydrologic soil group D includes soils with very slow infiltration rate or high runoff potential. The average permeability of the surface layer is lower than 8.4 mm/hour.

The NRCS hydrologic soil group classification is applied to the available soils in the Thau catchment. Attribution of the Thau catchment soils to HSG classes is based on the estimated saturated hydraulic conductivity (*Ks*).

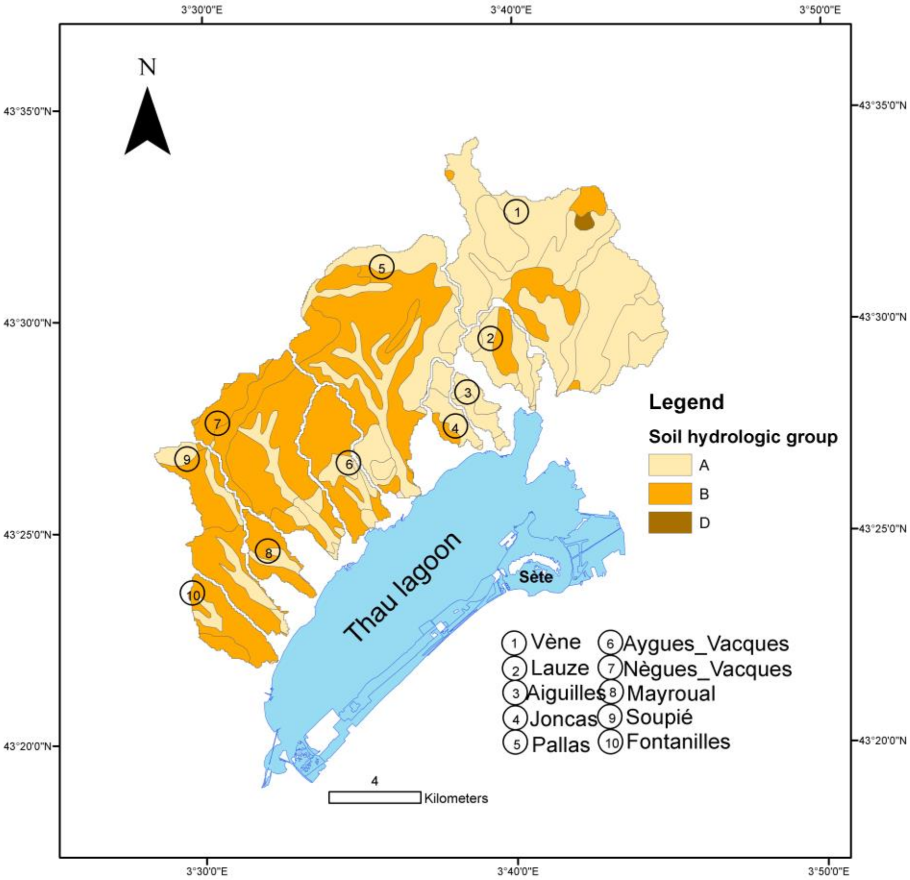

Figure 2-8: Hydrologic soil group of the Thau catchment

The presence of the karstic system in the eastern Thau catchment (see Figure 2-3) can explain the predominance of the soil hydrologic group A in this part of the Thau.

The land use map is provided within the frame work of *CLIMB* by Baghdadi et al. (2013). The land use parameterization in the hydrological model is made by linking each land use/cover class to the SWAT crop database, where most of the required parameters (Leaf Area Index, optimal temperature for plant growth, etc.) are available. Exceptions are made for vineyards and non-agriculture vegetation (the latter is locally known as *garrigue*) classes which are not included in the original SWAT crop database. Parameters related to these two missing land use/cover classes are extracted from Plus et al. (2006).

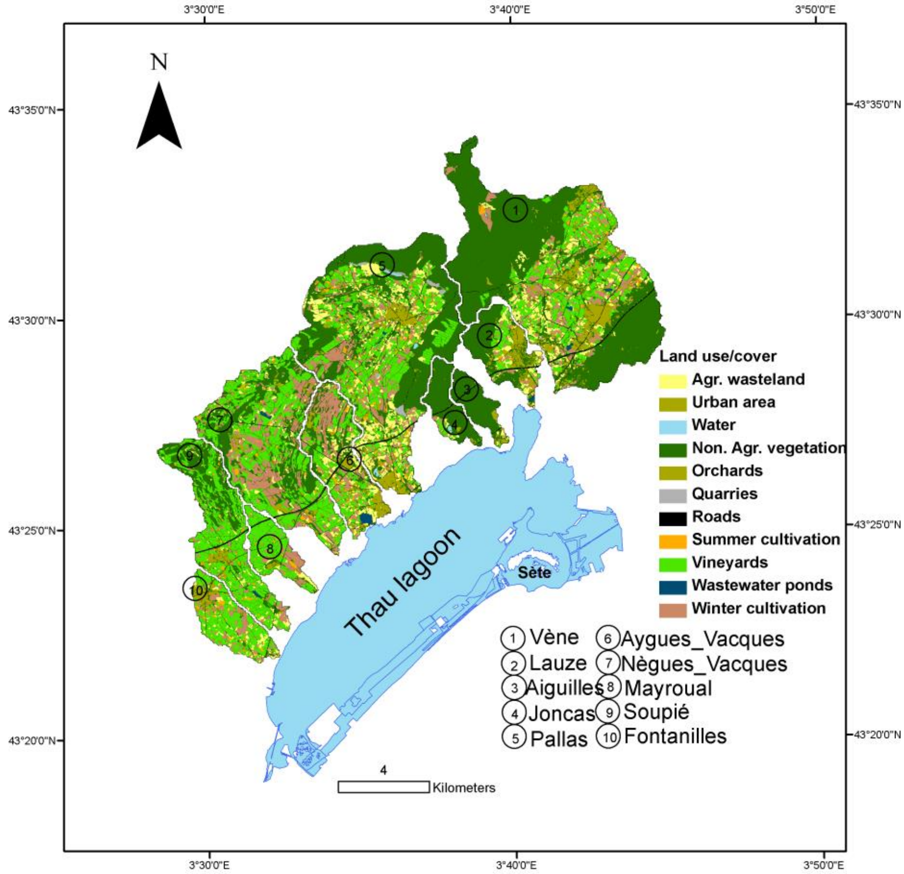

Figure 2-9: Land use/cover map of the Thau catchment (Source: Baghdadi et al., 2013 within the *ClIMB* project)

The Soil Conservation Service (SCS) runoff curve number (CN) method (SCS, 1972) is used to predict direct runoff or infiltration from rainfall excess within the SWAT model. The CN method is an empirical method developed for estimating the amount of surface runoff from a catchment with varying land use and soil types (SCS, 1972). SWAT assigns an initial CN value to each HRU in the catchment as a function of soil permeability, land use, and antecedent soil moisture conditions. Antecedent moisture conditions are the soil moisture conditions of a catchment at the beginning of a storm. These conditions affect the volume of runoff generated by a particular storm event. SCS (1972) defined three antecedent moisture conditions: moisture condition I, which refers to dry soil condition that leads to a permanent wilting point; moisture condition II, soils with average moisture condition; and moisture condition III, wet soil condition, where the soil is at field capacity. Typical Curve Numbers for moisture condition II (CN2) under varying land cover and soil types are provided by the National Engineering Handbook (SCS, 1986). SWAT adjusts the daily curve numbers based on the soil moisture content. Thus, daily curve numbers vary within the SWAT simulation but the CN2 is still the most important parameter for runoff generation.

Climatic data

To consider the spatial variability of the climatic conditions over the Thau catchment in the model, rainfall is specified for 5 conditions. First, precipitation data from the reference station of Sète (Météo France) are used. Second, data from 4 additional rain gauges are included in the SWAT model (Figure 2-2). Rainfall records differ in time length and period. For instance, both Florensac and Marsillon daily rain records cover the time period from 1995 to 1999, while the Montbazin and Mèze cover the time period from 1990 to 1999. Although more than one climatic station is implemented, the hydrological model always considers the geographically closest climatic station to the centroid of the subcatchment of interest and evenly distributes the climatic variable over the subbasin area. Thus, the spatial variability will be better represented in the model if the number of climatic stations is higher.

Table 2-4: Correlation coefficient between the daily rainfall records at different rain gauge stations in the Thau catchment

Rain gauge	Flore	Marse	Mèze	Montb	Sète
Flore	1				
Marse	0.28	1			
Méze	0.34	0.73	1		
Montb	0.31	0.69	0.94	1	
Sète	0.72	0.24	0.31	0.31	1

Note: Marse for Marseillon; Montb for Montbazin and Flore for Florensac

In Table 2-4, the correlation coefficient between the daily rain gauge stations datasets for the time period of 1995-1999 is calculated. It is clear that some differences exist in the recorded rainfall values between the different rain gauge stations. However, differences in the correlation coefficient between the rainfall data sets may not necessarily reflect the spatial variability of rainfall over the Thau catchment. It is possible that not all the rain gauge stations capture and record the same rainfall event due to measurement error or to occasional deficiencies of the rain gauge station.

2.3.2 SWAT on the Chiba catchment

Subcatchments delineation

The process of subcatchments delineation in the Chiba catchment is based on a digital elevation model (DEM) and drainage network both derived by digitizing several topographic maps at 1/50.000 of the CapBon region (north east Tunisia). The DEM accuracy is enhanced with additional topographic elevation points from the 1/25.000 topographic maps. Based on the discretization threshold value suggested by the SWAT model, the Chiba catchment is subdivided into 61 subcatchments and 129 HRUs (Figure 2-10).

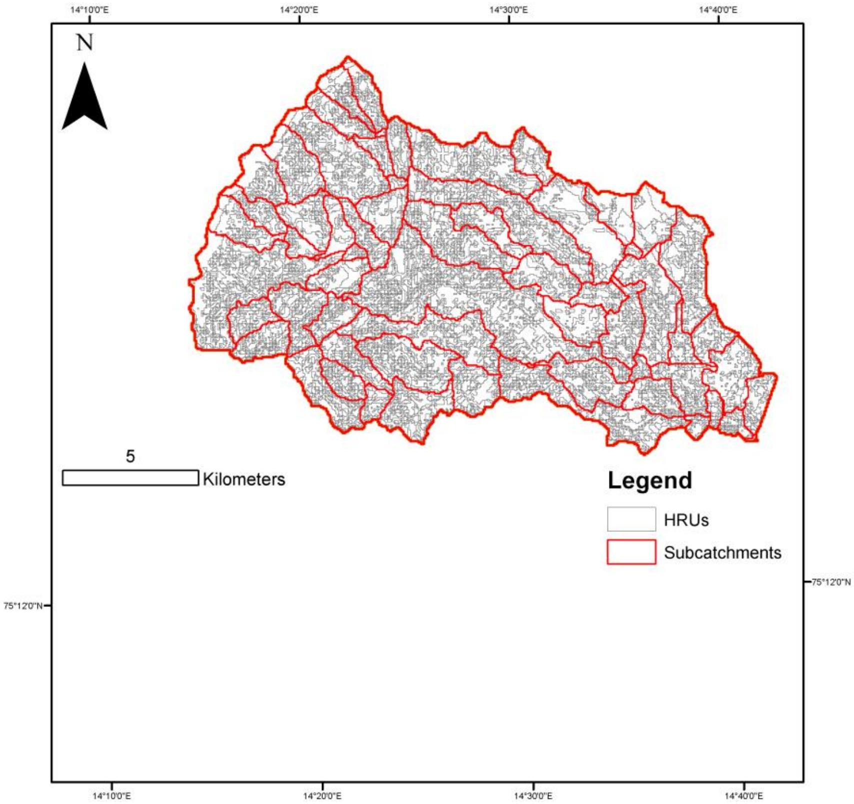

Figure 2-10: Subcatchments and HRUs delineation of the Chiba catchment

Similarly to the Thau catchment, during the delineation process of the Chiba catchment soil, land use and slope type less than 10% of the subbasin area, are considered negligible and therefore not included.

Soil and land use parameterization

The soil map (1/50.000) and soil physical properties (soil type and texture) are obtained from the Ministry of Agriculture and Hydraulic Resources of Tunisia and are improved with field observations, previous pedological studies (Chauvel, 1961; Calo, 1964) and other relevant pedological data within the study area. In absence of available pedotransfer functions (PTFs) adapted to the local study area, the missing soil parameters for implementing the SWAT model are estimated using the PTFs (Equation 2-2 to Equation 2-5), similarly to the Thau catchment.

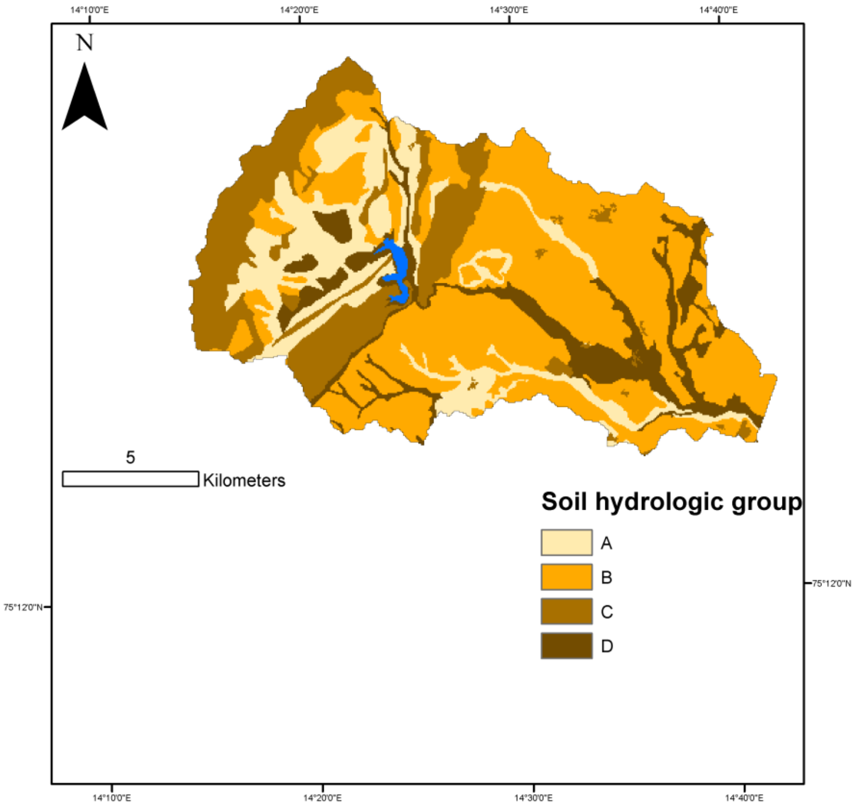

Figure 2-11: Hydrologic soil group in the Chiba catchment

The definition of the HSG is based on the U.S. Natural Resource Conservation Service classification (SCS, 1972). Soils of the Chiba catchment have the four HSG (A, B, C and D), but with the predominance of soils with medium to higher runoff potential (B and C) (Figure 2-11). It should be noted here that in many locations in the Chiba catchment soils are characterized by calcareous accumulation, at shallow depth due to the abundance of carbonates materials, referred to as lime crusts. These calcareous accumulations may reduce the soil permeability in contrast to high permeability of uncrusted soils (Rattan 2006).

The land use map of 2010 (provided within the *CLIMB* project) is used for SWAT implementation on the Chiba catchment. Additional field investigations were carried out to identify and improve some of the land use classes (Figure 2-12).

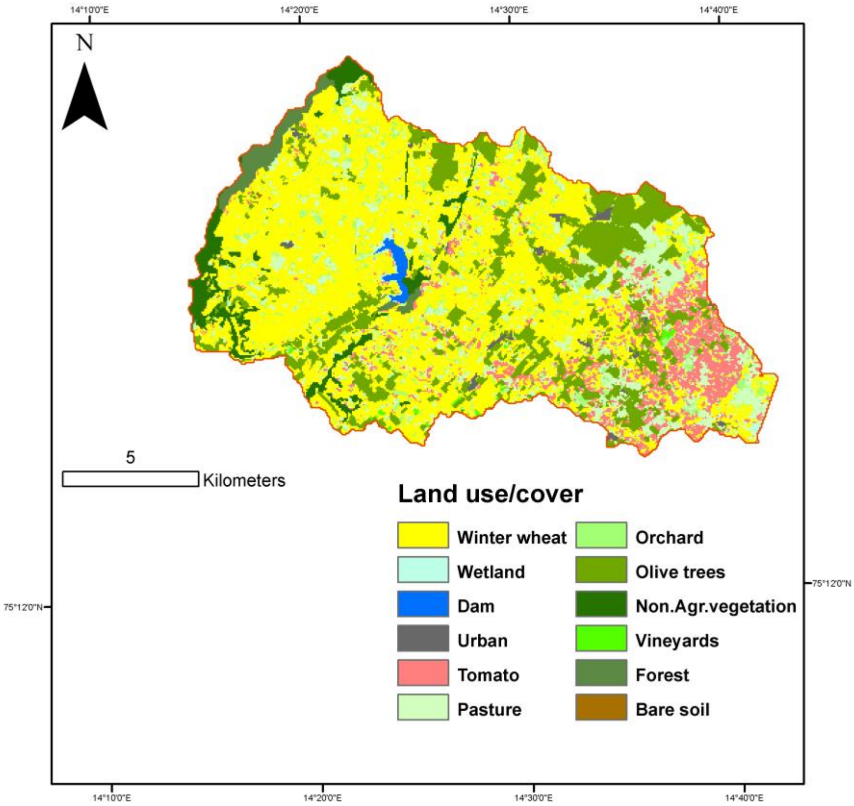

Figure 2-12: Land use/cover of the Chiba catchment

The main agriculture plots within the Chiba catchment are intended for winter wheat, olive trees, pasture and tomato cultivation. For the parameterization of the land use/cover, each land use/cover class is linked to the SWAT original crop database. Parameterization of vineyard land use class is made similarly to the one in the Thau catchment where most of the parameters are derived from Plus et al. (2006).

Climatic data

In addition to the reference climatic station of the Chiba dam, three additional rain gauge stations within or nearby the catchment are considered. Daily precipitation data are available from the several climatic station considered and cover the time period of 1970 to 2010. Other climatic variables required by the SWAT model are provided by the Kélibia climatic station located at 20 km from the Chiba catchment (Table 2-3).

2.4 General modelling approach

2.4.1 Discharge simulation

Although the SWAT model is able to simulate several hydrological variables, sediments, nutrients, etc., the main focus of this research work is only on catchment discharge. Thus, before running the SWAT model several configurations which are directly or indirectly related to the model flow component are required and summarized in Table 2-3. For both catchments, the modified SCS curve number method is chosen for surface runoff volume computing. The variable storage coefficient method is selected for the flow routing through the channel and potential evapotranspiration is estimated by the Penman-Monteith method. For the Thau catchment, discharge simulations are conducted from 1990 to 1996 while for the Chiba catchment the simulation time period extents from 1998 to 2010. The model simulation time period for each catchment is selected since it covers the time period of the available measured discharge data (Table 2-3). To minimize the effects of the initial state of the SWAT variables on the river flow, a warming-up period of two years (1998-1999) is considered for the Chiba catchment. However, due to the presence of the karst features in the Thau catchment, a longer warming-up period of four years (1990 to1993) is assumed sufficient to start with reasonable initial values for all storage volumes considered in the model.

2.4.2 Discharge measurements

Thau catchment

In the Thau catchment less than 2 years (1994-1996) of streamflow records are available for the Vène and the Pallas catchments (Figure 2-2). For the others rivers, streamflow records are either missing or either have missing values and gaps. Stream flow data in the Vène catchment cover 667 days from 02/08/1994 to 01/07/1996 while in the Pallas catchment only 208 days of discharge records are available from 25/11/1995 to 14/06/1996.

Chiba catchment

Since there is no streamflow gauge station in the Chiba catchment, discharge is computed from the dam water balance time series according to Equation (2-6).

$$\begin{cases} I_t = S_t - S_{t-1} + (Q_{irr} + Q_{spill} + E + Q_{release} - T_{imp} - R)_t \\ with, \\ I_t = 0, \quad if \quad (S_t - S_{t-1}) < 0; \end{cases} \qquad \text{Equation 2-6}$$

where, I_t is the inflow into the dam at the time step (t), $S_t - S_{t-1}$ is the change in the dam storage, Q_{irr} are the irrigation abstractions, Q_{spill} are the uncontrolled spills, E is the evaporation, $Q_{release}$ are flow releases from the dam, T_{imp} is the water transferred into the dam and R is the rainfall. The above parameters are in $m^3\ s^{-1}$. The calculated discharge at the dam location corresponds to the upstream part of the Chiba catchment (about 64 km^2) and not to the main catchment outlet. Thus, about 68% of the Chiba catchment area is ungauged. Such poor discharge data can hinder the calibration process and make the modelling task more challenging. Furthermore, it is expected that the discharge data at both Thau and Chiba catchment are affected with errors which may result in uncertain parameter estimation during the model calibration and, hence, increase uncertainty in simulated discharge. This may affect the performances of the hydrological model.

2.4.3 *Criteria for modelling performances assessment*

To evaluate the performances of the hydrological SWAT model the simulated discharge is compared to the observed data using one or more several statistical criteria. It is very common in hydrological studies to use the Nash and Sutcliffe (1970) efficiency coefficient (NS) for model performances assessment (Beven and Freer, 2001; Arabi et al., 2007; Shen et al., 2012).

$$NS = 1 - \frac{\sum_{i=1}^{n} (P_i - O_i)^2}{\sum_{i=1}^{n} (O_i - \overline{O})^2} \qquad \text{Equation 2-7}$$

with O_i is the observed discharge, $\overline{O}$ mean observed discharge values and P_i is the predicted discharge value. The range of NS lies between 1 and $-\infty$ with NS=1 being a perfect fit between model simulation and observation. NS value lower than zero indicates that the mean value of the observed time series would have been a better predictor than the model. The largest disadvantage of the NS efficiency is the fact that the differences between observed and predicted values are calculated as squared values which may overestimate higher values and neglect lower values. Motovilov et al. (1999) stated that according to common practice, the simulation of a model is considered good for NS greater than 0.75 and acceptable for NS between 0.75 and 0.36. These ranges are adopted in this study to classify SWAT performances.

$$R^2 = \left(\frac{\sum_{i=1}^{n} (O_i - \overline{O})^2 (P_i - \overline{P})^2}{\sqrt{\sum_{i=1}^{n} (O_i - \overline{O})^2} \sqrt{\sum_{i=1}^{n} (P_i - \overline{P})^2}} \right)^2 \qquad \text{Equation 2-8}$$

Besides the NS efficiency coefficient, the coefficient of determination R^2 is also used. R^2 is defined as the squared value of the coefficient of correlation according to Bravais-Pearson. R^2 lies between 0 and 1 which describes how much of the observed dispersion is explained by the prediction. A value of zero means no correlation at all whereas a value of 1 means that the dispersion of the prediction is equal to that of the observation. The fact that only the dispersion is quantified is one of the major drawbacks of R^2 if it is considered alone.

The above statistical criteria are used where observation data are available. In the opposite case, other criteria can be used such as graphical comparison, or a combination of both statistical and graphical comparison.

2.4.4 Modelling approach

The general modelling approach is summarized in the flow chart in Figure 2-13. After the ***implementation and parameterization of the SWAT model*** on the Thau and the Chiba catchments, the next step consists of the ***SWAT model parameter calibration and uncertainty assessment.*** Streamflow is the most important hydrological variable required for hydrological model calibration. However, as the Thau and the Chiba catchments are partially gauged, the SWAT model parameter calibration and uncertainty are performed only on subcatchments or part of the catchment where discharge data are available. In others words, parameter calibration and uncertainty analysis on the Thau catchment are conducted on the Vène and the Pallas subcatchments. For the Chiba catchment only the upstream part where the dam location is considered as the catchment outlet. This step is described in detail in the next chapter.

The second step consists of ***predicting discharge at the ungauged catchment through regionalization of hydrological model parameter.*** The “behavioral” model parameter sets (model parameter sets that lead to satisfied model performances) derived from the previous step are identified and transferred from gauged to ungauged catchments based on physical catchment similarity approach. The results are discharge estimation for the entire Thau and Chiba catchments. This step is described and treated in detail in chapter 4.

Once discharge for the entire Thau and Chiba catchment is available, the ***hydrological impacts of climatic change*** can be assessed through the development of some hydrological meaningfully indicators. This step is covered in chapter 5.

The last step in the modelling approach aims at comparing and quantifying the modelling uncertainty into ***hydrological parametric and climate models uncertainty sources***. To overcome the computational cost of the SWAT model, artificial neural networks (ANNs) are developed for each “behavioral” SWAT simulation. The ensemble ANNs is driven with the climate models and the resulting uncertainty is decomposed to hydrological and climate models uncertainty. This step is developed in chapter 6.

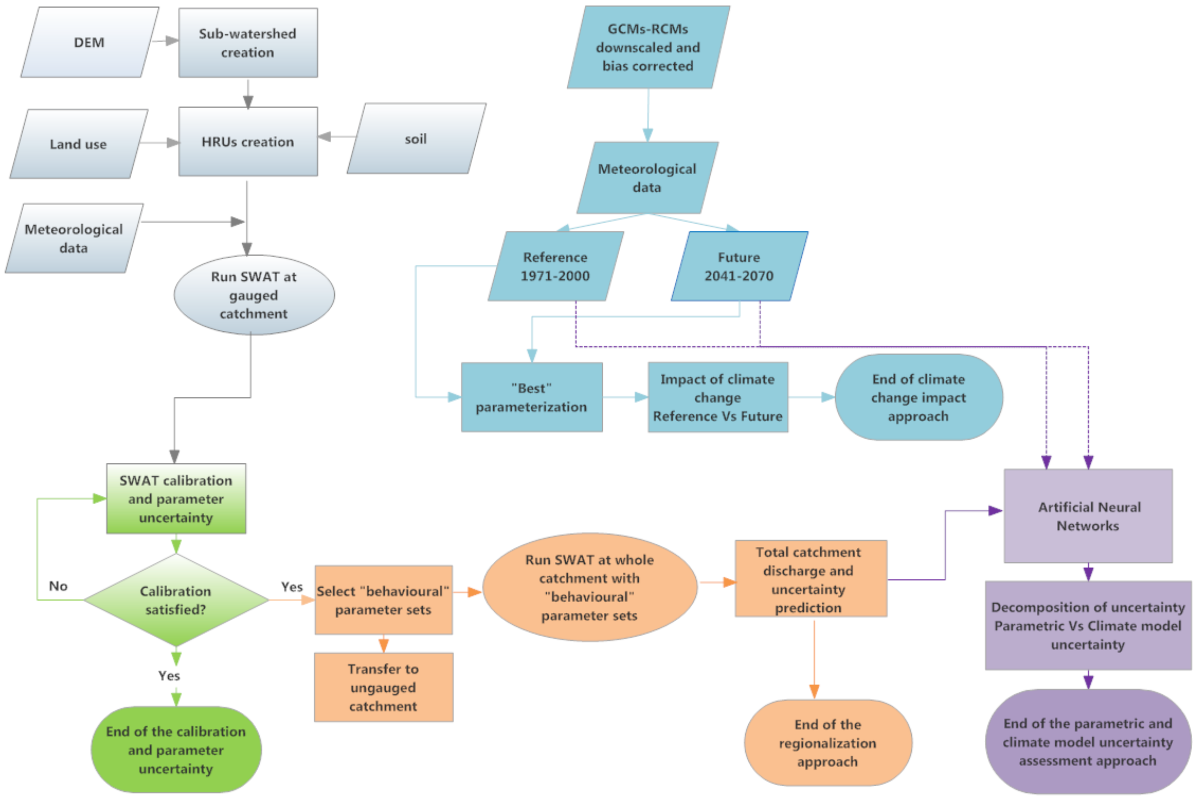

Figure 2-13: Flowchart of the general modelling approach

CHAPTER III[1]

[1] Based on: *Sellami H, La Jeunesse I, Benabdallah S, Vanclooster M. 2013. Parameter and rating curve uncertainty propagation analysis of the SWAT model for two small Mediterranean catchments. Hydrological Sciences Journal* ***58****: 1635-1657. doi:10.1080/02626667.2013.837222*

3 Hydrological model calibration and parameter uncertainty assessment

3.1 Abstract

Hydrological models predictions are always affected with uncertainty that have to be addressed in order to make appropriate use of these models in water resources studies and management. In this chapter, the efficiency of the SWAT model for discharge prediction of the Vène, Pallas and the Chiba catchments is tested. First, a sensitivity analysis is conducted using the LH-OAT method. Subsequent sensitive parameters calibration and uncertainty in the Thau catchment (Vène and Pallas subcatchments) are assessed simultaneously by using three different techniques (SUFI-2, GLUE and ParaSol). To efficiently compare the different uncertainty methods common criteria have been set for the likelihood function, the threshold value and the number of model simulations. Based on this comparison, the GLUE method is selected to investigate parameter uncertainty in the Chiba catchment during the SWAT calibration.

The effect of discharge uncertainty on the model prediction performances and uncertainty is also investigated, by considering firstly, deterministic discharge data (assuming no uncertainty in discharge data) and secondly, uncertainty in discharge data through the development of a methodology that accounts explicitly for error in the rating curve (stage discharge relationship). This approach is applied on the Vène and the Pallas catchments where the rating curves are available.

Results show that, model prediction uncertainty is not only study case specific, but also depends on the selected uncertainty analysis technique. It is found also that the 95% model prediction uncertainty interval is wider and more successful at bracketing the observations when uncertainty in discharge data is explicitly considered. The latter source of uncertainty adds additional uncertainty to the total model prediction uncertainty.

3.2 Introduction

Model calibration is the process of adjusting the values of model parameters such that the hydrological behaviour of the catchment can be simulated closely (Wagener et al., 2004). Although parameters of physically based hydrological models (e.g. SWAT model) represent physical properties they require an adjustment due to several uncertainty sources. Therefore, parameter uncertainty assessment should be an integrated part of the model calibration process.

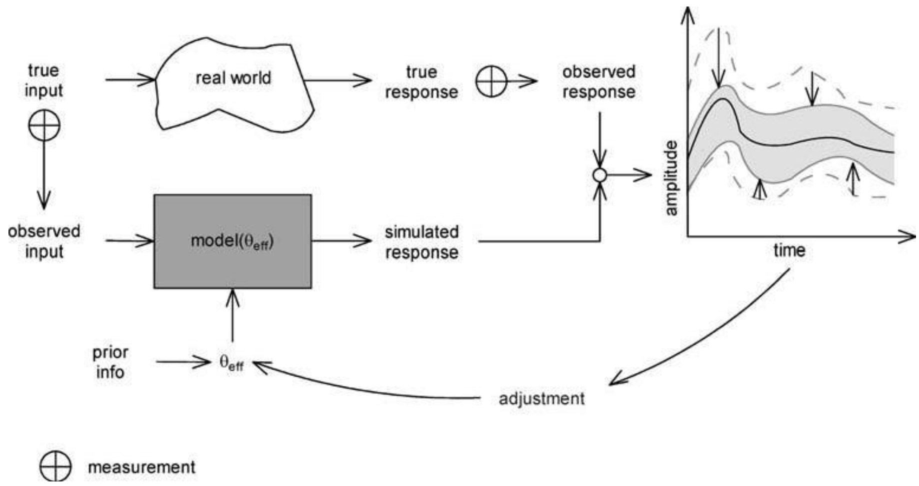

Figure 3-1: General hydrological model calibration process (Wagener and Gupta, 2005)

Hydrological model prediction uncertainty is a major point of concern for decision making in water resources management and planning. Therefore, uncertainty analysis must be performed in order to make full use of hydrological models as engineering and management tools. Uncertainties in hydrological models stem not only from model parameters, but also from inputs, outputs data (e.g. discharge) and model structure (Vrugt et al., 2005). Recently, the hydrological community has emphasized the need to explicitly treat the uncertainty of hydrological models through the modification and the development of robust methods. However, the traditional approaches to catchment model calibration have focused on methods to quantify only parameter uncertainty while neglecting the other uncertainty sources (Beven and

Binley 1992, Duan et al., 1992, Freer et al., 1996, Gupta et al., 1998, Vrugt et al., 2003).

Uncertainty assessment techniques are based on different concepts and assumptions. For example, the Shuffled Complex Evolution (SCE-UA) global optimization algorithm, developed by Duan et al. (1992) was modified by van Griensven and Meixner (2007) to an optimization and uncertainty analysis method known as Parameter Solution (ParaSol). The method investigates only parameter uncertainty and is implemented in recent SWAT model versions as an optimization and uncertainty analysis tool. Beven and Binley (1992) have developed the Generalized Likelihood Uncertainty Estimation (GLUE) based on Monte Carlo simulations. The philosophy behind GLUE is that no single optimum parameter set exists; rather a range of different sets of model parameter values may represent the process equally well. This is known as the *Equifinality Concept* (Beven and Binley 1992). The method has been extensively used for the uncertainty assessment of different hydrological models (Freer et al., 2004, Blasone et al., 2008, Viola et al., 2009 and Jin et al., 2010). It was also applied to assess the uncertainty analysis of the SWAT model (e.g. Yang et al., 2008, Setegn et al., 2009, Shen et al., 2012). Abbaspour et al. (2004) have developed the Sequential Uncertainty FItting procedure (SUFI-2) where the prediction uncertainty is quantified by a 95% uncertainty bands. SUFI-2 was used to calibrate and to assess parameter uncertainty of different hydrological models among them the SWAT model (e.g.Yang et al., 2008, Setegn et al., 2009).

While these methods are attractive solutions to the problem of accounting for model uncertainty, they are not yet part of the standard data analysis tool kit and challenging technical issues remain. Each of them has its own design, philosophy and its own working hypothesis and will not necessarily lead to the same uncertainty estimation for a given application. The selection of the uncertainty analysis method is not only based on its capacity in handling most of the uncertainty sources but also on its practical application regarding its computation time, the complexity in its implementation within the hydrological model, the modeler skills and the data available. However, one common result from all these applications is that parameter uncertainty is one of the most important uncertainty sources of model prediction uncertainty.

River discharge observations are always affected with uncertainty that strongly affect the rainfall-runoff model performance. Uncertainties in stage and discharge measurements propagate into the rating curve and affect the discharge values derived from it. Montanari (2004) simulated uncertainty in the measured discharge by adding Gaussian errors. Then he compared the optimized parameter sets resulting from different error realization to investigate the induced parameter uncertainty. Aronica et al. (2006) used the IHACRES model with the GLUE procedure to investigate the influence of the uncertainty of the rating curve on the final model prediction uncertainty. The upper and lower bands of the uncertain rating curves were constructed by randomly multiplying the original rating curve by a random variable. Their results showed a notable variation in the model prediction uncertainty when uncertainty of the rating curve was considered. McMilan et al. (2010) used the TopNet model to provide flow predictions in the Wairau River in New Zealand. They constructed around each discharge and stage value the confidence interval of the true values. Then they randomly sampled from these distribution to give possible pairs of true discharge and true stage values for each gauging point for the rating curve set. Using the Monte Carlo approach, multiple sets are taken and the uncertain rating curves were constructed. They showed that model prediction uncertainty bands obtained when uncertainty in the rating curve was considered were wider than these obtained without explicit consideration of uncertainty in the rating curve. Most of the aforementioned studies were done with conceptual hydrological models. Despite the agreement in literature that uncertainty in rating curves has a notable impact on model prediction uncertainty, (Clarke et al., 2000, McMilan et al., 2010, Aronica et al., 2006) studies that have considered uncertainty in discharge data in uncertainty analysis with spatially distributed hydrological models are, to the best of our knowledge, not widely available.

The aim of this chapter is to understand how parameter and discharge uncertainties affect the hydrological model performances and the prediction results. A first specific objective is to identify and quantify the uncertainty of daily discharge predictions using different uncertainty analysis techniques, considering deterministic observed discharge data. A second specific objective is to investigate the impact of the explicit consideration of the uncertainty of the stage discharge relationship (rating curve) on modelling prediction uncertainty.

3.3 Material and methods

3.3.1 Sensitivity analysis (SA)

Due to the large number of model parameters in the SWAT model the calibration process becomes tedious and challenging. A way to deal with such high-dimensional hydrological model is to conduct SA to select only the sensitive model parameters that are assumed to represent the real system behavior.

SA is conducted using the Latin Hypercube (LH) sampling (McKay et al., 2000) technique, combined with the one at a time (OAT) method (Morris 1991). This method is called the LH-OAT and is implemented in the SWAT model (van Griensven et al., 2006). The LH is a stratified sampling without replacement technique which divides the parameter range into *p* (*p*= 10) equal probability intervals. Only one input parameter is modified between two successive runs of the model. Therefore, the change in model output can be attributed to such a parameter modification by means of an elementary partial effect $S_{i,j}$ defined as (van Griensven et al., 2006):

$$S_{i,j} = \left[\frac{M(e_1,...,e_i \times (1+f_i),...,e_p) - M(e_1,...,e_i,...,e_p)}{f_i} \right] \quad \text{Equation 3-1}$$

where *M(.)* refers to the model functions (e.g. sum of squared error), f_i is the fraction by which the parameter e_i is changed and *j* refers to the LH point. According to Equation 3-1 the parameter is increased by a fraction f_i but it can also be decreased since the sign of the change is defined randomly. Considering *k* parameters, one loop involves performing (*k*+ 1) model runs to obtain one partial effect for each parameter. As the influence of a parameter may depend on the values chosen for the remaining parameters, the experiment is repeated for all the *p* LH intervals. Therefore, a total of *p* (*k*+1) model runs is required. A number of *m*= *p* (*k*+1) of elementary effects is obtained for each input factor. Based on this number of elementary effects calculated for each input factor, two sensitivity measures are proposed by Morris (1991); (i) the mean of the elementary effects, μ, which estimates the overall effect of the parameter on a given output, and (ii) the standard deviation of the effects, σ, which estimates the higher-

Table 3-1: Selected SWAT parameters for sensitivity analysis

Parameter	Initial distribution	Parameter description [Unit]
ALPHA_BF	U [0.1 – 1]	Base-flow alpha factor [days]
GW_DELAY	U [0 – 500]	Groundwater delay [days]
GW_REVAP	U [0.02 – 0.2]	Groundwater "revap" coefficient [none]
GWQMN	U [0 – 5000]	Threshold water depth in the shallow aquifer for flow [mm]
CN2*	U [0.1 – 0.9]	SCS CN II value [none]
ESCO	U [0.1 – 1]	Soil evaporation compensation factor [none]
EPCO	U [0 -1]	Plant uptake compensation factor [none]
SURLAG	U [1 – 24]	Surface runoff lag time [days]
CH_N2	U [0.1 – 0.3]	Manning's n value for main channel [none]
CH_K2	U [1 – 150]	Channel effective hydraulic conductivity [mm/hr]
SOL_AWC	U [0 – 1]	Available water capacity [mm/mm soil]
SOL_K	U [0–2000]	Soil hydraulic conductivity [mm/hr]
SOL_Z	U [0 – 3500]	Soil depth [mm]
SOL_ALB	U [0 – 1]	Moist soil albedo [none]
SLOPE*	U [0 – 0.5]	Average slope steepness [m/m]
SLSUBBSN	U [10 – 150]	Average slope length [m]
REVAPMN	U [0 – 500]	Threshold depth of water in the shallow aquifer for ‘‘revap’’ to occur [mm]

Note: U means uniform distribution. * Means fraction of variation by which the initial value of the parameter is changed.

order characteristics of the parameter (such as curvatures and interactions). The most sensitive parameter is ranked 1 and the less sensitive parameter is given a rank equals to the total number of parameters (van Griensven et al., 2006).

The selected objective function is the sum of the squared residuals SSQ (Equation 3-2) which provides the rank of the parameters based on the difference between measured and simulated daily flow.

$$SSQ = \sum_{i=1}^{l} (x_{i,measured} - x_{i,simulated})^2 \qquad \text{Equation 3-2}$$

where *l is* the number of pairs of measured ($x_{measured}$) and simulated ($x_{simulated}$) variables.

SA is performed on 17 SWAT model parameters that may have a potential to influence the flow river (Table 3-1). Snow parameters are not included in the SA since the study sites belong to a semi-arid climate and the flow is not affected by the snow melt process. The ranges of parameters variation are based on the SWAT manual (Neitsch et al., 2005) and are sampled by considering a uniform distribution in their physical range (Yang et al., 2008; Chahinian et al., 2011). The selected SWAT parameters for SA as well as their initial range, definition, units and initial distributions are reported in Table 3-1.

3.3.2 *Uncertainty analysis techniques (UA)*

As previously stated, three UA techniques are used for simultaneous parameter calibration and uncertainty assessment of the SWAT model on the Thau catchment. The aim behinds using more than one UA method is to investigate how different concepts and assumptions of UA methods influence the model prediction uncertainty and to select the most appropriate one for its application on the Chiba catchment and for further analysis. These UA techniques are described below.

Sequential Uncertainty Fitting (SUFI-2) (Abbaspour *et al.* 2004)
This calibration and uncertainty analysis method is an inverse optimization approach that uses the Latin Hypercube sampling procedure along with a global search algorithm to examine the behavior of objective functions. Parameterization is applied to a parameter set rather than to an individual parameter. The initial

parameter ranges are updated each iteration, and a narrower parameter uncertainty is obtained (Abbaspour et al., 2004). SUFI-2 is iterated until two stopping criteria quantifying the uncertainty are satisfied; (i) the *p-factor* (Equation 3-3) which is the percentage of discharge bracketed by the 95% prediction uncertainty interval (95PPU) calculated at the 2.5% and 97.5% levels of the cumulative distribution function of the output variables, and (ii) the *R-factor* (Equation 3-4) which is the average thickness of the 95PPU bands divided by the standard deviation of the measured data (Abbaspour *et al.* 2007).

$$p-factor = \frac{NQ_{in}}{n} \times 100 \qquad \text{Equation 3-3}$$

$$R-factor = \frac{\frac{1}{n}\sum_{t_{i=1}}^{n}(Q^{M}_{t_{i,97.5\%}} - Q^{M}_{t_{i,2.5\%}})}{\sigma_{obs}} \qquad \text{Equation 3-4}$$

where $Q^{M}_{t_{i,97.5\%}}$ and $Q^{M}_{t_{i,2.5\%}}$ represent the upper and lower simulated boundaries at time t_i of the 95PPU, n is the number of observed data points, M refers to modeled, t_i refers to the simulation time step, σ_{obs} stands for the standard deviation of the measured data and the NQ_{in} is the number of observed discharge in the 95PPU interval. The goodness of calibration and prediction uncertainty is judged on the basis of the closeness of the *p-factor* to 100% (i.e., all observations bracketed by the prediction uncertainty) and the *R-factor* to 0 (i.e., achievement of rather small uncertainty bound). If the above two criteria are considered as satisfactory then parameter uncertainty is depicted as a uniform distribution in the final parameter range. Previous studies (Schuol and Abbaspour, 2006, Yang et al., 2008, Andersson et al., 2009) showed that SUFI-2 is an efficient parameter optimization and uncertainty analysis procedure with low computational cost (between 500 and 1500 model runs). In this work two iterations are conducted with SUFI-2 each with 1500 model runs (with a total model runs of 3000) as suggested by Yang et al., (2008).

ParameterSolution (ParaSol) (van Griensven and Meixner 2007)
The technique is based on a modification of the global optimization algorithm SCE-UA (Duan et al., 1992). ParaSol calculates the objective function (OF) based on model outputs and observation time series for a selected variable and aggregates several fitting criteria to a

global optimization criterion (GOC). ParaSol minimizes the OF or a GOC using the SCE-UA algorithm. For the uncertainty analysis, the simulations performed are divided into “good” simulations and “not good” simulations based on a threshold value of the objective function which leads to “good” parameter sets and “not good” parameter sets. Then, the prediction uncertainty is constructed by equally weighting all “good” simulations. ParaSol was efficiently used for the calibration of the hydrological and water quality parameters of the SWAT model (Yang et al., 2008, Setegn et al., 2009 and Chahinian et al., 2011). In this study, the maximum number of model runs is set to 20,000 simulations before the optimization procedure is terminated. The computation demand of ParaSol depends only on the convergence of the SCE-UA algorithm. However, ParaSol can also stop if the criterion value is not changing. This has yielded 6,507 and 4,321 optimization loops in the Vène and in the Pallas catchment, respectively.

Generalized Likelihood Uncertainty Estimation (GLUE) (Beven and Binley 1992)
GLUE is a Monte Carlo based method for model calibration and uncertainty analysis (Beven and Binley 1992, Freer et al., 1996, for details). GLUE is based on a large number of model runs with different combinations of parameter values chosen randomly and independently from the prior distribution in the parameter space. By comparing predicted and observed responses, each set of parameter values is assigned a likelihood value (a function that quantifies how well that particular parameter combination simulates the observed system). Higher values of the likelihood function typically indicate better correspondence between the model predictions and observations. Based on a threshold value, the total sample of simulations is then split into “behavioral” and “non-behavioral”. The distribution of the likelihood value for the “behavioral” sets is treated as a probabilistic weighting function for the predicted variables (Beven and Binley 1992). According to this, a cumulative distribution of the model predictions is formulated and the desired quantiles are computed to represent the uncertainty interval that is likely to enclose the true value of the specific simulated variable. Therefore, the selection of these quantiles has an impact on the parameter uncertainty analysis (Blasone et al., 2008; Xiong and O’Connor, 2008; Jin et al., 2010; Gong et al., 2011). However, it is very common that the 95%

confidence interval is used to represent the prediction uncertainty interval which is also used in this study.

Other subjective choices are considered within the implementation of the GLUE framework in this study. The prior distributions of the selected parameters are assumed to follow a uniform distribution over their respective range (Table 3-1). This initial distribution is chosen since the real distribution of the parameter is unknown. The ranges of the parameters are selected based on the SWAT manual (Neitsch et al., 2005) and previous applications of the technique with the SWAT model (Yang et al., 2008; Shen et al., 2012).

To sample the prior parameter distribution, a simple random sampling is implemented. The number of sampling sets is set to 10,000. Such number of simulations was identified as sufficient for assessing uncertainty of about 10 sensitive SWAT model parameters (Yang et al., 2008, Gong et al., 2011). Moreover, it was showed by Yang et al. (2008) that no significant change is observed in the GLUE results between 10,000 and 20,000 model runs. So, the selected number of 10,000 simulations is considered reasonably sufficient for its application on the Vène and Pallas catchments. The likelihood function selected is the NS efficiency coefficient since it is widely used as a likelihood measure within GLUE in the literature (Beven and Freer, 2001; Arabi et al., 2007; Shen et al., 2012).

The cutoff threshold to separate “behavioral” from “non-behavioral” parameter sets is another subjective choice within the GLUE method. The selection of the threshold value is an entirely arbitrary choice that affects the prediction uncertainty (Montanari, 2005; Mantovan and Todini, 2006) and probably is the most important concern for the GLUE method. A small cutoff threshold will lead to larger “behavioral” simulations and larger uncertainty bands, while larger threshold value will decrease the numbers of “behavioral” models and will reduce the uncertainly interval width (Xiong and O’Connor, 2008; Blasone et al., 2008; Viola et al., 2009). Compared to previous applications of GLUE with the SWAT model (Gassman et al., 2007, Shen et al., 2012), model simulations that returned values of NS ≥ 0.5 are considered “behavioral” otherwise “non-behavioral” and, thus, they are discarded from further analysis.

3.3.3 *Integration of rating curve uncertainty in model prediction uncertainty*

This section focuses on the methodology used to develop the uncertainty related to the establishment of the rating curve, called hereafter "uncertain rating curve". A new model prediction uncertainty (due to "uncertain rating curve") and parameter uncertainty are introduced, based on an average prediction error calculation. The estimation of the flow discharge of the Vène and the Pallas catchments is based on fitting a single rating curve with a specific form. The power-law functional type (Equation 3-5) is found to be the best estimate of the rating curve for the cited catchments above (Figure 3-2 a).

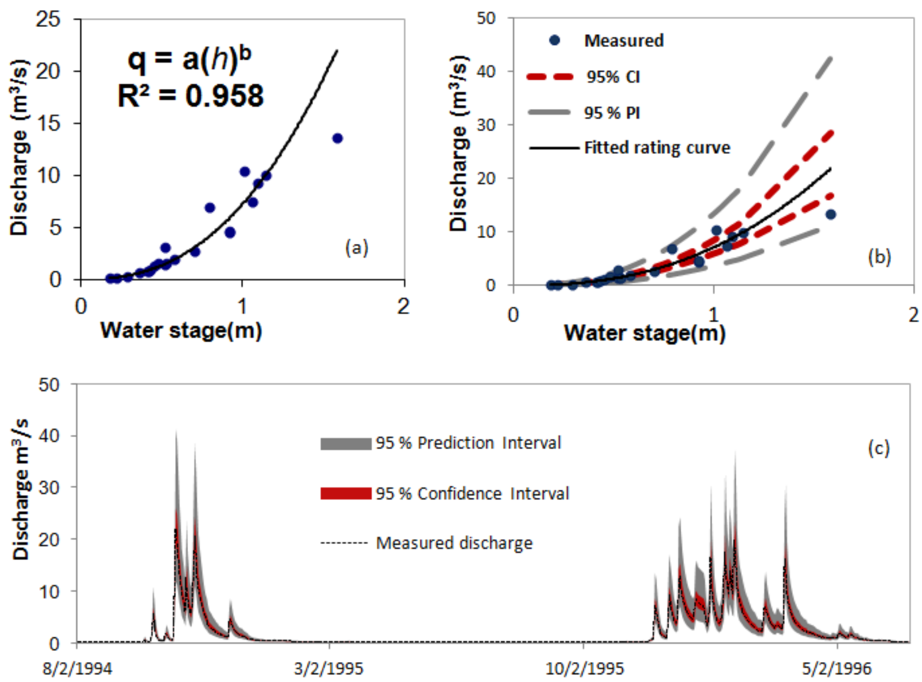

Figure 3-2: Schematic representation of the methodology used to construct the uncertain rating curve of the Vène catchment where 95% CI and 95% PI refer to the confidence and prediction intervals, respectively. (a): fitting the power law function to the stage discharge relationship. (b): constructing the confidence and prediction intervals of the uncertain rating curve and (c) is the uncertainty of the discharge data.

$$q = a(h)^{b} + \varepsilon \qquad \text{Equation 3-5}$$

where q is the discharge (m^3/s), h is the water level (m), a and b are parameters and ε is the residual. The power-law function is commonly used in hydrometric practice to fit the stage–discharge relationships (Clarke et al., 2000, Petersen-Øverleir and Reitan, 2005, McMillan et al., 2010).

For the purpose of constructing the confidence interval around the rating curve, the power-law function is linearized by logarithmic transformation to give a linear regression in the form of Equation 3-6.

$$\log_{10}(q) = \log_{10}(a) + b\log_{10}(h) + e \qquad \text{Equation 3-6}$$

Using the above equation it becomes easier to account for the increased dispersion between the measured discharge q_i and the predicted discharge $\hat{q}_i$ when discharge increases. Furthermore, it simplifies the calculation of the standard errors for the $\hat{q}_i$ Equation 3-6 can be written under the general form of:

$$y = A + Bx + e \qquad \text{Equation 3-7}$$

where y is $\log_{10}(q)$; A = $\log_{10}(a)$ is the intercept; $x = \log_{10}(h)$ and B=b which is the slope. The standard error of the predicted y, called hereafter y_{fit}, given at x_0, can be estimated as follow:

$$SE(y_{fit}) = \sqrt{\hat{\sigma}^2 \times \left[\frac{1}{n} + \frac{(x_0 - \bar{x})^2}{S_{xx}}\right]} \qquad \text{Equation 3-8}$$

where $\hat{\sigma}^2$ is the estimate of variance of the residual e about the regression line and is given by Equation 3-9, and S_{xx} is the sum of squared deviation of x from their mean $\bar{x}$ and is given by Equation 3-10.

$$\hat{\sigma}^2 = \frac{1}{n-1}\sum_{i=1}^{n}(y_i - y_{fit(i)})^2 \qquad \text{Equation 3-9}$$

$$S_{xx} = \sum_{i=1}^{n}(x_i - \bar{x})^2 \qquad \text{Equation 3-10}$$

where n is the number of data pairs (y,x) and $\bar{x}$ is the mean of x.

Using Equation 3-8, it is possible to calculate the standard error of y_{fit} or $\log_{10}(q)$ in terms of the standard error of x or $\log_{10}(h)$. For the purpose of constructing the confidence intervals, the residual e is assumed to be normally distributed with a constant variance. Analyses suggest that after the logarithmic transformation this assumption is reasonable. The 100(1-α) % confidence interval of y at a given value of $x=x_0$ can be constructed using according to Equation 3-11.

$$y_{fit} \pm t_{1-\alpha/2} \times SE(y_{fit}) \qquad \text{Equation 3-11}$$

where $t_{1-\alpha/2}$ is the appropriate value from the t-distribution (Student distribution) with n-1 degrees of freedom corresponding to the degree of confidence of 100 (1-α) %. For a 95 % CI, α is 0.05, for a 90 % CI α is 0.1, and so on.

When this calculation is made for all values of x in the observed range, the 100(1-α) % confidence interval of the position of the population regression line is obtained. Since the rating curve is used to derive the discharge values, uncertainty related to predict the discharge with h outside the measured range values will, intuitively, increase. Therefore, one can construct the prediction interval (PI) which is more appropriate to estimate the possible value of the discharge and its uncertainty region since it takes into account an additive prediction error term. The prediction interval for a particular value of x_0 can be constructed by adding one more standard error of y_{fit} about the regression line to Equation 3-8. Therefore, the standard error for the PI can be calculated using Equation 3-12.

$$SE(y_{fit}) = \sqrt{\hat{\sigma}^2 \times \left[1 + \frac{1}{n} + \frac{(x_0 - \bar{x})^2}{S_{xx}}\right]} \qquad \text{Equation 3-12}$$

Then, by replacing the new calculated standard error (Equation 3-12) in Equation 3-11, the PI can be constructed. Because of the last term of Equations 3-8 and 3-12, the confidence and prediction intervals become wider with increasing distance of x_0 (or h_0) from $\bar{x}$ (or $\bar{H}$) (see Figure 3-2 b).

The constructed uncertain rating curves allow association with each single discharge observation q_i (i =1, 2,..., n, where n is the total number of measured discharge data), a probability density function, pdf ($q_{true,i}$) where the log transformed true discharge (log($q_{true,i}$)) is centered on the reconstructed log(q_i) following a normal distribution, $N(\log q_{i,}\sigma_i^2)$.

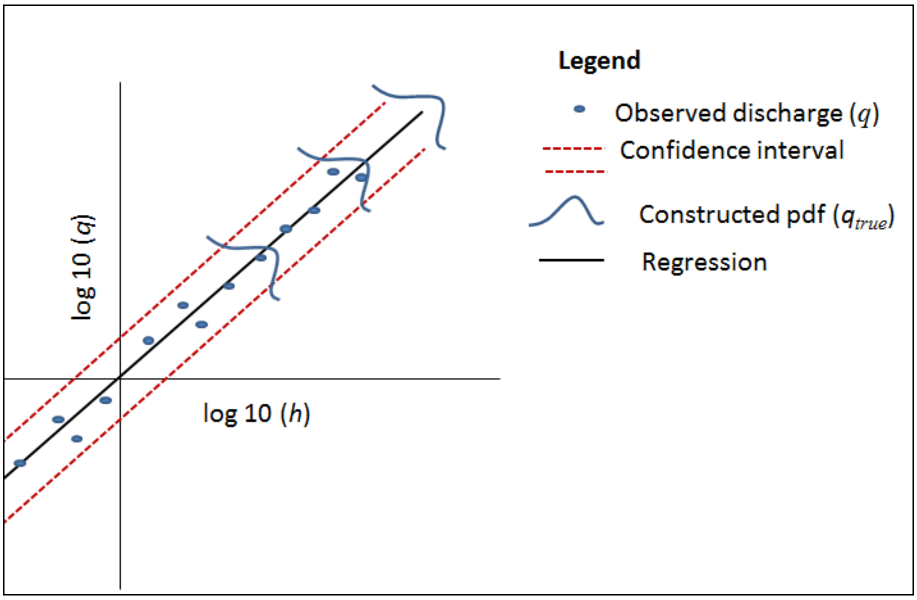

Figure 3-3: Schematic illustration of the reconstructed uncertain discharge

From the log($q_{true,i}$) pdf, the upper log($q_{U(true,i)}$) and lower log($q_{L(true,i)}$) limits are selected, corresponding to the 97.5th and 2.5th percentiles, respectively. Then, the model uncertainty is assessed using SUFI-2, GLUE and ParaSol, against the selected upper and lower values of the true discharge. By taking the upper and lower confidence limits as the true discharge, it is assumed that we can estimate an upper and lower error limits (Equations 3-13 and 3-14, respectively) where all the errors would fall if different samples of $q_{(true,i)}$ were taken from their pdfs. For each single simulation j and true discharge $q_{(true,i)}$ the upper and lower errors are calculated using Equations 3-13 and 3-14, respectively.

$$\varepsilon_j(q_{U(true,i)}) = \left(\hat{q}_{U(true,i,j)} - q_{U(true,i)}\right) \qquad \text{Equation 3-13}$$

$$\varepsilon_j(q_{L(true,i)}) = \left(\hat{q}_{L(true,i,j)} - q_{L(true,i)}\right) \qquad \text{Equation 3-14}$$

where i is the i^{th} observed point, j is the number of simulations and $\hat{q}_{U(true,i,j)}$ and $\hat{q}_{L(true,i,j)}$ are the predicted discharge of the j^{th} simulation of the $q_{U(true,i)}$ and $q_{L(true,i)}$, respectively.

The distributions of the errors estimated by Equations 3-13 and 3-14 are found to be dependent on the true discharge values which results in a skewed distribution. Hence, a logarithmic transformation is applied to the predicted true discharge and to the true discharge values in order to reach or to approximate normality of those errors.

$$\varepsilon(\log_{10}(q_{U(true,i)})) \approx N\begin{pmatrix} \log_{10}(\hat{q}_{U(true,i)}) - \\ \log_{10}(q_{U(true,i)}), \sigma^2{}_{\log_{10}(\hat{q}_{U(true,i)})} \end{pmatrix} \qquad \text{Equation 3-15}$$

$$\varepsilon(\log_{10}(q_{L(true,i)})) \approx N\begin{pmatrix} \log_{10}(\hat{q}_{L(true,i)}) - \\ \log_{10}(q_{L(true,i)}), \sigma^2{}_{\log_{10}(\hat{q}_{L(true,i)})} \end{pmatrix} \qquad \text{Equation 3-16}$$

In the second step, from the distribution of the errors given by Equations 3-15 and 3-16, and after logarithmic back transformation, an average error around each measured discharge q_i is derived as below.

$$\varepsilon_{av(i)} \approx N\begin{pmatrix} \dfrac{\hat{q}_{U(true,i)} - q_{U(true,i)} + \hat{q}_{L(true,i)} - q_{L(true,i)}}{2}, \\ \dfrac{\sigma^2_{\hat{q}_{U(true,i)}} + \sigma^2_{\hat{q}_{L(true,i)}}}{4} \end{pmatrix} \qquad \text{Equation 3-17}$$

Finally, from the $\varepsilon_{av(i)}$ pdf**,** the 2.5th and 97.5th percentiles are sampled corresponding to the new lower and upper model prediction errors around the measured discharge q_i. These new calculated uncertainty bands encompass both parameter uncertainty and discharge measurement uncertainty caused by uncertainties in the rating curve.

3.3.4 *Common criteria for uncertainty analysis techniques comparison*

As the uncertainty analysis techniques are based on different philosophies and assumptions, an exact comparison is not straightforward. Therefore, common criteria are used with regards to the practical application of these techniques such as the likelihood measure, the threshold value to define “behavioral” from “non-behavioral” models and the prediction uncertainty interval. The following are kept similar for all the methods to ensure an unbiased comparison: (i) the range and prior distribution of parameters, (ii) the likelihood measure and acceptance threshold, (iii) the statistical criteria for assessing model performances and prediction uncertainty.

The range of the SWAT model parameters is based on literature (Neitsh et al., 2005). A uniform parameter prior distribution is considered for all methods justified by the lack of information about parameter behavior. Indeed, as demonstrated by Freni and Mannina (2010), a uniform distribution is preferred, unless relevant prior parameter information is available. All the selected parameters are uniformly and independently sampled from their initial ranges while restricting to their physical range. The parameter ranges are listed in Table 3-1. The NS efficiency coefficient is selected as the likelihood measure for all the selected techniques. Comparison of the uncertainty results of the methods is based on model simulations with NS ≥ 0.5. The statistical criteria NS, R^2, *p_factor*, *R-factor* and the derived 95 % prediction interval are used for all the techniques to evaluate the uncertainty prediction.

To compare the effect of discharge uncertainty on the model prediction uncertainty, the number of simulations of each technique is kept similar to the one used to assess parametric uncertainty using deterministic rating curve. In addition, all the aforementioned criteria are kept constant. This is to ensure that differences in model prediction uncertainty, if any, are only related to the rating curves uncertainty.

3.4 Results and discussions

3.4.1 Sensitive SWAT parameters

Vène and Pallas catchments

The mean of the elementary effects (μ) and the standard deviation (σ) (Equation 3-1) for each analyzed parameter are plotted in a Cartesian plane in Figure 3-4 and their corresponding ranking is given in Table 3-2.

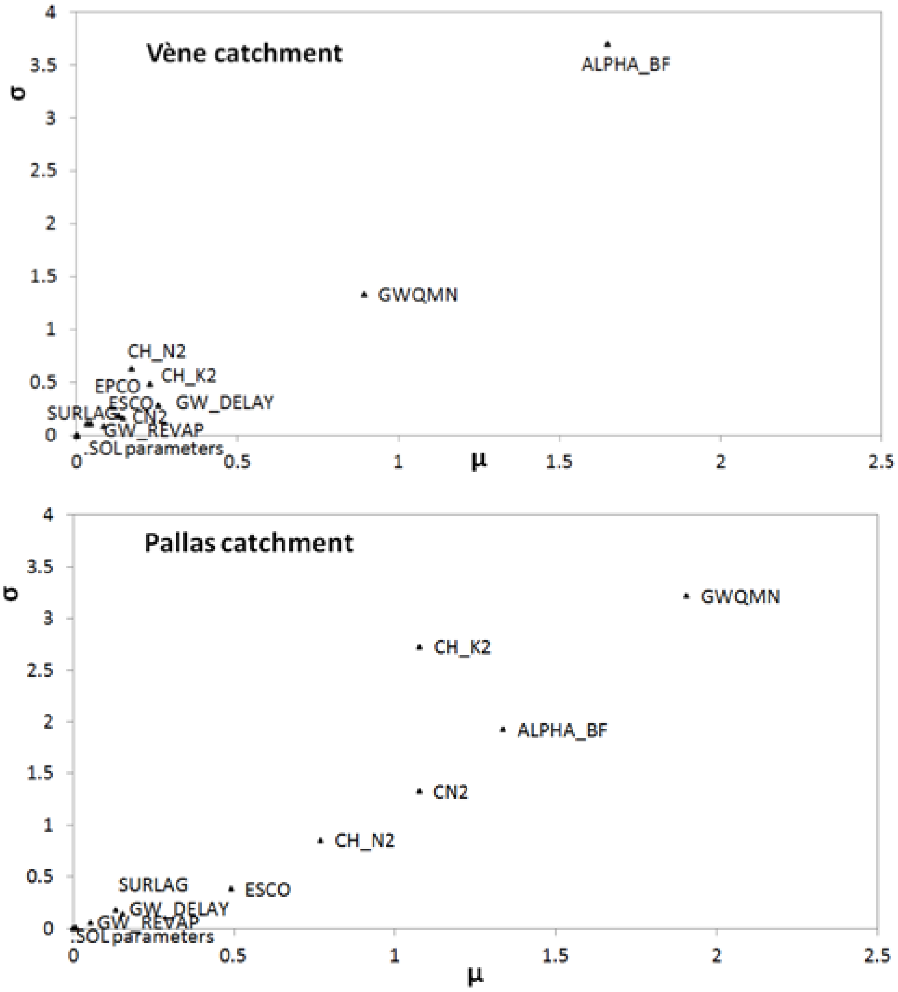

Figure 3-4: Morris plot of the average elementary effects (μ) of each parameter (17 parameters) against its standard deviation (σ) for the Vène and Pallas catchments

ALPHA_BF, a parameter that expresses the recession or the rate at which the groundwater is returned to the flow, and GWQMN, a threshold depth of water in the shallow aquifer required to return flow, are the most sensitive parameters in the Vène catchment. These two parameters show a high variability as expressed by the high value of their corresponding standard deviation which may reflect possible correlation between others parameters or between each other. A less sensitive but important parameter is the GW_DELAY, ranked third, which is defined as the required time for water leaving the bottom of the root zone to reach the shallow aquifer. These results suggest that the streamflow of the Vène catchment is highly dependent on the baseflow contribution. This is in agreement with the physical characteristics of the catchment. Indeed, the Vène catchment was found to be highly influenced by the karstic nature of the underground (Plus et al. 2006, Gallart et al., 2008, Perrin and Tournoud 2009, Chahinian et al., 2011).

Table 3-2: SA parameter ranking for the Vène, Pallas and Chiba catchments

Parameter	Vène	Pallas	Chiba
ALPHA_BF	**1**	**2**	**5**
GW_DELAY	**3**	**7**	11
GW_REVAP	**6**	**8**	13
GWQMN	**2**	**1**	8
CN2	**9**	**3**	**1**
ESCO	**8**	**6**	**2**
EPCO	**7**	**9**	7
SURLAG	**10**	**10**	9
CH_N2	**5**	**5**	10
CH_K2	**4**	**4**	**6**
SOL_AWC	13	14	**3**
SOL_K	15	11	**4**
SOL_Z	12	16	14
SOL_ALB	16	17	12
SLOPE	14	12	16
SLSUBBSN	17	15	17
REVAPMN	11	13	15

For the Pallas catchment, the most sensitive parameters are GWQMN, ALPHA_BF, CN2 and CH_K2. The two latter parameters are surface runoff related. The CN2 parameter is used to compute runoff depth from total rainfall depth. It is a function of catchment properties that include soil type, land use and antecedent soil moisture condition. CH_K2 is the hydraulic conductivity of the channel. The ranking of the most sensitive parameters (Table 3-2) suggests that the simulated Pallas streamflow depends on both baseflow and surface runoff components. The Vène and the Pallas streamflow are moderately sensitive to CH-N2, ESCO, EPCO and SURLAG parameters. The CH_N2 parameter is controlling the surface runoff while ESCO, EPCO and SURLAG are indirectly related to the surface runoff. CH_N2 is the manning's value of the tributary channel. ESCO is the soil evaporation compensation factor which directly influences the evapotranspiration losses from the catchment. The relative importance of this parameter is due to the long dry period that affects both the Vène and the Pallas catchments, especially in summer time. EPCO is the plant uptake compensation factor and expresses the amount of water needed to meet the plant uptake demand. SURLAG controls the fraction of the total water that is allowed to enter the stream on any specific day. The first ranked ten parameters given in Table 3-2 (in bold character) are identified as significantly sensitive and are selected for the calibration and uncertainty analysis for the Vène and the Pallas catchments.

The selection of the first 10 ranked parameters for the Vène and Pallas catchments is not based only on the results of the SA but also on the knowledge of the hydrological processes occurring in the catchment and on the previous applications of the SWAT model in the study area. In fact, it is known that the hydrological processes are complex in the study area due to the presence of the karstic features. Therefore, it is important to select besides parameters that influence the surface flow, model parameters that govern the groundwater flow and the interactions between subsurface and surface flow. In previous applications of the SWAT model in the study site, Plus et al. (2006) calibrated 8 parameters related to the flow simulation while Chahinian et al. (2011) selected 14 SWAT model parameters related to flow and to nutrient simulation, among 12 parameters were directly and indirectly related to flow simulation processes. Hence, selecting the 10 sensitive parameter described above ensures that the model does not omit one or more hydrological processes important for this particular case study.

Chiba catchment

The most sensitive SWAT parameters are those that govern the surface response including CN2, ESCO, SOL_AWC, SOL_K, ALPHA_BF and CH_K2. The SOL_AWC and SOL_K are sol related parameters that express the volume of water that is available to plants if the soil is at field capacity and the soil hydraulic conductivity, respectively. The last SWAT sensitive parameter is the hydraulic conductivity of the channel (CH_K2) which is a catchment response parameter. This parameter governs the movement of water from the riverbed to the subsurface for ephemeral or transient streams.

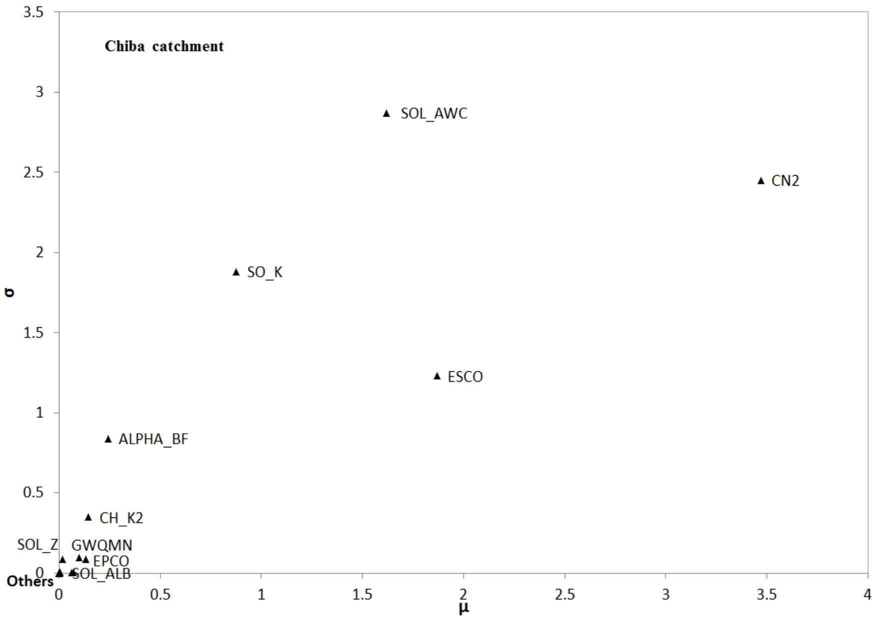

Figure 3-5: Morris plot of the average elementary effects (μ) of each parameter (17 parameters) against its standard deviation (σ) for the Chiba catchments

The sensitive soil and CN2 parameters have higher σ values than the others parameters. This may imply that the elementary effects relative to each of these parameters are different from each other and, thus, they are sensitive to the chosen values of the other parameters. However, the LH_OAT sensitivity analysis technique cannot quantify the correlation between the parameters, it just provides a qualitative results. Based on the SA results it is clear that the first six sensitive SWAT parameters should be selected for further analysis and parameter uncertainty assessment in the Chiba catchment (Table 3-2).

Conversely to the Vène and Palls catchments, the sensitive parameters in the Chiba catchment encompass only one groundwater parameter which is the ALPHA_BF but more soil related parameters. This can, *a priori*, reflect the difference in the hydrologic regime between the catchments. It seems that surface runoff has bigger influence on the hydrologic regime of the Chiba catchment than on the Pallas and Vène catchments. On the other hand, groundwater flow does not play an important role in the hydrologic regime of the Chiba catchment as it is obviously the case in the Vène and the Pallas catchment.

3.4.2 SWAT model efficiency for the Vène and Pallas catchments

To assess the performances of the SWAT model in reproducing the observed discharge of the Vène and the Pallas catchments, the results of the likelihood function (NS) for the "behavioral" model runs derived by each method are summarized in box plots in Figure 3-6. The best model simulation leading to the highest NS value for each method at each study catchment is scattered against the observed data in Figure 3-7. This figure also provides the R^2 coefficient to evaluate the SWAT ability in reproducing the variability of the discharge time series. In Table 3-3, these statistical criteria are summarized for each method at each of the Vène and Pallas catchments.

It is clear from Figure 3-6, Figure 3-7 and Table 3-3 that the maximum NS values and R^2 of all the techniques for both catchments are higher than 0.55 and 0.65, respectively, indicating that SWAT is able to satisfactorily predict the observed discharge at the Vène and the Pallas catchments. However, SWAT tends to under-predict the flows for both catchments, as it is shown in Figure 3-7.

95% of the NS values of the "behavioral" simulations derived from the ParaSol application are within the range of (0.5-0.67) and (0.5-0.58) in the Pallas and in the Vène catchments, respectively. The median NS value in the Pallas catchment (NS = 0.58) is superior to that in the Vène catchment (NS = 0.54). In a previous work (Chahinian et al., 2011), ParaSol was successfully applied at the Vène catchment with NS higher than 0.86.

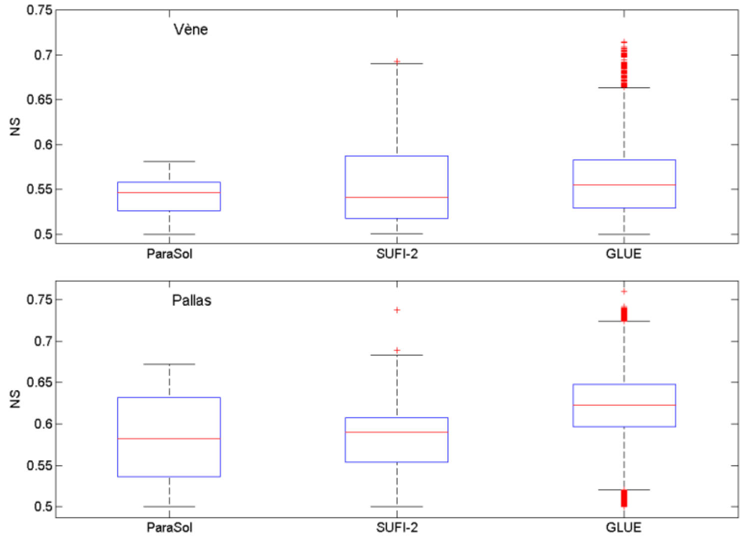

Figure 3-6: Boxplot of the likelihood function (NS) derived from the "behavioral" simulations of all the methods applied at the Vène and the Pallas catchments

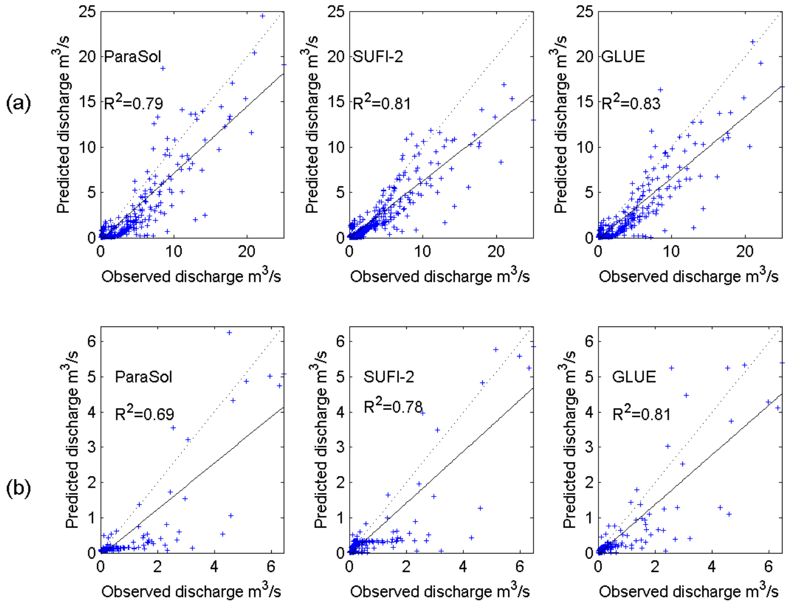

Figure 3-7: Scatter plot of the observed discharge against the best discharge simulation derived by each method at (a) the Vène catchment and (b) the Pallas catchment

The difference in the ParaSol performances between the results of this study and those reported by Chahinian et al. (2011) can be attributed to different causes. Firstly, Chahinian et al. (2011) used measured data of 4 years for calibration and validation of the SWAT model while in this study less than 2 years measured flow data are available. Secondly, Chahinian et al. (2011) calibrated the SWAT model at the upstream of the catchment (56% of the total area of the Vène catchment) while the entire Vène catchment is considered for model calibration in this study. Finally, Chahinian et al. (2011) used manual calibration followed subsequently by ParaSol while in our case, ParaSol is applied without prior manual calibration.

While the median NS value of the “behavioral” simulations of SUFI-2 is higher in the Pallas catchment (NS = 0.58) than in the Vène catchment (NS = 0.54), the 95% of NS values are within the same interval (0.5-0.69) for both catchments. The difference between the performances of SUFI-2 in both catchments is due to the presence of one extreme value in the Pallas catchment corresponding to the maximum NS reached by SUFI-2 (NS = 0.73). However, the limits of the confidence interval of NS values derived from SUFI-2 in both catchments are quite similar to these derived by ParaSol.

95% of the NS values of the “behavioral” simulations obtained by the GLUE method range from 0.52 to 0.72 and 0.50 to 0.66 in the Pallas and in the Vène catchments, respectively. However, the presence of many outliers suggests that NS values vary widely with GLUE compared to the other methods. In addition, theses extreme values of NS indicate that much more “behavioral” simulations are derived by the GLUE method than those derived by SUFI-2 and ParaSol.

All three methods provide better results, in terms of reproducing the observed discharge, in the Pallas catchment than in the Vène catchment. The GLUE method is the most efficient, followed by SUFI-2 and ParaSol (Table 3-3). These results indicate clearly that each method performs differently from the other and from one catchment to another.

Table 3-3: Uncertainty analysis techniques performances for the Vène and Pallas catchments

Statistical criteria	Method	Deterministic rating curve		Uncertain rating curve	
		Catchment			
		Vène	Pallas	Vène	Pallas
NS*	SUFI-2	0.69	0.73	---	---
	GLUE	0.71	0.76	---	---
	ParaSol	0.58	0.67	---	---
R^{2*}	SUFI-2	0.81	0.78	---	---
	GLUE	0.83	0.81	---	---
	ParaSol	0.79	0.69	---	---
p-factor (%)	SUFI-2	38	48	47	54
	GLUE	50	61	67	75
	ParaSol	19	28	21	29
R-factor	SUFI-2	0.38	0.36	0.44	0.41
	GLUE	0.46	0.44	0.67	0.59
	ParaSol	0.13	0.10	0.20	0.18

Note: * Corresponds to the "best" simulation.

3.4.3 *Model uncertainty using deterministic rating curve in the Vène and Pallas catchments*

For each method, the 95% model uncertainty bands (95PPU), derived from the "behavioral" simulations, with the observed discharge time series of the Pallas and the Vène catchment are produced in Figure 3-8. The *p-factor*, which expresses the percentage of observed data bracketed in the 95PPU and the *R-factor*, which is the average width of the 95PPU for each method are given in Table 3-3.

Results of SUFI-2 show that 38% of the observed Vène flow is bracketed in the 95PPU with an *R-factor* of 0.38 while in the Pallas catchment the 95PPU is bracketing around 48% of the observations with an *R-factor* of 0.36 (Table 3-3). GLUE is more successful at bracketing the Pallas discharge than the observations of the Vène discharge with respective values of *p-factors* of 61% and 50% and *R-factors* of 0.44 and 0.46. The 95PPU derived by ParaSol brackets only 19% of the observed Vène discharge with an *R-factor* of 0.13 against 28% of the observed Pallas discharge with an *R-factor* of 0.10. Although wider 95PPU is always found in the Vène than in the Pallas catchment for all the tested methods, which is also clear from the graphical investigation of Figure 3-8, the *R-factors* of each single technique calculated at both catchments are quite similar (Table 3-3). This is because the variance of the Pallas discharge is much lower than that of the Vène discharge which leads to an underestimation of the *R-factor* in the former catchment (See Equation 3-4). This also indicates that the quality of the observation data used to calibrate the model can affect the model prediction uncertainty.

From these statistics and the graphical inspection of Figure 3-8, it is clear that all techniques perform better in the Pallas catchment than in the Vène catchment which suggests that catchment properties may influence the prediction uncertainty results. In fact, a careful examination of Figure 3-8 shows that the 95PPU derived from all the techniques do not effectively capture the observations in the recession flow in both catchments especially in the Vène catchment. This can be attributed to the karstic feature in the Vène catchment.

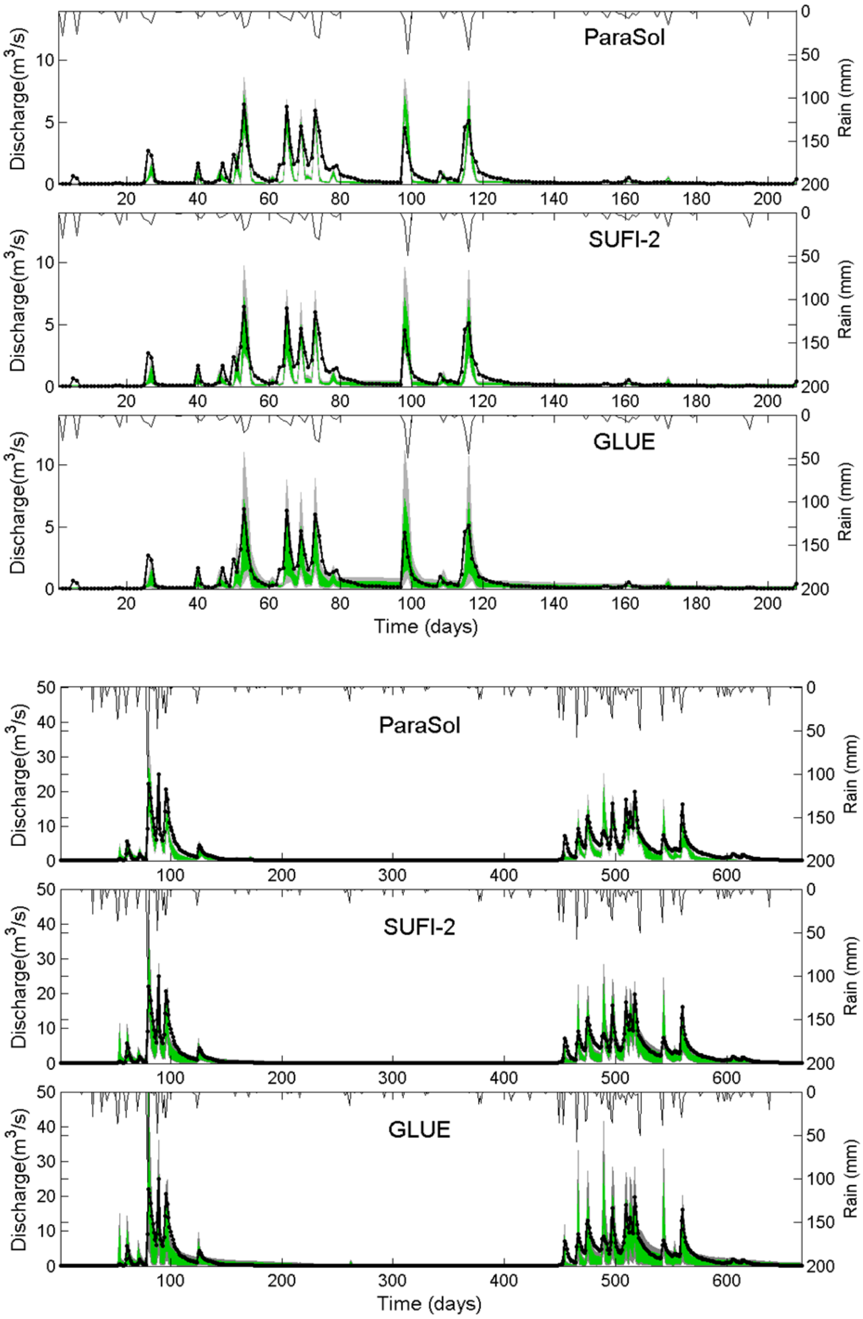

Figure 3-8: 95% prediction uncertainty interval derived using all the methods in the Pallas (upper panel) and in the Vène (lower panel) catchments. The grey shaded area corresponds to the 95% uncertainty interval derived using deterministic rating curve while the green shaded area corresponds to the 95% uncertainty interval derived using uncertain rating curve. The black line corresponds to the observed discharge.

Indeed, it was shown in previous studies (Gallart et al., 2008, Perrin and Tournoud, 2009, Chahinian et al., 2011) that the Vène streamflow is considerably influenced by the karst contribution. In fact, in the SWAT model, water that infiltrates through soil, sinkholes and loosing streams in a subbasin, recharges the aquifer and contributes to return flow within the same subbasin. But transfer of water from one subbasin to another is not allowed within the model. This can be a limitation for SWAT to adequately simulate karstic catchments where usually the hydrogeological boundaries exceed the topographic ones as is the case for the Vène catchment. This can explain the discrepancy and the larger uncertainty in the recession flow and in the baseflow of the predicted hydrograph of the Vène catchment. Other studies (Spruill et al. 2000, Coffey et al. 2004; Benham et al., 2006) reported the difficulty of the SWAT model to accurately represent karstic-fed catchment. Afinowicz et al. (2005) concluded that SWAT needs major change to adequately simulate baseflow and return flow. Baffaut and Benson (2009) modified the SWAT (2005) code to allow faster percolation through the soil substrate and recharge of the aquifer to simulate quick movement of water through vertical conduits that characterize karst topography. Their main modification consisted of splitting the original recharge of SWAT into two elements: the recharge from infiltration through the soil profile, and the recharge from sinkholes and losing streams. Their results showed an improved partitioning of streamflow between surface and return flow and significant sustainable flow even during summers with lack of precipitation. However, application of such a modified model code to improve discharge prediction in karstic system is beyond the scope of this research. In addition, for an accurate representation of the karstic features in the modelled study system, the loosing stream, sinkholes and springs have to be precisely located within the catchment and well characterized (drainage area, hydraulic conductivity, groundwater conduits network, etc.). Unfortunately, such information regarding the karstic features in our study area are not available.

Another observation that can be made from Figure 3-8 is that a relationship exists between the wet period and the width of the uncertainty interval. Model prediction uncertainty is more important under wet conditions than under dry conditions. This can be due to the inherent uncertainty in precipitation data (e.g. tempo-spatial variability, error in gauged stations, and variability in the intensity).

Applications of the different methods result in different parameter uncertainty ranges. Figure 3-9 provide the dotty plot which illustrates the parameter value against the performance measure (NS) for each model run for the Vène catchment (Figure 3-9 a) and for the Pallas catchment (Figure 3-9 b). The importance of the various model parameters can be depicted from these plots. Table 3-4 reports the final posterior parameters ranges for each uncertainty method for the Vène and the Pallas catchments.

Figure 3-9 shows that all the tested techniques are able to map all the parameter space. However, the number of the identified “behavioral” parameter sets, corresponding to model simulation that returned NS ≥ 0.5, varies from one technique to another and from one catchment to another. GLUE has the largest “behavioral” parameter sets followed by ParaSol and finally SUFI-2. In addition, more “behavioral” parameter sets are always found in the Pallas catchment than in the Vène catchment indicating that all methods have better performances in the Pallas than in the Vène catchment. From the dotty plots it appears that all the methods tend to flatten the response surface so that sharp peaks and valleys are not clear for all the parameters. This is because all the methods tend to find regions in the parameter space resulting in “behavioral” simulations and flatten the response surface of the parameter by given equally weight to the “behavioral” parameter sets. Therefore, in highly dimensional parameter space it is expected that one or many parameters will not be well identified. This finding is consistent with a previous study (Yang et al., 2008). Furthermore, different “behavioral” parameter sets lead to similar model prediction (Figure 3-9). This equifinality (Beven and Freer 2001) originates from the imperfect knowledge of the system under consideration and from different error sources (errors in input and boundaries conditions, errors in using an approximate model structure of the real system and error in the observation variable being modelled) that can interact in a non-linear way (Beven 2006). In addition, the subjective choice of the threshold value and the likelihood function can lead to additional uncertainty in the simulation results (Viola et al., 2009, Jin et al., 2010).

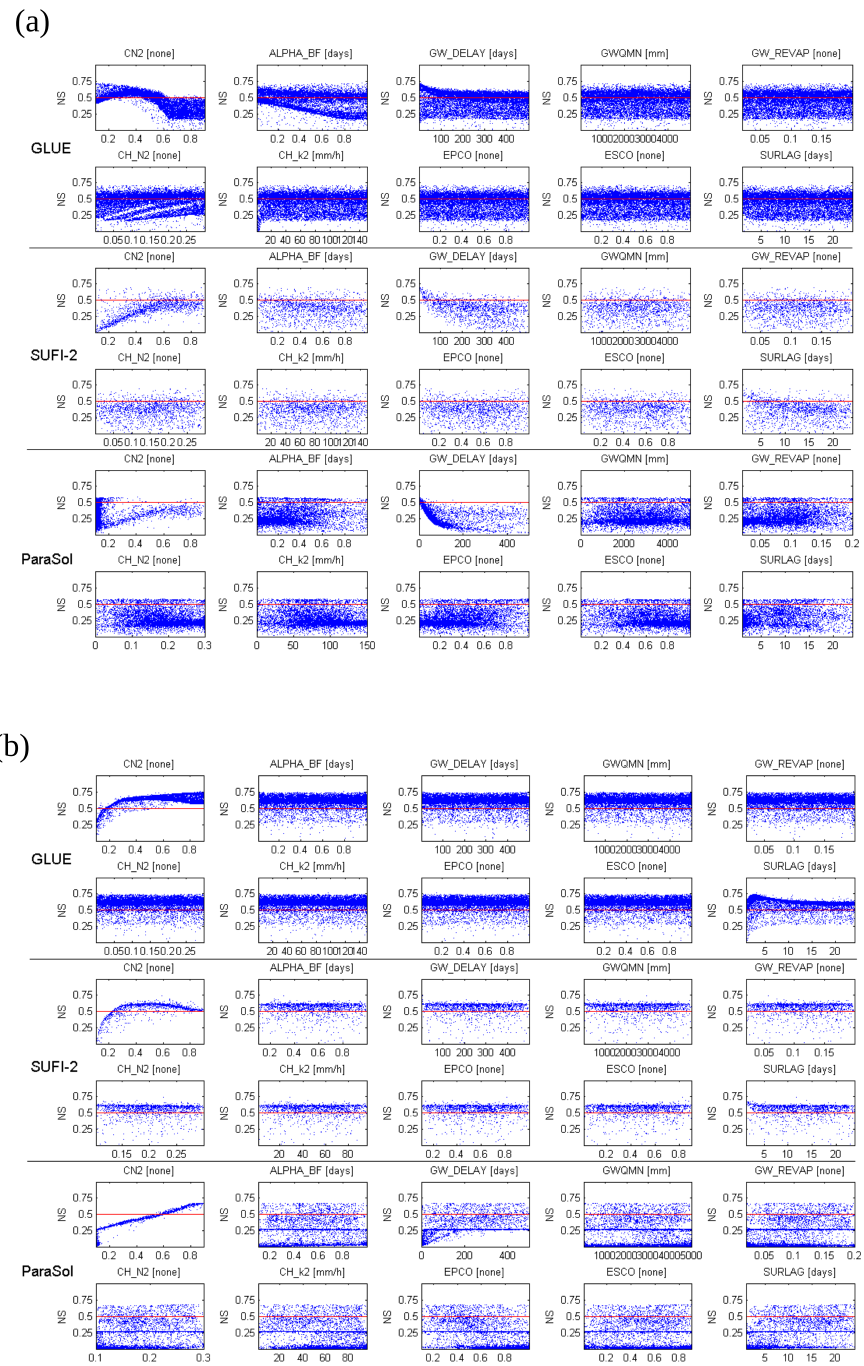

Figure 3-9: Dotty plot of the NS coefficient derived from all the methods at the Vène (a) and Pallas (b) catchments. The red line refers to the threshold value.

Table 3-4: Posterior uncertainty ranges of the SWAT model parameters from all the methods applied at the Vène and Pallas catchments.

Parameter	GLUE		SUFI-2		ParaSol	
	Vène	Pallas	Vène	Pallas	Vène	Pallas
CN2	0.17-0.53	0.21-0.86	0.23-0.85	0.28-0.83	0.1-0.22	0.58-0.86
ALPHA_BF	0.04-0.94	0.05-0.95	0.05-0.87	0.17-0.92	0.01-0.799	0.16-0.90
GW_DELAY	21.3-470	25.84-475	13.3-352	41.39-455	0-15.52	42-470
GWQMN	273-4768	265-4756	492-4607	493-4519	222-4997	503-4623
GW_REVAP	0.02-0.19	0.02-0.19	0.038-0.18	0.037-0.18	0.02-0.17	0.039-0.184
EPCO	0.05-0.94	0.05-0.94	0.09-0.93	0.17-0.91	0.012-0.97	0.17-0.88
ESCO	0.05-0.95	0.06-0.95	0.10-0.89	0.09-0.81	0.03-0.99	0.10-0.83
CH_N2	0.016-0.28	0.014-0.28	0.03-0.27	0.12-0.28	0.009-0.29	0.11-0.27
CH_K2	9.72-143	7.37-142	18.7-134	9.79-86.8	3.66-148	11-89.7
SURLAG	2.03-22.8	2.40-22.8	1.87-20.6	3.06-21.90	1-20.46	3.05-22.1

The dotty plots can also reflect the sensitivity of model performance to the parameter value. For instance, CN2 and GW-DELAY are the most sensitive parameters derived by all the techniques in the Vène catchment while only CN2 is depicted as sensitive for the Pallas catchment (Figure 3-9). CN2 has always been found to be sensitive within the SWAT model applications (Yang et al., 2008, Chahinian et al., 2011, Shen et al., 2012). This pointed to the significance of this parameter in the runoff process. Concerning the GW_DELAY, Spruill et al. (2000) highlighted the importance of this parameter when dealing with karstic aquifers. This parameter estimation depends on the depth of the water table and on the hydraulic properties of the geologic formation in the vadose and groundwater zones. Sensitivity of this parameter highlights the importance of the karstic features in the Vène catchment. The remaining parameters are distributed across wide range of values and are considered as non-identifiable parameters. It should be noted here that a parameter that shows a uniform posterior distribution may still be important in the context of a set of other parameters values due to possible parameters correlations and interactions. So, it is the combination of parameters that is important to produce “behavioral” model runs, given the selected model structure, the likelihood function, the acceptance threshold value and the sampling strategy. Therefore, results of the uncertainty analysis methods may not reveal the sensitivity of a single parameter as it is revealed by the LH-OAT sensitivity analysis technique.

Figure 3-10 shows the posterior cumulative density function of the “behavioral” parameters derived from each technique for the Vène and the Pallas catchments. The degree of the parameter uncertainty is expressed by the confidence interval (95% CI) taken at the 2.5% and 97.5% threshold values of the posterior cumulative density function. It is clearly seen from Figure 3-10 and Table 3-4 that different methods lead to different posterior parameter distributions (PDs). Most of the parameters have large 95% CIs which are close to their prior ranges which confirm that all the methods try to flatten the confidence region response surfaces. The 95% CI of some parameters, such as CN2, are different from one method to another and from one catchment to another Table 3-4.

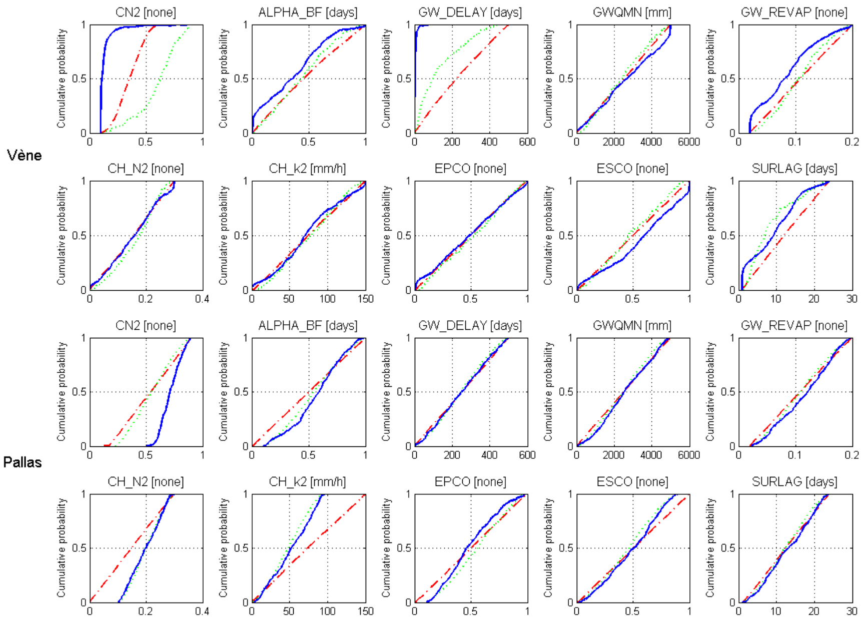

Figure 3-10: Posterior cumulative distribution function of "behavioral" parameters derived from all the methods for the Vène and the Pallas catchments (red for GLUE, green for SUFI-2 and blue for ParaSol).

In comparison, in the Vène catchment, SUFI-2 shows the largest 95% CI of CN2 parameters (0.23-0.85) followed by GLUE (0.17-0.53) and ParaSol (0.1-0.22) while in the Pallas catchment, for the same parameter, the largest 95% CI is derived by GLUE (0.21-0.86), followed by SUFI-2 (0.28-0.83), and finally ParaSol (0.58-0.86) (see Table 4). GLUE leads to the widest 95% CI of posterior parameter range followed by SUFI-2 and ParaSol. For instance, in the Pallas catchment the final 95% CI uncertainty range of CN2 derived by GLUE contains the corresponding interval of SUFI-2 and ParaSol. These results are in line with previous studies (Yang et al., 2008, Setegn et al., 2009). The parameter uncertainty is suspected to propagate in substantial model prediction uncertainty. However, this is difficult to verify because apart from the parameters, model structure and data quality also cause uncertainty in model prediction (Li et al., 2010).

When investigating the possible correlation between the model parameters, all three methods show weak correlation values. It seems that all the techniques do not explicitly account for parameter interactions. This can be related to the parameter sampling strategy or to the concept behinds the uncertainty technique. For example, in GLUE, one explanation can be that the selected sampling strategy cannot account for parameter interactions since each parameter is individually randomly sampled from its initial distribution. Moreover, as GLUE is built on the concept of equifinality, the method tends to evenly distribute the “behavioral” parameter sets with significant weight over the parameter space. In SUFI-2 parameter uncertainty is depicted as a uniform distribution in the final parameter range; therefore, parameter interactions are neglected.

3.4.4 Effect of the discharge uncertainty on the model prediction uncertainty in the Vène and Pallas catchments

In this section the results of the SWAT model prediction uncertainty derived from using all methods with explicit consideration of uncertainty in rating curves (discharge uncertainty) are provided and compared against model prediction uncertainty using the deterministic rating curve. It is worth noting here that for an unbiased comparison of the results, the initial distribution of the parameter, the numbers of model runs and the threshold value to separate “behavioral” from “non-behavioral” parameter sets are kept the same as in model prediction uncertainty using the deterministic rating curve. The simulated discharge and the 95PPU obtained by considering the deterministic rating curve and the 95% model prediction uncertainty interval obtained by explicit consideration of discharge uncertainty (95MPU) by applying each method, on the Pallas and the Vène catchments, are shown in Figure 3-8 (green shaded area).

Results show that ParaSol does not show a significant improvement in enclosing more observations in both catchments. As shown in Figure 3-8, the 95MPU derived from ParaSol in the Vène and the Pallas catchments, considering the uncertain rating curve, is hardly distinguishable from the 95PPU using the deterministic rating curve. One explanation for this result can be that the number of model runs is insufficient to provide a large number of “behavioral” model parameters given the selected threshold value.

The uncertainty prediction interval derived by GLUE is the widest and the most successful in bracketing the discharge observation in both catchments when uncertainty in rating curve is considered (Table 3-3). About 17% and 14% of additional Vène and Pallas discharge observation points, respectively, are falling in the 95MPU obtained using the uncertain rating curve. These added observations correspond mainly to the peak discharge and to the recession flow. These findings are in line with those of Aronica et al. (2006) and McMillan et al. (2010).

For SUFI-2, the additional percentages of the enclosed observations in the 95MPU are about 9% and 6% for the Vène and the Pallas, respectively. These results are lower than those achieved by the GLUE method. This is because the results of SUFI-2 are based on the second iteration where the uncertainty of the model prediction is smaller than the one obtained in the first iteration. The improvement of the methods, mainly for GLUE and SUFI-2, in bracketing more observation data comes at the cost of wider model prediction uncertainty reflected by an increase in the *R-factor* values of the uncertainty interval derived using the uncertain rating curve (Table 3-3). It is also clear from Figure 3-8 that uncertainty in the rating curve leads to wider uncertainty in the discharge peak flows under wet conditions than under dry conditions. It should be noted here, that the 95MPU, derived by the methods using the uncertain rating curve, are assumed to encompass both parameter and discharge uncertainty. Model structure and input uncertainty (e.g. rainfall) are not explicitly considered or may slightly be covered through parameter uncertainty.

Although the explicit consideration of uncertainty in the discharge data lead to wider uncertainty interval than the one of deterministic rating curve, the *p-factors* for all the methods are still far from the suggested value of 100%. This means that parameter uncertainty cannot fully account for all sources of model uncertainty even when discharge uncertainty is explicitly accounted for. Therefore, besides parameter and discharge uncertainty, model structure and model input uncertainty have to be explicitly considered to provide modelling uncertainty interval able to capture the observation data. However, given all these sources of uncertainty and their possible interaction and propagation from one model component to another, quantifying and separating each uncertainty source is a difficult and remains challenging.

As the implementation of all the methods with the uncertain rating curve is kept unchanged in comparison to the one using the deterministic rating curve, the difference between these two model prediction uncertainty intervals can be assumed to be related to the additional uncertainty of the rating curve. Therefore, the contribution of this last uncertainty factor can be estimated by variance decomposition. The uncertainty due to "uncertain rating curve" ($\sigma^2_{\varepsilon(obs)}$) can be estimated by subtracting the model residual variance obtained by the "deterministic rating curve" ($\sigma^2_{\varepsilon(d)}$) from the model residual variance obtained by the "uncertain rating curve" ($\sigma^2_{\varepsilon(av)}$).

$$\sigma^2_{\varepsilon(obs)} = \sigma^2_{\varepsilon(av)} - \sigma^2_{\varepsilon(d)} \qquad \text{Equation 3-18}$$

As the model residual variances obtained by the deterministic rating curve $\sigma^2_{\varepsilon(d)}$ are heteroscedastic, a logarithmic transformation is applied to become approximately constant or independent on the model output discharge value. Based on the above assumptions and Equation 3-18, the contribution of discharge uncertainty to the total model prediction uncertainty can be roughly estimated. Based on the GLUE results, about 28% and 14% of the modelling uncertainty is originating from discharge uncertainty in the Vène and Pallas catchments, respectively. Results of SUFI-2 suggest that discharge uncertainty contributes by an average of 13% and 9% to the total model uncertainty in the Vène and the Pallas catchments, respectively. Such information is very useful towards a global quantification of different uncertainty sources and their contribution to the total model prediction uncertainty.

3.4.5 Advantages and limitations of the uncertainty methods

GLUE leads to the largest model prediction uncertainty interval and is the most successful method in enclosing the observation data. Furthermore, its implementation is straightforward and can be used easily without major change to its original method. The concept behind the GLUE approach which is based on rejecting the idea of "optimal" parameter value and accepting that several parameter sets can be "behavioral" for describing the system is appealing and consistent in the face of inputs error, model structure, parameter errors and observation errors. However, as it is based on random Monte Carlo sampling, it requires a large number of model runs which makes it the most computationally burdensome technique with respect to SUFI-2 and ParaSol. The selection of the likelihood function and the threshold value within the implementation of the GLUE framework are arbitrary. This may add some additional uncertainty in the prediction results.

SUFI-2 is efficient in providing “behavioral” simulations that satisfactorily matched the observation data with less computational time than the GLUE method. Another advantage of SUFI-2 is that it can be implemented with different likelihood measures. However, implementation of SUFI-2 is more complicated than GLUE due to the global optimization procedure involved in it. In addition, the technique requires interactive checking of the final posterior parameter range by the modeler. The *p-factor* and the *R-factor* are the two main statistical criteria used to assess the final acceptable model prediction uncertainty within SUFI-2. However, a higher *p-factor* can be achieved by increasing the *R-factor*. Also, additional iterations lead to narrower model prediction uncertainty which makes SUFI-2 losing its objectivity in deriving realistic uncertainty bands.

ParaSol This method is difficult to implement and to use. Based on the SCE-UA optimization tool, in principle ParaSol is able to locate the “optimal” parameter value but it is not the case in this work. Its computational demand depends on the convergence of the search which can be higher in a high dimensional model. ParaSol is the least performing method compared to GLUE and SUFI-2 in this study.

In the light of these results and the comparison between the uncertainty analysis techniques and their efficiency in assessing the modelling prediction uncertainty, the GLUE methodology is selected for further analysis and applications to the Chiba catchment.

3.4.6 SWAT model efficiency and parameter uncertainty in the Chiba catchment

In this section, the SWAT model efficiency is evaluated and parameter uncertainty is investigated using the GLUE approach on the gauged part of the Chiba catchment.

SWAT model performances

Although more extensive GLUE simulations are conducted in the Chiba (13,000) in comparison to the Vène and the Pallas catchments (10,000), the identified “behavioral” parameter sets, with respect to the selected threshold value of NS ≥ 0.50, is very weak and does not exceed 1.5% of the total model runs. Others authors have also reported similar limitation of GLUE to provide a sufficient number of “behavioral” parameter sets. For instance, Jia and Culver (2008) reported that only 0.8% of 50,000 generated parameter sets were considered as “behavioral”. Kuczera and Parent (1998) explained that it is possible that even after billions of model runs no even one “behavioral” solution can be retained. Of course for the same generated parameter sets, the number of “behavioral” model parameter sets is not influenced only by the defined threshold value but also by the number of the selected parameters, their initial range and the parameter sampling schema adopted.

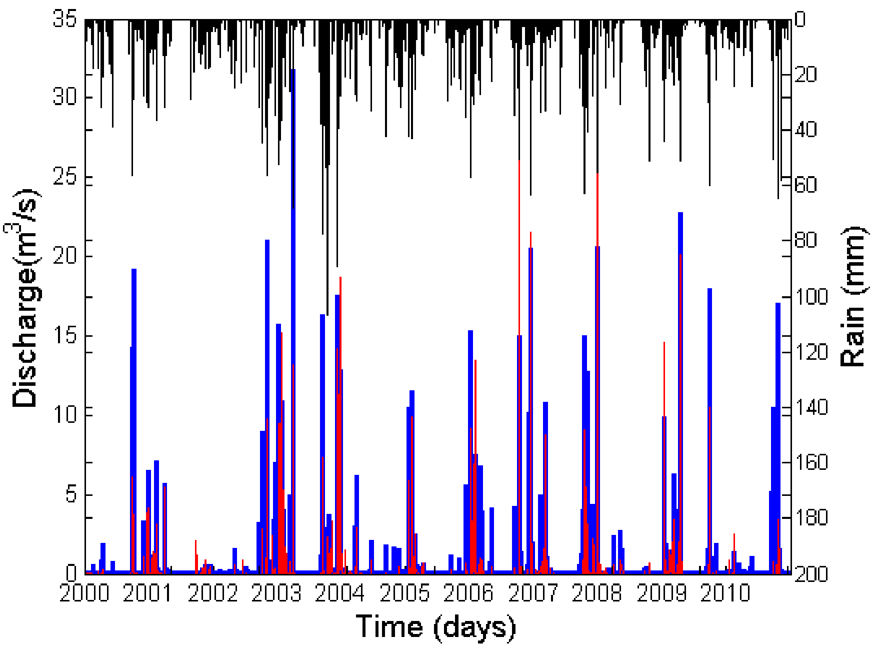

Figure 3-11: Predicted versus observed discharge at the Chiba dam location. (The red line corresponds to the observed discharge calculated from the dam water balance and the blue lines represent the 95% of the “behavioral” model simulations).

The “behavioral” SWAT model simulations are compared to the observed discharge in Figure 3-11. The NS and R^2 values derived by the “behavioral” model runs for the 10-years simulation period, range between 0.5 and 0.624 and 0.80 and 0.81, respectively. These statistics suggest that the overall model performance can be classified as acceptable according to Motovilov et al. (1999). However, the inter-annual model performance is marked by high variability. For instance, the NS values are negative for years 2000, 2002, 2004 and 2010, while they are acceptable for 2001, 2003, 2005 and 2008 and good for 2005, 2006, 2007 and 2009 (Figure 3-12).

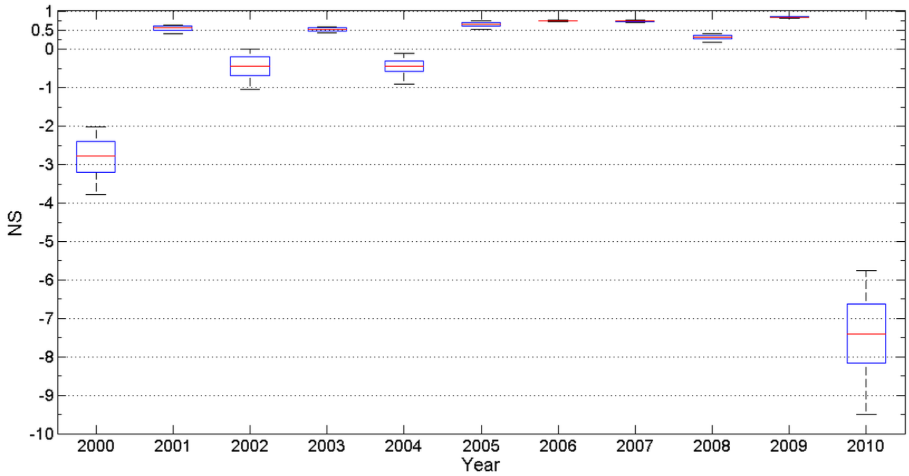

Figure 3-12: Box plot of the model efficiency (NS) showing the inter –annual variability of the “behavioral” model prediction performances. (The red central line is the median, the blue edges of the box are the 25th and 75th percentiles, and the whiskers extend to the most extreme data points not considered outliers)

Given the same model parameter sets, input data and model structure, this inter-annual variability in the model prediction performance can be attributed to the spatio-temporal variability of the rainfall data. For instance, Figure 3-13 illustrates the temporal and spatial variability in rainfall within and surrounding the Chiba catchment. In this figure, the ratio of the yearly rainfall value by the 10-years average rainfall values at the rain gauges retained by the SWAT model undergoes high variability from one year to another and from one rain station to another. For example, the average annual rainfall value of 2003 reaches more than twice the 10-years average rainfall value measured at the KORBA rain gauge while at the CHIBA rain gauge this ratio is about 1.6.

This high spatio-temporal variability of rainfall is a typical climate characteristic of semi-arid regions (Bouraoui et al., 2005) and can affect the accuracy of the discharge prediction.

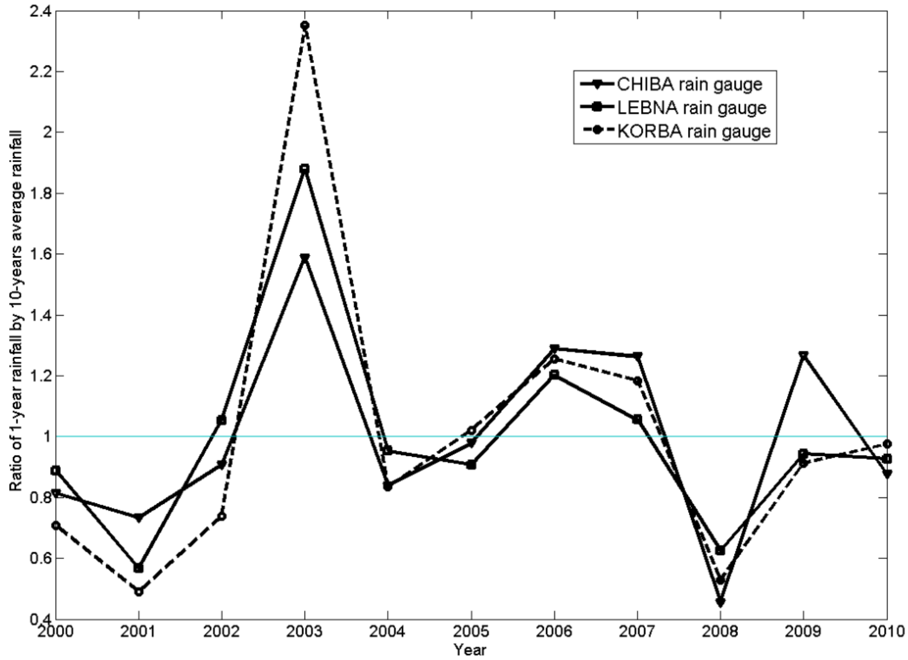

Figure 3-13: Spatial and inter-annual variability of the rainfall data from the rain gauge stations retained by SWAT in the Chiba catchment

To better investigate the model performances and the discrepancy between simulations and observations, the flow duration curves (FDCs) of the "behavioral" simulations are constructed and plotted against the observed FDC in Figure 3-14. FDC provides the percentage of time (duration) a daily or monthly (or some other time interval) streamflow is exceeded over a period for a particular river basin (Castellarin et al., 2004). FDC may also be viewed as the complement of the cumulative distribution function of the considered streamflow and is probably one of the most informative methods for displaying the complete range of river discharges, from low flows to flood events. Empirical FDCs can be easily constructed from streamflow observations using standardized non-parametric procedures (see Vogel and Fennessey, 1994, 1995; Smakhtin, 2001; Castellarin et al., 2004).

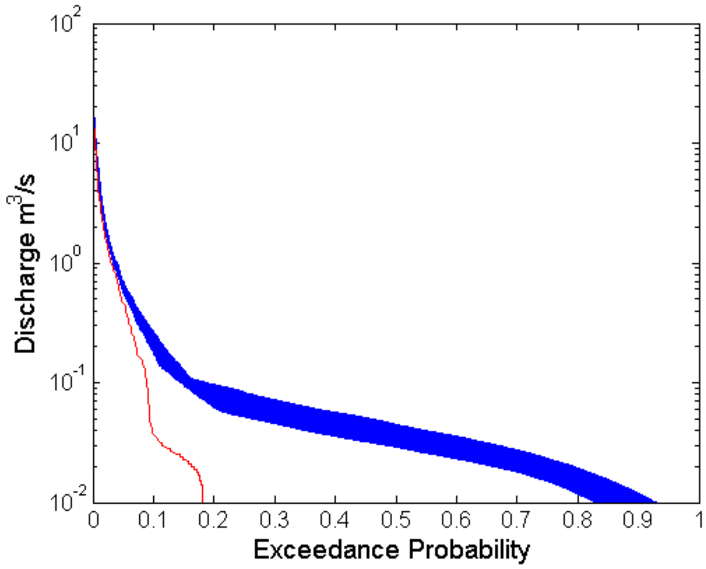

Figure 3-14: Observed (red) versus predicted (blue) "behavioral" 10-years daily FDCs for the Chiba catchment.

The flow percentiles conceptually represent different segments of the FDC: high flows (≤ Q10 or Q0.1), median flows (Q20- Q70 or Q0.2-Q0.7) and low flows (>Q70 or Q0.7). The predicted daily 10-years-FDCs show a relatively steep slope within the high flows percentile (exceedance probability ≤0.1) indicating that floods discharge occur shortly and intermittently and are affected with high inter-annual variability. The observed FDC is marked with a steep slope throughout denoting a highly variable stream whose flow is largely from direct runoff. The predicted high flow values, median and range of variation match well the observed ones (NS= 0.90-0.96, R^2= 0.93-0.96). These high flows occur as direct catchment response to rainfall event or storm. Therefore, the high variability in the predicted high flow values as well as in the observed ones can be attributed to the inter-annual variability of the rainfall in the study area.

The lower tail of the FDC, corresponding to low flows (exceedance probability > 0.7), suggests that the observed Chiba streamflow ceases flowing at 80% over the specified time period whereas the predicted FDCs overestimate the flowing time period to more than 80%. Low flows most likely come from soil, channel storage release or groundwater contribution and are influenced by the geology, soil moisture and land use characteristics (Mohamoud, 2008). The discrepancy between the predicted and the observed low flows can be attributed to the uncertainty in the inflow data derived from the dam water balance and used to evaluate the model performances. Nevertheless, for this specific study case, it is more important that the model reproduce better the high flows than the low flows since the latter is not an important component in the catchment flow regime as suggested by the observed FDC (Figure 3-14). However, losses in low flows can be also attributed to the volume of water abstracted through river bed transmission. In fact, many semi-arid catchments especially intermittent rivers have alluvial channels that abstract large volume of water when the flood wave is traveling downstream.

SWAT parameter uncertainty using the GLUE approach for the Chiba catchment

About 14% of the observation data are bracketed in the 95% uncertainty interval (95PPU) with an *R_factor* of 0.066. While the latter is close to the suggested value of zero reflecting narrow uncertainty interval, the *p_factor* reflects the poor percentage of the observed data falling inside the 95 PPU. Most of these observation data are within the high flows percentile which can be clearly seen in Figure 3-14. However, as previously discussed interpretation of the model prediction uncertainty derived by GLUE is conditioned by the choice of the threshold value among others. For instance, an increase in the threshold value induces a decrease in the *R_factor* and the *p_factor* and declines the number of the retained “behavioral” parameter sets. Table 3-5 reports the posterior range of the sensitive parameters derived from the “behavioral” model runs. The dotty plot of NS against each parameter values for the “behavioral” GLUE simulations are illustrated in Figure 3-15. Most of the parameters, except for ESCO, have narrower final range than their initial range. However, except CN2, all the parameters have a uniform distribution within their respective final range which makes their distribution non-identifiable (Figure 3-15). This is because the GLUE approach is not intended to seek the best likelihood value and to derive the optimal parameter value. Instead, it tends to find regions in the parameter space resulting in acceptable simulations and flatten the response surface of the parameter by given equally weight to “behavioral” parameter sets. Therefore, in highly dimensional parameter space it is expected that one or many parameters will not be well identified.

Table 3-5: Posterior range of sensitive parameters in the Chiba catchment

Parameter	Initial range	Posterior range	Unit
CN2*	[0.1- 0.9]	[0.26-0.40]	none
ESCO	[0-1]	[0-1]	none
SOL_AWC	[0 - 1]	[0.1-0.28]	mm/mm soil
SOL_K	[0-2000]	[0.8-1.2]	mm/hr
ALPHA_BF	[0-1]	[0.01-0.06]	days
CH_K2	[0-150]	[1.1-3]	mm/hr

* Relative change

Investigations of the parameters correlation (data not shown) show very low correlation between the parameters. For instance the highest correlation coefficient is R= 0.17 between the CN2 and the CH_K2 parameters. This confirms that GLUE does not explicitly account for parameters interaction.

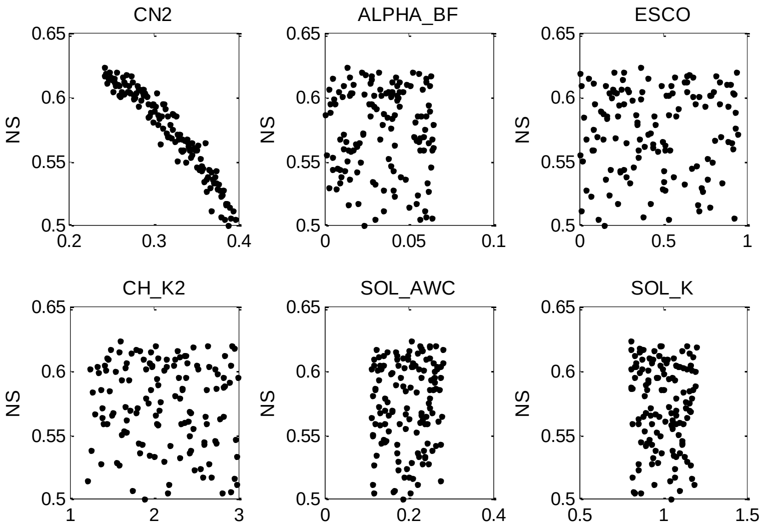

Figure 3-15: Dotty plot of the NS coefficient derived from all the “behavioral” GLUE runs for the Chiba catchment

Since there is no discharge gauge station in the Chiba catchment, uncertainty related to rating curve could not be assessed. Therefore, only parameter uncertainty has been addressed in the Chiba catchment, thus, modelling uncertainty in this case could be underestimated.

3.5 Conclusions

In this chapter, the SWAT model efficiency and its associated prediction uncertainty in predicting the discharge of the Vène, Pallas and Chiba catchments are investigated.

The model calibration results were satisfactory despite several uncertainty sources and the data scarcity in the tested catchments. However, the application and the comparison of the different uncertainty techniques revealed that SWAT model predictions are always affected with uncertainty whose quantification is a challenging task. The assessed uncertainty depends on the technique used and the way it is implemented. The application of the uncertainty techniques in different catchments highlights how the complexity of the system affects the prediction uncertainty assessment. For instance, it was demonstrated how the presence of the karstic features in the Vène catchment leads to larger prediction uncertainty than in the other catchments.

Although all the methods are implemented as similarly as possible their results are different, not only from one catchment to another but also from one technique to another. Each technique has its advantages and limitations. The selection of the most appropriate uncertainty method depends not only on its prediction results but also on the theory behind it, its simplicity, its computational efficiency, the data available, and the modeler's knowledge and skills. In this regard, the GLUE was selected as the preferred technique due to its several advantages and mainly to its concept.

Due to the fact that all sources of uncertainty must be considered, a methodology was developed that explicitly took the uncertainty in discharge data into account. Uncertainty in discharge data is principally due to the uncertainty in the rating curve. It was demonstrated that explicit consideration of uncertainty in the discharge data leads to wider model prediction uncertainty bands. The latter are more successful at enclosing the observations. This suggests that parameter uncertainty alone cannot compensate for all modelling uncertainty sources and that other additional uncertainty sources (input and model structure uncertainty) must be considered for a complete and comprehensive uncertainty assessment.

CHAPTER IV[2] [3]

[2] Based on : *Sellami, H., La Jeunesse, I., Benabdallah, S., Baghdadi, N., and Vanclooster, M.: Uncertainty analysis in model parameters regionalization: a case study involving the SWAT model in Mediterranean catchments (Southern France), Hydrology and Earth System Sciences Discussions, 10, 4951-5011, 10.5194/hessd-10-4951-2013, 2013.*

[3] *Sellami H, Vanclooster M, Benabdallah S, La Jeunesse I. 2013. Assessment of the SWAT model prediction uncertainty using the GLUE approach A case study of the Chiba catchment (Tunisia). IEEExplore. doi:10.1109/ICMSAO.2013.6552605*

4 Streamflow prediction at the ungauged catchments: hydrological parameter regionalization and uncertainty propagation

4.1 Abstract

In this chapter a method for propagating the hydrological model uncertainty in discharge predictions of the ungauged subcatchments of the Thau and the Chiba catchments is developed and presented. The method is based on model parameter regionalization approach. Regionalization of model parameters based on physical similarity between gauged and ungauged catchments attributes is a popular methodology for discharge prediction in ungauged basins. However, the methods are often confronted with an arbitrary criterion for selecting the “behavioral” model parameters sets (Mps) at the gauged catchment. A more objective method is provided in this chapter where the transferrable Mps are selected based on the similarity between the donor and the receptor catchments. In addition, the method allows propagating the modelling uncertainty while transferring the Mps to the ungauged catchments. Results indicate that physically similar catchments located within the same geographic and climatic region may exhibit similar hydrological behavior and can also be affected by similar model prediction uncertainty. Furthermore, the results suggest that model prediction uncertainty at the ungauged catchment increases as the dissimilarity between the donor and the receptor catchments increases. The methodology presented in this paper can be replicated and used in regionalization of any hydrological model parameters for estimating streamflow at ungauged catchment.

4.2 Introduction

Hydrological models are generally calibrated against observation variable(s), typically streamflow, to estimate some parameters that cannot be measured directly and to achieve a reliable prediction of the catchment response. However, in many cases, observed streamflow data are not available or are insufficient. Therefore, the catchment is considered as ungauged (Sivapalan et al., 2003) which may undermine the planning and the management of the water resources in the ungauged catchment. To overcome this problem, various regionalization techniques have been developed to estimate streamflow in ungauged catchments including methods based on the similarity approach (Vandewiele and Elias, 1995; Idrissi et al., 1999; Merz and Blöschl, 2004; McIntyre et al., 2005; Oudin et al., 2008) and/or statistical approach (Sivapalan et al., 2003; Yadav et al., 2007). The latter approach consists in deriving statistical relationships between catchment attributes (CAs), such as topography, soil, drainage area, etc., and the optimized model parameters (Mps). Once these relationships have been established, one can determine the parameters of an ungauged basin using its CAs. Although it can be considered as the most common regionalization approach for ungauged catchment (Wagener and Wheater, 2006), statistical approaches were deeply criticized due to the assumption that most statistical models consider linearity between CAs and optimized Mps (Merz and Blöschl, 2004 ; Parajka et al., 2005; McIntyre et al., 2005). On the other hand, regionalization based on similarity approach consists of transferring the information from donor catchment(s) to receptor catchment(s). It starts by identifying one or more donor catchments which are usually gauged catchments and that are most likely to be hydrologically similar to one or more receptor catchments. Subsequently, the relevant information (Mps or streamflow records) from donor to receptor catchments is transferred. Typically, Mps transfer from donor to receptor catchment(s) rely on physical similarity measures. In this case, the same CAs as used in the statistical technique can be adopted to identify similar catchments. Alternatively, use can be made of spatial proximity measures (e.g. the distance between the centroids of the catchments). The similarity regionalization approach is based on the assumption that similar catchments behave hydrologically similarly. So, the definition of the similarity measure, certainly subjective, will condition the success of the selected regionalization approach (Heuvelmans et al., 2006).

Several studies have focused on the transfer of Mps based on similarity approach for predicting streamflow records at ungauged catchments (Merz and Blöschl, 2004; McIntyre et al., 2005; Parajka et al., 2005; Bàrdossy, 2007; Oudin, et al., 2008). For instance, McIntyre et al., (2005) found that Mps transfer outperformed as compared to the statistical regression approach using a five parameters version of the Probability Distribution Model (Moore, 1985) applied on 127 UK catchments. Similar conclusions were drawn by Oudin et al., (2008) using two conceptual rainfall-runoff models on 913 French catchments; the GR4J (modèle du Génie Rural à 4 paramètres Journalier) developed by Perrin et al. (2003) and the TOPMO model which is a six parameters version of the TOPMODEL (Beven, 1997). Parajka et al. (2005) have used 4 groups of regionalization approaches. The first group is based on spatial averaging of calibrated model parameters, the second is based on spatial proximity (spatial distance) between the catchments, the third uses multiple regression between catchments attributes and model parameters and the last group is based on similarity between catchment attributes. They have found that regionalization methods based on spatial proximity and catchment attributes similarity performed better than multiple regression and spatial averaging methods. However, other studies have reported that even nearby catchments can be hydrologically different (Ouarda et al., 2001; Shu and Burn (2003); McIntyre et al., 2005; Beven, 2000).

The similarity approach for regionalization of Mps in ungauged catchments implies the “good” performance of the calibrated hydrological model at the donor catchment. Then, Mps that lead to “good” or “behavioral” model simulations are selected and transferred to the ungauged catchment. However, it is argued that hydrological model predictions, even in well gauged catchments are subject to inherent uncertainty that stems from different uncertainty sources (e.g. inputs, parameter uncertainty, model structure, and observed data). Because of all these uncertainty sources, it is expected and argued that model calibration will lead to non-unique sets of parameters (Beven and Binley, 1992). Therefore, it becomes difficult to associate the calibrated parameters with the physical characteristics of the catchment.

While model parameters uncertainty at well gauged catchment has received considerable attention during the past two decades (Beven and Binley 1992, Duan et al., 1992; Abbaspour et al., 1997; Muleta and Nicklow, 2005; Vrugt et al., 2008; Yang et al., 2008; Zhang et al., 2009, Shen et al., 2012), little attention has been given to the uncertainty resulting from Mps regionalization at ungauged sites (Wagener and Wheater, 2006). Furthermore, additional uncertainty related to the regionalization procedure that stems from the arbitrary choices of the CAs, the similarity measure, the selection of the candidate parameter sets to be transferred can have a significant effect on the model prediction uncertainty in the ungauged catchments. Addressing all these sources of uncertainty and understanding the way they can affect the model prediction in the ungauged catchment is a challenging task (Sivapalan et al., 2003 and Wagener et al., 2004).

This chapter aims to contribute to this challenge by addressing the following question: how can Mps uncertainty of donor catchments be propagated through regionalization schemes based on the similarity approach, and how does it affect the prediction uncertainty in ungauged catchment?

4.3 Material and methods

The approach is firstly developed on the Thau catchment then applied to the Chiba catchment. As the Vène and Pallas catchments have been subject to many previous studies (Aquilina et al., 2002; La Jeunesse et al., 2002; Plus et al., 2006; Chahinian et al., 2011, Sellami et al., 2013) more detailed data are available for these subcatchments. Therefore, the Vène and the Pallas catchments are considered as gauged catchments, while all other eight small subcatchments are considered ungauged.

4.3.1 The regionalization approach

Selection of catchment attributes

The adopted regionalization method for this study is the transfer of Mps from donor to receptor catchment based on the similarity between their physical attributes (topography, geology, soils, drainage area, etc.). The physical similarity approach is based on the assumption that catchment physiographic characteristics predetermine the hydrological behavior. Therefore, the selection of relevant CAs is crucial for the success of the regionalization procedure. The catchments attributes selected and used to define similarity are related to topography, land cover, drainage area, soil and geological features and are given in Table 2-1. They are derived from the available data such as land use maps, soil maps, digital elevation model and geology maps. These CAs are generally considered as the main drivers of the hydrological process in the literature (Merz and Blöschl, 2004;

Heuvelmans et al., 2006; Wagener et al., 2007; Bastola et al., 2008) and are the most common ones used to define similarity between catchments in model parameter regionalization schemes. For instance, Heuvelmans et al. (2006) have considered catchment area, average slope, dominant land use and soil texture classes as the most appropriate catchment descriptors in model parameters regionalization in the Flemish part of the Scheldt river basin (Belgium). Besides these CAs, others authors have used flow indices or characteristics using flow duration curve (FDC) such as (Masih et al., 2010), indices of hydrological responses (Yadav et al., 2007) or hydro-meteorological long term data (Bastola et al., 2008) as relevant catchment descriptors. However, the selection of the appropriate CAs depends also on the physical meaning of the selected model parameters, on the objective of the regionalization procedure and on the knowledge about the key hydrological processes occurring within the catchment. For example, when the objective of the regionalization procedure is to estimate the flow in ungauged catchments, as in our case, the use of flow characteristics or indices as input is useless. Model parameters, especially those of physically based model such as SWAT, are assumed to be closely related to CAs and, thus, representing the functional behavior of the catchment response. For instance, in the SWAT model the curve number parameter (CN2) depends on the soil and land use characteristics of the catchment which are considered among the relevant catchment descriptors. Knowledge about the key processes in the system can also assist the selection of the relevant CAs. As an example, the geology is considered as relevant catchment descriptor in our study case since it is known that the Jurassic limestone aquifer in the eastern part of the Thau catchment strongly influences the hydrological regime of the Vène catchment (Sellami et al., 2013a).

Within each catchment, the dominant soil physical texture based on the relative proportion of sand, silt and clay is considered to identify the CAs related to soil type. The main geological features considered is the surface catchment percentage covered by the Jurassic limestone estimated using the GIS tools based on the simplified geological map of the Thau catchment. Other geomorphologic and topographic descriptors (mean elevation, mean slope, drainage area) are also calculated using GIS tools and are reported in Table 2-1. Besides the CAs, it is very common that climatic characteristics such as long-term precipitation characteristics, the annual precipitation, annual potential evapotranspiration index, solar radiation, etc. (see, Wagener et al., 2007), are used for the similarity measure between the catchments. However, in our case study such climatic descriptors are omitted since we are dealing with small and geographically close catchments located within a relatively small area under the same climate regime.

Definition of the similarity measure and catchments clusters

Unfortunately, there does not exist a universally accepted metric or combination of metrics to quantify catchments similarity in the catchment attributes dimension. Some authors have used the inverse of the Euclidean distance (Heuvelmans et al., 2004) or the normalized sum of the absolute difference (Parajka et al., 2005). Others authors (Masih et al., 2010) have used the weighted normalized sum of the absolute difference where equal or more weights are assigned to individual catchment attributes in order to consider their varying assumed importance.

To identify similar catchments groups, CAs are normalized and each catchment is assigned to its own cluster and the similarity matrix between clusters, in the catchment attributes dimension, is calculated. Then, clusters with the largest similarity measure are linked together into binary clusters based on the average linkage method where the distance between two clusters is defined as the average distance between all objects belonging to these clusters. These steps are repeated and the similarity matrix between clusters is updated until all clusters are linked together in a hierarchical tree.

The Pearson's correlation coefficient, denoted hereafter as R, is used as a similarity metric between catchments attributes; the higher the R between the target and the donor catchments, the more similar they are. Once the clusters are established, information can be transposed from donor(s) to receptor(s) catchment(s). In complex hydrological models this transfer of information is a difficult task due to the parameter uncertainty, to their interdependency, to the non-unique solution and to other various sources of uncertainty (Bárdossy, 2007). Some authors (Heuvelmans et al., 2004; McIntyre et al., 2005; Bárdossy 2007; Oudin et al., 2008; He et al., 2011) suggest transferring the entire parameter sets to the ungauged catchment(s).

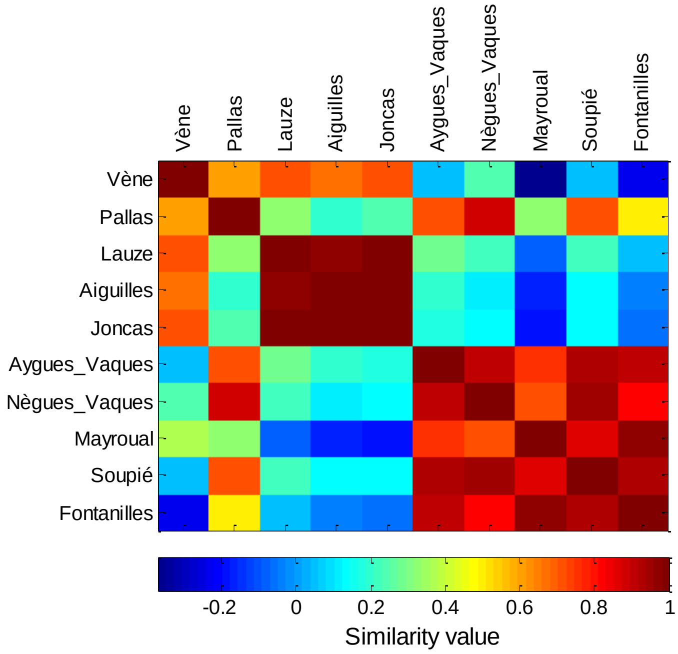

Figure 4-1: Matrix of similarity measure between all Thau subcatchments attributes

The traditional way of transferring the Mps from donor(s) to receptor(s) catchment(s) can also be based on the selection of the "behavioral" Mps obtained from simulations with likelihood values (e.g. NS) above certain user defined threshold value at the donor(s) catchment(s). However, in this way all the receptor(s) catchment(s) will receive equal number of Mps despite the fact that they are not equally similar to the donor(s) catchment(s). This may overestimate the prediction uncertainty at the closest receptor(s) catchment(s) and may underestimate it at catchments that are further from the donor(s) catchment(s). Furthermore, the selection of the "behavioral" Mps is often based on an arbitrary and entirely subjective choice of a threshold value which may add to the uncertainty of the final regionalization results.

New approach to select and propagate parameter uncertainty from gauged to ungauged catchments

In this section a new and more objective method for selecting the appropriate Mps to be transferred from the gauged to the ungauged catchment is proposed. First, the similarity measure ($R_{(d,r)}$) between gauged and ungauged catchment in their CAs dimension is calculated and clusters with similar catchments are constructed. Then, based on the GLUE results at the Vène and Pallas catchments, Mps sets that lead to positive NS values between observation and model simulation are retained. After that, based on the similarity measure and the maximum NS value derived by GLUE at each of the donor catchments (Vène and Pallas), a new threshold value, denoted hereafter *Thresh*, is calculated using Equation 4-1 that serves as a cutoff value to identify the candidates Mps to be transferred from the donor to the receptor catchment.

$$Thresh_{(d,r)} = R_{(d,r)} \times \max NS_d \qquad \text{Equation 4-1}$$

where $R_{(d,r)}$ is the similarity measure between the donor catchment *(d)* and the receptor catchment *(r)*, and NS_d is the highest likelihood value reached in the GLUE simulations at the donor catchment *(d)*.

By applying Equation 4-1 the number of the candidate Mps will increase linearly as the dissimilarity between the donor(s) and the receptor(s) catchment(s) increases. Furthermore, besides parameter uncertainty, additional uncertainty related to the regionalization schemes is explicitly accounted in the final model prediction at the ungauged catchment(s) by introducing the similarity measure in the above equation. As the dissimilarity between the donor(s) and the target catchment(s) increases, model prediction uncertainty in the target catchment(s) intuitively increases and vice versa. Another advantage of using this new method is that the selection of the threshold value to define the number of the candidate Mps is based on the similarity metric rather than on a subjective choice of the modeler which may reduce this additional uncertainty component in the final regionalization procedure. Finally, once the threshold value (*Thresh*) is calculated the entire selected Mps are transferred from the donor catchment(s) to the receptor(s) catchment(s) and discharge can be predicted within an uncertainty framework. Because updating manually the parameter values in the text SWAT file is a time consuming and tedious task, a sampling and rewriting program in the MATLAB® computing language is developed that samples and provides the Mps from the donor catchment to the receptor catchment in the SWAT model format and runs the model.

4.3.2 Evaluation criteria

The modelling performances and the uncertainty prediction assessment of the regionalization approach are conducted using the statistical criteria of NS, R^2 and *p_factor*. However, as no observation data is considered or available in the ungauged catchment, the *R_factor*, a measure of the uncertainty interval width, cannot be used. Therefore, for more efficient comparison the ARIL (Average Relative Interval Length) metric proposed by Jin et al., (2010) is modified here by normalizing the upper and lower boundary values (upper and lower 95% uncertainty limits) of a simulated discharge by its mean value. The modified ARIL is called, hereafter, the Average Standardized Relative Interval Length (*ASRIL*) and reflects the average width of uncertainty interval (95PPU).

$$ASRIL = \frac{1}{m}\sum_{t=1}^{m}\frac{Q_{t,97.5\%}^{M} - Q_{t,2.5\%}^{M}}{Mean(Q_t^M)} \qquad \text{Equation 4-2}$$

where $Q_{t,97.5\%}^{M}$ and $Q_{t,2.5\%}^{M}$ represent the upper and lower simulated boundary, respectively, at time *t* of the 95PPU, *m* is the length of simulations, the subscript *M* refers to simulated, *t* refers to the simulation time step. A smaller value of *ASRIL* indicates a thin uncertainty interval. If there is no uncertainty than the value of *ASRIL* is zero. To assess the relative performances of the regionalization procedure for flow estimation in ungauged catchments, usually the simulated flow is compared to the observed one and/or sometimes gauged catchments are considered in turn as if they are ungauged (Oudin et al., 2008). In the Thau catchment, catchments have very scarce streamflow records. Therefore, any available observation data, field knowledge and/or previous work conducted in the area of interest can be precious and helpful to check the performance of the adopted regionalization method. Performance assessment of the regionalization procedure is based on three evaluation criteria. The first one namely fit to observation (van Griensven et al., 2012) and consists of the quantitative assessment of model accuracy simulations compared to measurements using some statistical criteria. In this regard, the simulated FDCs flow percentiles are compared to the observed ones by using the NS coefficient and the model prediction uncertainty is assessed through the *p-factor* wherever observation data are available. The second one is called fit to reality (van Griensven et al., 2012) and consists of the evaluation of the model capability in reproducing the real hydrological process and in reflecting the reality of the field. For instance, the predicted mass balance can be calculated and used to assess the performance of the regionalization procedure in representing the main hydrological processes that govern the hydrology of the study system. The third evaluation criterion is called fit to geography and it consists of mapping the predicted variable in order to check the soundness of its spatial distribution with some observed data such as soil moisture maps.

4.4 Results and discussions

4.4.1 Catchments clustering

The similarity metric based on the multidimensional space of CAs resulted into 4 ungauged catchments similar to the Vène catchment (Lauze, Aiguilles, Joncas and Mayroual) and 4 ungauged catchments similar to the Pallas catchment (Fontanilles, Aiguilles, Nègues_Vacques and Soupié). Catchments within the same group are assumed to have similar hydrological behavior. The catchments clusters and the numbers of the candidate Mps transferred from the donor to the receptor catchments, calculated using the similarity measure, are given in Table 4-1.

Table 4-1: Results of catchments clustering and number of Mps transferred from the donor to the receptor catchment based on the similarity measure

Donor catchment	Receptor catchment	Similarity	Threshold (*Thresh*)	% of Mps
Vène	Joncas	0.71	0.50	44.10
	Lauze	0.70	0.49	46.95
	Aiguilles	0.66	0.46	54.62
	Mayroual	0.36	0.25	89.18
Pallas	Nègues_Vacques	0.88	0.66	16.60
	Aygues_Vacques	0.71	0.54	85.16
	Soupié	0.70	0.53	86.47
	Fontanilles	0.50	0.38	96.52

The Vène and the Pallas catchments are identified as the donor catchments while all the other ungauged catchments are considered as receptor catchments. The highest threshold value (*Thresh*) calculated is *Thresh* = 0.50 and 0.66 for the Vène and the Pallas catchments, respectively. These *Thresh* values are frequently used in literature to identify "behavioral" Mps (Gassman et al., 2007, Shen et al., 2012). The lowest *Thresh* values range between 0.25 and 0.38 corresponding to a transfer of 89.18% and of 96.52% of the total Mps sets of the Vène and the Pallas catchments, respectively (Table 4-1). These *Thresh* values correspond to poor model performances at the gauged catchments and can be seen as low compared to what has been usually used in literature. However, as it was reported by Oudin et al., (2008), it is not straightforward to state whether or not poorly modeled gauged catchment(s) parameters should be transferred to ungauged catchment(s). From one side, it is expected that Mps associated with poorly modeled hydrographs in gauged catchment(s) will yield poor model performances at the ungauged catchment(s). On the other side, transfer of Mps of poorly modeled gauged catchment(s) may add a diversity which can be beneficial for modelling the ungauged catchment (Oudin et al., 2008).

4.4.2 Predicted Flow Duration Curves (FDCs) at the Thau ungauged catchments

The results of the predicted discharge at the Thau ungauged catchments based on the regionalization approach are presented as FDCs since the latter display the complete range of river discharges, from low flows to flood events. The simulated FDCs resulting from the transfer of the GLUE Mps sets of the Pallas and the Vène catchment to the ungauged catchments, within their corresponding group, are plotted in Figure 4-2. The slope of the simulated FDCs within the high flow percentiles is relatively steep for the two catchments groups indicating that flood discharges are not sustained for a long period of time. The slope of the end tail of the simulated FDCs, corresponding to low flow, is steeper in the Pallas catchment group, while it is flattened out considerably in the Vène catchments group. This reflects the difference in the low flow regime between the two catchments groups. Catchments of the Pallas group cease flowing at 20% to 40% of the simulation time period, while catchments of the Vène group have more sustained baseflow contribution.

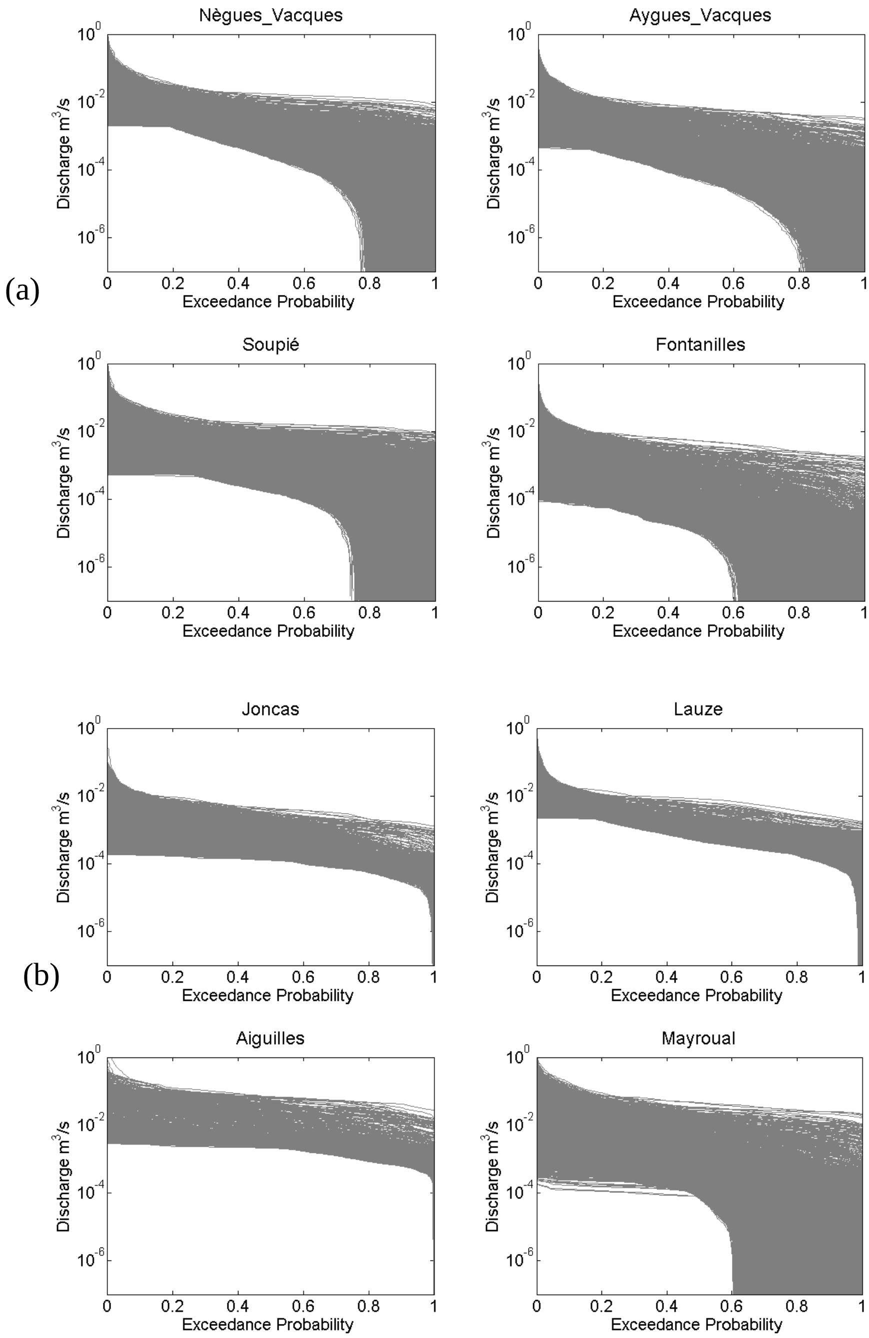

Figure 4-2: Simulated uncertain FDCs for the ungauged catchments of the Pallas group (a) and Vène group (b) based on model parameters regionalization

Figure 4-3 shows the coefficient of variation (CV= Standard deviation/Mean) and the mean magnitude of the simulated FDCs flow percentiles for all the catchments and quantify their inter- and intra-catchments groups variability.

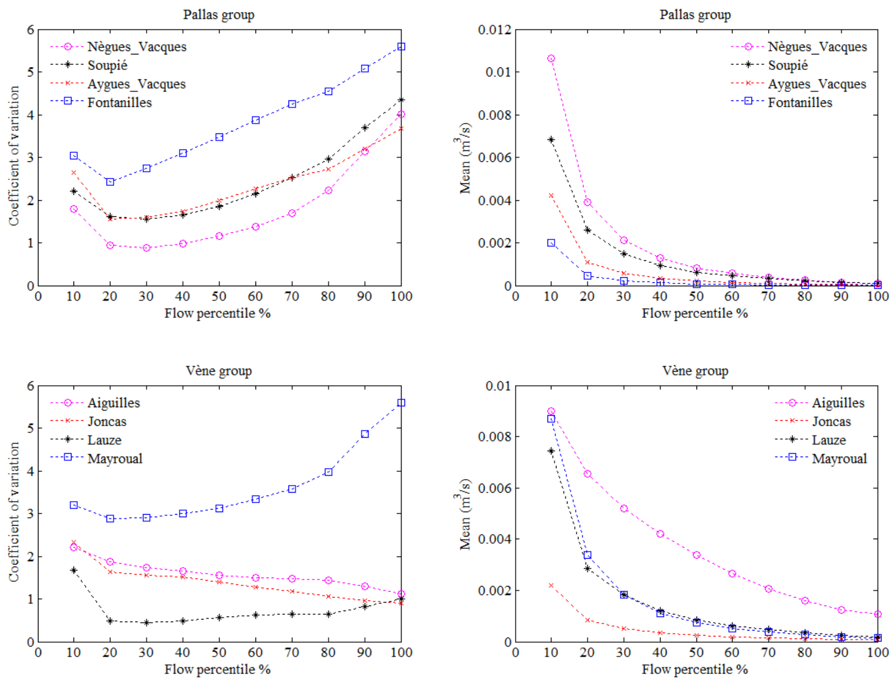

Figure 4-3: Mean and coefficient of variation of the predicted FDCs percentiles based on the physical similarity approach for the Pallas and Vène catchments groups

It is clearly seen from Figure 4-3 that the CV of the mean for all the FDCs flow percentiles within the Pallas catchments group is higher at low flows than at high flows. However, for the Vène catchments group, the CV is more or less steady across the flow percentiles, except for the Mayroual catchment. The intra-catchments variability of the CV of the flow percentiles within each catchment group shows that catchments within each group converge to a similar low flow CV value, except for the FDCs of the Fontanilles within the Pallas group and the Mayroual within the Vène group. It is worth noting here, that these catchments exhibit the largest dissimilarity in their physical attributes form their corresponding donor catchments. It is also clear in the same figure that the simulated mean flow magnitude of the different flow percentiles is very low in both catchments group. The mean values of the high flow percentiles in both catchments group do not exceed $0.015m^3.s^{-1}$. However, the variation in the mean values of the simulated FDCs is more important in high flow percentiles than in low flow percentiles in both catchment groups. In the Pallas catchment group, the mean flow magnitude decreases rapidly from Q10 to Q20, then progressively from Q20 to Q50 leading to progressive increase in the CV within these flow percentiles and tends to be steady for flow percentile higher than Q50, which results in higher CV values. In addition, at low flow percentiles (> Q70), all the simulated FDCs of the Pallas catchment group tend to have similar mean flow values which resulted in less variability of the CV at the low flow percentiles. Also, catchments within the Vène group have much more variability in their simulated flow percentiles mean values than these of the Pallas group. The flow percentiles of the simulated FDCs of the Aiguilles catchment have the highest mean values while the Mayroual and Lauze FDCs flow percentiles are very similar and these of the Joncas catchment are the lowest values.

4.4.3 Uncertainty in the Predicted Flow Duration Curves (FDCs) at the Thau ungauged catchments

The uncertain simulated FDCs are represented in Figure 4-2 in such a way that dissimilarity between the donor and the receptor catchment, within each catchments group, increases from the left to the right and from top to down. It is clearly seen form Figure 4-2 that the FDCs uncertainty interval in both catchments groups is wider as the receptor catchment is further from the donor catchment in the CAs space. This is also confirmed by the relationship that exists between the number of Mps transferred from the donor to the receptor catchments and the *ASRIL* factor plotted in Figure 4-4. While the average FDCs uncertainty width (*ASRIL*) in both catchments groups tends to increase as the dissimilarity between the donor and the receptor catchments increases, catchments of the Pallas group show wider uncertainty interval than these of the Vène group. Another observation that can be made from Figure 4-2 and Figure 4-4 is that catchments that are very similar to each other have similar uncertain FDCs shape and very close *ASRIL* factor values (Table 4-2). This is the case for the Joncas and Lauze catchments in the Vène group and for the Nègues_Vacques and Aygues_Vacques catchments in the Pallas group.

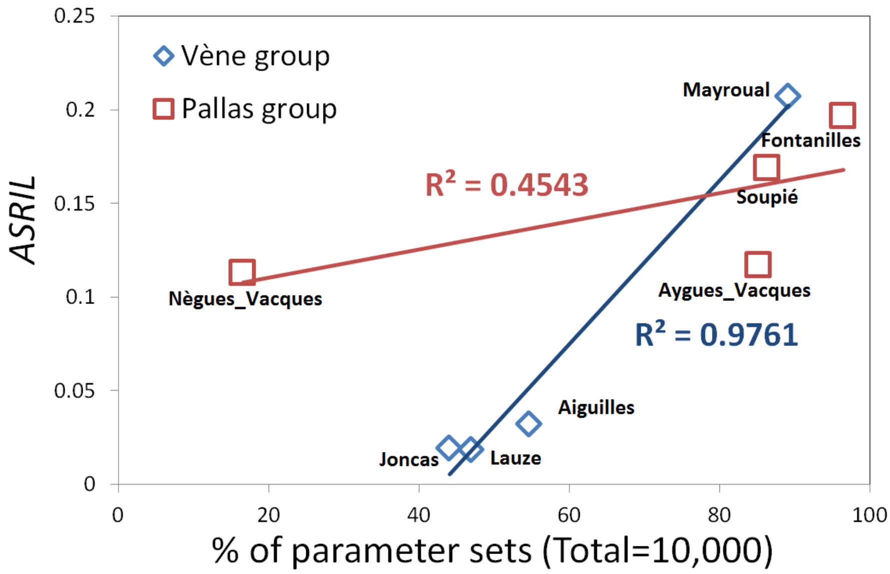

Figure 4-4: Relationship between the number of transferred model parameter sets and the *ASRIL* factor at the ungauged catchments.

These results suggest that high similarity between CAs may lead to similar hydrological responses and model prediction uncertainties of catchments that are under the same climatic and geographic region. However, this assumption is far to be validated in this work and needs to be further investigated and checked in future work with larger number of similar catchments or by simply gauging the catchments.

In order to check the consistency of the developed methodology attempts are conducted to investigate if relationships between parameter uncertainty of the donor catchment and the predicted uncertainty of the FDCs in the receptor catchments exist. This has been done through the calculation of the coefficient of variation (CV) of the transferred Mps within each ungauged catchment. The CV can be used as a dimensionless measure of parameter uncertainty (Bastola et al., 2008). The variability of the CV of Mps transferred to the ungauged catchments within each catchment group is given in Figure 4-5. Results show that the CV of Mps varies between the catchments depending on the parameter itself and on the similarity distance between the receptor and the donor catchments.

Table 4-2: Measure of the *ASRIL* factor of the predicted FDCs uncertainty intervals in the ungauged catchments

Ungauged catchment	Donor catchment	
	Vène	Pallas
Lauze	0.018	-----
Aiguilles	0.031	-----
Joncas	0.019	-----
Mayroual	0.207	-----
Fontanilles	-----	0.196
Aygues_Vacques	-----	0.117
Nègues_Vacques	-----	0.113
Soupié	-----	0.169

In the Pallas catchment group, the CN2 and the SURLAG parameters show a clear variability in their corresponding CV values across the catchments. It is obvious that uncertainty in CN2 and SURLAG parameters increases from the closest (Nègues-Vacques) to the furthest ungauged catchment (Fontanilles) from their respective donor catchment (Figure 4-5a). Moreover, the variability trend of the CV of the CN2 parameter follows closely the trend of the *ASRIL* factor across the catchments, with a determination coefficient of R^2= 0.66 while the CV of the SURLAG parameter is less correlated to the *ASRIL* factor (R^2= 0.40). In the Vène catchment group, 3 out of 10 transferred parameters show variable CV values across the catchments. These parameters are CN2, GW_DELAY and ALPHA_BF (Figure 4-5b). While all the other remaining parameters show a constant CV at its maximum value across all the catchments, uncertainty in CN2, GW_DELAY and ALPHA_BF parameters increases progressively from the closest similar ungauged catchment (Joncas) to the furthest one, but in different trends. The variability of the CV of CN2 is better correlated to the *ASRIL* factor (R^2= 0.83) than these of the GW_DELAY and ALPHA_BF (R^2= 0.545 and 0. 540, respectively). These results suggest that relationships exist between the transferred parameter uncertainty and the predicted uncertainty width of the FDCs and between the CAs similarity distance and the predicted uncertainty in the ungauged catchment.

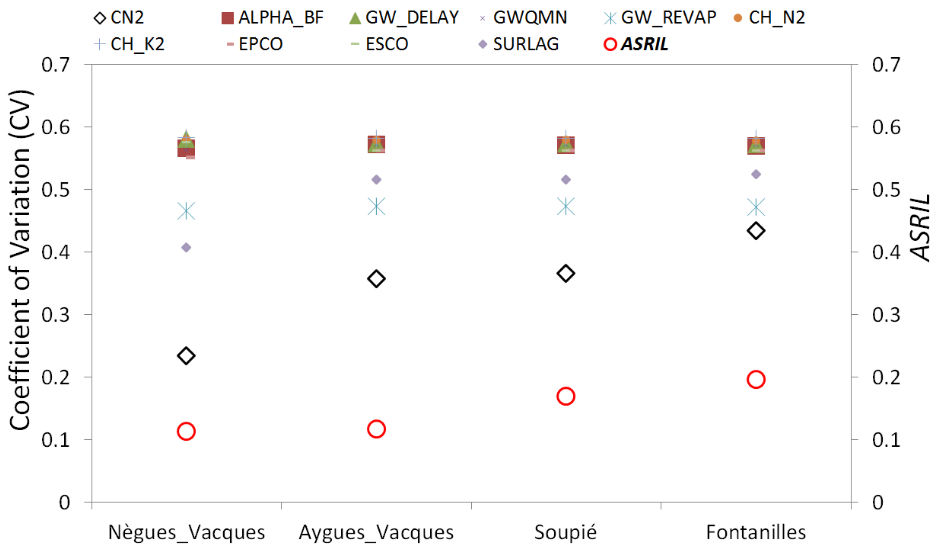

(a) Pallas catchments group

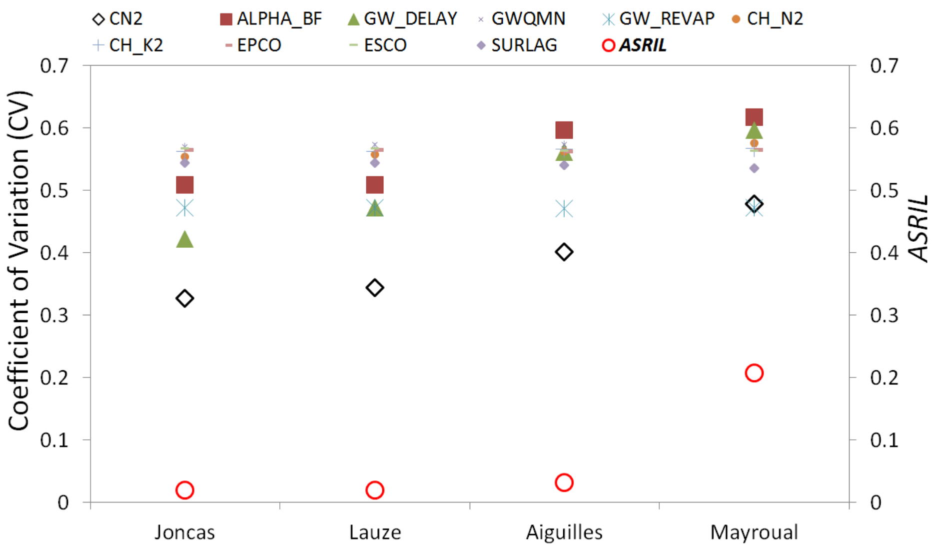

(b) Vène catchments group

Figure 4-5: Relationship between the CV variability of the transferred model parameter from gauged to the ungauged catchments and the *ASRIL* factor within each catchments group

The results are consistent with the proposed methodology in this work which is based on the principle that model prediction uncertainty intuitively increases as the dissimilarity in CAs between the donor and the receptor catchments increases. However, these results need to be interpreted with care and precaution. Indeed, the CV is calculated for each model parameter individually without taking simultaneously into account the uncertainty and the interactions between the other parameters while it is the whole parameter set that was transferred in the regionalization schemes. By relating the parameter CV to the model prediction uncertainty in ungauged catchment, it is assumed that linear relationship exists between parameter uncertainty and model prediction uncertainty at the ungauged catchments. However, this linearity is difficult to check and to establish because of the possible interdependency of the parameters, non-linearity and non-monotonicity of the hydrological model and other various sources of uncertainty (uncertainty in input and model structure). Moreover, model parameters that have steady CV across the ungauged catchments may contribute to model prediction uncertainty when they are transferred in a set of parameters. Therefore, the CV of individual parameter may not reflect its real uncertainty. In addition to Mps, input and model structure uncertainty, regionalization procedures are known to have additional uncertainty on model prediction in ungauged catchments (Wagener et al., 2004; Heuvelmans et al., 2006; Bastola et al., 2008). In the proposed methodology it is assumed that uncertainty that stems from the regionalization schemes is propagated to model prediction in the ungauged catchment through the integration of the similarity measure in defining the Mps sets to be transferred from the donor to the receptor catchments. However, partitioning each uncertainty source and telling to which extent it can affect the model prediction is a very difficult task to perform.

4.4.4 Performance evaluation of the regionalization approach

Fit to observation

The 95% uncertainty interval and the median of each flow percentile values of the observed and the simulated FDCs for the ungauged catchments, where observed data are available, are constructed and plotted in Figure 4-6.

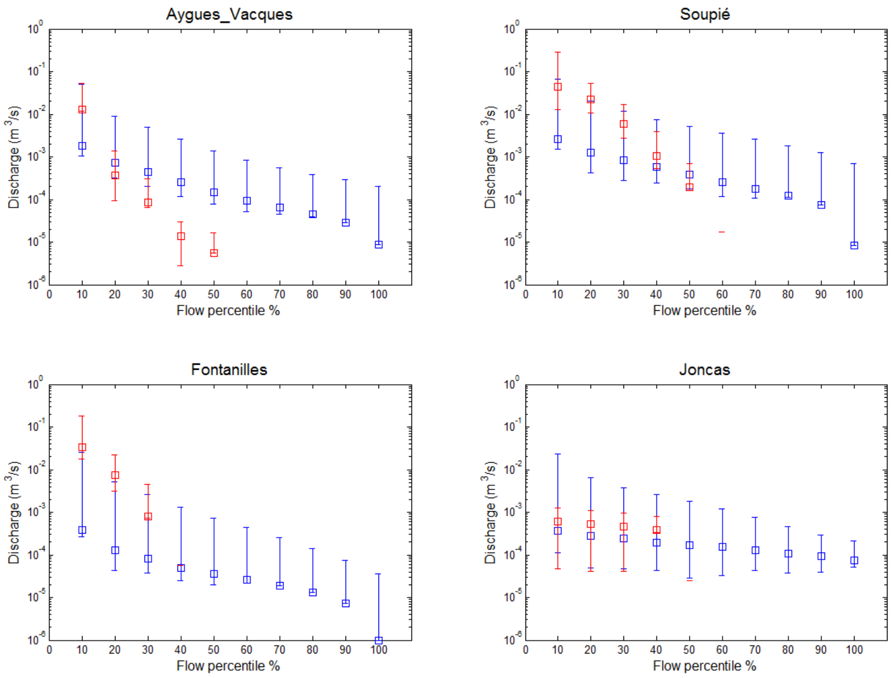

Figure 4-6: 95% uncertainty interval of the simulated FDCs flow percentiles versus 95% of the observed FDCs flow percentiles resulting from the model parameters regionalization approach. Results correspond to the transfer of the Pallas model parameter sets to the Aygues_Vacques, Soupié and Fontanilles catchments and transfer of the Vène model parameters sets to the Joncas catchments. The blue color is for simulation and the red color is for observation. The bar corresponds to the 95% flow percentile value while the square corresponds to the flow percentile median value.

Only 4 ungauged catchments have some observed data that can be used to compare the results of the regionalization approach. According to the observed FDCs, ungauged catchments cease flowing at 50 to 60 % of the time while the predicted FDCs indicate that ungauged catchments flow for longer period between 60 and 100% of the simulation time period reflecting the ephemeral hydrological behavior of the catchments (Figure 4-6).

Table 4-3: Statistical criteria of the regionalization approach results

Catchment	Aygues_Vacques	Soupié	Fontanilles	Joncas
NS	0.169	-0.131	-0.144	0.518
P_factor (%)	18	65	73	87

The calculated NS coefficient between the observed and the simulated median flow percentiles and the average *p-factor* values, corresponding to the average percentage of the observed flow percentile values bracketed in the predicted uncertainty flow percentile interval, are summarized in Table 4-3. Given the observation data available, the NS coefficient values are negative for the Soupié and Fontanilles catchments (NS = -0.131 and -0.144, respectively), indicating that the observed median values of the different flow percentiles are poorly reproduced by the model in these ungauged catchments. On the other hand, positive NS values of 0.169 and 0.518 are obtained in the Aygues_Vacques and in the Joncas catchments, respectively, showing better model prediction of the flow percentiles median values. While the simulated flow percentiles uncertainty intervals are able to bracket most of the observation data there is a clear tendency of the *p-factor* increase with the decrease of the distance between the donor and the receptor catchment. As it was demonstrated previously, the average relative width of the uncertainty interval (*ASRIL*) increases as the dissimilarity between the donor and the receptor catchments increases. Therefore, more observation data are bracketed in the flow percentile uncertainty interval of the ungauged catchments that are located far from the donor catchment.

Fit to reality

The annual mass balance is calculated based on the average annual values of the different hydrological components that are computed by the SWAT model according to the following equation:

$$WYLD = Surf\_Q + Lat\_Q + GW\_Q - TLosses \qquad \text{Equation 4-3}$$

where WYLD is the net water yield to reach (mm), Surf_Q is the surface runoff (mm), Lat_Q is the lateral flow contribution to reach (mm), GW_Q is the groundwater discharge into the reach (mm) and T Losses is the amount of water removed from the tributary channel by transmission (mm).

The average annual water budget, its components and their corresponding uncertainty (calculated as the standard deviation) for each ungauged catchment are plotted in Figure 4-7. The results of the regionalization approach suggest that surface runoff is the major component of the water budget (65% in average) followed by the lateral flow (22.7% in average) and by the groundwater flow (12.3% in average). However, all the hydrological balance components are estimated with large uncertainty. For instance, about 65% of the WYLD uncertainty is attributed to the uncertainty of the estimated surface runoff (Surf_Q). In fact, in the SWAT model, Surf_Q is estimated using the modified Soil Conservation Service (SCS, 1972) curve number (CN) method which depends on the soil moisture and land cover. Therefore, any uncertainty in the soil and land cover is translated to the associated curve number and affects the predicted Surf_Q. Moreover, in SWAT the runoff coefficient is calculated as the ratio of runoff volume to rainfall. Therefore, uncertainty of the latter can affect the predicted peak flow which in turn affects the predicted Surf_Q.

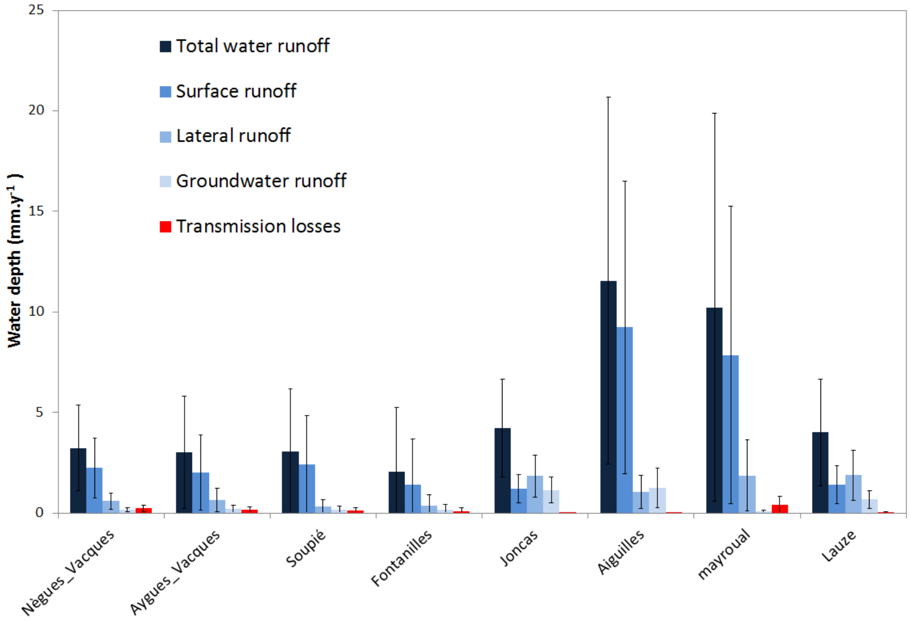

Figure 4-7: Average annual water balance simulated at the ungauged catchments based on the regionalization approach. The error bars represent the standard deviation calculated based on all model simulations

The groundwater component (GW_Q) has more important average contribution rate to the total water budget in the Vène catchments group (Joncas, Lauze, Aiguilles and Mayroual) with an average of 11.71%, than in the Pallas catchments group (Nègues_Vacques, Aygues_Vacques, Soupié and Fontanilles), with an average of 6.47%.

In addition, groundwater contribution (GW_Q) to the streamflow within the Pallas catchments group is intermittent, while it seems more sustained, but also more uncertain, within the Vène catchments group (Figure 4-7). Because of the different sources of uncertainty (e.g. precipitation, evapotranspiration, uncertainty in groundwater parameters) and the rainfall seasonal variability, the groundwater volume and its level of fluctuation are estimated with uncertainty that is translated into an uncertain GW_Q. These results suggest that streamflow in the Vène catchments group (corresponding more or less to the eastern part of the Thau catchment) is more influenced by the groundwater flow contribution than in the Pallas catchments group (corresponding to the central and western part of the Thau catchment). However, the validation of this result is not straightforward since no information or data on groundwater are available in the study area and more hydrogeological measurements are required to check the results and to reduce the groundwater discharge uncertainty.

About 2.5% of the total water budget is lost via leaching through the stream bed (TLosses). This type of losses is more important in the Pallas catchments group (5.3%), than in the Vène catchment group (1.37%). Transmission losses become more important when GW_Q decreases and vice versa. Because the SWAT model creates more sustained shallow aquifer with larger water storage in the eastern part than in the western part of the Thau catchment, the Vène catchments group are gaining much more water through baseflow (GW_Q + Lat_Q) leading to smaller losses of water through channel transmission.

Based on the Mps regionalization results at the ungauged catchments and the model calibration results at the donor (Vène and Pallas) catchments, it is possible to estimate the different flow components for the entire Thau catchment. Figure 4-8 shows the estimated average annual flow components as well as their associated uncertainty as predicted by the SWAT model for the total Thau catchment. It is clear that total runoff is mainly originating from surface runoff (63%) followed by groundwater flow (26%) and lateral flow (9%). About 2% of the annual water volume is wasted via transmission losses. The Vène and the Pallas catchments are the main contributors to the total runoff in the Thau catchment. Together, they account for more than 80% while the other small subcatchments have negligible contribution less than 1/5 of the water volume of the Thau.

It should be noted here that this is the first time that the total water volume as well as each subcatchments contribution in the Thau catchment are estimated.

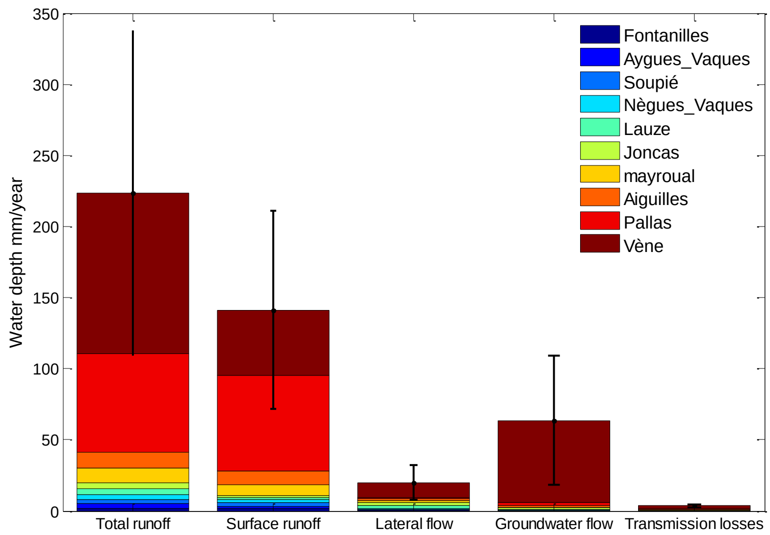

Figure 4-8: Average annual water balance simulated at the entire Thau catchment based on the regionalization approach. The error bars represent the standard deviation calculated based on all model simulations

Fit to geography

This criterion is used here to assess the performances of the regionalization procedure in reproducing the actual spatial distribution of the soil moisture in the Thau catchment. Baghdadi et al. (2012) proposed a method to estimate the volumetric soil moisture from RADARSAT-2 image (space Synthetic Aperture Radar «SAR» sensor) for bare agricultural fields or fields with thin vegetation cover over the Thau basin for ten dates between November 2010 and March 2011. Their estimated soil moisture values showed a good agreement with the measured in situ soil moisture with a RMSE = 0.065 cm^3/cm^3 (see Baghdadi et al., 2012 for details). These estimated soil moisture maps, referred hereafter as "observed" soil moisture (Figure 4-9), are compared to the soil moisture derived from the regionalization results which are referred hereafter as predicted soil moisture (Figure 4-10). Since the "observed" soil moisture maps are available only for three different dates (November 18, December 4 and 12, 2010) within the model simulation period, the comparison between the "observed" and the predicted soil moistures is restricted to these 3 dates.

The SWAT predicted soil moisture is spatially correlated to the "observed" one but with different degree of satisfaction. The latter can be broadly and arbitrary set to good, satisfactory and poor based on the graphical comparison of Figure 4-9 and Figure 4-10. The spatial correlation between the distribution of the predicted and the "observed" soil moisture can be considered as good for the Vène, Aiguilles and Fontanilles catchments, as satisfactory for the Joncas, Lauze, Pallas and Soupié and as poor for the Aygues_Vacques, Mayroual and Nègues_Vacques catchments. Overall, the predicted soil moisture has an acceptable spatial distribution with the "observed" one which is more clear in the eastern part (corresponding to the Vène catchments group) than in the western part (corresponding to the Pallas catchments group) of the Thau catchment.

Table 4-4: Statistical criteria of the 95% confidence "observed" and predicted soil moisture values (cm^3/cm^3) on the three dates of 2010 at the Thau catchment

	"Observed"			Predicted		
Date	11/18	12/04	12/12	11/18	12/04	12/12
Prec.*	2.2	0.6	0	2.2	0.6	0
Min	0.08	0.10	0.03	0.08	0.04	0.01
Max	0.27	0.26	0.19	0.33	0.30	0.28
Median	0.167	0.162	0.07	0.142	0.102	0.07
Mean	0.169	0.166	0.08	0.167	0.127	0.09

*Note: Prec. is the cumulative precipitation in (mm) from the 3 previous days to the selected date.

The predicted soil moisture values on the three different dates at the Thau catchment are also compared to the "observed" ones. Table 4-4 presents some statistical characteristics of the 95% "observed" and predicted soil moisture values on the three selected dates. The predicted soil moisture values ranges are slightly larger than the "observed" ones. The variability of the predicted soil moisture on a given day is larger as this day is preceded by wet days. Nevertheless, the median and the mean of the "observed" and predicted soil moisture values are in a good agreement.

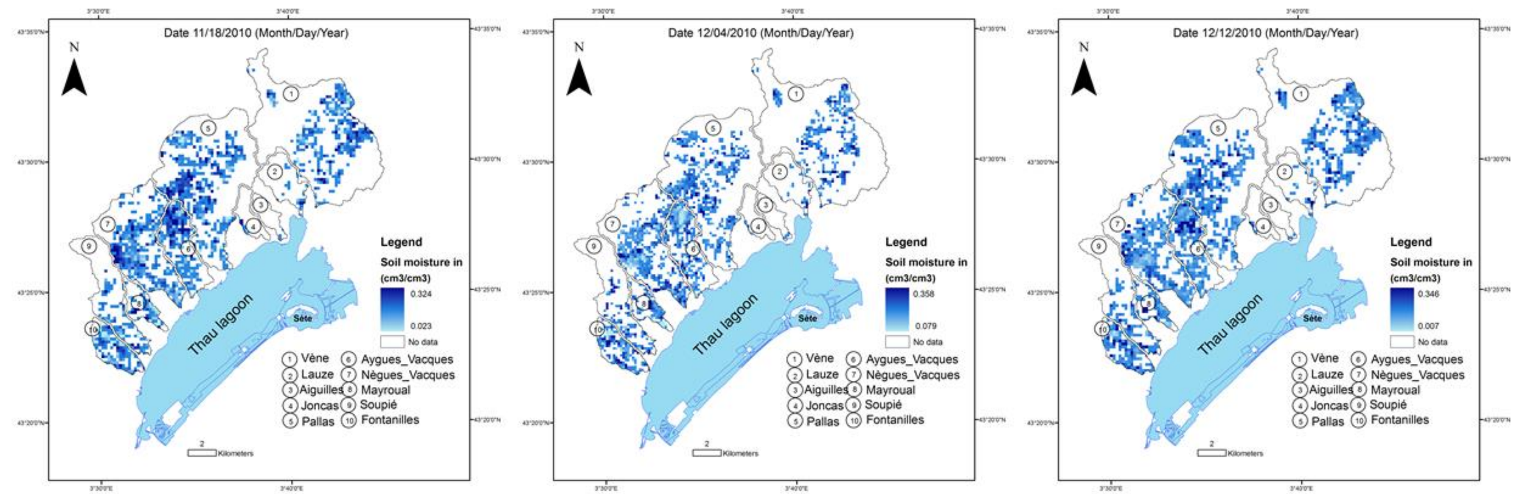

Figure 4-9: Distribution of the "observed" soil moisture within the Thau catchment for 3 different dates (based on: Baghdadi et al., 2012)

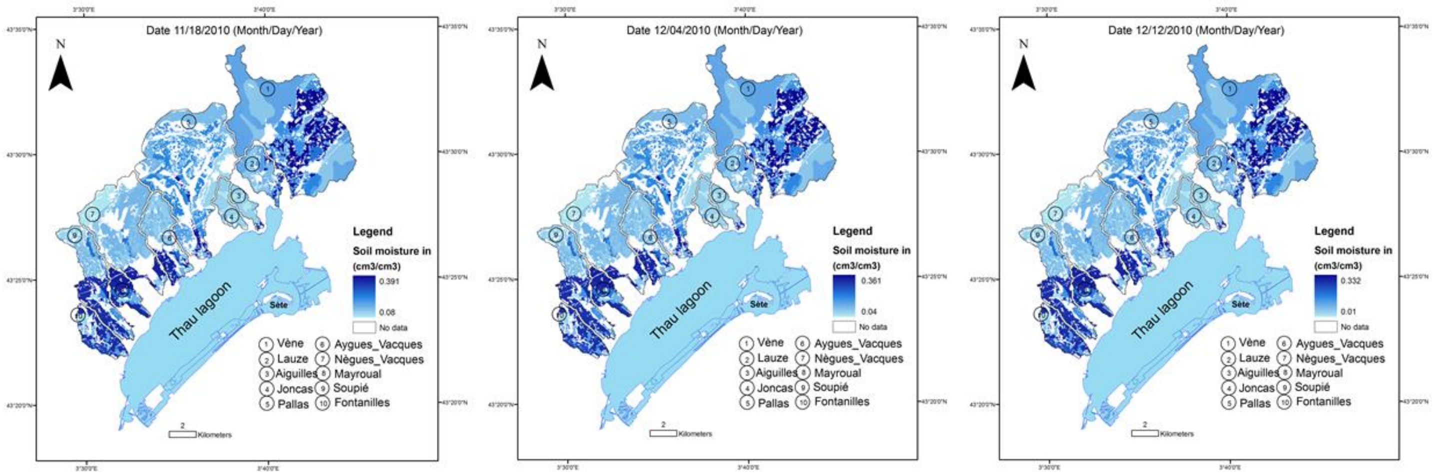

Figure 4-10: Distribution of the predicted soil moisture within the Thau catchment for 3 different dates as based on the regionalization results

However, the comparison of the "observed" and predicted soil moisture values is not straightforward since the model is predicting the soil moisture at the HRU scale for soils with different vegetation type cover, while the "observed" soil moisture values are made up for bare soils or soils with thin vegetation cover. In addition, "observed" soil moisture values are made up for the top 5 to 10 cm of the soil profile whereas the predicted ones might be estimating by SWAT for the entire soil layer that can be much more than 10 cm depth.

4.4.5 Model parameter regionalization and discharge estimation for the Chiba catchment

Given, the model performances and prediction uncertainty discussed in the previous Chapter, the "behavioral" Mps are assumed to represent satisfactory the real hydrological processes of the Chiba upstream part. In the absence of discharge gauge station within the Chiba catchment, the identified "behavioral" Mps are transferred from the upstream to the downstream (corresponding to catchment area from the dam outlet to the main catchment outlet) part of the catchment (Figure 4-11). It is assumed that by transferring the entire parameter set the hydrological processes are considered at once and that transferring all the "behavioral" Mps the uncertainty and interdependency of the parameters are conserved within the structure of the Mps.

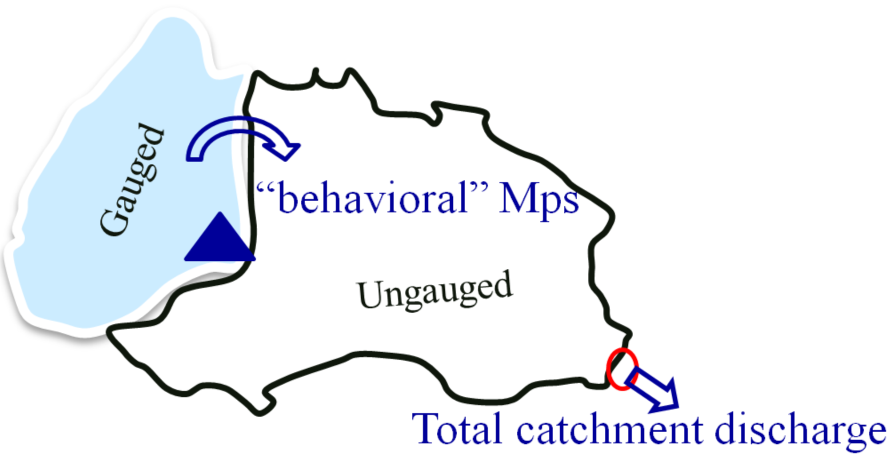

Figure 4-11: Schematic illustration of the Mps regionalization method applied to the Chiba catchment (scale is not respected)

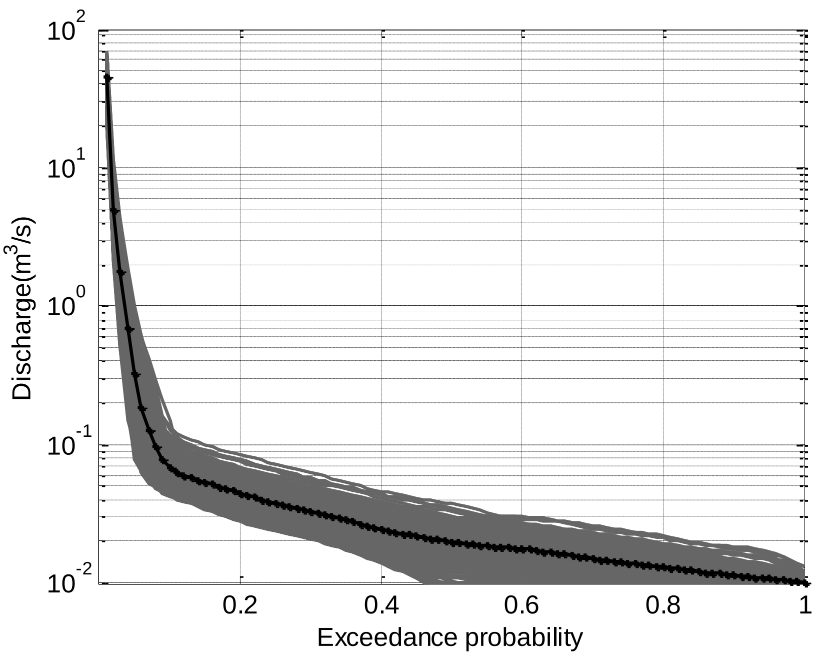

Figure 4-12: Predicted uncertain FDCs at the Chiba catchment outlet based on the results of the Mps regionalization. The black line with the black dots refers to the mean FDC

Similarly to the Thau catchment, the regionalization results and the predicted discharge at the Chiba catchment outlet are presented in terms of FDCs in Figure 4-12**.** The predicted FDCs of the "behavioral" model runs at the entire catchment outlet are steeper and affected with higher variability than those at the upstream catchment. They (FDCs at the entire catchment outlet) also suggest more extensive zero flow period which can reach 50% of the simulation time period. The results suggest that the Chiba streamflow occurs as a direct response to rainfall with a small or without groundwater contribution. Discharge flow values at the catchment outlet reach almost two times the predicted ones at the upstream catchment despite the same model parameter sets. This difference can be explained by the difference in the physical attributes between the upstream and downstream parts of the Chiba catchment rather than by the model parameter. The fact that the downstream catchment has less forest cover, larger drainage area and more urbanized lands than the upstream catchment, the predicted flow magnitudes are expected to be higher.

The predictions of high flows are associated with larger uncertainty than in low flows. As it was previously mentioned, the inter-annual variability of rainfall can play an important role in the uncertainty associated with high flows.

Performances of the regionalization approach for the Chiba catchment

Unfortunately, there are no observed hydrological available data to assess the performances of the regionalization approach on the Chiba catchment. Nevertheless, the different flow processes within the catchment modeled by the SWAT model are analyzed and investigated hereafter.

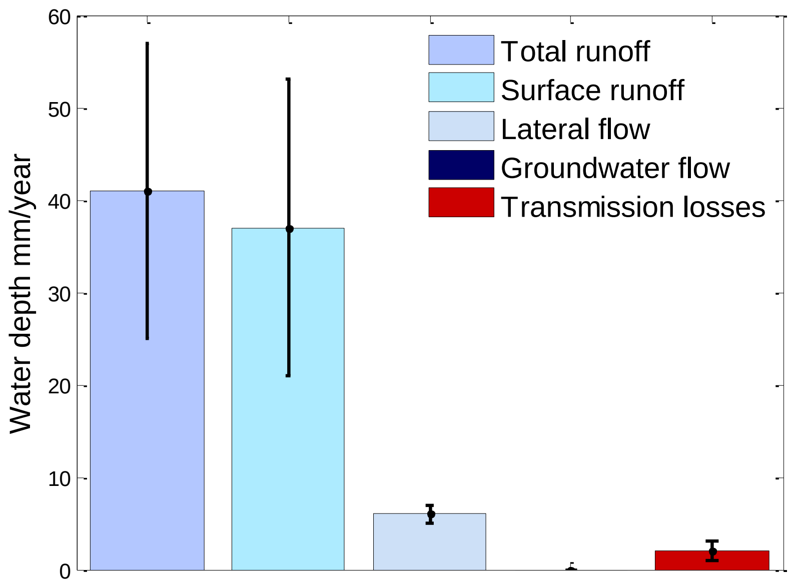

Figure 4-13: Average annual water balance simulated at the entire Chiba catchment based on the regionalization approach. The error bars represent the standard deviation calculated based on all model simulations

It is evident from Figure 4-13 that the flow processes in the Chiba catchment are dominated by surface runoff which contributes to more than 90% to the total water runoff of the catchment. However, surface runoff prediction is affected with the largest uncertainty in comparison to the others flow components. This uncertainty can be explained by the errors associated with the surface runoff model parameters such as

CN2, SOL_AWC and ESCO. In fact, in the SWAT model surface runoff is estimated using the curve number (CN) method which depends on the soil moisture condition and land use. Therefore, any uncertainty in the soil and land use data or parameterization is translated to the associated curve number and affects the predicted flow component. Furthermore, in SWAT the runoff coefficient is calculated as the ratio of runoff volume to rainfall. The latter, being uncertain, can add uncertainty to the prediction results. However, due to the non-linearity and non-monotonicity of the SWAT model, other parameters (soil and/or groundwater parameters) can interact in a non-linear way with surface runoff parameters and, thus, can contribute to the predicted uncertainty. Lateral flow has an average contribution to the total water yield around 16%. There is no contribution of groundwater to the catchment runoff as predicted by the SWAT model. This can be explained by the weak water depth stored in the shallow aquifer that cannot reach the threshold value to be released to the stream as groundwater flow. It is worth noting here that the shallow aquifer in SWAT works like a reservoir located somewhere below the soil profile but not referenced to any datum or distance from the soil surface. Thus, the thickness of the shallow aquifer built by SWAT in terms of depth of water stored does not correspond to the field groundwater table depth. Therefore, SWAT may suggest a deeper shallow aquifer than the actual one which may lead to an under-prediction of the groundwater flow. Consequently, the weak simulated groundwater flow in the Chiba catchment should be carefully considered since its related parameters are suggested without any knowledge about the actual subsurface aquifer properties and groundwater movement in the catchment.

The final flow component considered in the SWAT water balance is the transmission losses. Many catchments especially in semiarid areas have alluvial channels that abstract large volume of water when the flood wave is traveling downstream. For instance, in a river bed that has been dry for long period, the transmission losses following an event of rainfall is expected to be initially high and decreases progressively. These losses in SWAT are function of the geometry and geomorphologic characteristics of the channel (width, length, CH_K2, Manning's coefficient, etc.). For example, for catchments where the groundwater level is beyond the river bed, there shouldn't be a waste of water via channel transmission and, thus, the value of the CH_K2 should be equal to zero (van Griensven et al., 2012). This parameter should not be too high in humid catchments. Unexpectedly, the annual average water volume abstracted via transmission losses in the Chiba catchment as predicted by the SWAT model is low and does not exceed 8% of the total water volume. This can be due to the low value assigned to the CH_K2 parameter. Therefore, the volume of water lost via channel transmission is under-predicted or may not realistic.

4.5 Conclusions

The need for estimating discharge for the entire Thau and Chiba catchments has led to the development of a new regionalization approach where discharge at the ungauged catchments is predicted within an uncertainty framework. Similarity measure between catchments attributes was adopted to identify similar catchments clusters. Within each cluster, the degree of similarity between the donor and the receptor catchment was used as a threshold to select the appropriate transferrable model parameter sets.

Results showed that within the same catchments cluster, ungauged catchments can exhibit similar hydrologic behavior if they exhibit high degree of similarity in their physical attributes and have received similar model parameter sets.

The performance of the regionalization method at the ungauged catchments was assessed through statistical and field reality criteria. The predicted water balance revealed the prevailing of the surface runoff component in the hydrology of the Thau and Chiba catchments. The findings suggest that the SWAT model parameters can be regionalized to predict discharge at ungauged catchments and the results can fit the reality of the study case. However, thorough evaluation and criticism of model performances is constrained by the availability of the observation data at the ungauged catchments. Therefore, other evaluation criteria such as fit to reality and fit to geography can be used to describe the model performances in these ungauged catchments.

It was also shown in this chapter how parameter uncertainty can affect model prediction uncertainty at ungauged catchment through the regionalization of the model parameters. The assumptions behind the developed methodology were that physically similar catchments are hydrologically similar and model prediction uncertainty increases as the dissimilarity between the donor and the receptor catchment increases. The developed methodology allows propagating model parameter uncertainty proportionally to the degree of similarity between catchments attributes. Furthermore, it makes the selection of the donor catchment parameter sets more objective than the traditional approach which is based on modeler subjective choice.

It was shown that model prediction uncertainty was influenced by the similarity distance between the donor and the receptor catchment. Wider prediction uncertainty is obtained as the dissimilarity between the donor and the receptor catchment increases. In addition, the findings showed that the selected threshold values and, hence, the number and the uncertainty of the parameters transferred can affect the prediction uncertainty at the ungauged catchment. If a higher degree of similarity exists between the donor and the receptor catchments then a higher threshold value is selected. Consequently, a lower parameters uncertainty is propagated to the ungauged catchment leading to lower prediction uncertainty in the ungauged catchment. Otherwise, a lower threshold value is selected and a wider uncertain parameter sets are transferred which will yield a larger uncertain model prediction at the target catchment. However, it is not pretended with these results that uncertainty in the transferred parameter sets is the only one source for model prediction uncertainty at the ungauged catchment. As it was demonstrated by the results, although the relationship between uncertainty in the parameter and in the prediction results at the ungauged catchments exists, this relationship is far to be linear. This is due to other sources of uncertainty (e.g. model structure, inputs uncertainty), parameter correlation and equifinality. Therefore, all sources of uncertainty should be considered in an integrated framework for more effective parameter regionalization.

To our knowledge, a hydrological study of the entire Thau and Chiba catchments was never done before. Therefore, building on the regionalization approach, this work can be considered as a starting point for further research study of hydrological issues in these catchments.

We think that the developed methodology in this work provides more objectivity in the selection of the transferrable model parameters sets for estimating the discharge at the ungauged catchments. This can reduce a part of the additional uncertainty that can be introduced by the user through his subjective selection of the transferrable model parameters. However, some subjective choices are inevitable such as the choice of the similarity measure and the selection of the catchment attributes which can have an additional source of uncertainty.

We think also that the speculation behinds the developed methodology such as model prediction uncertainty at the ungauged catchments increases as the dissimilarity between the donor and the receptor catchment increases is appealing and reasonable. It provides more reliable prediction uncertainty at the ungauged catchment than the traditional approach. The method is easy and can be replicated with any model parameter transfer approach for estimating flow at ungauged catchments within an uncertainty propagation framework.

CHAPTER V

5 Assessment of climate change impacts on flow regime of the Thau and the Chiba catchments

5.1 Abstract

Projected future changes in climate and their possible impacts on river flow are major concerns for the Mediterranean region. In this chapter the projected alterations in the flow regimes of the Thau and Chiba catchments due to climatic change projections are assessed by means of several hydrological indicators through the conjunctive use of the hydrological SWAT model driven by an ensemble of multiple climatic models underpinned with the A1B greenhouse gas emissions scenario. Results indicate that both catchments are likely to experience drier conditions in the future period (2041-2070) with respect to the reference period (1971-2000) as consequence to the projected decrease in precipitation and increase in temperature. Both catchments are likely to experience a decrease in soil water content, actual evapotranspiration and runoff. Furthermore, high and low flow frequencies and flow extremes magnitudes at various time durations, are also expected to decrease in both catchments in 2050s. The use of multi-climate models allows assessing the degree of uncertainty related to the projected relative change in the reference values of the hydrological indicators. It is found that hydrological future prediction is affected with large uncertainty particularly during the wet period.

5.2 Introduction

Since the middle of the 20th century, the number of hydrometeorological observation data in the Mediterranean area has remarkably increased which allowed scientists to analyze long-term chronological climate data. Their investigations showed a general tendency towards drier climate conditions with decreases in total precipitation and increases in temperatures (IPCC 2007; Giorgi and Lionello 2008; López-Moreno et al. 2011). According to the different Global Circulation Models (GCMs) projections underpinned with different greenhouse gas emissions scenarios, these changes are projected to amplify in the 21st century and the Mediterranean basin will be particularly sensitive to future climate changes and variability (Ludwig et al., 2011; IPCC 2007). For instance, a projected increase in temperatures is expected to range between 5-7°C in summer and 3-4°C in winter in the Iberian Peninsula (Ludwig et al., 2011). Räisänen et al. (2004) have predicted an increase in temperature varying between 4-6°C in summer and 2-4°C in winter for the future time period of 2071-2100. While Hertig and Jacobeit (2008) have projected an increase in temperature by 4°C by the end of this century for the overall Mediterranean basin, Schneider et al. (2013) have found that annual temperatures are likely to increase by an average of 2.3°C.

Concerning precipitation, the projected changes are affected by large regional and seasonal disparity. For instance, winter precipitation over the ensemble Mediterranean basin is projected to decrease by a range of -19 to -6.9 % while summer precipitation will be diminished by -29.3 to -19% in the future (2041-2070), as reported by Schneider et al. (2013). Räisänen et al. (2004) have found that winter precipitation in the future period of 2071-2100 is likely to decline by a range of -30 to -50% against -50 to -60% for summer months and possibly up to -70% in Southern Europe. A generalized drying condition over the Mediterranean region by the end of this century has been reported by Giorgi and Lionello (2008) in their review of climate change projections based on sets of climate models. The authors have also highlighted the particular decrease in summer precipitation that exceeds -25%. García-Ruiz et al. (2011) have reported that a marked decrease in annual precipitation in the future (2040-2070), in comparison to the baseline period (1960-1990), over the entire

Mediterranean basin is evident with the south of Spain, North Africa and the Middle East being the most affected regions (around − 15%). They also added that a decrease in precipitation around 10% is also projected for southern Italy, Greece, and south of Turkey.

Since the hydrological cycle, in general and particularly in Mediterranean region, is very sensitive to climate change and variability, several studies have attempted to quantify the impact of the projected climate change on river flow regime. The combined decrease in precipitation and increase in temperature is likely to reduce the amount of water reaching the soil, increase the soil evaporation and plants transpiration (Foley et al., 2005), reduce the soil moisture and decrease the magnitude of river discharge (García-Ruiz et al., 2011). It is further expected that hydrologic regime alteration will decrease the fresh water availability, increase risks of droughts and floods with more exacerbated forms of water pollution (Ludwig et al., 2009, 2011). Lespinas et al. (2014) have projected a general water discharge decrease ranging between -26% and -54% in Mediterranean French coastal river basins for 2071-2100 in comparison to 1961-1990. Koutroulis et al. (2013) reported that average water availability is expected to drop during 2000-2050 to a devastating 70% of the observed average which is already insufficient to cover current demand in Crete Island (Greece). Schneider et al. (2013) have found that simulated discharge of Europe Mediterranean rivers for the future period (2041-2070) is likely to be lower during the entire year in comparison to the reference period (1971-2000). Their results revealed also a substantial decrease in magnitude of monthly flow, maximum and minimum flows which, according to the authors, will lead to more intermittent flow with an increasing of zero flow events. In assessing the impact of climate change in southern Italy, Senatore et al. (2011) have noted annual reductions in soil moisture during the whole year with the highest deficits during summer (up to −40%) in the future period (2070-2099) with respect to the reference period (1961-1990). They have also noted a reduction in groundwater storage (−6.5±1.4% and −11.6±1.6%), surface runoff (−25.4±6% and −41.2±5%) and a significant increase in future runoff variability.

Most of the climate change impact studies on Mediterranean flow regime have focused on global or regional scale rather than on catchment scale which is more useful and more appropriate to guide practical mitigation and adaptation policy for water resources management. As reported by several authors (Lespinas et al. 2014; Elguindi et al., 2011) the plausible reason behind neglecting small Mediterranean catchments in climate change impact studies could be related to the coarse resolution and uncertainty of the GCMs to provide reliable information for the hydrological model at the local scale. Indeed, both climate and hydrological models are prone to considerable uncertainty related to their structure, parameters, inputs and boundaries conditions (Koutroulis et al., 2013; Schneider et al., 2013; Sellami et al., 2013). Thus, it is expected that this uncertainty will propagate throughout the modelling chain and affect the quantification of the projected change in catchment flow regime due to climatic change (Arnell, 1999). Together, modelling uncertainty with the variability in catchment characteristics (e.g. morphology, geology, and climate) and hydrological processes make the quantification of the possible impacts of climate change on the flow regime more challenging and uncertain at the local scale than at the regional or global scale.

Assessing the impact of climate change on catchment hydrology is usually based on quantitative measures of hydrologic change between pre-impacted and post-impacted conditions. The difficulty lies in the identification of these metrics that should be hydrologically meaningful to draw a comprehensive picture of the effect of climate change on catchment hydrology. Ideally, these hydrologic indicators should be also with a great potential to support operational river management (DeGasperi et al., 2009; Richter et al., 1996). A broad range of hydrologic metrics, also known as hydrologic indicators, exist in literature (Richter et al., 1996, 1998; Olden and Poff, 2003; Gao et al., 2012). However, their selection varies from one study to another depending on the objectives, the data available and characteristics of the study site. For instance, Schneider et al. (2013) have selected 12 parameters from the Indicator of Hydrologic Alteration (Richter et al., 1996) to investigate climate change impact on river flow regimes over Europe. Although their selected indicators cover magnitude, frequency, duration, timing and rate of change of the flow, they did not reflect changes related to other facets of the flow regime such as evapotranspiration, soil moisture and runoff. Others (Senatore et al., 2011) have selected snow accumulation, root zone soil moisture, evapotranspiration, groundwater storage, surface runoff and runoff on annual basis to assess the impact of climate change in the Crati basin in Calabria region (Italy). But they did not investigate the possible change in the frequency, timing and duration of the flows. Gain et al. (2011) investigated the effect of climate change by selecting metrics related to both low and high flows of the lower Brahmaputra catchment located in the glaciated areas of the Kailash range in Tibet (China). Thus, there is no a unique universal set of hydrologic indicators recommended for climatic change impact studies. Furthermore, studies that combine hydrologic indicators related to water balance (evapotranspiration, runoff, soil moisture, etc.) with these to the frequency, timing and magnitude of the flow to derive a comprehensive picture of the climate change effect on local scale hydrology are rare, specifically in the Mediterranean.

The objective of this chapter is to quantify and derive an overall picture of the possible impacts of climate change on the hydrology of the Thau and Chiba catchments by means of relevant hydrologic indicators. To address the question of uncertainty, the hydrological model is driven by an ensemble of climate models and the degree of alteration of the flow regime is quantified in an uncertainty framework.

5.3 Material and methods

5.3.1 The CLIMB project

Climate models used in the present study as well as the approaches used for their downscaling, bias correction intercomparison and validation are produced within the framework of the European *CLIMB* project (*Climate Induced Changes on the Hydrology of Mediterranean Basin;*). Thus, a brief description of the *CLIMB* project is given here.

Funded by the EU, *CLIMB* aims to reduce the uncertainty in assessing the impacts of climate change on 7 Mediterranean catchments including the Thau and the Chiba catchments (Ludwig et al., 2010). To achieve this goal, *CLIMB* relies on improving modelling capabilities and developing new appropriate tools through novel field monitoring concepts, remote sensing techniques, integrated hydrological modelling and socioeconomic factor analysis (Ludwig et al., 2010). Thus, the outcomes of the project will provide the necessary information to support and guide the design of adaptive water resources management plans in the Mediterranean region under climatic change conditions. More details about the *CLIMB* project can be found on http://www.climb-fp7.eu/home/home.php.

Furthermore, *CLIMB* is forming a cluster with two projects; *WASSERMed* from the Environment and *CLICO* from Socio-Economic Sciences and Humanities Call of FP7. The cluster joins the forces between the three projects by exchanging data, methods, model results and scientific expertise towards better understanding of the climate change impacts on Mediterranean region and reducing its assessment uncertainty to an unprecedented level. For the projects cluster the reader can refer to http://www.cliwasec.eu/home/home.php

5.3.2 *Future climate scenario*

Assessment of climate change impact on catchment hydrology is usually conducted with a conjunctive use of climate and hydrological models. Traditionally, the calibrated hydrological model is forced by the climate model outputs to investigate the change in catchment hydrology between reference and future conditions due to change in climate.

Future climate scenarios were developed by Deidda et al. (2013) within the framework of *CLIMB* project. A summary of the approach used to select the climate models is report hereafter. For more details the reader can refer to the work of Deidda et al. (2013).

From the EU-FP6 ENSEMBLES project 14 combinations of GCMs and Regional Climate Models (RCMs) underpinned with the A1B emission scenario (IPCC, 2007) were selected. Then, the climate models (GCM-RCM combination) were ranked based on their performances in reproducing precipitation and temperature of the state-of-the art reference data set E-OBS (http://www.ecad.eu and hosted by the Climate Research Unit (CRU) of the Hadley Centre) over some Mediterranean catchments including the Thau and the Chiba, for the control time period of 1951-2010. The four best rated climate models were selected with additional constraint by considering at least two different RCMs nested in the same GCM, and two different GCMs forcing the same RCM to maintain diversity between the climate models (Deidda et al., 2013).

Table 5-1: Acronyms of the selected GCMs and RCMs for the Thau and Chiba catchments

Acronym	Climatological center and model
GCM	
HCH	Hadely Center for Climate Prediciton, Met Office, UK HadCM3 Model (high sensitivity)
ECH	Max Planck Institute for Meteorology, Germany ECHAM5/MPI OM
RCM	
RCA	Swedish Meteorological and Hydrological Institute (SMHI), Sweden RCA Model
REM	Max Planck Institute for Meteorology, Hamburg, Germany REMO Model
RMO	Royal Netherlands Meteorological Institute (KNMI), Netherlands RACMO2 Model

Therefore, the retained climate models for the Thau and Chiba catchments were these derived from the combination of:

- ECHAM5/MPI-OM model with RCA model, referred hereafter as ECH-RCA,
- ECHAM5/MPI-OM model with REMO model, referred hereafter as ECH-REM,
- ECHAM5/MPI-OM model with RACMO2 model, referred hereafter as ECH-RMO,
- HadCM3 model with RCA model, referred hereafter as HCH-RCA.

These climate models provided meteorological variables (e.g. precipitation, temperature, solar radiation, wind speed and humidity) at a coarse resolution (24 km grid) which were not compatible for SWAT application at the catchments scale. Therefore, Deidda et al. (2013) have performed downscaling procedures for the climate models outputs to field scale. Precipitation downscaling was performed using the multi-fractal approach described in details in Deidda (2000) while temperature was downscaled according to Liston and Elder (2006), which combines a spatial interpolation scheme with orographic corrections. However, some discrepancy between the modelled and the observed variables remained. Thus, Deidda et al.

(2013) have applied bias and quantiles correction technique to reduce the bias and obtain better fit between the observed and predicted probability distribution of the climatic variables. It should be noted here that Deidda et al. (2013) validated the climate model simulations against the E-OBS data using several metrics. However, the E-OBS data may not accurately reflect the on-site measured climatic variables.

5.3.3 Selection of the hydrologic indictors

Once the meteorological climate models outputs are available they are used to drive the hydrological SWAT model on a daily basis for the reference (1971-2000) and future (2041-2070) periods. Changes in catchment flow regime between these two time periods can be assessed using a broad range of existing hydrologic indicators (Richter et al., 1996, 1998; Olden and Poff, 2003; Gao et al., 2012). As discussed in the introduction, the selected hydrologic indicators depend on the aims, data available and the catchment characteristics. Based on that and on additional knowledge regarding the hydrology of the catchment, a set of 9 hydrological indicators deemed relevant for the Thau and the Chiba catchment are selected (Table 5-2).

Table 5-2: Selected hydrologic indicators for climatic change impact assessment

Process group	Hydrologic indicator
Climate conditions	- Cumulative monthly precipitation - Monthly temperature
Water balance	- Evapotranspiration (ETP) - Monthly runoff - Soil water content (SWC)
Flow magnitude and frequency	- Number of low flow days per month - Number of high flow days per month - FDC (30 years daily discharge)
Flow duration	- Minimum flow duration (7, 30, 90 days) - Maximum flow duration (7, 30, 90 days)

These indicators are able to reflect the projected changes in;(i) climate and meteorological conditions through changes in monthly precipitation and temperature, (ii) changes in catchment hydrological processes by investigating changes in monthly runoff, actual evapotranspiration (ETP) and soil water content (SWC), and (iii) changes related to magnitude, frequency and duration of flows based on analysis of catchment flow duration curve (FDC), low and high flows duration and frequency. Therefore, the overall facet of the catchment hydrologic regime is well characterized by these selected indicators.

5.3.4 Multi-climate models ensemble average and uncertainty approach

One way to improve the prediction impact of climate change and to obtain more accurate results is to use an ensemble of multiple climate models commonly knowing as multi-models ensemble approach (Kwon, 2012). The reason is that each single climate model has its own structure, sensitivity to the input data and parameterization, strength and limitations in reproducing the observed climate. Therefore, there is no reason to believe that good climate model skills based on past relationships between climate forecasts and verifications implies good skills in climate predictions. Furthermore, the multi-models approach is used and recommended by the Intergovernmental Panel on Climate Change (IPCC) to derive the mean of long-term climate change projections as the best guess projection (IPCC, 2001). The suggested approach has shown to be more efficient in improving the accuracy and consistency of the predictions than a single climate model (Giorgi and Mearns, 2002; Tebaldi and Knutti 2007; Knutti, 2010; Koutroulis et al., 2013). In addition, the use of the multi-models ensemble makes the characterization of the model structural uncertainty possible.

For each climate model the projected deviation (Δv, either relative change or absolute difference) in the hydrologic indicator (v) is calculated and the values are averaged to consider a multi-climate models ensemble mean ($\overline{\Delta v}$).

$$\Delta v = \begin{cases} \dfrac{v_{Fut} - v_{\mathrm{Re}f}}{v_{\mathrm{Re}f}} \times 100, & \text{relative change (\%)} \\ v_{Fut} - v_{\mathrm{Re}f}, & \text{absolute change (indicator unit)} \end{cases} \qquad \text{Equation 5-1}$$

Positive value of Δv indicates an increase of the reference value in the future; negative value indicates a decrease of the reference value in the future while null value indicates no change to the reference value in the future.

Then, the uncertainty in the magnitude of deviation of the regarded ensemble climate models is constructed by $\overline{\Delta v} \pm \delta_{\Delta v}$.

$$\delta_{\Delta v} = \left[\frac{1}{N} \sum_{i=1}^{N} (\Delta v_i - \overline{\Delta v})^2 \right]^{1/2} \qquad \text{Equation 5-2}$$

where $\delta_{\Delta v}$ corresponds to the root-mean-square difference of the change in the indicator v, N is the total number of climate models used (in the present study N=4), $\overline{\Delta v}$ is the climate multi-models ensemble (CME) average relative change for v and the average uncertainty interval is then given by $\overline{\Delta v} \pm \delta_{\Delta v}$.

5.3.5 Assumptions of the approach

In this approach all the climate models are given an equal weight. Of course, one can weigh each climate model according to its skill in simulating the actual climate conditions or any other hydrological variable. From one hand, it makes perfect sense to trust, thus, weigh better model, on the other hand, there is no guarantee that model that performs better in the present conditions will be superior to other models in the future. Thus, the difficulty lies in deriving model weights according to their performances. However, this is not followed in this study since the selected climate models are considered as the "best" in reproducing the E-OBS data thus are all equally performants.

As the focus of this chapter is to assess the hydrological implications of climate change while considering only uncertainty related to climate models, hydrological uncertainty is neglected. Therefore, the "best" parameter sets (it is meant by "best" here the parameter sets that led to the highest NS values during the calibration process) at each subcatchment is selected and the hydrological model, without any further tuning, is driven by the climate models. However, doing this, the model structure and the parameter sets are considered to be correct and that any departure in the hydrologic indicator from the reference condition is only related to climatic change. Thus, the predicted uncertainty is “unambiguously” originating from the climate models uncertainty. Actually, this is a strong assumption since additional uncertainty can arise from the instability and sensitivity of the hydrological model parameters due to the possible difference in climatic or catchment characteristics between the reference and the future period. However, it remains the classical adopted approach in climate change impact studies (Brigode et al., 2013).

5.4 Results and discussions

5.4.1 Performances of the climate models

Before assessing the projected changes in the catchments hydrology due to changes in climate, it is useful to provide an overall picture of the performances of the climate models ensemble in simulating the actual climatic conditions. For this purpose, 30 years of daily precipitation and temperature recorded by the Sète climatic station in the Thau catchment and the Chiba climatic station in the Chiba catchment are used.

Figure 5-1 compares the climate multi-models ensemble (CME) prediction of temperature and cumulative precipitation against observations for the reference period (1971-2000) on a monthly basis. For both catchments, the observed monthly cumulative precipitations are mostly within the 25th and 75th percentiles of the CME predictions. In addition, the monthly variability and seasonality of the actual precipitation is well mimicked by the climate models. However, the bias between the observed precipitation values and the median predictions of the CME tends to increase as moving from the dry season (May to September) to the wet season (October to April) as it can be depicted from the dispersion of the predicted precipitation in Figure 5-1. The estimated overall annual average error between climate models simulations and measurements is less than 10% for both catchments. On annual basis, average measured and predicted precipitations are about 600 and 550mm, respectively, for the Thau catchment and 450 and 405mm, respectively, for the Chiba catchment.

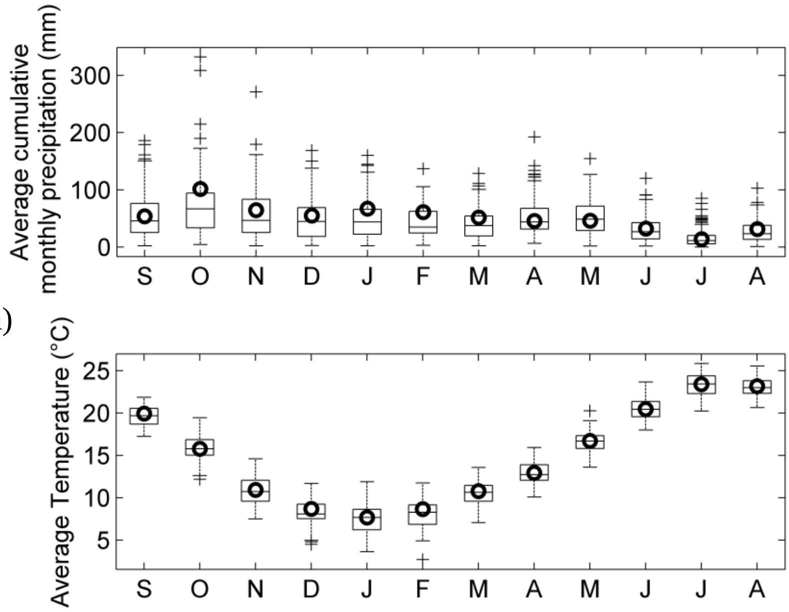

(a)

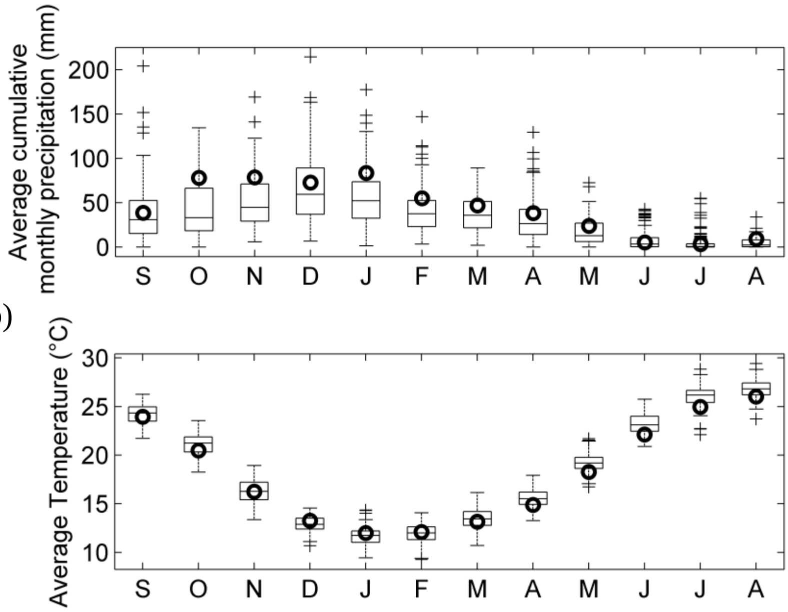

(b)

Figure 5-1: Measured versus CME prediction for monthly precipitation and temperature for the Thau (a) and the Chiba (b) catchments. The boxplots are the CME predictions where the central line is the median, the edges of the box are the 25th and 75th percentiles, the whiskers extend to the most extreme data points, without outliers, and outliers are plotted individually. The circles refer to the measured values.

The climate models predict well not only the magnitude but also the seasonality of the observed temperature at both catchments. Measured monthly temperatures for both catchments are within the first and the third quartile range of the CME prediction. Climate models are better predictor for actual temperature than precipitation.

Based on the performances of the climate models in reproducing the actual climatic conditions of the reference period for the Thau and the Chiba catchments, climate simulations can be considered as very good and, thus, reliable to be used for future projections.

5.4.2 Projected changes in precipitation and temperature

Projected changes in climate conditions for the future period are assessed by calculating the CME average relative deviation for monthly cumulative precipitation and absolute changes in monthly temperature with respect the reference period (1971-2000) at each study site.

Projected changes in climatic conditions for the Thau catchment

While the projected precipitation in 2050s by the CME respects and closely follows the seasonality and the monthly variability of the reference period, there is a clear tendency to a generalized decrease in the magnitude values across all the months over the Thau catchment (Figure 5-2). The reduction of precipitation is expected to range between -14 to -2% according to the CME mean values. Exception is made for February where the mean trend projects an increase of +5% in precipitation which can be due to an outlier in the simulated values. However, the CME uncertainty interval suggests that these values can range between -18 to -5% from September to December, from -14 to +10% from January to April and between -15 to -2% in the late of spring and during the summer months. Thus, there is a large uncertainty and variability in the projected change in precipitation in particular in the winter months in the Thau catchment. In general, the projection uncertainty tends to increase as moving from the dry months to the wetter months.

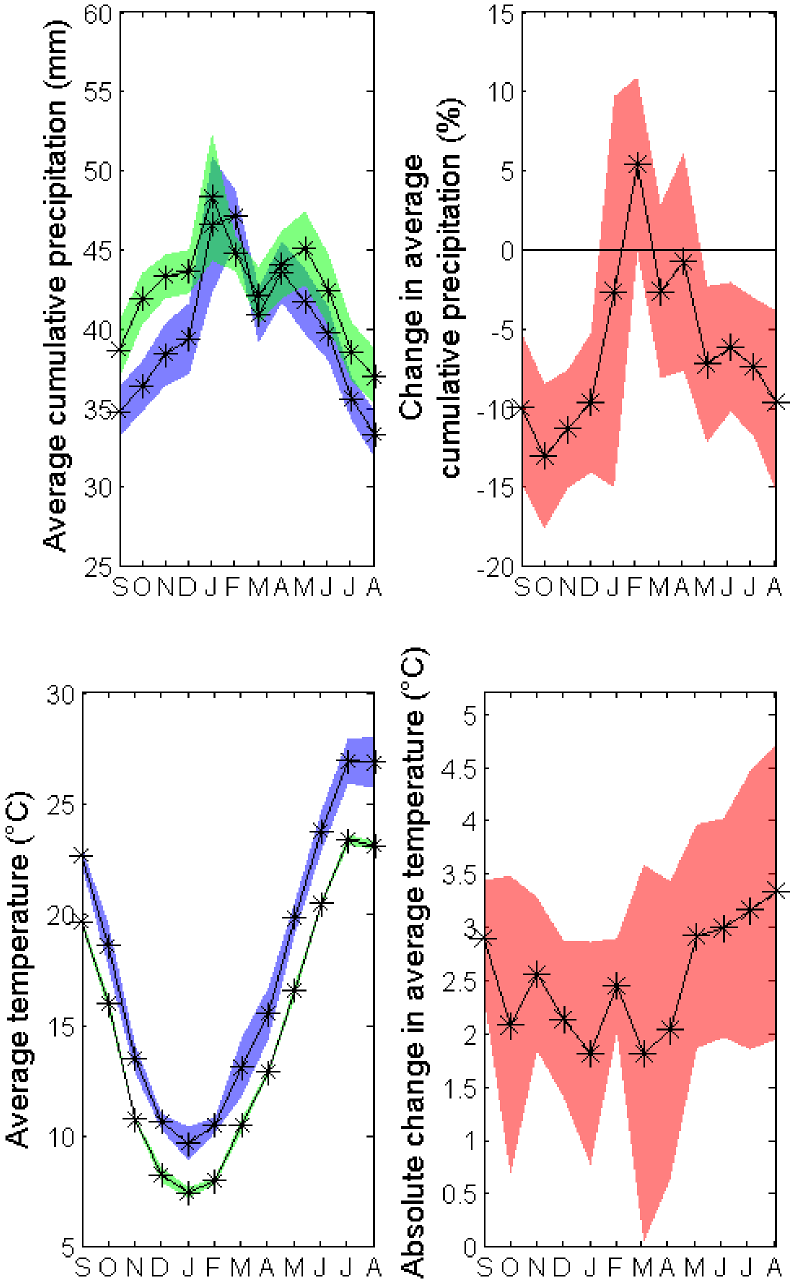

Figure 5-2: Projected change in monthly cumulative precipitation (upper) and monthly temperature (lower) over the Thau catchment as calculated by the CME. Green, blue and red colors are CME uncertainty intervals for the reference, future and relative change, respectively. Black line with black starts refers to the CME mean values.

On annual basis, the average yearly reference precipitation (550 mm) is projected to range between 453 mm and 500 mm when considering the CME uncertainty leading to an average annual reduction ranging between -18 and -9%.

Figure 5-2 also shows the CME predicted magnitudes and projected absolute change of the average monthly temperature for the reference and future period. When comparing the magnitude of average monthly temperature projection to those of the reference period, there is clear evidence that climate models become more uncertain in simulating temperature in 2050s. All climate models project a general tendency towards warmer conditions over the Thau catchment. The projected magnitudes of change suggest that reference monthly temperature is likely to increase by 1.7 to 3.2°C depending on the season. The highest increase in temperature is projected for summer months where summer season (JJA) reference average temperature will increase by 3.1°C in the 2050s, according to the CME mean value. Conversely, to precipitation, the projected uncertainty in the magnitude of change in temperature decrease as moving from the dry months to the wetter months. By considering the uncertainty range of the values, average monthly reference temperature is likely to increase by [2 to 4.6°C] in summer, [1 to 3°C] in winter, [0.1 to 4°C] in spring and [0.7 to 3.4°C] in Autumn.

Projected changes in climatic conditions for the Chiba catchment

The predicted monthly cumulative precipitation and monthly temperature as calculated by the CME over the Chiba catchment for the reference and future periods are illustrated in Figure 5-3. The projected changes in precipitation and temperature, as well as their associated uncertainty intervals, as derived from the CME are also plotted in the same figure. Similarly to the Thau catchment, the projected precipitation in 2050s is likely to follow the reference seasonality and monthly variability of rainfall in the Chiba catchment. The rainy and dry seasons in the future period seems to be very similar to these in the reference period.

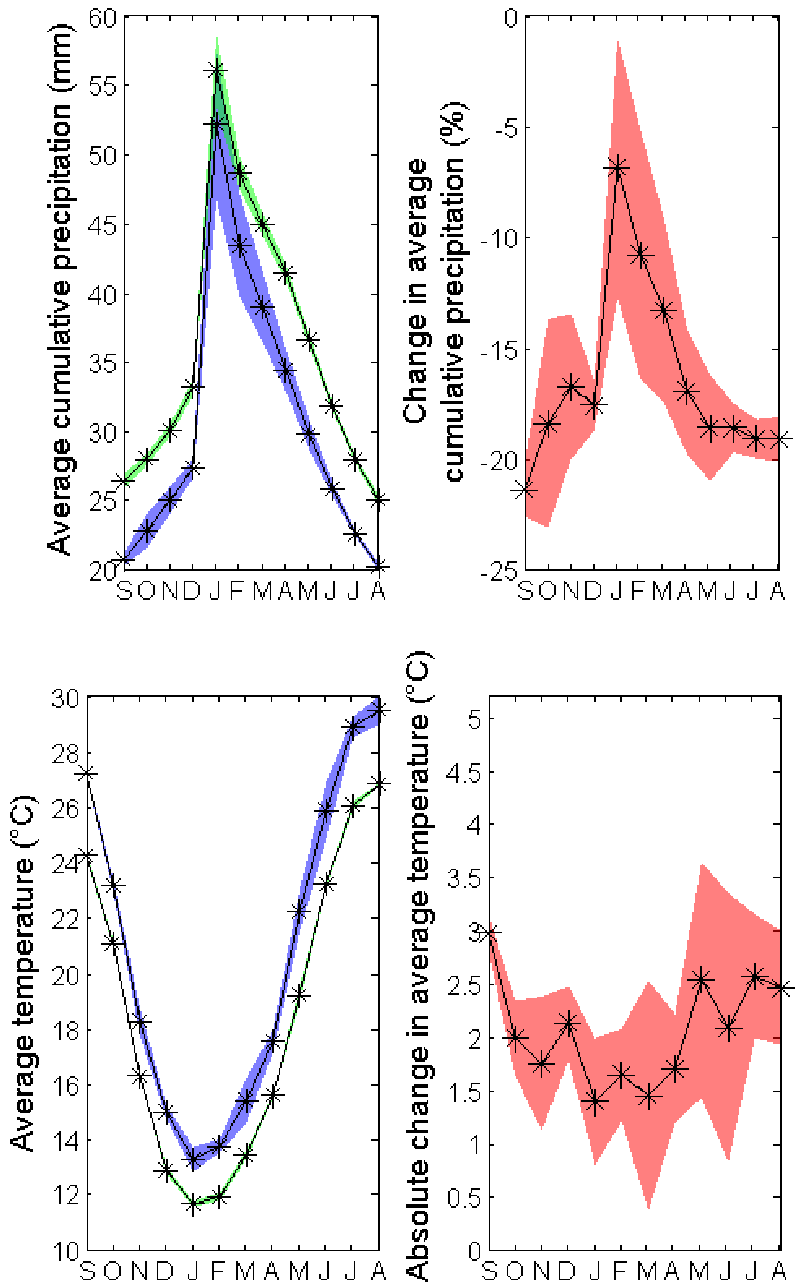

Figure 5-3: Projected change in monthly cumulative precipitation (upper) and monthly temperature (lower) over the Chiba catchment as calculated by the CME. Green, blue and red colors are CME uncertainty intervals for the reference, future and relative change, respectively. Black line with black starts refers to the CME mean values.

There is an evident negative evolution in monthly precipitation with respect to the reference conditions suggesting that the Chiba catchment is likely to experience drier conditions in 2050s. The CME projected magnitudes of precipitation are affected with larger uncertainty than these in the reference period. Furthermore, this uncertainty is likely to increase as moving from dry months (May to September) to wet months (October to April). The CME mean and uncertainty of the projected relative change magnitudes of precipitation reflect the agreement of all the climate models regarding the negative sign of the change. The fact that the uncertainty interval is below the reference line (Figure 5-3) reinforces the beliefs of the generalized decrease in monthly precipitation over the Chiba catchment in the future. The decrease in precipitation is very likely to be more pronounced in the dry months, particularly in summer, than in winter months. By considering the spread of the possible relative change values, reference precipitation is expected to diminish in the future by ranges of [-18 to -20%] in summer, [-17 to -4%] in winter, [-22 to -14%] in autumn and [-18 to -13%] in spring. On an annual basis, the projected decrease in average annual reference precipitation is likely to range between -19 and -14% leading to an average annual precipitation between 365 and 387 mm in 2050s in comparison to 450 mm in the reference conditions.

For temperature, while the reference seasonal variability is likely to be conserved, there is larger uncertainty in the projected magnitude values than these in the reference period in the Chiba catchment (Figure 5-3). CME projects a general increase in reference temperature with an average value of +2.5°C in the dry period against 1.72°C in the wet period. However, uncertainty in the projected increase of temperature suggests that summer values are likely to range between +2.08 and 2.46°C while winter temperature is likely to vary between +1.4 to 2.1°C.

In both Thau and Chiba catchments, there is a general tendency for drier and warmer conditions in the future period in comparison to the reference period which may severely amplify the current rainfall geographical disparities and the water scarcity in the areas. These projected results at the catchment scale confirm the general consensus existing in literature about precipitation decrease over the Mediterranean region (Ludwig et al., 2011; García-Ruiz et al., 2011; Schneider et al, 2013). However, despite this general agreement the reported ranges of change vary from one study to another depending on the study site, climate model, the emission scenario, the prediction time horizon and the approach used to calculate these changes. For temperature, literature agrees more or less on a similar range of increase, roughly, between 4 and 6°C in summer and between 2 and 4°C in winter over the Mediterranean basin (Räisänen et al., 2004; IPCC, 2007; Ludwig et al., 2011). The projected increases in temperature for the Thau and the Chiba catchments perfectly lie within these reported ranges. These projected increases in temperature particularly in summer can have very dangerous effects in both study areas if we know that the ceiling on global temperature increase argued to avoid the most dangerous effects of global warming is 2°C.

5.4.3 Projected changes in catchment soil water content (SWC)

It is well recognized that soil moisture plays an important role in the hydrological and meteorological processes (Parajka et al., 2005). It controls the portioning of rainfall into runoff and infiltration. Accurate soil moisture estimation and measurement can improve hydrological model prediction through data assimilation (Tran et al., 2013; Vernieuwe et al., 2011; Minet et al., 2011). In the SWAT model, the soil water content at the end of the simulation time step corresponds to the amount of water stored (mm) in the soil profile (m). SWAT records the water content of the different soil layers but assumes that the water is uniformly distributed in the horizontal direction within that layer. Therefore, for more accurate representation of the predicted SWC, only the water stored in the first layer is considered hereafter. Moreover, the results are presented in volumetric soil water content expressed as the volume of water per volume of soil by considering the depth of the first soil layer.

Projected changes in SWC in the Thau catchment

SWC as predicted by the CME for the reference and future periods over the Thau catchment is given in Figure 5-4. Uncertainty prediction and projected relative change of SWC are also plotted in this figure.

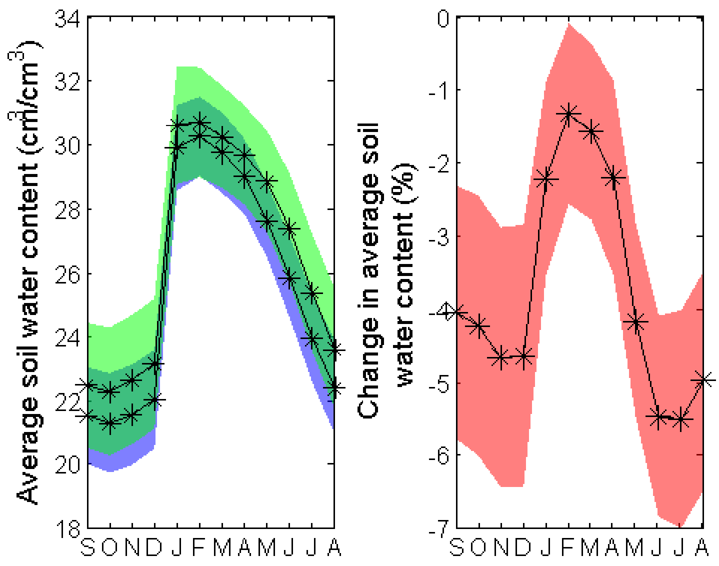

Figure 5-4: Projected change in average soil water content over the Thau catchment as calculated by the CME. Green, blue and red colors are CME uncertainty intervals for the reference, future and relative change, respectively. Black line with black starts refers to the CME mean values

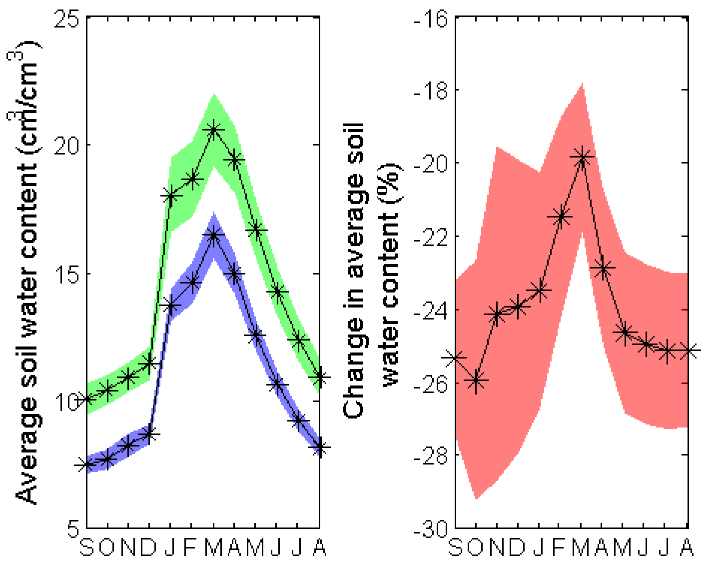

Figure 5-5: Projected change in average soil water content over the Chiba catchment as calculated by the CME. Green, blue and red colors are CME uncertainty intervals for the reference, future and relative change, respectively. Black line with black starts refers to the CME mean values

In the Thau catchment, for both reference and future periods, CME predicts higher SWC in the wet period than in the dry period with the highest values are in winter months [29-32 cm^3/cm^3] and the lowest values are in summer months [20-25 cm^3/cm^3]. Predicted average annual SWC as calculated by the CME is about 26.5 cm^3/cm^3 in the reference period against 25.4 cm^3/cm^3 in 2050s. Furthermore, CME prediction uncertainties of SWC in both projection periods are similar in width and temporal variability and are overlapping in most of the months of the year. These results suggest that the projected changes in reference SWC are likely to be insignificant and that the monthly variability and seasonality of the reference SWC in the Thau catchment is likely to be conserved in the future period (Figure 5-4).

While there is a general tendency that the Thau catchment will experience a decrease in SWC in the future with respect to the reference period, the magnitudes of the projected relative changes are very weak and ranging between -7 and 0% (Figure 5-4). In winter months the projected relative change is lower than 3% of the reference SWC values while in the dry period, these changes are expected to vary between -2.2 and -7%.

Projected changes in SWC in the Chiba catchment

Similarly to the Thau catchment, the predicted SWC in the Chiba catchment for the reference and future periods exhibits similar monthly and seasonal variability suggesting that that no changes in the timing of the SWC are expected (Figure 5-5). However, it is clear that the projected SWC values are likely to be lower than these in the reference period. Average annual SWC in the Chiba catchment is expected to decrease from 14.45 cm^3/cm^3 to 11 cm^3/cm^3, thus an overall annual decrease of 23.8%. The latter projected decrease is better represented through the negative sign of the projected relative changes in the reference SWC across all the months of the year in the future period (Figure 5-5, right panel). The projected relative change values are expected to range between [-27 and -23%] in summer, [-28 to -19%] in winter, [-29 to -19.5%] in autumn and [-18 to -22%] in spring season. These statistics suggest that a higher deficit in SWC is expected to be in the future period than in the reference period with a probable marked decrease in summer and autumn season. The projected decrease in SWC is likely to be more pronounced in the

Chiba catchment than in the Thau catchment. This is consistent with the projection in precipitation in both catchments.

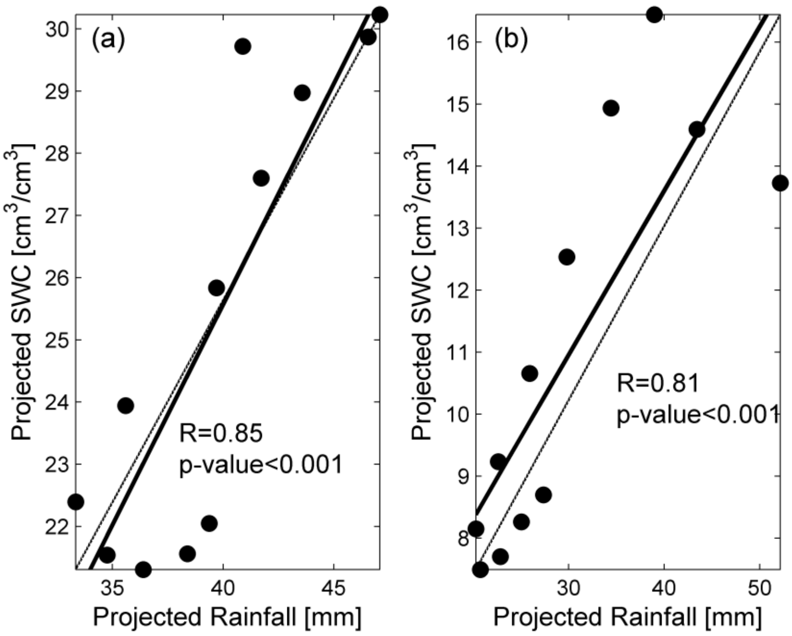

Figure 5-6: Relationships between projected precipitation and SWC in the Thau (a) and the Chiba (b) catchments. Dashed line is the 1:1 line and the black line is the regression model.

There is a clear and significant relationship between the average monthly projected precipitation and soil moisture values in the future period in the Thau and the Chiba catchments (Figure 5-6). Thus, it is very likely that the projected decrease in reference precipitation will decrease the soil moisture in both catchments. However, it is widely admitted that others factors besides precipitation can influence the soil moisture. For instance, canopy can influence the soil water regime by offsetting drier conditions through decreased transpiration, particularly in summer months (Holsten et al., 2009). Senatore et al. (2011) have attributed the projected decrease in SWC to the projected decrease in ETP and increase in temperature. However, in both catchments the projected decrease in SWC is not significantly correlated either with ETP or with temperature. The projected decrease in SWC can cause a negative feedback to the hydrological cycle by amplifying the magnitude and duration of the meteorological droughts in both study catchments. It can also increase the demand for water irrigation under less water availability.

5.4.4 Projected changes in catchment evapotranspiration (ETP)

ETP is the water that can be lost by plants transpiration and bare soils and surface water bodies through evaporation. ETP is commonly used by hydrological models to calculate runoff thus making it a major component of the water balance. In Mediterranean area, around 90% or more of annual rainfall can be lost through evapotranspiration (Wilcox et al., 2003). Thus, estimating ETP is important for a better understanding of the relationships between climate and water balance.

Projected change in ETP in the Thau catchment

The predicted magnitudes and projected change in average monthly ETP, as well as their associated uncertainty interval over the Thau catchment as calculated by the CME are given in Figure 5-7.

The predicted trend in the ETP in the Thau catchment for both reference and future periods shows that higher ETP values are within the dry season while lower ETP values are within the wet season. However, the CME uncertainty reveals that the projected monthly ETP values are more uncertain than these in the reference period and that uncertainty becomes larger as moving from dry season to wet season. The average annual ETP as calculated by the CME is about 418.23 mm in the reference period against 406.5 mm in the future period. These values suggest that about 82% of reference annual precipitation is lost via ETP in the reference period against 80% in the future conditions. Thus, the projected changes in reference ETP are likely to be insignificant over the Thau catchment. This statement is confirmed by the low projected relative change values of the reference ETP in the 2050 horizon. The projected relative changes suggest a slight decrease (less than 11%) of the reference ETP during the dry season and a slight increase (less than 10%) in winter months.

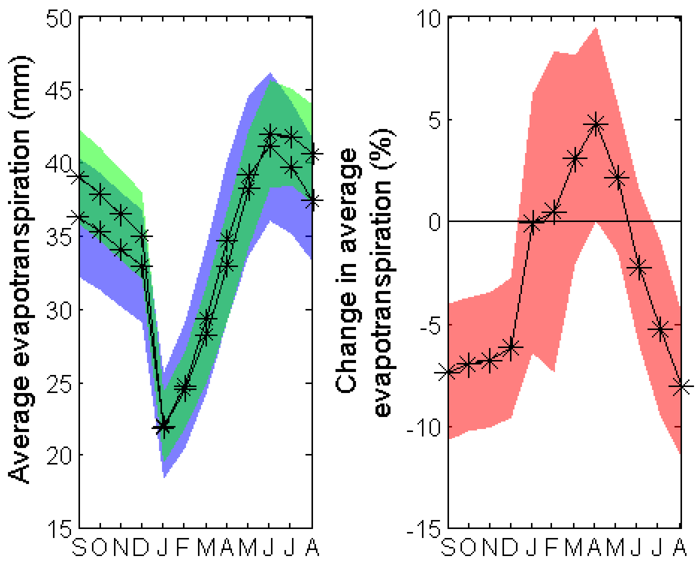

Figure 5-7: Projected change in average monthly ETP over the Thau catchment as calculated by the CME. Green, blue and red colors are CME uncertainty intervals for the reference, future and relative change, respectively. Black line with black starts refers to the CME mean values

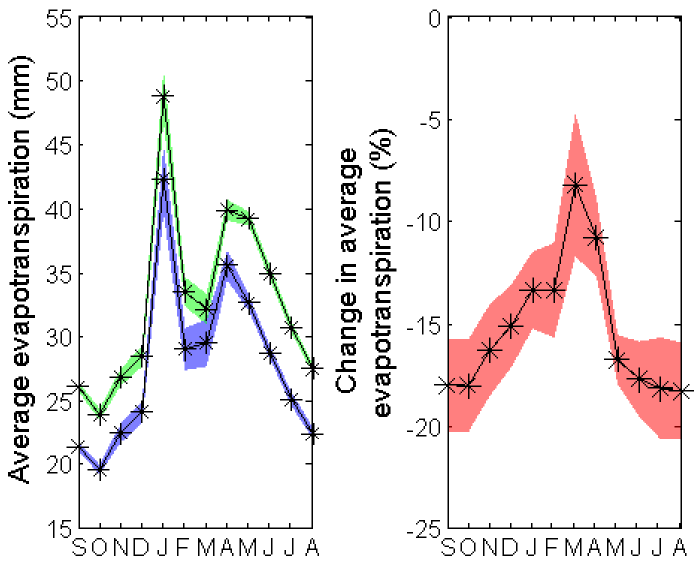

Figure 5-8: Projected change in average monthly ETP over the Chiba catchment as calculated by the CME. Green, blue and red colors are CME uncertainty intervals for the reference, future and relative change, respectively. Black line with black starts refers to the CME mean values

In the Chiba catchment, changes in ETP as predicted by the CME for the reference and the future periods can be depicted in Figure 5-8. Results show a clear tendency towards a general decrease in ETP in the future period, with respect to the reference period, in the Chiba catchment. In both reference and future periods, higher ET are projected in the dry season while lower ETP are in the wet season, except in January which could be due to the higher precipitation peak. In general, the seasonality and monthly variability of the reference ETP is likely to be preserved in the projection horizon. However, the average annual reference ETP (392 mm) is projected to decrease by an average rate of -15% leading to an annual average ETP value of 333mm. These statistics suggest that the average annual ratio of ETP/precipitation is 90% in both reference and future periods. These results are in a perfect line with the runoff and precipitation prediction over the Chiba catchment if we know that the annual average runoff/precipitation ratio, as predicted by the CME, is about 9.5% in both reference and future period. The project relative changes in the reference ETP in the Chiba catchment are negative across all the months in the future period. A marked projected decrease is likely to occur in the dry season, where the relative change values range between -20 to -15.5%, in comparison to the wet period where the values are expected to range between -17 to -5%. The projected decrease in reference ETP in the Chiba catchment is likely to be more severe than in the Thau catchment.

As the ETP includes evaporation from soils and transpiration from vegetation, a large fraction of the soil moisture in the first soil horizon in semi-arid catchments can be directly lost through soil evaporation (Wang et al., 2012). Therefore, it is expected that a reduction in the soil moisture decreases soil evaporation, thus decreases the ETP. However, while investigating the possible relationships between ETP, SWC and precipitation, there is no clear and significant statistical link between these variables in the study sites despite that they exhibit similar monthly and temporal behaviors. Furthermore, although temperature can indirectly affect the water balance through ETP no significant relationships are found between these two variables. Relating ETP dynamic to hydroclimatic variables in Mediterranean catchments can be difficult because apart from soil evaporation (when water is available), vegetation under Mediterranean climate has developed optimal water use strategies to decrease transpiration.

5.4.5 Projected changes in catchment runoff

Runoff includes not only the waters that travel over the land surface and through channels to reach a stream but also all the others flow components such as interflow, groundwater flow, etc. Therefore, runoff is one of the important components of the catchment hydrological balance. Assessing the impacts of climatic change on catchment runoff is of paramount importance to guide appropriate future management of the water resources at the catchment scale.

Projected change in runoff in the Thau catchment

The projected changes in average monthly runoff and its associated uncertainty interval as predicted by the CME over the Thau catchment are illustrated in Figure 5-9. The projected seasonality and monthly variability of the runoff are quite similar to these in the reference period suggesting that there will be no shifting in the runoff timing. High runoff values will be during the wet period, particularly in winter months (DJF) while low values are expected to be during the dry months, specifically during the summer months (JJA). On the other hand, there is a clear tendency to less runoff in the future with respect to the reference period in the Thau catchment. All months are likely to experience less runoff flow with a marked decrease in the wet months, from October to December, with an average reduction of -20% of the reference value. Summer monthly runoff is also expected to decrease with an average value of -8%. There will be no changes to the reference runoff magnitude of February as derived by the CME mean value. This could be due to the projected increase in precipitation for the same month which is suspected to be an outlier. As it can be depicted in Figure 5-9, there is a large uncertainty in the projected relative change of the reference runoff values in the future period. The direction of the uncertainty in the projected runoff is quite similar to the one of projected precipitation, meaning that, uncertainty is likely to increase as moving from the dry period to the wet period. Considering this uncertainty, it becomes more appropriate to communicate a range of plausible values of the projected relative change in runoff rather than the mean value. Thus, reference runoff in the Thau catchment is expected to decrease in 2050s by a range of [-13 to -3%] in summer, [-33.8 to -1.8%] in winter (without considering February), [-31 to -5.5%] in autumn and [-10.3 to -2.2%] in spring season.

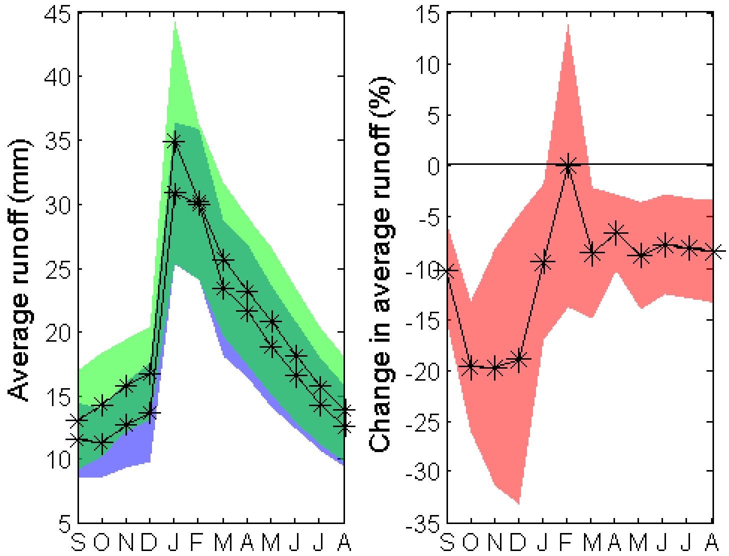

Figure 5-9: Projected change in average monthly runoff over the Thau catchment as calculated by the CME. Green, blue and red colors are CME uncertainty intervals for the reference, future and relative change, respectively. Black line with black starts refers to the CME mean values.

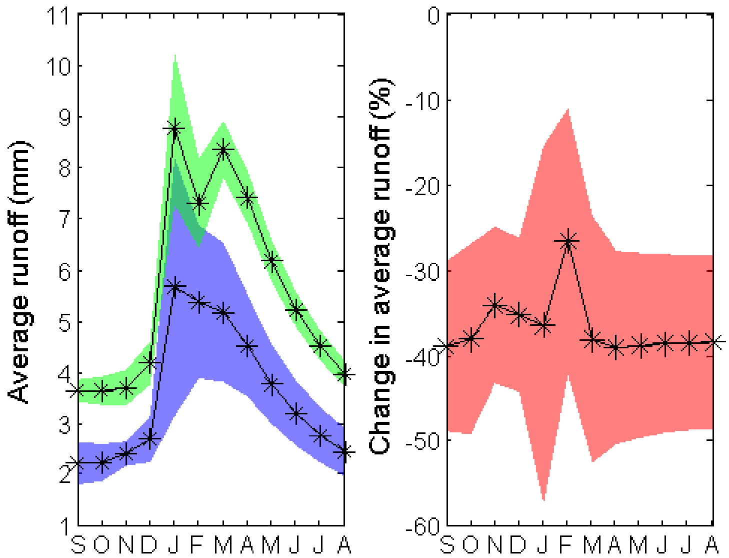

Figure 5-10: Projected change in average monthly runoff over the Chiba catchment as calculated by the CME. Green, blue and red colors are CME uncertainty intervals for the reference, future and relative change, respectively. Black line with black starts refers to the CME mean values

On an annual basis, the average annual runoff for the Thau catchment as predicted by the hydrological model for the reference period is ranging between 345 and 120 mm while it is projected to range between 338 and 80 mm.

Projected change in runoff in the Chiba catchment

Predicted runoff in the Chiba catchment for the reference and future periods, as well as the projected relative change and CME uncertainty prediction are given in Figure 5-10. The latter reveals that future runoff seasonal and monthly dynamic is very likely to remain similar to the reference period. Thus, no shift in the reference runoff timing is projected in the future. However, the predicted runoff monthly magnitudes for the future period are more uncertain than these in the reference period as easily depicted by the difference in the width of their respective CME uncertainty intervals (Figure 5-10 left panel). This predicted uncertainty is translated into large uncertainty in the calculated relative change of the average monthly runoff in 2050s with respect to the reference period (See right panel of Figure 5-10). While the mean CME projection suggests a decrease of the reference runoff by -34.45% and -39% in the wet and dry periods, respectively, the CME uncertainty interval suggests wider range of these values between [-11.5 and -57.4%] and [-27.85 and -50.3%], respectively. The aforementioned ranges of the projected relative change values reveal that larger uncertainty is projected in the wet period in comparison to the dry period. A similar statement is reported for projected change of precipitation over the Chiba catchment. Similar results are also reported in the Thau catchment regarding the direction of the projected uncertainty in the future runoff. On annual basis, the Chiba catchment is likely to lose between -25 and -48% of its annual reference runoff which has been estimated between 25 and 58 mm.

The projected changes in reference runoff for the Thau and the Chiba catchments revealed some similarity but also some differences. The similarity consists mainly in the general agreement about the projected decrease in monthly runoff across all the months of the year. Both catchments also show similar trend in the projected CME uncertainty interval of the relative change. The latter is found to be more uncertain as moving from dry to wet period. The main difference between the two catchments is related to both magnitude values and uncertainty range of the projected runoff. Projected runoff reduction in the Chiba catchment is likely to be more critical and more uncertain than in the Thau catchment. Two reasons can be behind this difference. The first one can be a direct consequence of the increase in temperature and decrease in precipitation which is more important in the Chiba catchment than in the Thau catchment. The second reason can be related to the difference in the hydrological regime between the two catchments. Indeed, the flow regime of the Thau catchment is highly influenced by the discharge dynamic of the Vène subcatchment which is considerably influenced by the karst contribution (Sellami et al., 2013a). Thus, non-explicit consideration of climatic change impact on groundwater flows may attenuate the projected amplitude of the runoff changes in this catchment. In contrast to the Thau, the hydrologic regime of the Chiba catchment depends in 90% on surface runoff. Therefore, the runoff is very sensitive to direct change in climatic conditions.

To investigate the possible relationships between the projected runoff and the other hydroclimatic indicators in both catchments, basic regressions are conducted but only the significant ones are represented. As it is shown in Figure 5-11, the projected runoff magnitude is heavily dependent on the project precipitation. This relationship is found strong with correlation coefficient $R > 0.90$ significant at 0.1% in both catchments. Thus, it is expected that a decrease in the projected precipitation will likely decrease the runoff.

While the role of precipitation in catchment runoff is dominant, SWC also shows high ($R > 0.90$) and significant correlation ($p\text{-value} < 0.001$) to the runoff evolution in both Thau and Chiba catchments (Figure 5-12). These relationships highlight the combined roles of precipitation and SWC in runoff process generation in the catchments under study. However, this is not to pretend that changes in runoff are only related to changes in precipitation and SWC. ETP can also play an important role in the catchment water balance. However, due to the nonlinearity of the hydrological processes occurring within the catchments, and also to their complexity to be effectively represented within the hydrological model structure, the effect of one or many factors cannot be visible.

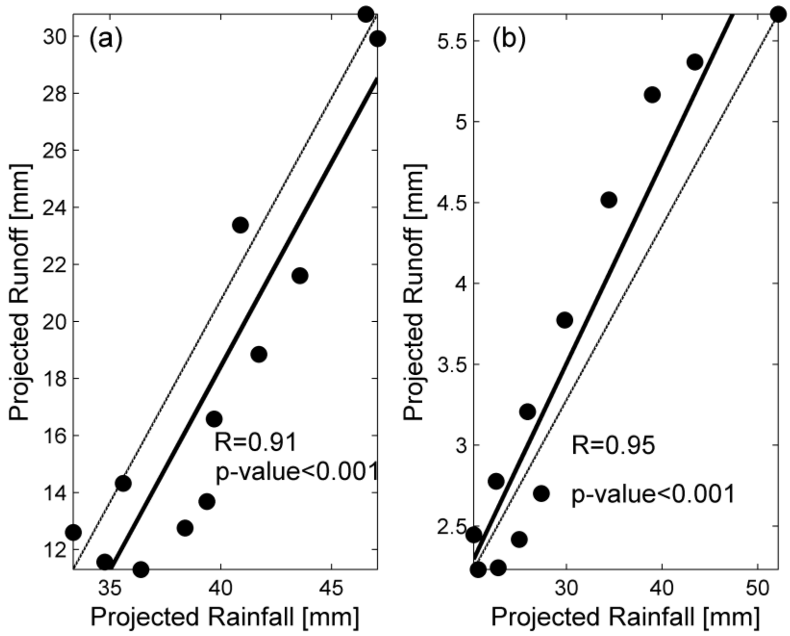

Figure 5-11: Relationships between projected precipitation and runoff in the future period for the Thau (a) and the Chiba (b) catchments

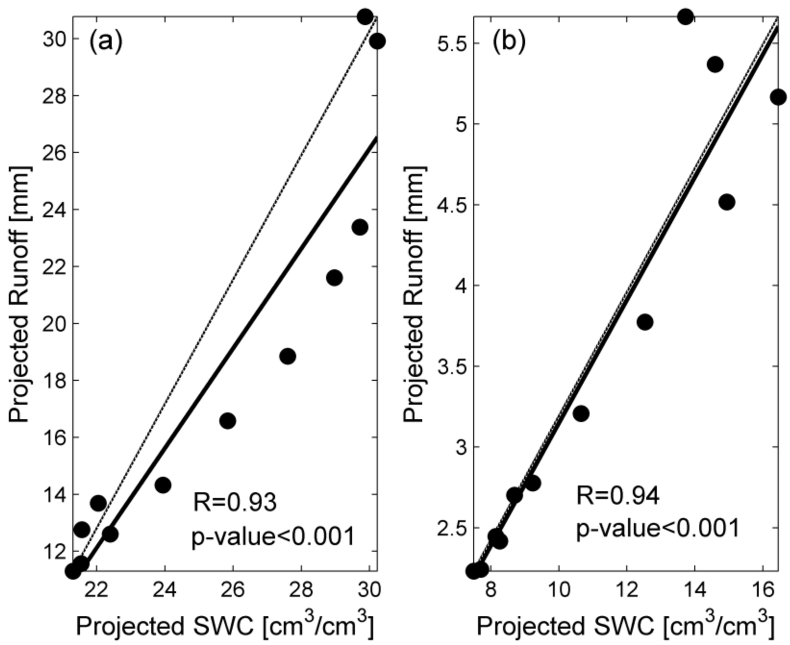

Figure 5-12: Relationships between projected SWC and runoff in the future period for the Thau (a) and the Chiba (b) catchments

5.4.6 *Projected changes in low flow and high flow days*

Projected changes in low flow and high flow days in the Thau catchment

The predicted values and uncertainty interval of the numbers of low flow and high flow days for the reference and future periods as calculated by the CME for the Thau catchment are given in Figure 5-13. Low flow days correspond to days where the reference flow magnitude is less than the discharge value at FDC flow percentile Q70 while high flow days correspond to days where the reference flow magnitude is higher or equals to the discharge value at FDC flow percentile Q10.

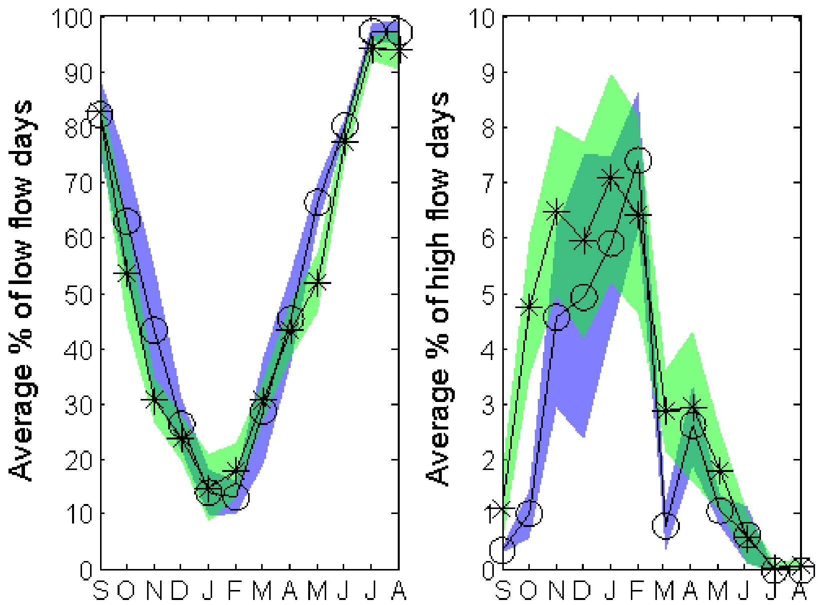

Figure 5-13: Predicted low flow and high flow days for the reference and future periods over the Thau catchment. Green and blue colors are the CME uncertainty interval for reference and future, respectively. Black line refers to the CME mean value, with stars for the reference and with circle for the future periods.

The monthly variability and seasonality of the low flow days and high flow days as predicted by the CME in the reference period is likely to be well preserved in the future period. Low flow days are more frequent in the dry period than in the wet period. Conversely, high flow days are more frequent in the wet period than in the dry period. This is true for both simulations time periods. This suggests that the actual timing of the low flows and high flows in the Thau catchment will not change in the future. However, the monthly frequency of the reference low flow days is projected to increase by 2050s except from January to March where it is likely to remain steady. The projected increase in the reference low flow days is not significant and rarely exceeds 7%. On the other hand, there is a clear tendency to decrease in the reference number of days with high flows in the future. This reduction is more evident in the wet period than in the dry period (Figure 5-13). These results are consistent with the projected reduction in precipitation and runoff over the Thau catchment.

Projected changes in low flow and high flow days in the Chiba catchment

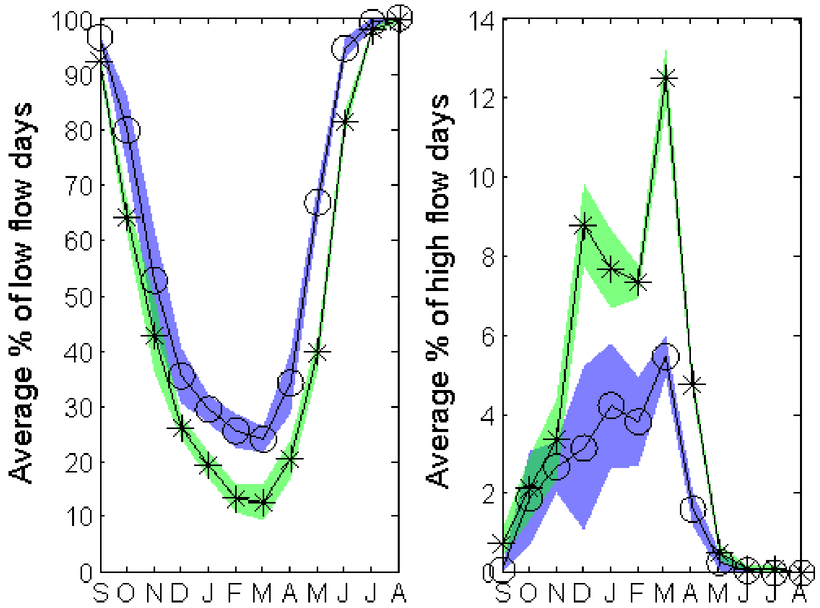

Figure 5-14: Predicted low flow and high flow days for the reference and future periods over the Chiba catchment. Green and blue colors are the CME uncertainty interval for reference and future, respectively. Black line refers to the CME mean value, with stars for the reference and with circle for the future periods.

While the number of reference low flow days per month in the Chiba catchment is expected to increase, high flow days are expected to decrease by the 2050s. It is likely that the temporal dynamic for both indicators will remain unchanged (Figure 5-14). The number of low flows days in the Chiba catchment is projected to increase by 20 to 90% of the reference values during the wet period, particularly during January to March, while it is expected to be less significant during the dry period and lower than 10% of the reference values. This suggests that the number of low flows days is expected to be prolonged in all the months of the year in the Chiba catchment by the 2050s. The number of the reference high flow days will be significantly reduced in particular during the wet period with a magnitude ranging between -11 to -66% with an average of -45% of the reference values. During the summer season reduction in the high flows days is projected to be higher than 90% of the reference values, but this is more related to the extremely low values of high flows days during this season.

There is a strong and significant relationship between the projected numbers of low flow days and temperature in the Thau and the Chiba catchment (Figure 5-15). It is very likely that a projected increase in average monthly temperature will result in an increase in the number of low flow days per month for the future period as expressed by the high correlation $R > 0.90$ significant at 0.1% in both catchments. On the other hand, a negative trend between the projected rainfall and the number of low flow days is found in both catchments (Figure 5-17). A decrease in precipitation is likely to result in an increase in the frequency of low flow days in both catchments. However, it seems that the effect of precipitation is weaker and less significant than temperature. Nevertheless, the combination of the projected decrease in precipitation and increase in temperature is likely to have strong effects on the projected increase of the low flow indicator in the study sites. For high flow days, a negative but strong and significant relationship with the projected increase in temperature over the Thau and the Chiba catchments is found (Figure 5-16). Conversely, a decrease in precipitation is likely to decrease the high flow days monthly frequency in both catchments (Figure 5-18). Although precipitation exerts strong effects on the high flow indicator, its effects seem to be less significant than those of temperature.

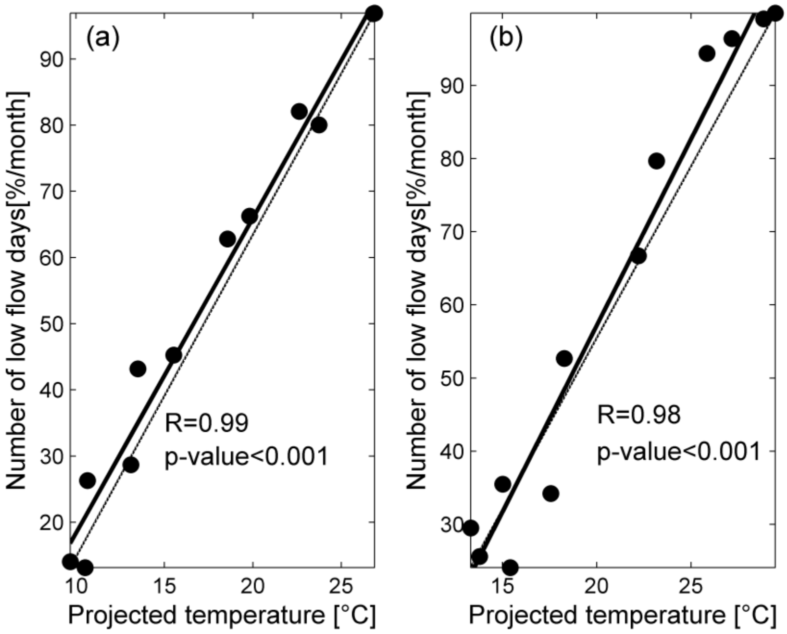

Figure 5-15: Relationships between the projected temperature and the number of low flow days for the Thau (a) and the Chiba (b) catchments

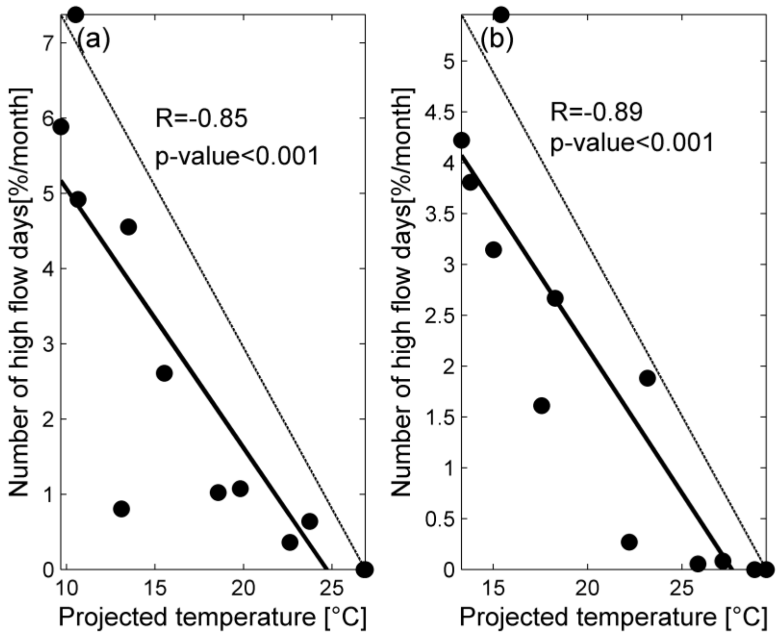

Figure 5-16: Relationships between the projected temperature and the number of high flow days for the Thau (a) and the Chiba (b) catchments

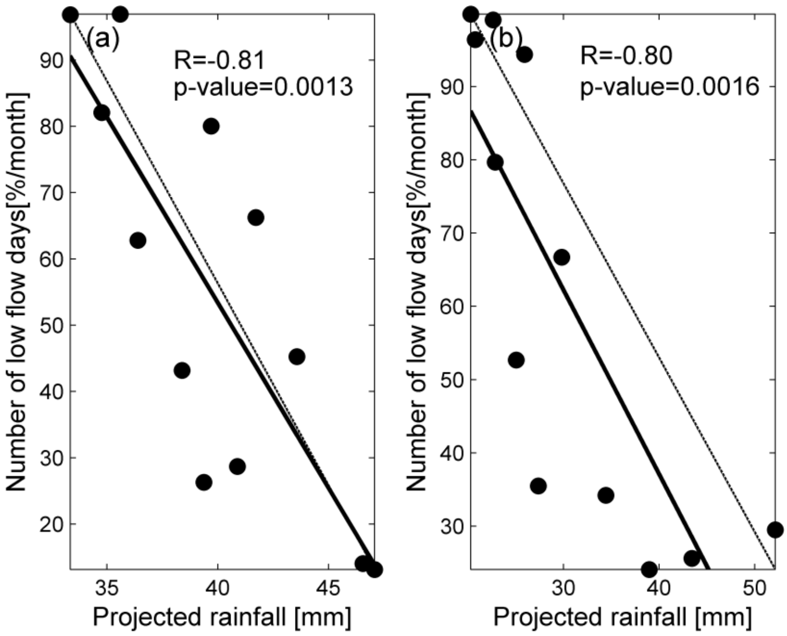

Figure 5-17: Relationships between the projected rainfall and the number of low flow days for the Thau (a) and the Chiba (b) catchments

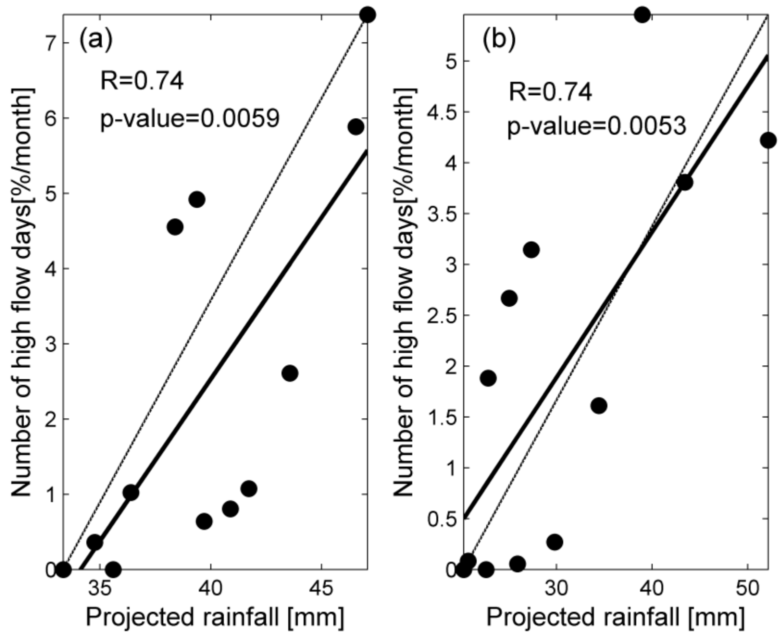

Figure 5-18: Relationships between the projected rainfall and the number of high flow days for the Thau (a) and the Chiba (b) catchments

In both Thau and Chiba catchments the combined effects of the projected increase in temperature and decrease in precipitation is likely to reduce the numbers of high flow days but also increase the frequency of the low flow days per month. In others words, for both catchments it is expected that the current dry condition will be prolonged and the wet period will be shortened in the 2050s. These results are in line with theses reported by Döll and Zhang (2010) at the Mediterranean scale.

5.4.7 Projected changes in flow duration curve (FDC)

The FDCs are constructed by considering 30 years daily discharge values. For each subcatchment of the Thau, the FDCs are constructed than summed together at each flow percentile (1%) to obtain general FDCs for the entire Thau catchment for the reference and the future periods.

Projected change in FDCs for the Thau catchment

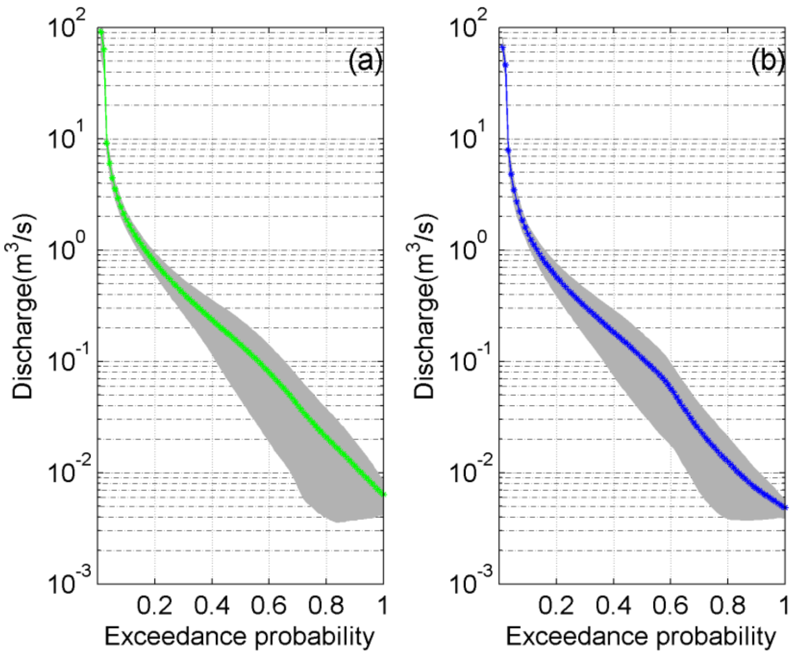

Figure 5-19: FDCs mean and uncertainty interval as derived by the CME for the reference (a) and the future (b) periods for the Thau catchment

Figure 5-19 displays the 30 years daily FDCs for the reference and future periods as projected by the CME for the Thau catchment. The shape of the predicted FDC is likely to remain similar to the one of the reference period suggesting that there will be no changes in the main drivers of the hydrological processes within the catchment. The CME predicted FDCs suggest a sustained baseflow ranging between 0.0041 and 0.0086 $m.s^{-1}$ with an average of 0.0064 $m.s^{-1}$ for the reference condition while for the projection period the values range between 0.0039 and 0.0058 $m.s^{-1}$ with an average value of 0.0048 $m.s^{-1}$. This sustained baseflow is due to the contribution of the Vène catchment which is the only perennial river in the Thau catchment.

To better compare the reference FDCs to the projected ones, Figure 5-20, shows the mean FDC and the relative change between the reference and the future periods for each 1% flow percentile as calculated by the CME for the Thau catchment.

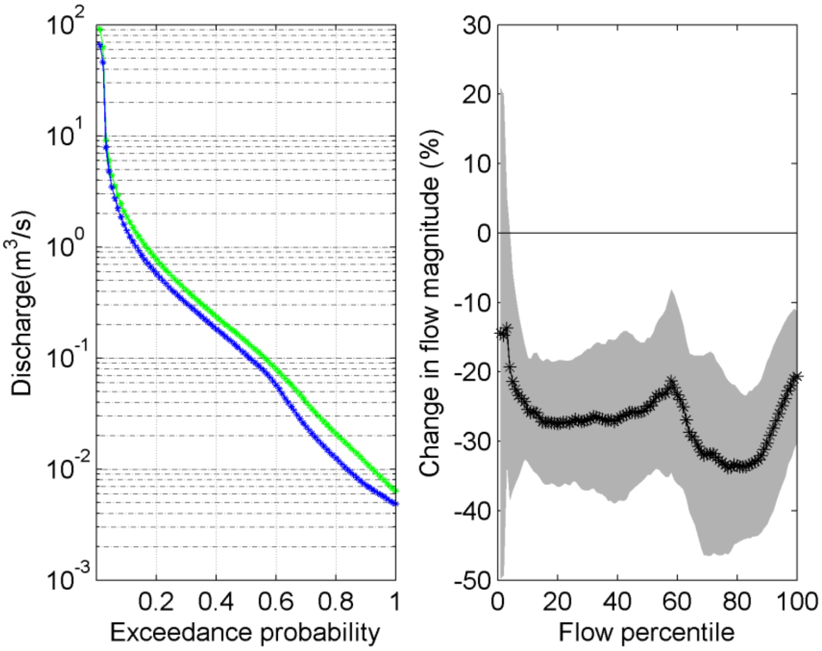

Figure 5-20: CME mean FDCs for the reference (green) and future period (blue) and mean projected relative change for each 1% flow percentile (black) and CME uncertainty interval (grey) for the Thau catchment

When comparing the CME mean reference FDC to the projected one it is likely that the Thau catchment will experience a decrease in the daily discharge magnitude in the future. All the projected FDC flow percentiles are lower than these in the reference period. This is also reflected in the negative evolution of the mean CME relative change across all the FDC percentiles. However, the CME projected relative change shows large uncertainty regarding the magnitude of change, in particular for the high flows (≤Q10) where the values range between [-50% to +20%] of the reference values. This is because some climate models predict a reduction in the high flows magnitudes while others suggest an opposite trend in the sign of changes reflecting the large uncertainty in the flood regime that the Thau catchment is likely to have in the future. Uncertainty in the predicted high flows can be related to the uncertainty in the projected rainfall by the climate models especially in the wet season when most of the high flows occur. Medium flows are likely to be reduced by a range of [-10% to -37%] while low flows are projected to decrease by a range of [-10% to -46%]. Despite this uncertainty, the mean CME relative change suggests an expected reduction in the streamflow availability which is in accordance with the projected reduction in precipitation and runoff in the Thau catchment.

Projected change in FDCs for the Chiba catchment

In Figure 5-21 the 30-years daily FDCs as predicted by the CME for the reference and the future periods have similar shape and trend across all the flow percentiles suggesting that no changes are projected in the main drivers of the hydrological processes within the catchment; high flows will not probably be sustained for a long period and will occur as flash floods as response to rainfall events while low flows reflect the intermittent regime of the flow. In contrast, to the Thau catchment, the predicted CME mean FDCs for the Chiba catchment in both projection periods are hardly distinguishable from their respective uncertainty intervals. This is because there is less inter-climate models variability for the Chiba catchment than for the Thau catchment. Figure 5-22 clearly shows that the predicted CME mean FDC for the reference period is projected to decrease in the future period. The estimated relative change magnitude in each flow percentile shows large uncertainty in particular for high flows. Reference high flows changes are expected to range between [+30 to -70%] while medium and low flows are expected to decrease by [-20 to -40%] and [-10 to -40%], respectively.

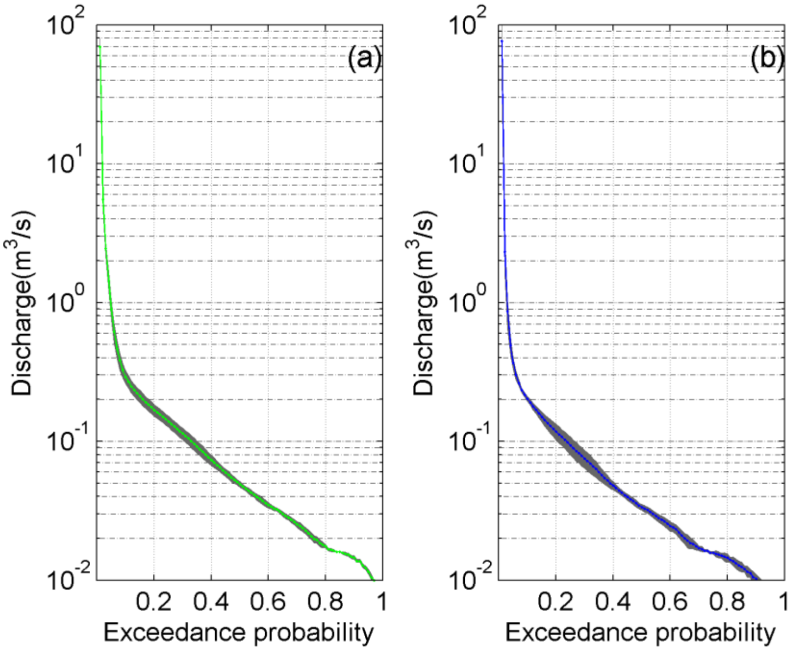

Figure 5-21: FDCs mean and uncertainty interval as derived by the CME for the reference (a) and the future (b) periods for the Chiba catchment

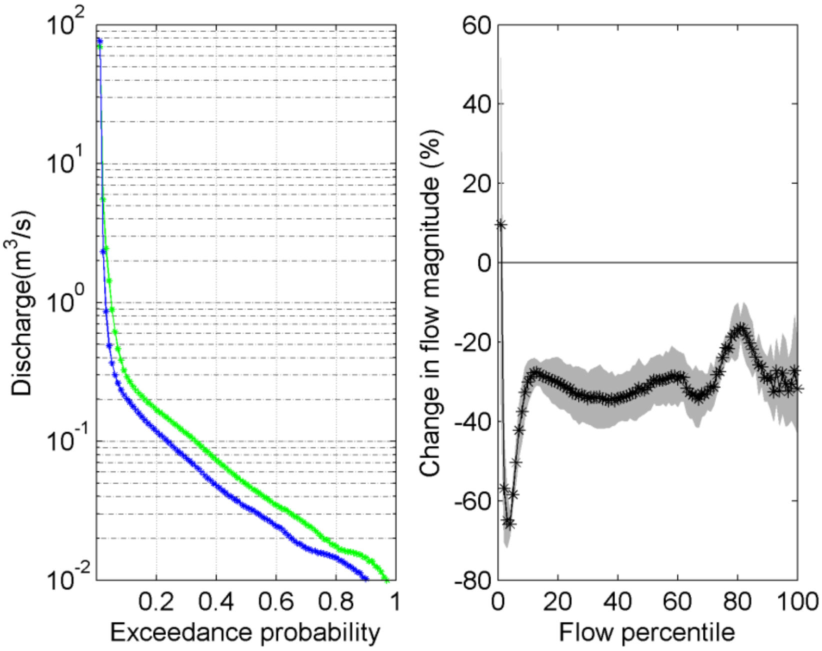

Figure 5-22: CME mean FDCs for the reference (green) and future period (blue) and mean projected relative change for each 1% flow percentile (black) and CME uncertainty interval (grey) for the Chiba catchment

In both Thau and Chiba catchments, CME projects a general decrease in the reference FDCs reflecting a possible reduction in the streamflow available for both catchments. However, the projected magnitudes of change in reference FDCs are highly uncertain particularly for high flows. This is true for both catchments. Indeed, FDC high flows are an indicator of catchment response to direct rainfall (Mohamoud, 2008). Thus, their uncertainty can be attributed to the one associated with the predicted precipitation. The projected increase in high flows are exclusively due to the extremes flow percentiles (1% and 2%) values which also can be related to outliers in precipitation. By considering of all flow percentiles within the high flows segment, the average reference high flows are projected to decrease by [-20% and -43%] by the 2050s in the Thau and the Chiba catchments, respectively.

The projected decrease in the reference discharge for the Thau and the Chiba catchments fall within the range of -26% and -54% estimated by Lespinas et al. (2014) for Mediterranean French coastal river basins for the future period of 2071-2100 in comparison to 1961-1990.

5.4.8 Projected changes in magnitude of flow extremes durations

Extreme flow conditions (minimum and maximum) for various time duration (7, 30 and 90 days) are taken from moving averages of the appropriate length calculated for every projection. These metrics are important not only for water resources operational management (e.g. dam construction, droughts and floods protection) but also for aquatic ecosystems, agriculture, domestic and industrial sectors (Richter et al., 1997; Gain et al., 2011).

Changes in the flow extremes for the various time durations and the CME uncertainty between the reference and the future periods for the Thau and Chiba catchments are illustrated in Figure 5-23. As the time days duration increases minimum flow magnitudes increases because it contain more non-zero flow values. The results indicate that maximum and minimum flow magnitudes of the different time durations are likely to experience a significant decrease at the horizon of 2050 for both catchments.

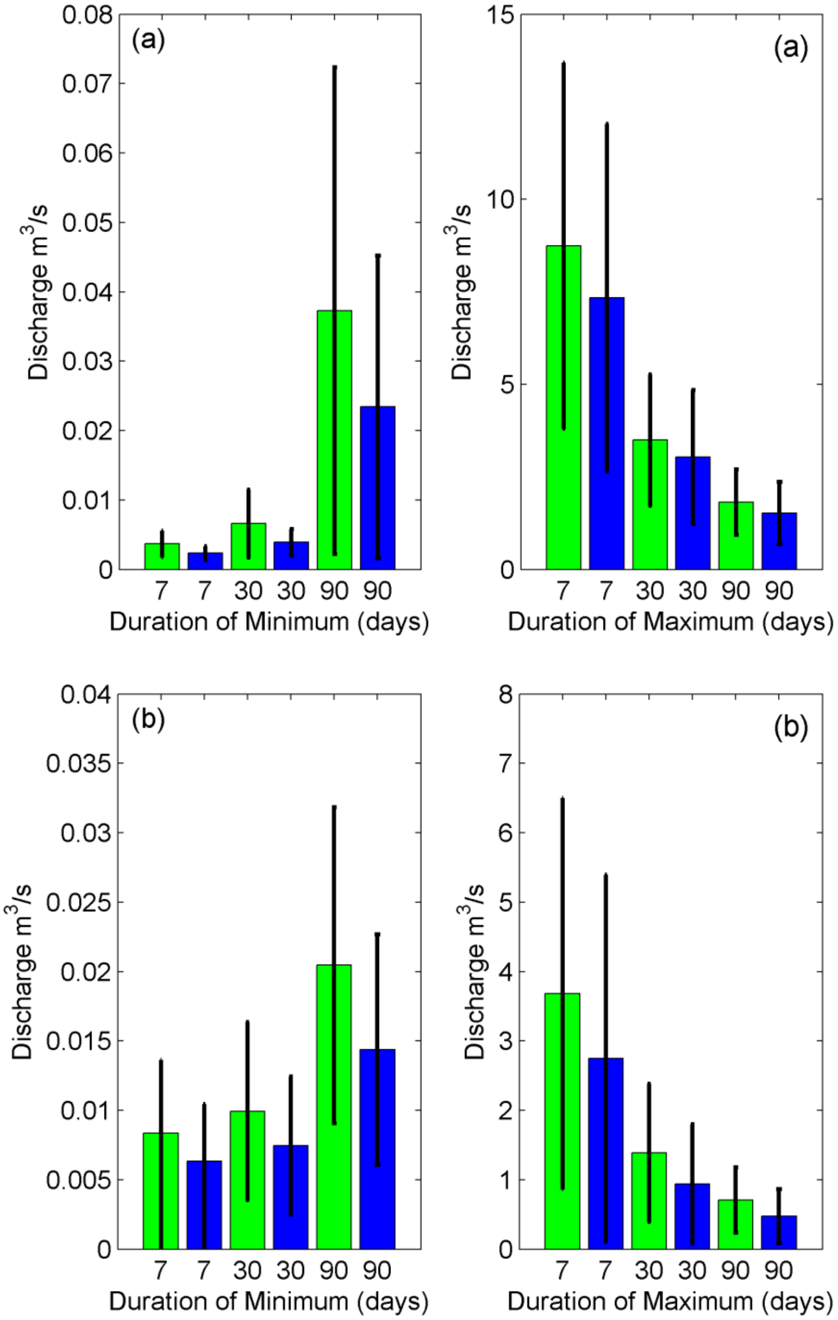

Figure 5-23: Changes in minimum and maximum flow extremes for various time durations for the Thau (a) and the Chiba (b) catchments. Green color is for reference period, blue color is for future period and error bar is CME uncertainty interval.

The annual average extremes flows for the various time durations are expected to decrease with the most critical reduction is likely for the 90-days duration with an average of -30% for the Chiba catchment against -37% for the Thau catchment. For the same time duration, the annual average maximum flow is likely to decrease by an average of -16% for the Thau catchment against -33% for the Chiba catchment. These projected average relative changes in extreme flows conditions can be more dramatic if the possible range of the values within the uncertainty interval is considered as shown in Figure 5-23. The results suggest that drier conditions with notable reduction in average annual flow extremes are likely to occur in the future period in both Thau and Chiba catchments.

5.4.9 Overall picture of climate change impacts

In Figure 5-24 are summarized the average CME uncertainty projected change for the selected hydrological metrics for the Thau and the Chiba catchments. The projected degree of alteration is evaluated based on a subdivision of the projected magnitude of change into several intervals as given in Table 5-3. The projected trend in all hydrological indicators due to climate change in the Thau catchment is quite similar to the one in the Chiba catchments. In both catchments there is a clear tendency towards a decrease in all the reference indicator values except for temperature and low flow days indicators (LFD). The latter indicators are expected to increase but with moderate to high degree of alteration with respect to their reference values in both catchments. The projected alteration level in average precipitation is likely to induce an additional alteration level in average catchment runoff. The latter is projected to be the most altered water balance indicators with moderate to very high degree reduction in the Thau and the Chiba catchment, respectively.

Table 5-3: Overall degree of alteration intervals

Magnitude of projected change	Degree of alteration
≤5%	Very low
5% < and ≤10%	Low
10%< and ≤20%	Medium
20%< and ≤30%	High
>30%	Very high

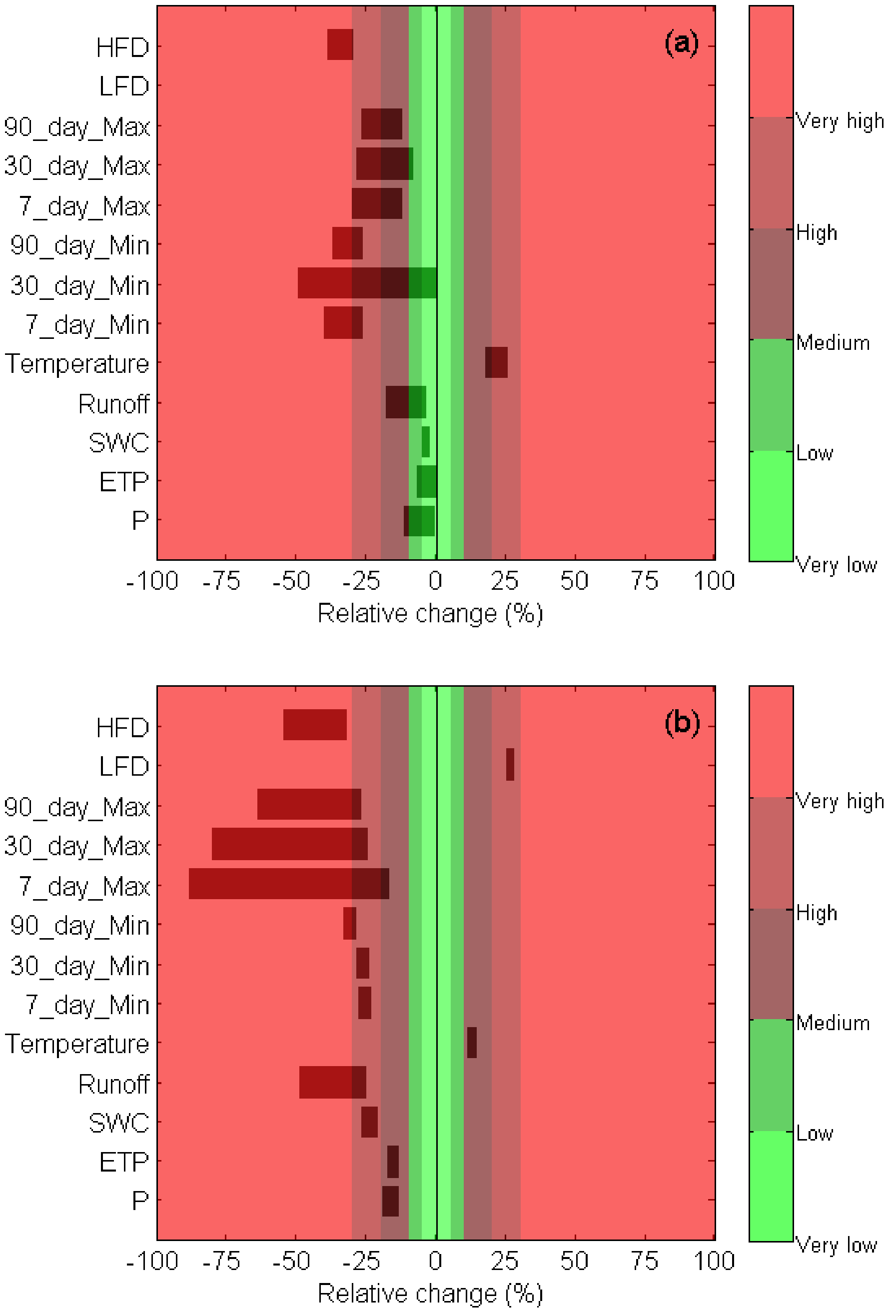

Figure 5-24: Overall picture of CME projected change in the hydrological indicators for the Thau (a) and the Chiba (b) catchments

Average flow extremes frequencies and magnitude at various time durations are likely to experience moderate to high degree of alteration in the Thau catchment while they are expected to be highly and very highly altered in the Chiba catchment. In general, climate change is likely to exert stronger negative impacts on the flow regime of the Chiba catchment than on the Thau catchment.

5.5 Conclusions

The use of multi-climate models ensemble driven by the plausible emission scenario A1B (IPCC, 2007) in a conjunction with the hydrological model SWAT has allowed to quantify the possible impacts of climate change on the hydrologic regime of the Thau and the Chiba catchments. The results of this study show that climate change at the horizon of 2050 is likely to induce moderate to severe changes on several flow facets related to magnitude, frequency and extremes of the flow in both catchments. In both catchments, the projected decrease in precipitation, together with the projected increase in temperature, is likely to reduce soil water content and actual evapotranspiration with stronger alteration in catchments runoff. It is also demonstrated that high and low flow frequency, as well as flow extremes magnitudes at various time durations, are expected to decrease in both catchments in 2050s. These findings at the catchment scale converge with the general agreement about the projected alterations in rivers flow regime at the Mediterranean scale.

The strongest impacts of climate change are likely to be for the Chiba catchment where the prevailing hydrological processes are mainly related to surface runoff. In the Thau catchment, the flow regime is considerably influenced by the groundwater contribution which may attenuate the real impact of climate change. Therefore, the impact magnitude of the climate change within the same climatic region (e.g. Mediterranean climate regime) varies from one catchment to another depending on the local hydrological processes governing the catchment functioning and considered in the assessment study.

The quantification of the impact of climate change is not straightforward due to the inherent uncertainty in the predicted results. Although there are several uncertainty sources that propagate in a cascade throughout the different steps of the methodology, the considered uncertainty in this study is only linked to the climate projections through the use of multi-climate models. Thus, hydrological parametric uncertainty was neglected. This possibly underestimated the prediction uncertainty in the final results. Therefore, the results should be considered with care especially in the context of Mediterranean catchments where these uncertainties may vary locally.

The possible impacts of change in the flow regime induced by change in climate of the Thau and the Chiba catchment are manifold. Changes in the natural flow conditions may severely impact the ecosystem and the environment leading to considerable socio-economic impacts. By providing a complete picture of the possible impacts of climate change on the flow regimes of the Thau and the Chiba catchments, this study can help to guide the water resources management actions to mitigate these effects on the hydrologic regime and, therefore, on the ecosystem of the Thau and the Chiba catchment.

CHAPTER VI

6 Comparison of hydrological and climate models uncertainties in climate change impact assessment

6.1 Abstract

While it is widely admitted that both hydrological and climate models are prone to uncertainty, combining both uncertainty sources is still not a common practice in climate change impact studies. We propose an approach for propagating climate models uncertainty through hydrological parameter uncertainty and assessing each respective uncertainty sources. An ensemble of "behavioral" parameter sets of the GLUE method is approximated by feed-forward artificial neural networks (FF-NNs). Then, the latters are driven by an ensemble of climate multi-models (CME) for predicting changes in monthly runoff and flow duration curves. The study is developed for the Thau and the Chiba catchments. The predicted uncertainty is partitioned into CME uncertainty and hydrological parametric uncertainty. The study reveals that CME uncertainty is dominating hydrological parameters uncertainty when moving from drier to wetter conditions. This suggests that particular attention should be given to the seasonality when assessing uncertainty in climate impact assessment studies.

6.2 Introduction

Assessment of climate change impacts on water resources is usually conducted with a conjunctive use of hydrological and climate models. However, it is well established that both forecast models are prone to considerable uncertainties that need to be addressed to make an appropriate use of the prediction results (Tebaldi and Knutti 2007; Bhat et al., 2011; Koutroulis et al., 2013). In both hydrological and climate models, uncertainties stem from several sources including parametric and model structure uncertainty. As with climate models, it is widely accepted that no single optimum hydrological parameter set exists to approximate the real catchment response and, thus, parameter uncertainty is recognized as one of the most important source of hydrological modelling uncertainty (Beven 2006; Sellami et al., 2013a). However, it is still not a common practice to combine a multi-models climate ensemble approach with hydrological model parameter uncertainty when assessing the impact of climate change on water resources. This can be due to the various issues and challenges associated with the application of such approach. The complexity in the interaction and the propagation of different error sources in climate and hydrological modelling makes the prediction uncertainty assessment challenging, despite the existing wide panoply of techniques and approaches. Other technical issues can also be related to the high computational cost when combining several climate models with different hydrological model(s) parameterizations.

Teng et al. (2011) showed that uncertainties stemming from fifteen climate models are larger than theses originating from five hydrological models in several south eastern Australian catchments.
A similar statement was reported by Arnell (2011) while assessing future hydrological evolution in the UK. Bastola et al. (2011) have assessed parameter and structural hydrological model uncertainty in climate change impact studies on four Irish catchments. They have reported the remarkable role of hydrological model uncertainty and have suggested that they should routinely be considered in impact studies. Kwon et al. (2012) have quantified and compared the uncertainty associated with climatic and hydrological models in seasonal streamflow forecasts in Northeastern Brazil. In contrast to the study of Bastola et al. (2011), they suggested that the uncertainty of the climate model is predominant in comparison to the hydrological parameter uncertainty. The different conclusions in aforementioned studies are due to the fact that the climate and hydrological models, uncertainty sources and studies scale are different from one application to another. Thus, the role of the different uncertainty components in the hydrological impacts of climate change prediction is still not well investigated.

The objective of this chapter is therefore to quantify and partition the prediction uncertainty of the climate change impact as assessed by a combined CME and hydrological multi-parameter sets ensemble on the flow of Mediterranean catchments. In a first step, different parameterizations of the hydrological model are driven by the CME. Then, the average projected changes on monthly runoff and FDCs indicators are calculated and the predicted uncertainty is assessed. Finally, the predicted uncertainty is partitioned into CME uncertainty and hydrological parametric uncertainty.

6.3 Material and methods

6.3.1 Artificial Neural Networks as substitute to the SWAT model

To simultaneously consider the SWAT parameter uncertainty with the CME uncertainty, each of the identified “behavioral” parameter set needs to be driven by each of the CME output for the reference and future period. However, such approach is computationally intensive and time consuming. To alleviate the task, the SWAT “behavioral” simulations have been approximated with artificial neural networks models (ANNs).

ANNs in Rainfall-Runoff modelling

ANNs, are usually presented as artificial systems inspired by biological neural network that are able to compute and solve complex non-linear systems (Wang et al., 2006). In the context of rainfall-runoff (R-R) modelling, ANNs fall into the category of empirical black-box models where the physical laws that govern the R-R processes are not considered (Shamseldin, 2010). In comparison to the SWAT model, ANNs have faster execution time and are more parsimonious in terms of data requirements (Zhang et al., 2009). Several studies have reported the robustness and effectiveness of ANNs in R-R modelling and forecasting (Shamseldin et al., 1999; Wang et al., 2006, among others).

Structure and principles of the selected ANNs

One of the most popular forms of ANNs used in R-R forecasting is the three-layered feed-forward neural network (FF-NN) which consists of an input layer, one hidden layer and one output layer interconnected by a number of computational elements called neurons (Wang et al., 2006; Zhang et al., 2009a; Shamseldin, 2010). In the FF-NN, the information flows from the input to the output layer in one direction without any feedback (Figure 6-1).

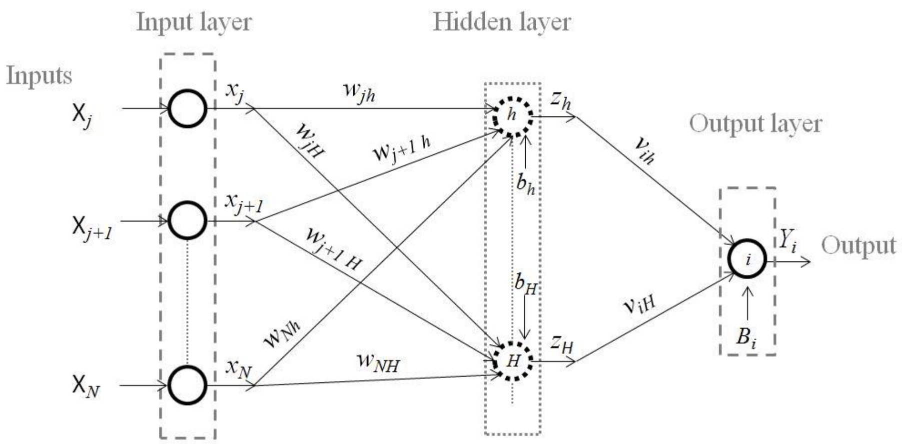

Figure 6-1: Architecture of the Multi-layer Feed-Forward Neural Network used for rainfall-runoff forecasting

At the entrance of the FF-NN, each external input is assigned to a neuron in the input layer but no processing is taking place at this stage, it simply feeds the data into the FF-NN. In the present study, the input layer consists of four neurons corresponding to the external input signals of daily precipitation, maximum and minimum daily temperature, and precipitation of the previous day. The latter variable is added to the input signals as an indirect indicator of the hydrological state of the catchment. Others studies have shown that the use of hydrological state indicators (e.g. previous values of discharge, evaporation time series, etc.) as external input signal can improve the ANNs performances (De Vos and Rientjes 2005; Shamseldin, 2010).

The connection between each hidden neuron and all the input neurons is expressed as the summation of the weighted outputs from the input neurons. A bias value is added and the results are processed by the hidden neuron to provide a single output using a non-linear transfer function. The mathematical functionality of a hidden neuron can be expressed as:

$$Z_h = f(z_h) = f\left(\sum_{j=1}^{N} w_{hj} x_j + b_h\right) \qquad \text{Equation 6-1}$$

where Z_h is the output of the h^{th} hidden neuron for h going from 1 to H, with H is the total number of the neurons in the hidden layer, w_{hj} is the connection weight between the h^{th} hidden neuron and j^{th} input neuron for j going from 1 to N, with N is the total number of neurons in the input layer, x_j is the output of the j^{th} input neuron, b_h is the bias associated with the h^{th} hidden neuron, and f ( ) is the activation function which is a non-linear transfer function that is commonly chosen to be the tan-sigmoid function which is also used in this study.

$$f(z_h) = \frac{2}{1+e^{-2z_h}} - 1 \qquad \text{Equation 6-2}$$

Unlike the input layer, the number of neurons in the hidden layer is unknown a priori and it has to be estimated using either automatic procedures (e.g. pruning and constructive algorithms) or by trial-and-error approaches which is by far the most common choice (Wang et al., 2006). The latter approach is also used in this study and the "optimal" hidden neurons number is set to ten.

In the output layer each neuron receives the outputs from the previous layer and processes the data similarly to the hidden neuron to produce the final network output according to

$$Y_i = f(y_i) = f\left(\sum_{h=1}^{H} v_{ih} Z_h + B_i\right) \qquad \text{Equation 6-3}$$

where Y_i is the output of the ith neuron in the output layer for i going from 1 to I, with I is the total number of the neurons in the output layer, v_{ih} is the connection weight between the ith output neuron and hth hidden neuron, Z_h is the output of the hth hidden neuron, B_i is the bias associated with the ith output neuron. In the present study, one single output neuron is used.

Training and validation of the selected ANNs

The constructed FF-NN is trained (calibrated) using the Levenberg-Marquardt Backpropagation procedure which seeks to reduce the error between the FF-NN output and the target data by updating the weights and the bias values. To appropriately stop the training and to ovoid an overtraining (the neural network starts learning or describing the noise in the data instead the underlying relationship between the input and output) or undertraining (the neural network does not learn all the information in the data) of the FF-NN, the data available are split into three sub-data called training set, cross-validation set and test set. The first sub-data set have been used to train the neural network by considering 70% of the available data. The remaining 30% of the data have been evenly divided between the second and the third sub-data sets which have been used to stop the learning process and to validate the performances of the trained network.

FF-NNs for the Thau and the Chiba catchments

In this experiment, only the Vène and the Pallas catchments are considered. This is because, together they account for more than 80% of the total water volume of the Thau catchment. As previously discussed in Chapter IV, the other small subcatchments have a negligible contribution to the Thau discharge. For each of the Vène and Pallas catchments, each selected “behavioral” SWAT simulation, identified from the GLUE yields a “behavioral” FDC at each corresponding catchment. Then, an average FDC is calculated by taking the mean at each FDC 1% flow percentile. This step is repeated until all the “behavioral” SWAT simulations are used at each catchment. For practical reasons the same number of “behavioral” SWAT simulations are considered for both Vène and Pallas catchments. Therefore, an ensemble of 3998 average FDCs is constructed for the entire Thau catchment (Figure 6-3a). For the Chiba catchment, the SWAT simulations derived from “behavioral” Mps obtained from the regionalization approach at the catchment outlet are considered and the ensemble FDCs is constructed (Figure 6-4a).

Because the aim in developing the neural network is to reproduce the SWAT “behavioral” simulations as consistently as possible, and because it was not possible to get satisfactory results by using only one single FF-NN for all the “behavioral” simulations, a FF-NN has been developed and trained for each single SWAT “behavioral” simulation for each of the Thau and the Chiba catchment. Thus, 3998 FF-NNs are constructed for the Thau against 166 FF-NNs for the Chiba. All the FF-NNs have the same structure (Figure 6-1) but differ in their parameters values (weights and biases). Subsequently, the FF-

NNs have been fed by the climate models for both time periods, allowing, first, to assess the projected change in the monthly mean runoff and in the 30 years daily flow duration curve (FDC), second, to quantify the overall prediction uncertainty, and, third, to partition this overall prediction uncertainty into hydrological and climate models uncertainty. The climate models used in this study are these presented and discussed in the previous chapter.

6.4 Results and discussions

6.4.1 Performances of the FF-NNs

The skills of the FF-NNs in reproducing the SWAT "behavioral" simulations based on NS and R^2 coefficients for the Thau and the Chiba catchments are given in Figure 6-2. For the Thau catchment, the NS values range between 0.75 and 0.97 with an average value of 0.91 while NS ranges between 0.80 and 0.95 with an average value of 0.90 for the Chiba catchment. The R^2 values are higher and exceed an average of 0.90 in both catchments. These results reflect the good performances of the FF-NNs in approximating the "behavioral" SWAT simulations at the Thau and the Chiba catchments. However, the discrepancy between the SWAT and FF-NNs in both catchments is mainly related to the low flows prediction. This may be due to several factors. First, it is possible that the best weights derived from the training of the FF-NNs do not necessarily lead to the best validation performances. In this regard, a better approach would be to consider an average of ensemble weights that lead to acceptable FF-NNs simulations rather than considering the best single weight. Another possible reason can be related to the sensitivity of the FF-NNs to the data preprocessing procedure which aims to rescale the data within the interval of the transfer function (Wang et al., 2006). Another plausible reason can be related to the SWAT performance itself. For instance, Sellami et al. (2013b) have shown that SWAT performed better in predicting high flows than low flows in the Chiba catchment. They have also pointed out the problem of the equifinality and the large uncertainty affecting the low flow in SWAT predictions in the Thau catchments.

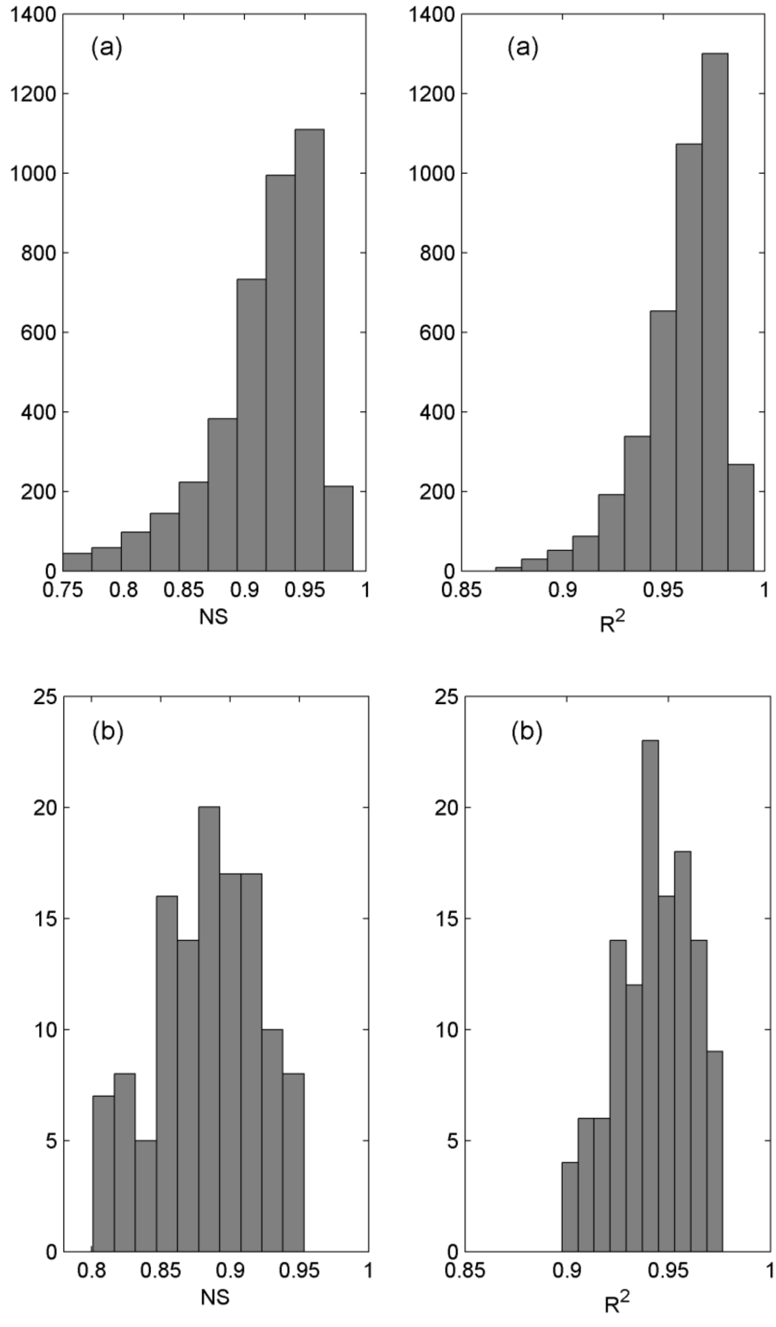

Figure 6-2: Distribution of NS and R^2 coefficients between SWAT and FF-NNs predictions for the Thau (a) and the Chiba (b) catchments

To be appropriately used as a substitute for the SWAT model, the developed FF-NNs should also be able to replicate the prediction uncertainty interval of the original model.

Figure 6-3 and Figure 6-4 compare the uncertainty interval of the SWAT predictions and the ensemble of the FF-NNs models in terms of FDCs of the Thau and the Chiba catchments, respectively Graphically, there is a good resemblance between the FF-NNs and the SWAT model simulations in both shape and uncertainty intervals of the predicted FDCs in the Thau and the Chiba catchments. The mean FDCs as derived by the FF-NNs ensemble are quite similar to the ones derived by the SWAT "behavioral" simulations ensemble in both study cases.

To quantitatively compare the uncertainty intervals of the SWAT and FF-NNs simulations, the standardized difference between the upper and lower predicted values for each 10% FDCs percentile is used as a dimensionless measure of the uncertainty interval width. For this purpose, Figure 6-5 shows the percentage deviation in the standardized width of the uncertainty interval for each 10% FDCs percentile predicted by the FF-NNs from these predicted by SWAT for the Thau (a) and the Chiba (b) catchments. The FF-NNs produce quite similar uncertainty intervals widths across the entire FDC percentiles to these produced by the SWAT model in the Thau and the Chiba catchments. Although the FF-NNs underestimate the low flow uncertainty intervals widths of the SWAT model, the differences remain lower than 5% in the Chiba. For the Thau catchment, FF-NNs slightly under-predict the SWAT uncertainty intervals in particular for flow percentiles Q>50%. Nevertheless, the deviation errors remain lower than 10% and do not exceed 3% for high flow percentiles.

The qualitative and quantitative performances assessments of the FF-NNs suggest that the latters can be a good substitute to the SWAT hydrological model in both Thau and Chiba catchments. Hence, their benefits in terms of rapid execution time, data parsimony and ease of use can be reliably exploited in R-R modelling in these catchments. Similar conclusions were also reported by Zhang et al., (2009a).

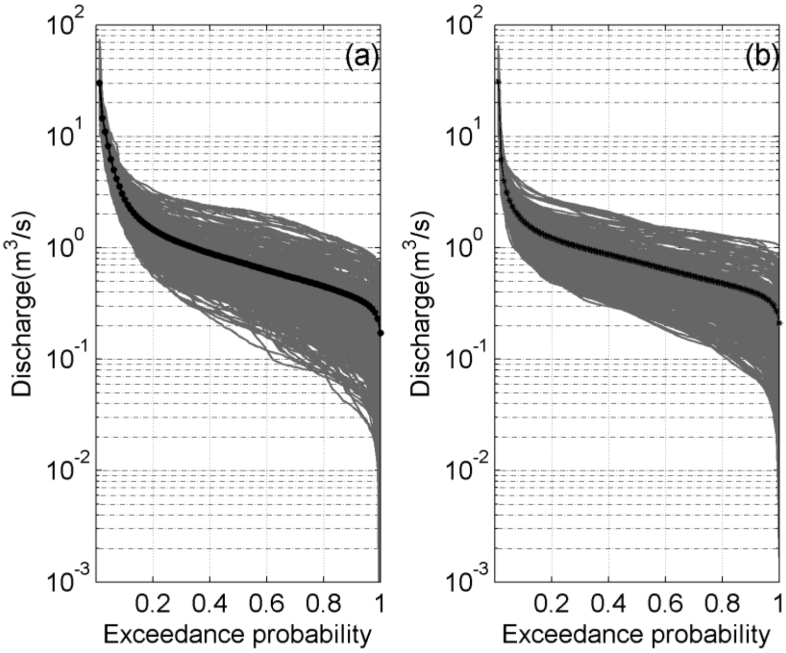

Figure 6-3: FDCs and uncertainty interval as predicted by the SWAT model (a) and FF-NNs models (b) for the Thau catchment

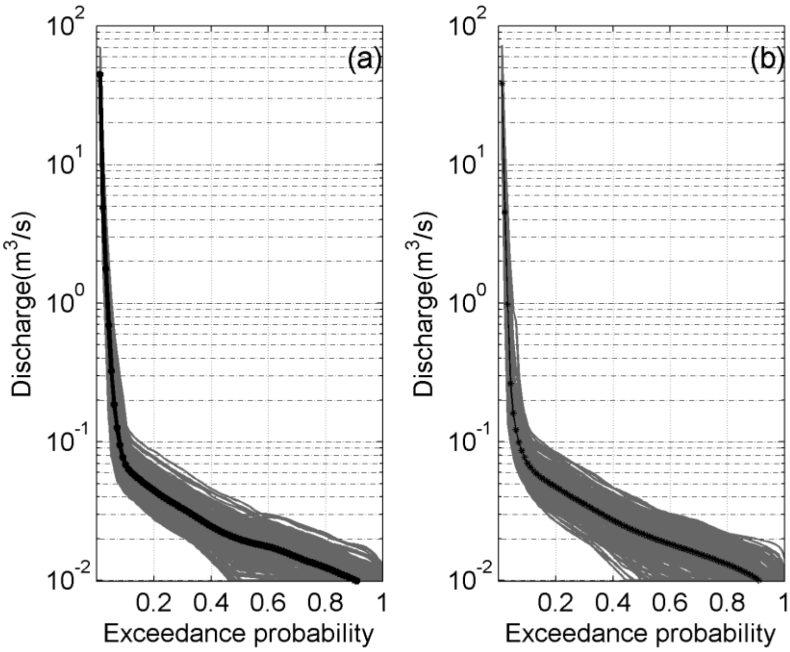

Figure 6-4: FDCs and uncertainty interval as predicted by the SWAT model (a) and FF-NNs models (b) for the Chiba catchment.

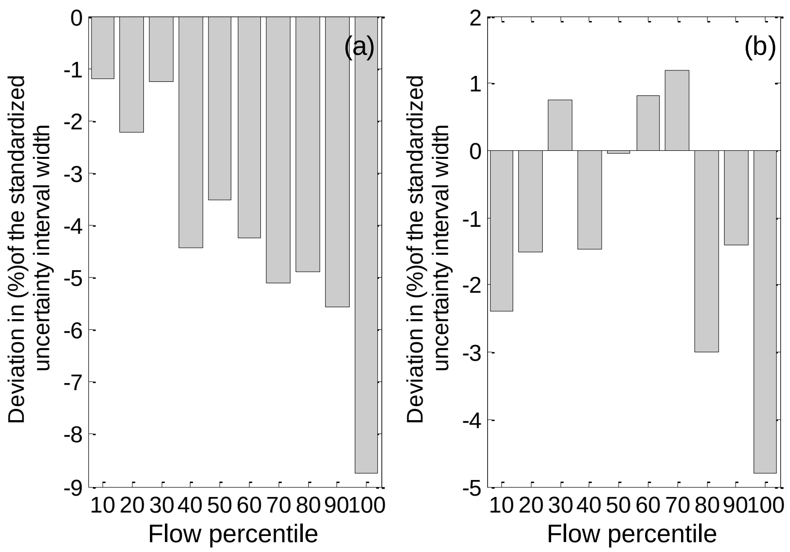

Figure 6-5: Measure of the deviation in (%) of the standardized uncertainty interval width of the FDCs flow percentiles predicted by the FF-NNs from these predicted by SWAT for the Thau (a) and the Chiba (b) catchments

6.4.2 Projected changes under hydrological parameter and climate models uncertainties

Given the appropriate substitution capacity of the FF-NNs to the SWAT model simulations, we further use the FF-NNs to assess the possible effect and uncertainty of climatic change on the Thau and the Chiba catchments discharge, considering both hydrological parameters and CME uncertainty sources. It should be noted that hereinafter the FF-NNs uncertainty is referred to as hydrological parameter uncertainty, while the uncertainty envelope resulting from the combination of hydrological parameter and CME uncertainties is referred as the average ensemble modelling uncertainty (AMU). To construct the average ensemble modelling uncertainty interval around the mean magnitude of change for a given hydrological indicator, the Equation (5-2) is modified to encompass both hydrological parameter and CME uncertainties as follow:

$$\delta_{\Delta v(m)} = \left[\frac{1}{NJ} \sum_{i=1}^{N} \sum_{j=1}^{J} (\Delta v_{ij(m)} - \overline{\overline{\Delta v}}_{(m)})^2 \right]^{1/2} \qquad \text{Equation 6-4}$$

where $\delta_{\Delta v(m)}$ is the root mean square difference for the element *m* (month or FDC percentile), *N* is the total number of climate models, *J* is the total number of "behavioral" hydrological model simulations (or total number of FF-NNs simulations), $\Delta v_{ij(m)}$ is the relative change in the hydrological indicator for the element *m* from the *j*th simulation driven by the *i*th climate model and $\overline{\overline{\Delta v}}_{(m)}$ is the mean relative change in the hydrological indicator for the element *m* from all the *J* simulations and all the *N* climate models. Thus, the AMU interval around the magnitude of change for a given hydrological element *m* is defined by $\overline{\overline{\Delta v}}_{(m)} \pm \delta_{\Delta v(m)}$.

The impact of climatic change and the average ensemble modelling uncertainty are assessed on the monthly flow runoff and on each ten flow percentile of the 30-yrs daily FDCs of the Thau and the Chiba catchments. These hydrological indicators are selected since they are hydrologically and ecologically meaningful and have been developed and used in literature in order to quantify the degree of hydrological alteration of catchment flow regime (Richter 1996; Olden and Poff 2003; Gao et al., 2009).

Projected change in catchment monthly runoff under hydrological parameter and climate model ensemble uncertainties

To illustrate the role of the different uncertainty sources (CME and Mps) on the ensemble modelling uncertainty we analyze the probability density functions (PDFs) of the relative change in monthly runoff for each individual climate model in the Thau (Figure 6-6) and the Chiba catchments (Figure 6-7). The figures illustrate that the PDFs in the dry period months are quite similar for each climate model indicating that the average ensemble modelling uncertainty is mainly dominated in these cases by hydrological parameters. On the other hand, the PDFs in the wet period months are different in shape and width reflecting the domination of climate model uncertainty in this case.

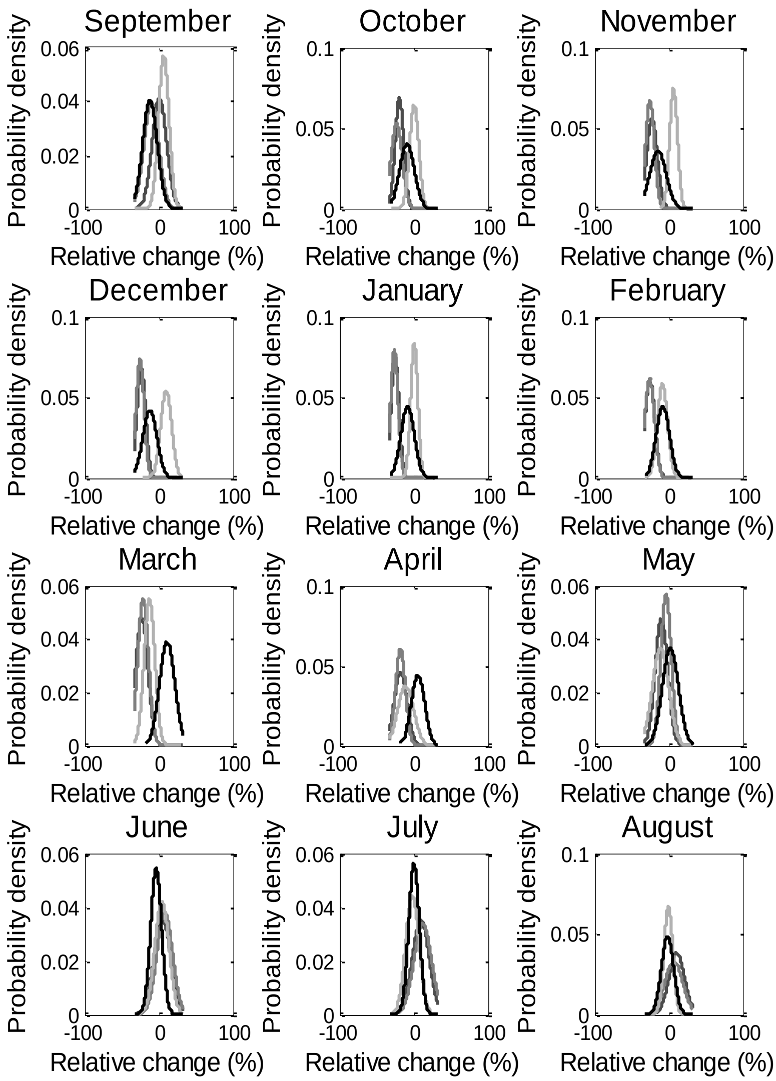

Figure 6-6: Probability density function (pdf) for the projected relative change in monthly flow magnitude derived from all FF-NNs simulations fed with each single climate model for the Thau catchment. Each curve is the pdf of the relative change calculated from the all the ensemble FF-NNs simulations driven by each climate model (4 climate models, hence, 4 pdfs).

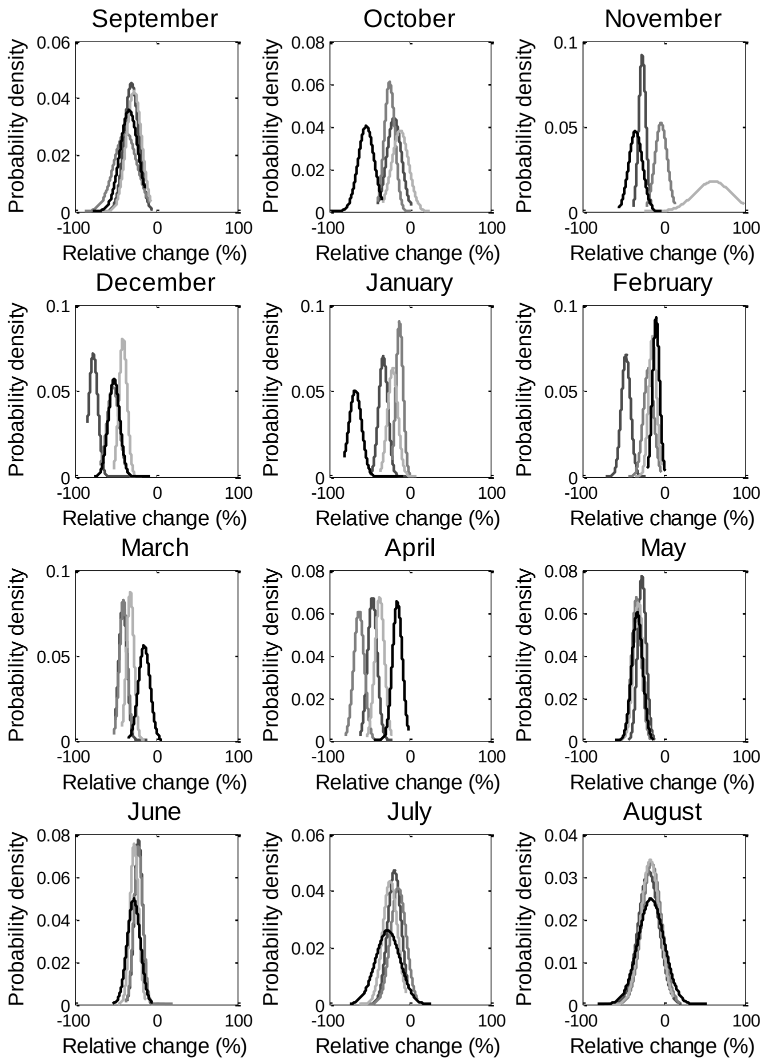

Figure 6-7: Probability density function for the projected relative change in monthly flow magnitude derived from all FF-NNs simulations fed with each single climate model for the Chiba catchment. Each curve is the pdf of the relative change calculated from the all the ensemble FF-NNs simulations driven by each climate model (4 climate models, hence, 4 pdfs).

Figures 6-6 and 6-7 also show that the uncertainty range in the relative change of the monthly runoff fed with each single climate model is larger than the constructed CME uncertainty interval as inferred from Figures 5-9 and 5-10. This is consistent with the results of Knutti (2010) who showed that the average uncertainty band of the multi-models ensemble may not resemble those of any single model. The difference can be explained by the method used to construct the average uncertainty interval which is based on the simple mean of all the models and, is thus, very sensitive to outliers. Furthermore, this approach is also sensitive to the performance of each single model and to its deviation from the ensemble mean. For instance, when calculating the average uncertainty interval of the multi-models ensemble using the simple approach as used in this study, all models are equally weighted and, thus “poor” models or predictions which can be considered as outliers can induce large shift in the ensemble mean value. To avoid this, some authors proposed weighted average approaches where models are weighted according their skills in reproducing either observed climate (Giorgi and Mearns 2002; Tebaldi and Knutti 2007; Bhat et al., 2011) or measured discharge (Gain *et al*., 2011). The use of weighted average approaches, however, implies additional subjectivity related to the weight assignments. Therefore, the choice of the method to represent the average effect of multi-models ensemble can add additional source of uncertainty and impact the interpretation of the results.

Projected change in catchment FDC under hydrological parameter and climate model ensemble uncertainties

To consider the ensemble modelling average change and its associated uncertainty on the long term FDCs of the Thau and the Chiba catchments, results are presented for the three conceptual FDC segments corresponding to high, medium and low flows. The latter correspond respectively to flow percentiles lower than 10%, between 10 and 70% and higher than 70%. To construct the AMU interval for each flow type, all the values within the respective intervals mentioned above are extracted from the reference and future projections in FDCs and their ensemble mean relative change and uncertainty are calculated. The results are presented in Figure 6-8 and show the projected change uncertainty in high, medium and low flows in the FDCs of the Thau and the Chiba catchments, constructed by considering hydrological parameter and climate models uncertainties.

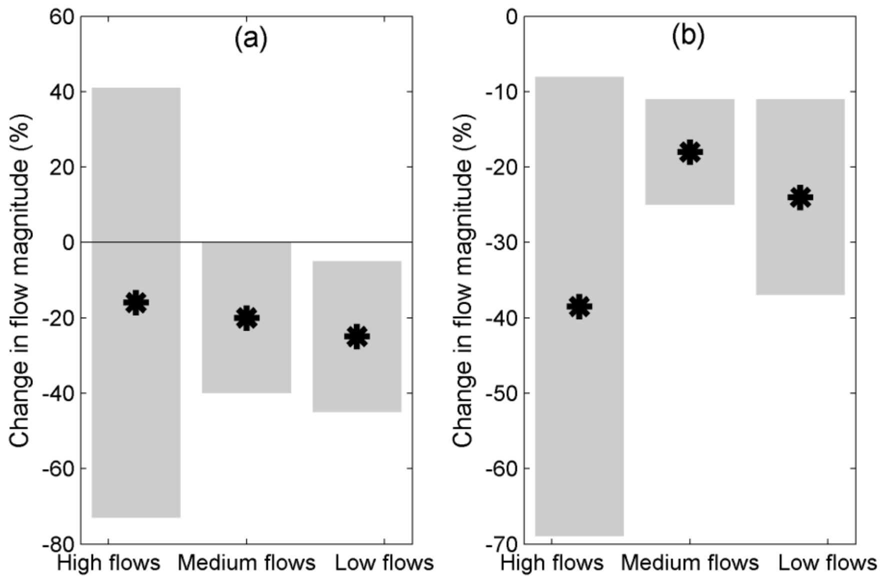

Figure 6-8: Uncertainty intervals for the mean projected change on FDCs high, medium and low flows as predicted by the ensemble modelling for the Thau (a) and the Chiba (b) catchments. The black stars refer to the mean value

In both catchments, FDCs high flows are likely to experience the largest decrease in the future with average values of -19% and -38% in the Thau and the Chiba catchment, respectively. The combination of hydrological parameter and climate models uncertainties lead to wider uncertainty intervals in the projected relative changes of the FDCs flow segments than those calculated by considering only CME uncertainty. In both results the projected changes in high flows are likely to be the most uncertain in comparison to medium and low flows. Indeed, high flows most often are caused by intense rainstorms and occurring during the wet period either in the Thau or in the Chiba catchments. These results are consistent with the observations previously made showing that projected uncertainty in monthly precipitation and runoff changes are larger and more uncertain in the wet period than in the dry period. Therefore, the large predicted uncertainty in the projected change in FDC high flows can be attributed to climate models uncertainty in predicting heavy rainfall events. This will be better investigated in the next section.

Changes in medium flows as derived from the combination of the hydrological parameter and CME uncertainties are also projected to decrease in both catchments. However, their associated ensemble modelling uncertainty is smaller than the one of high flows but larger than the one derived from CME. For instance, in the Thau catchment medium flows are projected to decrease by a range of 0 to -40% when both uncertainty sources are considered against -10 to -37% when only CME uncertainty is considered. This is because the FDC medium flows are more dependent on soil moisture condition, land use/cover characteristics and other basin properties than on direct climate influence.

Changes in low flows may have negative effects on maintaining river ecological state, agriculture and domestic water supply (Smakhtin 2001). From the ensemble modelling results, the average change in low flows is likely to decrease by range of [-5 to -45%] and [-11 to -37%] with respect to the reference period in the Thau and the Chiba catchments, respectively. Uncertainty in the projected decrease of low flows in both catchments as derived from the combination of the hydrological parameter and CME uncertainties is slightly larger than the calculated uncertainty using CME alone. The projected reduction in the low flows can be related to several factors including reduction in precipitations and increase in temperature during the dry period. Consequently, it is very likely that the Chiba flow becomes more intermittent leading probably to more extended drier conditions and to several types of droughts in the future (e.g. agricultural and hydrological droughts).

6.4.3 *Uncertainty sources decomposition*

When assessing the impact of climate change on catchment hydrology there is always uncertainty involved at each stage of the study approach. These uncertainties interact and propagate in a complex nonlinear way affecting the final projected magnitude of change in the catchment response. Thus, it is not surprising that this issue has drawn specific intention in recent literature (Bastola et al., 2011; Knutti 2010; Kwon et al., 2012). In this section, the average ensemble modelling uncertainty surrounding the projected mean of change in monthly runoff and FDC flow segments is decomposed into hydrological model parameters and CME uncertainty by fractioning the total ensemble modelling variance according to Equation 6-5.

$$FMPU_{(m)} = \frac{\delta^2_{MP(m)}}{\delta^2_{\Delta v(m)}} \qquad \text{Equation 6-5}$$

with *FMPU* is the fraction of the total ensemble modelling variance, $\delta^2_{\Delta v(m)}$ (Equation 6-4), explained by the hydrological model parameters variance, $\delta^2_{MP(m)}$, for the element *m* (*m* can be a month or a FDC percentile). The latter can be calculated as follows:

$$\delta^2_{MP(m)} = \frac{1}{J}\sum_{j=1}^{J}(\overline{\Delta v}_{j(m)} - \overline{\overline{\Delta v}}_{(m)})^2 \qquad \text{Equation 6-6}$$

with $\delta^2_{MP(m)}$ is the variance of the hydrological model parameters, $\overline{\Delta v}_{j(m)}$ is the mean relative change of the climate model ensemble for the hydrological model parameter set simulation *j*. Figure 6-9 illustrates the fraction of the ensemble modelling variance explained by the hydrological model parameter variance based on the monthly runoff and FDCs projected results for the Thau and the Chiba catchments. The monthly runoff indicator results in the Thau catchment reveal that in the dry period hydrological model parameter uncertainty contributes by 45 to 81% to the average ensemble modelling uncertainty whereas CME uncertainty is responsible for more than 60% of the total uncertainty during the wet period. This statement is confirmed in the Chiba catchment where hydrological parameter uncertainty contributes by 55 to 93% to the average ensemble modelling uncertainty in the dry period, whereas during the wet period, more than 85% of the average ensemble modelling uncertainty is explained by uncertainty of the CME. The results of the uncertainty decomposition in the FDCs flow segments (Figure 6-10) in both catchments corroborate these findings. Climate models uncertainty dominate the high flow prediction uncertainty while hydrological parameter uncertainty sources is prevailing for the medium and low flows. These results suggest that in both catchments, the average ensemble modelling uncertainty tends to amplify due to the increase in the CME prediction uncertainty as moving from the dry period to the wet period.

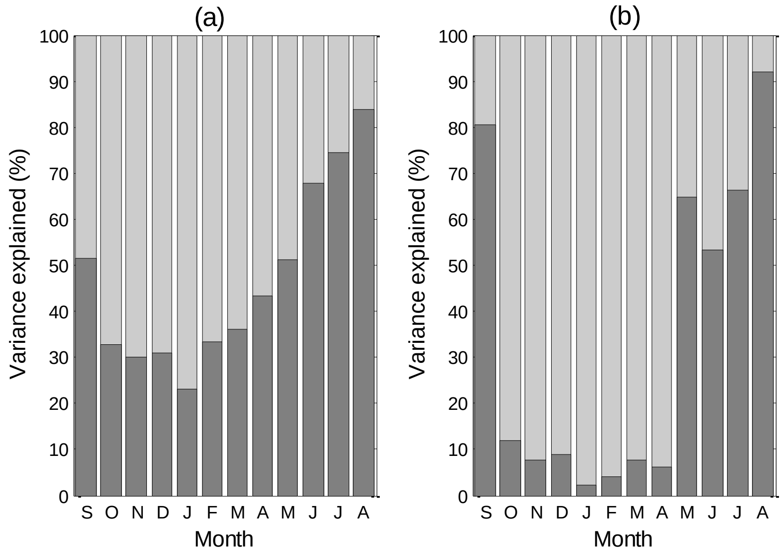

Figure 6-9: Decomposition in % of the ensemble modelling variance of the projected relative change into hydrological parameter variance (dark grey) and climate multi-models ensemble (light grey) calculated from monthly flow magnitude for the Thau (a) and the Chiba (b) catchments

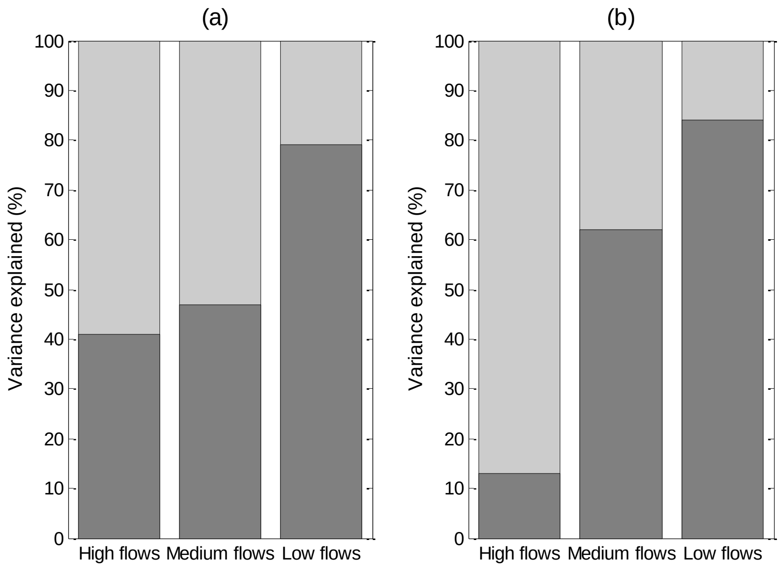

Figure 6-10: Decomposition in % of the ensemble modelling variance of the projected relative change into hydrological parameter variance (dark grey) and climate multi-models ensemble (light grey) calculated from FDCs for the Thau (a) and the Chiba (b) catchments

6.5 Conclusions

Feed-forward artificial neural networks (FF-NNs) have been developed and used as substitute for the physically based hydrological model (SWAT) to propagate uncertainty in a climate change impact study for the Thau and the Chiba catchments. In this study, uncertainty related to both the climate scenarios and hydrological model parameterization is explicitly considered. Climate change impacts are analyzed on monthly runoff and FDC curves.

Throughout this study it has been demonstrated that FF-NNs are appropriate to substitute complex hydrological model and, thus, can be effectively and efficiently used in rainfall-runoff modelling in the Thau and the Chiba catchments. When it comes to investigate the impact of climate change on catchment hydrology, the issue of uncertainty in models projections needs to be addressed. In this regard, the conjunctive use of an ensemble of four climate models with different parameterizations of the hydrological model has offered the possibility to characterize the average magnitude of change in monthly runoff and FDC indicators and the associated ensemble modelling uncertainty. It has been confirmed that the combined effect of the projected decrease in precipitation and increase in temperature over the Thau and the Chiba catchments is likely to induce a reduction in the future monthly and daily flow magnitude.

The propagation and the decomposition of the uncertainty have shown that uncertainty in climate models is dominating hydrological parameters uncertainty when moving from drier to wetter conditions. This suggests that particular attention should be given to the seasonality when assessing uncertainty in climate impact assessment studies. Since many sources of uncertainty are not considered in this study (e.g. uncertainty related bias correction, downscaling approach, hydrological models structure, etc.), the interpretations and the conclusions drawn from the current results should be considered within the spectrum of the modelling choices and assumptions made. Numerous open issues need to be addressed related to the selection of the appropriate climate and hydrological models member to construct the ensemble-multi-models, to the statistical approach to derive the ensemble multi-models mean and to the construction of the uncertainty interval combing all possible sources of uncertainty.

CHAPTER VII

7 General conclusions and perspectives

7.1 General conclusions

Hydrological models are valuable tools for assessing the impact of climate change on catchment hydrology. However, they are prone to uncertainty that needs to be assessed for accurate use of the prediction results in operational and practical water resources management under uncontrolled changes such as these related to climate change.

Uncertainty in hydrological impacts of climate change stems from several sources including model parameter, structure, and observation data. Both hydrological and climate models suffer from these uncertainties and others additional uncertainty sources. Thus, the challenge is to assess the uncertainty prediction while investigating the impacts of climate change projections on catchment hydrology. In this thesis attempts are made to achieve this ambitious goal in small Mediterranean catchments by addressing several research questions. These can be summarized as follows.

1) Is the selected hydrological model appropriate for discharge prediction in the selected catchments?

The SWAT model, acronym of the Soil and Water Assessment Tools (Arnold et al., 1998), was applied and evaluated for daily discharge prediction in the Thau (South France) and the Chiba (North East Tunisia) catchments. The model calibration results were satisfactory despite the data scarcity suggesting that the selected hydrological model (SWAT) is suitable for discharge prediction in the selected catchments.

2) How do parameter and discharge uncertainties affect the hydrological model performances and the prediction results?

Hydrological model predictions are always affected with uncertainty whose quantification is a challenging task that depends on the uncertainty technique used and the way it is implemented. Different uncertainty techniques were used to assess model parameter uncertainty. This source of uncertainty is important and should be routinely considered while evaluating the performances of the selected hydrological model. Furthermore, it is not unusual that different parameter set combinations lead to similar results. This is what Keith Beven has called equifinality. The latter originates from parameter uncertainty, model structure error, and from the propagation of others various uncertainty sources in a complex way. Thus, the equifinality should be accepted in model uncertainty assessment when dealing with high dimensional complex model such as SWAT. This is particularly true in Mediterranean catchments where the spatial and temporal variability of the local hydrological processes, catchment features and climatic conditions increase the complexity of the model calibration and evaluation.

Hydrological model are usually calibrated against discharge data. But the uncertainty related to this observation variable is rarely considered in the model uncertainty assessment. In this regard, we have developed a new approach where uncertainty of the discharge data is integrated with model parameter uncertainty. By contributing from 14 to 28% to the model parameter uncertainty in the Thau catchment, uncertainty in the discharge is far to be a negligible source in the modelling results. It was also demonstrated that parameter uncertainty alone cannot compensate for all modelling uncertainty sources and that other additional uncertainty sources (input and model structure uncertainty) must be considered for a complete and comprehensive uncertainty assessment.

3) How can discharge be estimated in ungauged or partially gauged catchments within an uncertainty framework?

There are two main challenges in this research question that hydrologists are currently facing. The first issue is related to the discharge estimation in ungauged catchments and the second is related to the assessment of the uncertainty of discharge prediction in ungauged catchments. We have simultaneously addressed these challenges through a new developed approach based on similarity between gauged and ungauged physical catchments attributes. Based on the speculation that physically similar catchments are hydrologically similar, “behavioral” or good model parameters are transferred from the gauged to the ungauged catchments functioning to their degree of physical similarity. The developed approach allows propagating the modelling uncertainty while transferring the model parameter sets to the ungauged catchments. Therefore, model prediction uncertainty at the ungauged catchments increases as the dissimilarity between the donor and the receptor catchment increases. The approach was applied to the Thau and the Chiba catchments and found to be appealing and reasonable. Furthermore, it provides more reliable prediction uncertainty at the ungauged catchments and more objectivity in selecting the transferrable model parameter sets. This has allowed to estimate for the first time the total discharge and water balance of the entire Thau and Chiba catchments.

4) How climate change will impact the hydrological regime of Mediterranean catchments?

Projected future changes in climate and their possible impacts on river flow regime are major concerns for the Mediterranean region identified as “a hot spot” to future climate changes and variability (Ludwig et al., 2011; IPCC 2007). We investigated the hydrological climate-impact projections based on the hydrological model simulations driven with four climate models underpinned with the A1B emission scenario. We assessed the projected changes in hydrological indicators related to climatic conditions, water balance, flow magnitudes and frequency and flow durations for the future scenario period (2041-2070) with respect to reference period of 1971-2000 for the Thau and the Chiba catchments.

The combined effects of the projected decrease in precipitation and increase in temperature by 2050s are likely to induce a decrease in soil water content, actual evapotranspiration and catchments runoff. It is also demonstrated that high and low flow frequency, as well as flow extremes magnitudes at various time durations, are expected to decrease in both catchments with more pronounced effects in the Chiba catchment than in the Thau catchment. These findings at the catchment scale converge with the general agreement about the projected alteration in rivers flow regime at the Mediterranean scale.

It was also demonstrated that the projected degree of flow alteration depends also on the nature of the hydrological processes occurring in the catchment. For instance, where groundwater contributions to the catchment flow are important, climate change impacts on the catchment flow regime can be attenuated unless their impacts on the groundwater flow regime is considered. In catchments where the hydrologic regime is mainly dependent upon surface runoff, the impacts of climate change can be more critical than in the previous example.

The use of multi-climate models ensemble allow quantifying the hydrological prediction uncertainty related to climate models ensemble in the projected changes of the flow regime. In both Thau and Chiba catchments, it was found that projection uncertainty became wider as moving from the dry period to the wet period highlighting the effect of seasonality on hydrological simulations under climate change in Mediterranean catchments.

5) How can climate models uncertainty be propagated into the hydrological model and how much each uncertainty sources contribute to the climate change projection impacts uncertainty?

The fact that hydrological simulations dependent on the climate models used emphasizes the need for considering both climate and hydrological uncertainty sources in climate change impact assessment. Uncertainty related to both the climate scenarios and hydrological model parameterization is explicitly considered through the development of an approach based on feed-forward artificial neural networks (FF-NNs). The latter has been developed to overcome the computational cost of the SWAT model and to approximate each "behavioral" SWAT simulations. FF-NNs have shown to be appropriate to substitute the complex hydrological model and, thus, they can be effectively and efficiently used in rainfall-runoff modelling in the Thau and the Chiba catchments. Then, each FF-NNs are driven with the climate models outputs for the baseline and future periods and the uncertainty in the projected change in monthly runoff and flow duration curves was assessed. This uncertainty encompasses both uncertainty related to the climate models and hydrological parameter.

The variance decomposition has identified the climate models to be the dominant source of uncertainty during the wet period and, thus, resulting in large uncertainty in catchment runoff and high flows during this time period. In the dry period, however, the dominance of the climate models uncertainty diminishes, and the hydrological parameter uncertainty becomes more important. The contribution of the climate models uncertainty to the total modelling uncertainty was estimated about 60 and 85% for the wet period in the Thau and the Chiba catchments, respectively. Whereas in the dry period, the average contribution of hydrological parameter uncertainty to the total modelling uncertainty was 63 and 74% for the Thau and the Chiba catchments, respectively.

The diversity and variability in local hydrological processes and climatic conditions coupled with the uncertainty in both hydrological and climate models make the assessment of hydrological impacts of climate change projections in small Mediterranean catchment difficult. Nevertheless, climate change impact studies at the local scale can provide valuable information to assist water managers in their local operational management plans. In addition, as most of water monitoring programs are usually established at the local scale, assessing the impact of climate change at this spatial level can offer base of data for implementing regional water management plan and suggest relevant policy measure.

7.2 Perspectives

Whilst the results and approaches developed and presented in this thesis suggest a number of improvements to the most challenging scientific questions related to the uncertainty assessment of climate change impacts in catchment hydrology, there is a long list of open research questions and issues that needs to be addressed in the future for better understanding the effects of climate change on catchment hydrology.

By considering only uncertainty in the hydrological model parameters and discharge data it is assumed that the model structure is correct and that model inputs are error free. However, model structure uncertainty is well known to be one of the most important uncertainty sources, and, thus, it should be considered while assessing the hydrological model performances and predictions. Furthermore, the utility of the hydrological prediction results with respect to future changes in catchment water resources is constrained by the uncertainty of the climate models in addition to the one emerging from the hydrological models. This emphasizes the need for using multi-model ensembles to sample a wider range of structural uncertainties and to increase the confidence in future models predictions. However, the list of open issues and questions associated with the development and interpretation of multi-model ensemble is long including the lack of robust methods and approaches for combining multiple models and deriving a common probabilistic projections.

Whilst further uncertainty in hydrological predictions under climate change can arises from hydrological model parameter instability due to possible changes in climatic conditions between the model calibration period and future projections period (Brigode et al., 2013), is not considered in the current work and requires a particular future attention.

The need for better understanding the role and interactions of uncertainty sources is apparent to guide future improvement in model predictions. New approaches and techniques for a complete and integrated assessment and combination of all uncertainty sources in hydrological modelling are urgent.

When assessing uncertainty of climate change impacts on catchment hydrology there is always a part of the results associated to the natural variability in hydrological and climate models. This natural variability can be more important in Mediterranean catchments than elsewhere. Thus, for better understanding the effects of climatic change and more accurate quantification of model prediction uncertainty it is may be useful to discriminate in the projection results between what is related to the natural variability and to the models themselves.

Despite the substantial uncertainty associated with the model predictions, our results showed that climate change is expected to alter the hydrologic regime and decrease the fresh water availability of Mediterranean catchments. In addition, further negative impacts are also expected in the region such as increasing risks of droughts and floods with more exacerbated forms of water pollution (Ludwig et al., 2009, 2011) and consequent threats to water availability and management. This emphasizes the needs for deeper investigations and studies of these projected changes at the local scale to assist regional water resources management strategies. However, a key challenge is how to incorporate high uncertain information about potential impacts of climate change from the local scale into regional climate change adaptation strategy.

Bibliography

Abbaspour, K.C., van Genuchten, M.T., Schulin, R., Schläppi, E., 1997. A sequential uncertainty domain inverse procedure for estimating subsurface flow and transport parameters. Water Resour. Res., 33(8): 1879-1892.

Abbaspour, K.C., Johnson, C.A., van Genuchten, M.T., 2004. Estimating Uncertain Flow and Transport Parameters Using a Sequential Uncertainty Fitting Procedure. Vadose Zone Journal, 3(4): 1340-1352.

Abbaspour, K.C., Yang, J., Maximov, I., Siber, R., Bogner, K., Mieleitner, J., Zobrist, J., Srinivasan, R., 2007. Modelling hydrology and water quality in the pre-alpine/alpine Thur watershed using SWAT. Journal of Hydrology, 333(2-4): 413-430.

Abbaspour, K.C., 2008. Swat calibration and uncertainty programs, Version2. A User Manual. Department of Systems Analysis, Integrated Assessment and Modelling (SIAM), Eawag, Swiss Federal Institute of Aquatic Science and Technology. (2008): 95.

Abouabdillah, A., Ouslati, O., De Girolamo, A.M., Lo Porto, A., 2010. Modelling the impact of climate change in a Mediterranean catchment (Merguellil, Tunisia) Fresenius Environmental Bulletin, 19: 14.

Afinowicz, J. D., Munster, C. L. and Wilcox, B. P., 2005. Modelling effects of brush management on the rangeland water budget: Edwards Plateau, Texas. *Journal of the American Water Resources Association,* 41 (1), 181-193.

Ajami, N. K., Duan, X. G. and Sorooshian, S., 2005). Multi-model combination techniques for hydrologic forecasting: Application to distributed model intercomparison project results, J. Hydrometeorol., 7 (4), 755-768.

Ajami, N. K., Duan, Q. and Sorooshian, S., 2007. An integrated hydrologic Bayesian multimodel combination framework: Confronting input, parameter, and model structural uncertainty in hydrologic prediction. *Water Resources Research,* 43 (1), W01403.

Andersson, J. C. M., Zehnder, A. J. B., Jewitt, G. P. W. and Yang, H.,2009. Water availability, demand and reliability of in situ water harvesting in smallholder rain-fed agriculture in the Thukela River Basin, South Africa. *Hydrology and Earth System Sciences,* 13 (12), 2329-2347

Alpert, P., Krichak, S.O., Shafir, H., Haim, D., Osetinsky, I., 2008. Climatic trends to extremes employing regional modelling and statistical interpretation over the E. Mediterranean. Global and Planetary Change, 63(2–3): 163-170.

Aouissi, J., Benabdallah, S., Lili Chabaâne, Z., Cudennec C.; 2012. Modelling Water Quality to Improve Agricultural Practices and Land Management in a Tunisian Catchment using SWAT. Journal of Environmental Quality, doi:10.2135/jeq2011.0375. 2012

Aquilina, L., Ladouche, B., Doerfliger, N., Seidel, J.L., Bakalowicz, M., Dupuy, C., Le Strat, P., 2002. Origin, evolution and residence time of saline thermal fluids (Balaruc springs, southern France): implications for fluid transfer across the continental shelf. Chemical Geology, 192(1–2): 1-21.

Arabi, M., Govindaraju, R.S., Hantush, M.M., 2007. A probabilistic approach for analysis of uncertainty in the evaluation of catchment management practices. Journal of Hydrology, 333(2–4): 459-471.

Arnell, N.W., 2011. Uncertainty in the relationship between climate forcing and hydrological response in UK catchments. Hydrology and Earth System Sciences. 15(3), 897-912. doi:10.5194/hess-15-897-2011

Arnell, N.W., 1999. The effect of climate change on hydrological regimes in Europe: a continental perspective. Global Environmental Change, 9(1): 5-23

Arnold, J.G., Fohrer, N., 2005. SWAT2000: current capabilities and research opportunities in applied catchment modelling. Hydrological Processes, 19(3): 563-572.

Arnold, J.G., Srinivasan, R., Muttiah, R.S., Williams, J.R., 1998. Large area hydrological modelling and assessment. Part I: Model development1. Journal of the American Water Resources Association, 34(1): 73-89.

Aronica, G. T., Candela, A., Viola, F. and Cannarozzo, M., 2006. Influence of rating curve uncertainty on daily rainfall-runoff model predictions. *In:* IAHS Publication, *Predictions in Ungauged Basins: Promise and Progress. (Proceedings of symposium S7 held during the Seventh IAHS Scientific Assembly at Foz do Iguaçu,* Brazil, April 2005*).* Brazil:IAHS Publication, 303, 116-124.

Bacher, C., Millet, B., Vaquer, A., 1996. Modelling the impact of cultivated filter feeders on phytoplanctonic biomass of the Thau lagoon (France). Compte-Rendu de l'Académie des Sciences, Paris, Sciences de la Vie/Life sciences: 8.

Baffaut, C. and Benson, V. W., 2009. Modelling flow and pollutant transport in a karst watershed with SWAT. Transactions of the ASABE, 52, 469-479.

Baghdadi, N., Cresson, R., El Hajj, M., Ludwig, R., La Jeunesse, I., 2012. Estimation of soil parameters over bare agriculture areas from C-band polarimetric SAR data using neural networks. Hydrol. Earth Syst. Sci., 16(6): 1607-1621.

Bàrdossy, A., 2007. Calibration of hydrological model parameters for ungauged catchments. Hydrol. Earth Syst. Sci., 11(2): 703-710.

Bastola, S., Ishidaira, H., Takeuchi, K., 2008. Regionalisation of hydrological model parameters under parameter uncertainty: A case study involving TOPMODEL and basins across the globe. Journal of Hydrology, 357(3–4): 188-206.

Bastola, S., Murphy, C., Sweeney, J., 2011. The role of hydrological modelling uncertainties in climate change impact assessments of Irish river catchments. Advances in Water Resources, 34(5): 562-576.

Benham, B. L., Baffaut, C., Zeckoski, R. W., Mankin, K. R., Pachepsky, Y. A., Sadeghi, A. M., Brannan, K. M., Soupir, M. L. and Habersack, M. J., 2006. Modelling bacteria fate and transport in watersheds to support TMDLS. Transactions of the ASABE, 49 (4), 987-1002.

Beven, K., Binley, A., 1992. The future of distributed models: Model calibration and uncertainty prediction. Hydrological Processes, 6(3): 279-298.

Beven, K., 1997. TOPMODEL: a critique, Hydrological. Process., 11(9),1069–1086, 1997.

Beven, K., 2000. On the future of distributed modelling in hydrology. Hydrological Processes, 14(16-17): 3183-3184.

Beven, K., Freer, J., 2001. Equifinality, data assimilation, and uncertainty estimation in mechanistic modelling of complex environmental systems using the GLUE methodology. Journal of Hydrology, 249(1-4): 11-29.

Beven, K., 2006. A manifesto for the equifinality thesis. Journal of Hydrology, 320(1-2): 18-36.

Bhat, K.S., Haran, M., Terando, A., Keller, K., 2011. Climate Projections Using Bayesian Model Averaging and Space–Time Dependence. JABES, 16(4): 606-628.

Blasone, R.-S., Madsen, H., Rosbjerg, D., 2008. Uncertainty assessment of integrated distributed hydrological models using GLUE with Markov chain Monte Carlo sampling. Journal of Hydrology, 353(1-2): 18-32.

Bollen, M. J. S., Bekhuis, F. H. W. M., Reiling, R., Scheper, E., 1995. Toward a spatial pattern of the vulnerability of soil and groundwater. RIVM report n°711901012, Bilthoven, the Netherlands, 69 p.

Bouraoui, F., Benabdallah, S., Jrad, A., Bidoglio, G., 2005. Application of the SWAT model on the Medjerda river basin (Tunisia). Physics and Chemistry of the Earth, Parts A/B/C, 30(8–10): 497-507.

Briffa, K.R., van der Schrier, G., Jones, P.D., 2009. Wet and dry summers in europe since 1750: Evidence of increasing drought. International Journal of Climatology, 29(13): 1894-1905.

Brigode, P., Oudin, L., Perrin, C., 2013. Hydrological model parameter instability: A source of additional uncertainty in estimating the hydrological impacts of climate change? Journal of Hydrology, 476(0): 410-425.

Butts, M. B., Payne, J. T., Kristensen, M. and Madsen, H., 2004. An evaluation of the impact of model structure on hydrological modelling uncertainty for streamflow simulation. Journal of Hydrology, 298 (1-4), 242-266.

Calo, A., 1967. Etude pédologique du périmètre de l’Oued Chiba. Direction des Sols, Ministère de l’Agriculture, Tunisie, N° 264, PP. 21.

Cary, L., Casanova, J., Gaaloul, N., Guerrot, C., 2013. Combining boron isotopes and carbamazepine to trace sewage in salinized groundwater: A case study in Cap Bon, Tunisia. Applied Geochemistry, 34(0): 126-139.

Castellarin, A., Galeati, G., Brandimarte, L., Montanari, A., Brath, A., 2004. Regional flow-duration curves: reliability for ungauged basins. Advances in Water Resources, 27(10): 953-965.

Chahinian, N., Tournoud, M.-G., Perrin, J.-L., Picot, B., 2011. Flow and nutrient transport in intermittent rivers: a modelling case-study on the Vène River using SWAT 2005. Hydrological Sciences Journal, 56(2): 268-287.

Chauvel A., 1961. Etude pédologique du périmètre de l'Oued Chiba. Direction des Sols, Ministère de l'Agriculture, Tunisie, N° 187, PP. 65.

Clarke, R. T., Mendiondo, E. M. and Brusa, L. C., 2000. Uncertainties in mean discharges from two large South American rivers due to rating curve variability. Hydrological Sciences Journal, 45 (2), 221-236.

Coffey, M. E., Workman, S. R., Taraba, J. L. and Fogle, A. W., 2004. Statistical procedures for evaluating daily and monthly hydrologic model predictions. Transactions of the ASABE, 47 (1), 59-68.

Davis, J.M., Baxter, C.V., Minshall, G.W., Olson, N.F., Tang, C., Crosby, B.T., 2013a. Climate-induced shift in hydrological regime alters basal resource dynamics in a wilderness river ecosystem. Freshwater Biology, 58(2): 306-319.

Davis, J.M., Baxter, C.V., Rosi-Marshall, E.J., Pierce, J.L., Crosby, B.T., 2013b. Anticipating Stream Ecosystem Responses to Climate Change: Toward Predictions that Incorporate Effects Via Land–Water Linkages. Ecosystems.

De Luis, M., González-Hidalgo, J.C., Longares, L.A., Štepánek, P., 2009. Seasonal precipitation trends in the Mediterranean Iberian Peninsula in second half of 20th century. International Journal of Climatology, 29(9): 1312-1323.

De Vos, N.J., Rientjes, T.H.M., 2005. Constraints of artificial neural networks for rainfall-runoff modelling: trade-offs in hydrological state representation and model evaluation. Hydrol. Earth Syst. Sci., 9(1/2): 111-126.

DeGasperi, C.L., Berge, H.B., Whiting, K.R., Burkey, J.J., Cassin, J.L., Fuerstenberg, R.R., 2009. Linking Hydrologic Alteration to Biological Impairment in Urbanizing Streams of the Puget Lowland, Washington, USA1. JAWRA Journal of the American Water Resources Association, 45(2): 512-533.

Deidda, R., 2000. Rainfall downscaling in a space-time multifractal framework, Water Resour. Res., 36, 1779–1794.

Deidda, R., Marrocu, M., Caroletti, G., Pusceddu, G., Langousis, A., Lucarini, V., Puliga, M., Speranza, A., 2013. Regional climate models' performance in representing precipitation and temperature over selected Mediterranean areas. Hydrol. Earth Syst. Sci., 17(12): 5041-5059.

Di Luzio, M., Arnold, J.G., Srinivasan, R., 2005. Effect of GIS data quality on small catchment stream flow and sediment simulations. Hydrological Processes, 19(3): 629-650.

Dotto, C.B., Mannina, G., Kleidorfer, M., Vezzaro, L., Henrichs, M., McCarthy, D.T., Freni, G., Rauch, W., Deletic, A., 2012. Comparison of different uncertainty techniques in urban stormwater quantity and quality modelling. Water research, 46(8): 2545-58.

Duan, Q., Sorooshian, S., Gupta, V., 1992. Effective and efficient global optimization for conceptual rainfall-runoff models. Water Resour. Res., 28(4): 1015-1031.

Duan, Q., Sorooshian, S., Gupta, V.K., 1994. Optimal use of the SCE-UA global optimization method for calibrating catchment models. Journal of Hydrology, 158(3-4): 265-284.

Eckhardt, K., Fohrer, N., Frede, H.-G., 2005. Automatic model calibration. Hydrological Processes, 19(3): 651-658.

Elguindi, N., Somot S., Déqué, M., Ludwig, W., 2011. Climate change evolution of the hydrological balance of the Mediterranean, Black and Caspian Seas: impact of model resolution. Clim. Dyn. 36(1-2) 205-228. doi: 10.1007/s00382-009-0715-4.

El Kenawy, A.M., López-Moreno, J.I., Vicente-Serrano, S.M., Mekld, M.S., 2009. Temperature trends in Libya over the second half of the 20th century. Theoretical and Applied Climatology, 98(1-2): 1-8.

Engeland, K. and Gottschalk, L., 2002. Bayesian estimation of parameters in a regional hydrological model", Hydrol. Earth Syst. Sci., vol 6,2002, pp. 883-898.

Foley, J.A., DeFries, R., Asner, G.P., Barford, C., Bonan, G., Carpenter, S.R., Chapin, F.S., Coe, M.T., Daily, G.C., Gibbs, H.K., Helkowski, J.H., Holloway, T., Howard, E.A., Kucharik, C.J., Monfreda, C., Patz, J.A., Prentice, I.C., Ramankutty, N., Snyder, P.K., 2005. Global consequences of land use. Science, 309(5734): 570-574.

Freer, J., Beven, K., Ambroise, B., 1996. Bayesian Estimation of Uncertainty in Runoff Prediction and the Value of Data: An Application of the GLUE Approach. Water Resour. Res., 32(7): 2161-2173.

Freni, G., Mannina, G., 2010. Bayesian approach for uncertainty quantification in water quality modelling: The influence of prior distribution. Journal of Hydrology, 392(1–2): 31-39.

Fujihara, Y., Tanaka, K., Watanabe, T., Nagano, T., Kojiri, T., 2008. Assessing the impacts of climate change on the water resources of the Seyhan River Basin in Turkey: Use of dynamically downscaled data for hydrologic simulations. Journal of Hydrology, 353(1-2): 33-48.

Gain, A.K., Immerzeel, W.W., Sperna-Weiland, F.C., Bierkens, M.F.P., 2011. Impact of climate change on the stream flow of lower Brahmaputra: trends in high and low flows based on discharge- weighted ensemble modelling. Hydrol. Earth Syst. Sci. Discuss., 8(1): 365-390.

Gallart, F., Amaxidis, Y., Botti, P., CanÈ, G., Castillo, V., Chapman, P., Froebrich, J., GarcÍA-Pintado, J., Latron, J., Llorens, P., Porto, A.L., Morais, M., Neves, R., Ninov, P., Perrin, J.-L., Ribarova, I., Skoulikidis, N., Tournoud, M.-G., 2008. Investigating hydrological regimes and processes in a set of catchments with temporary waters in Mediterranean Europe. Hydrological Sciences Journal, 53(3): 618-628.

Gao, B., Yang, D., Zhao, T., Yang, H., 2012. Changes in the eco-flow metrics of the Upper Yangtze River from 1961 to 2008. Journal of Hydrology, 448-449: 30-38.

Gao, Y., Long, D., 2008. Intercomparison of remote sensing-based models for estimation of evapotranspiration and accuracy assessment based on SWAT. Hydrological Processes, 22(25): 4850-4869.

Gao, Y., Vogel, R.M., Kroll, C.N., Poff, N.L., Olden, J.D., 2009. Development of representative indicators of hydrologic alteration. Journal of Hydrology, 374(1-2): 136-147.

García-Ruiz, J.M., López-Moreno, J.I., Vicente-Serrano, S.M., Lasanta–Martínez, T., Beguería, S., 2011. Mediterranean water resources in a global change scenario. Earth-Science Reviews, 105(3-4): 121-139.

Gassman, P.W., Reyes, M.R., Green, C.H., Arnold, J.G., 2007. The Soil and Water Assessment Tool: Historical developement , applications and future research directions. Transactions of the ASABE, 50(4): 1211-1250.

Gibson, C.A., Meyer, J.L., Poff, N.L., Hay, L.E., Georgakakos, A., 2005. Flow regime alterations under changing climate in two river basins: implications for freshwater ecosystems. River Research and Applications, 21(8): 849-864.

Giorgi, F., Lionello, P., 2008. Climate change projections for the Mediterranean region. Global and Planetary Change, 63(2-3): 90-104.

Giorgi, F., Mearns, L.O., 2002. Calculation of Average, Uncertainty Range, and Reliability of Regional Climate Changes from AOGCM Simulations via the “Reliability Ensemble Averaging” (REA) Method. Journal of Climate, 15(10): 1141-1158.

Gitau, M.W., Chaubey, I., 2010. Regionalization of SWAT Model Parameters for Use in Ungauged Catchments. Water, 2(4): 849-871.

Gong, Y., Shen, Z., Hong, Q., Liu, R., Liao, Q., 2011. Parameter uncertainty analysis in catchment total phosphorus modelling using the GLUE methodology. Agriculture, Ecosystems & Environment, 142(3–4): 246-255.

Goubanova, K., Li, L., 2007. Extremes in temperature and precipitation around the Mediterranean basin in an ensemble of future climate scenario simulations. Global and Planetary Change, 57(1-2): 27-42.

Grillot, C., 2006. Fonctionnement hydrologique et dynamique des nutriments d’une rivière intermittente méditerranéenne en étiage et en crues. Analyse spatiale et temporelle. Thèse de Doctorat, Université de Montpellier II, PP 294.

Groves, D.G., Yates, D., Tebaldi, C., 2008. Developing and applying uncertain global climate change projections for regional water management planning. Water Resources Research, 44(12): W12413.

Gupta, H. V., Sorooshian, S. and Yapo, P. O.,1998. Toward improved calibration of hydrologic models: Multiple and noncommensurable measures of information. Water Resources Research, 34 (4), 751-763.

Hasanean, H.M., 2004. Precipitation variability over the Mediterranean and its linkage with El Nino Southern Oscillation ENSO. Journal of Meteorology 29(289): 151-160

Hasanean, H.M., Basset, H.A., 2006. Variability of summer temperature over Egypt. International Journal of Climatology, 26(12): 1619-1634.

He, Y., Bàrdossy, A., Zehe, E., 2011. A review of regionalisation for continuous streamflow simulation. Hydrol. Earth Syst. Sci., 15(11): 3539-3553.

Hertig, E., Jacobeit, J., 2008. Downscaling future climate change: Temperature scenarios for the Mediterranean area. Global and Planetary Change, 63(2-3): 127-131.

Heuvelmans, G., Muys, B., Feyen, J., 2004. Analysis of the spatial variation in the parameters of the SWAT model with application in Flanders, Northen belguim. Hydrology and Earth System Sciences Discussions, 8(5): 931-939.

Heuvelmans, G., Muys, B., Feyen, J., 2006. Regionalisation of the parameters of a hydrological model: Comparison of linear regression models with artificial neural nets. Journal of Hydrology, 319(1–4): 245-265.

Holvoet, K., Vangriensven, A., Seuntjens, P., Vanrolleghem, P., 2005. Sensitivity analysis for hydrology and pesticide supply towards the river in SWAT. Physics and Chemistry of the Earth, Parts A/B/C, 30(8-10): 518-526.

IPCC (2001) Climate Change 2001: the Scientific basis. Contribution of Working Group I to the Third Assessment Report of the Intergovernmental Panel on Climate Change (eds J.T. Houghton, Y. Ding, D.J. Griggs, M. Noguer, P.J. Van der Linden, D. Xiaosu, X. Dai, K. Maskell & C.A. Johnson) Cambridge, UK: Cambridge University Press:881.

IPCC (2007) Climate Change 2007: The Physical Science Basis. Contribution of Working Group I to the Fourth Assessment Report of the Intergovernmental Panel on Climate Change [Solomon, S., D. Qin, M. Manning, Z. Chen, M. Marquis, K.B. Averyt, M. Tignor and H.L. Miller (eds.)]. Cambridge University Press, Cambridge, United Kingdom and New York, NY, USA,:996.

Jia Y, Culver TB., 2008. Uncertainty analysis for watershed modelling using generalized likelihood uncertainty estimation with multiple calibration measures. J Water Resour Plan Manage, 134(2):97-106.

Jin, X., Xu, C.-Y., Zhang, Q., Singh, V.P., 2010. Parameter and modelling uncertainty simulated by GLUE and a formal Bayesian method for a conceptual hydrological model. Journal of Hydrology, 383(3-4): 147-155.

Kim, B.-S., Kim, B.-K., Kwon, H.-H., 2011. Assessment of the impact of climate change on the flow regime of the Han River basin using indicators of hydrologic alteration. Hydrological Processes, 25(5): 691-704.

Knutti, R., 2010. The end of model democracy? Climatic Change, 102(3-4): 395-404.

Kostopoulou, E., Jones, P.D., 2005. Assessment of climate extremes in the Eastern Mediterranean. Meteorology and Atmospheric Physics, 89(1-4): 69-85.

Koutroulis, A.G., Tsanis, I.K., Daliakopoulos, I.N., Jacob, D., 2013. Impact of climate change on water resources status: A case study for Crete Island, Greece. Journal of Hydrology, 479(0): 146-158.

Koutsouris, A.J., Destouni, G., Jarsjö, J., Lyon, S.W., 2010. Hydro-climatic trends and water resource management implications based on multi-scale data for the Lake Victoria region, Kenya. Environmental Research Letters, 5(3): 034005.

Kuczera G. and Parent E., 1998. Monte Carlo assessment of parameter uncertainty in conceptual catchment models: the Metropolis algorithm. Journal of Hydrology, 211 69 - 85

Kwon, H.-H., de Assis de Souza Filho, F., Block, P., Sun, L., Lall, U., Reis, D.S., 2012. Uncertainty assessment of hydrologic and climate forecast models in Northeastern Brazil. Hydrological Processes, 26(25): 3875-3885

La Jeunesse, I., 2001. Etude intégrée dynamique du phosphore dans le système bassin versant Lagune de Thau. Thèse de Doctorat, Volume I+ Annexes, PP. 383. Université d'Orléans, France.

La Jeunesse, I., Deslous-Paoli, J.M., Ximénès, M.C., Cheylan, J.P., Mende, C., Borrero, C., Scheyer, L., 2002. Changes in point and non-point sources phosphorus loads in the Thau catchment over 25 years (Mediterranean Sea – France). Hydrobiologia, 475-476(1): 403-411.

La Jeunesse, I., Elliott, M., 2004. Anthropogenic regulation of the phosphorus balance in the Thau catchment–coastal lagoon system (Mediterraean Sea, France) over 24 years. Marine Pollution Bulletin, 48(7–8): 679-687.

Laizé, C.L.R., Acreman, M.C., Schneider, C., Dunbar, M.J., Houghton-Carr, H.A., Flörke, M., Hannah, D.M., 2013. Projected Flow Alteration and Ecological Risk for Pan-European Rivers. River Research and Applications: n/a-n/a.

Lespinas, F., Ludwig, W., Heussner, S., 2014. Hydrological and climatic uncertainties associated with modelling the impact of climate change on water resources of small Mediterranean coastal rivers. Journal of Hydrology.

Liston, G.E., Elder, K., 2006. A meteorological distribution system for high-resolution terrestrial modelling (MicroMet). Journal of Hydrometeorology. 7(April): 217-234

López-Moreno, J.I., Vicente-Serrano, S.M., Moran-Tejeda, E., Zabalza, J., Lorenzo-Lacruz, J., García-Ruiz, J.M., 2011. Impact of climate evolution and land use changes on water yield in the ebro basin. Hydrology and Earth System Sciences, 15(1): 311-322.

Louati, M., Bucknall, J., 2010. Tunisia's experience in water resources mobilization and management. World development report. Development and Climate Change. Background note: 24.

Luterbacher, J., Xoplaki, E., Casty, C., Wanner, H., Pauling, A., Küttel, M., Rutishauser, T., Brönnimann, S., Fischer, E., Fleitmann, D., Gonzalez-Rouco, F.J., García-Herrera, R., Barriendos, M., Rodrigo, F., Gonzalez-Hidalgo, J.C., Saz, M.A., Gimeno, L., Ribera, P., Brunet, M., Paeth, H., Rimbu, N., Felis, T., Jacobeit, J., Dünkeloh, A., Zorita, E., Guiot, J., Türkes, M., Alcoforado, M.J., Trigo, R., Wheeler, D., Tett, S., Mann, M.E., Touchan, R., Shindell, D.T., Silenzi, S., Montagna, P., Camuffo, D., Mariotti, A., Nanni, T., Brunetti, M., Maugeri, M., Zerefos, C., Zolt, S.D., Lionello, P., Nunes, M.F., Rath, V., Beltrami, H., Garnier, E., Ladurie, E.L.R., 2006. Chapter 1 Mediterranean climate variability over the last centuries: A review. In: P. Lionello, P.M.-R., Boscolo, R. (Eds.), Developments in Earth and Environmental Sciences. Elsevier, pp. 27-148.

Ludwig, R., May, I., Turcotte, R., Vescovi, L., Braun, M., Cyr, J.F., Fortin, L.G., Chaumont, D., Biner, S., Chartier, I., Caya, D., Mauser, W., 2009. The role of hydrological model complexity and uncertainty in climate change impact assessment. Adv. Geosci., 21: 63-71.

Ludwig, R., Soddu, A., Duttmann, R., Baghdadi, N. S. B., Deidda, R., Marrocu, M., Strunz, G., Wendland, F., Engin, G., Paniconi, C., Prettenthaler, F., Lajeunesse, I., Afifi, S., Cassiani, G., Bellin, A., Mabrouk, B., Bach, H., and Ammerl, T. 2010. Climate-induced changes on the hydrology of mediterranean basins – a research concept to reduce uncertainty and quantify risk, Fresen. Environ. Bull., 19, 2379–2384, 2010.

Ludwig, R., Roson, R., Zografos, C., Kallis, G., 2011. Towards an inter-disciplinary research agenda on climate change, water and security in Southern Europe and neighboring countries. Environmental Science & Policy, 14(7): 794-803.

Mantovan, P., Todini, E., 2006. Hydrological forecasting uncertainty assessment: Incoherence of the GLUE methodology. Journal of Hydrology, 330(1-2): 368-381.

Margat, J., Vallée, D., 2000. Mediterranean vision on water, population and the environment for the 21st Century. Plan Bleu: 62.

Masih, I., Uhlenbrook, S., Maskey, S., Ahmad, M.D., 2010. Regionalization of a conceptual rainfall–runoff model based on similarity of the flow duration curve: A case study from the semi-arid Karkheh basin, Iran. Journal of Hydrology, 391(1–2): 188-201.

McIntyre, N., Lee, H., Wheater, H., Young, A., Wagener, T., 2005. Ensemble predictions of runoff in ungauged catchments. Water Resour. Res., 41(12): W12434.

Mekonnen, M.A., Wörman, A., Dargahi, B., Gebeyehu, A., 2009 Hydrological modelling of Ethiopian catchments using limited data. Hydrological Processes, 23(23): 7.

Merz, R., Blöschl, G., 2004. Regionalisation of catchment model parameters. Journal of Hydrology, 287(1–4): 95-123.

Milano, M., Ruelland, D., Fernandez, S., Dezetter, A., Fabre, J., Servat, E., Fritsch, J.-M., Ardoin-Bardin, S., Thivet, G., 2013. Current state of Mediterranean water resources and future trends under climatic and anthropogenic changes. Hydrological Sciences Journal, 58(3): 498-518.

Minville, M., Brissette, F., Leconte, R., 2008. Uncertainty of the impact of climate change on the hydrology of a nordic catchment. Journal of Hydrology, 358(1-2): 70-83.

Mohamoud, Y.M., 2008. Prediction of daily flow duration curves and streamflow for ungauged catchments using regional flow duration curves. Hydrological Sciences Journal, 53(4): 706-724.

Montanari, A., 2005. Large sample behaviors of the generalized likelihood uncertainty estimation (GLUE) in assessing the uncertainty of rainfall-runoff simulations. Water Resour. Res., 41(8): W08406.

Moore, R.J. 1985. The probability-distributed principle and runoff production at point and basin scales, Hydrol. Sci. J., 30(2), 273-297.

Moriasi, D.N., Arnold, J.G., Van Liew, M.W., Bingner, R.L., Harmel, R.D and Veith, T.L., 2007. Model evaluation guidelines for systematic quantification of accuracy in catchment simulations", American Society of Agricultural and Biological Engineers, vol 50, 2007, pp. 885–900.

Mosbahi, M., Benabdallah, S. and Boussema, M. R. 2011. Determination of Critical Source Areas for Sediment Loss: Sarrath River Basin, Tunisia", International Journal of Civil and Environmental Engineering, vol 3, 2011, pp. 206-2010.

Motovilov, Y.G., Gottschalk, L., Engeland, K., Rodhe, A., 1999. Validation of a distributed hydrological model against spatial observations. Agricultural and Forest Meteorology, 98-99(0): 257-277.

Muleta, M.K., Nicklow, J.W., 2005. Sensitivity and uncertainty analysis coupled with automatic calibration for a distributed catchment model. Journal of Hydrology, 306(1-4): 127-145.

Nash, J.E., Sutcliffe, J.V., 1970. River flow forecasting through conceptual models part I — A discussion of principles. Journal of Hydrology, 10(3): 282-290.

Nathan, R.J., McMahon, T.A., 1990. Identification of homogeneous regions for the purposes of regionalisation. Journal of Hydrology, 121(1-4): 217-238.

Navarra, A. and Tubiana, L. 2013. Eds Regional Assessment of Climate Change in the Mediterranean. Advances in Global Change Research 50. doi 10.1007/978-94-007-5781-3.

Neitsh, S.L., Arnold, J.G., Kiniry, J.R., Srinivasan, R., Williams, J.R., 2005. Soil and Water Assessment Tool input/output file documentation, version 2005. Temple, Texas: Grassland, Soil and Water Research Laboratory, Agricultural Research Service.

Neubert, S., Benabdallah, S., 2003. La réutilisation des eaux usées traitées en Tunisie Etudes et rapports d'expertise 11/2003, Deutsches Institut für Entwicklungspolitik, 96p.

Nicault, A., Alleaume, S., Brewer, S., Carrer, M., Nola, P., Guiot, J., 2008. Mediterranean drought fluctuation during the last 500 years based on tree-ring data. Climate Dynamics, 31(2-3): 227-245.

NRCS, 2004. Part 630: Hydrology. Chapter 10: Estimation of direct runoff from storm rainfall: Hydraulics and hydrology:Technical references. In NRCS National

Engineering Handbook. Washington, D.C.: USDA National Resources Conservation Service.

Olden, J.D., Poff, N.L., 2003. Redundancy and the choice of hydrologic indices for characterizing streamflow regimes. River Research and Applications, 19(2): 101-121.

Oudin, L., Andréassian, V., Perrin, C., Michel, C., Le Moine, N., 2008. Spatial proximity, physical similarity, regression and ungaged catchments: A comparison of regionalization approaches based on 913 French catchments. Water Resour. Res., 44(3): W03413.

Ouessar, M., Bruggeman, A., Abdelli, F., Mohtar, R.H., Gabriels, D., Cornelis, W.M., 2009. Modelling water-harvesting systems in the arid south of Tunisia using SWAT. Hydrol. Earth Syst. Sci., 13(10): 2003-2021.

Ouarda, T. B. J. M., Girard, C., Cavadias, G. S., and Bobee, B. 2001. Regional food frequency estimation with canonical correlation analysis, J. Hydrol., 254(1-4), 157–173.

Panagopoulos, Y., Makropoulos, C., Baltas, E., Mimikou, M., 2011. SWAT parameterization for the identification of critical diffuse pollution source areas under data limitations. Ecological Modelling, 222(19): 12.

Parajka, J., Naeimi, V., Blöschl, G., Wagner, W., Merz, R., Scipal, K., 2005. Assimilating scatterometer soil moisture data into conceptual hydrologic models at the regional scale. Hydrol. Earth Syst. Sci. Discuss., 2(6): 2739-2786.

Perrin, C., Michel, C. and Andréassian, V. 2003. Improvement of a parsimonious model for streamflow simulation. J. Hydrol, 279(1-4), 275-289.

Perrin, C., Oudin, L., Andreassian, V., Rojas-Serna, C., Michel, C., Mathevet, T., 2007. Impact of limited streamflow data on the efficiency and the parameters of rainfall—runoff models. Hydrological Sciences Journal, 52(1): 131-151.

Perrin, J.-L., Tournoud, M.-G., 2009. Hydrological processes controlling flow generation in a small Mediterranean catchment under karstic influence. Hydrological Sciences Journal, 54(6): 1125-1140.

Plan Bleu, 2008. Changement climatique et énergie en Méditerranée Sophia Antipolis:578.

Pielke Sr, R.A., Stohlgren, T., Schell, L., Parton, W., Doesken, N., Redmond, K., Moeny, J., McKee, T., Kittel, T.G.F., 2002. Problems in evaluating regional and local trends in temperature: an example from eastern Colorado, USA. International Journal of Climatology, 22(4): 421-434.

Plus, M., Jeunesse, I., Bouraoui, F., Zaldivar, J., Chapelle, A., Lazure, P., 2006. Modelling water discharges and nitrogen inputs into a Mediterranean lagoonImpact on the primary production. Ecological Modelling, 193(1-2): 69-89.

Rattan, L., 2006. Encyclopedia of soil science. Second edition, 2. Taylor & Francis Group, New York, 584 pp.

Räisänen, J., Hansson, U., Ullerstig, A., Döscher, R., Graham, L.P., Jones, C., Meier, H.E.M., Samuelsson, P., Willén, U., 2004. European climate in the late twenty-first century: Regional simulations with two driving global models and two forcing scenarios. Climate Dynamics, 22(1): 13-31.

Richter, B.D., Baumgartner, J.V., Powell, J., Braun, D. P. , 1996. Method for Assessing Hydrologic Alteration within Ecosystems. Conservation Biology, 10(4): 11.

Richter, B.D., Baumgartner, J.V., Powell, J., Braun, D. P. , 1998. A spatial assessment of hydrologic alteration within a river network. Regulated Rivers: Research & Management, 14: 11.

Schneider, C., Laizé, C.L.R., Acreman, M.C., Flörke, M., 2013. How will climate change modify river flow regimes in Europe? Hydrology and Earth System Sciences, 17(1): 325-339.

Scoullos, M., V.Malotidi, Spirou, S., V.Constantianos, 2002. Integrated Water Resources Management in the Mediterranean. GWP-Med & MIO-ECSDE, Athens: 36.

SCS, 1986. Soil Conservation service Engineering Division, 1986. Urban hydrology for small watersheds. U.S.Department of Agriculture, Technical release 55.

SCS, 1972. SCS National Engineering Handbook. Section 4. Hydrology, Soil Conservation Service, US Department of Agriculture:Washington, DC.

Shafii, M., De Smedt, F., 2009. Multi-objective calibration of a distributed hydrological model (WetSpa) using a genetic algorithm. Hydrol. Earth Syst. Sci., 13(11): 2137-2149.

Sellami, H., La Jeunesse, I., Benabdallah, S., Baghdadi, N., Vanclooster, M., 2013a. Uncertainty analysis in model parameters regionalization: a case study involving the SWAT model in Mediterranean catchments (Southern France). Hydrology and Earth System Sciences Discussions, 10(4): 4951-5011.

Sellami, H., La Jeunesse, I., Benabdallah, S., Vanclooster, M., 2013b. Parameter and rating curve uncertainty propagation analysis of the SWAT model for two small Mediterranean catchments. Hydrological Sciences Journal, 58(8): 1635-1657.

Sellami, H., Vanclooster, M., Benabdallah, S., La Jeunesse, I., 2013c. Assessment of the SWAT model prediction uncertainty using the GLUE approach A case study of the Chiba catchment (Tunisia), Modelling, Simulation and Applied Optimization (ICMSAO), 2013 5th International Conference on, pp. 1-6.

Senatore, A., Mendicino, G., Smiatek, G., Kunstmann, H., 2011. Regional climate change projections and hydrological impact analysis for a Mediterranean basin in Southern Italy. Journal of Hydrology, 399(1–2): 70-92.

Setegn, S.G., Srinivasan, R., Melesse, A.M., Dargahi, B., 2009. SWAT model application and prediction uncertainty analysis in the Lake Tana Basin, Ethiopia. Hydrological Processes: n/a-n/a.

Shamseldin, A.Y., 2010. Artificial neural network model for river flow forecasting in a developing country. Journal of Hydroinformatics, 12(1): 17.

Shamseldin, A.Y., Nasr, A.E., O'Connor, K.M., 1999. Comparison of different forms of the Multi-layer Feed-Forward Neural Network method used for river flow forecasting. Hydrol. Earth Syst. Sci., 6(4): 671-684.

Shen, Y., Chen, Y., 2009. Global perspective on hydrology, water balance, and water resources management in arid basins. Hydrological Processes: n/a-n/a.

Shen, Z.Y., Chen, L., Chen, T., 2012. Analysis of parameter uncertainty in hydrological modelling using GLUE method: a case study of SWAT model applied to Three Gorges Reservoir Region, China. Hydrology and Earth System Sciences 8(4): 8203-8229.

Shu, C. and Burn, D.H. 2003. Spatial patterns of homogeneous pooling groups for flood frequency analysis, Hydrol. Sci. J., 48(4), 601-618, DOI: 10.1623/hysj.48.4.601.51417.

Shrestha, D.L., Kayastha, N., Solomatine, D.P., 2009. A novel approach to parameter uncertainty analysis of hydrological models using neural networks. Hydrol. Earth Syst. Sci., 13(7): 1235-1248.

Sivapalan, M., Takeuchi, K., Franks, S.W., Gupta, V.K., Karambiri, H., Lakshmi, V., Liang, X., McDonnell, J.J., Mendiondo, E.M., O'Connell, P.E., Oki, T., Pomeroy, J.W., Schertzer, D., Uhlenbrook, S., Zehe, E., 2003. IAHS Decade on Predictions in Ungauged Basins (PUB), 2003–2012: Shaping an exciting future for the hydrological sciences. Hydrological Sciences Journal, 48(6): 857-880.

Smakhtin, V.U., 2001. Low flow hydrology: a review. Journal of Hydrology, 240(3–4): 147-186.

Stedinger, J.R., Vogel, R.M., Lee, S.U., Batchelder, R., 2008. Appraisal of the generalized likelihood uncertainty estimation (GLUE) method. Water Resources Research, 44(12): W00B06.

Tayanç, M., Im, U., Doğruel, M., Karaca, M., 2009. Climate change in Turkey for the last half century. Climatic Change, 94(3-4): 483-502.

Tebaldi, C., Knutti, R., 2007. The use of the multi-model ensemble in probabilistic climate projections. Philosophical Transactions of the Royal Society A: Mathematical, Physical and Engineering Sciences, 365(1857): 2053-2075.

Teng, J., Vaze, J., Chiew, F.H.S., Wang, B., Perraud, J.-M., 2011. Estimating the Relative Uncertainties Sourced from GCMs and Hydrological Models in Modelling Climate Change Impact on Runoff. Journal of Hydrometeorology, 13(1): 122-139.

Tubiello, F., 2012. Climate change adaptation and mitigation: challenges and opportunities in the food sector. Natural Resources Management and Environment Department, FAO, Rome, High-level conference on world food security: the challenges of climate change and bioenergy, Rome, 3-5 June 2008: 29.

Van Genuchten, M.T., 1980. A closed-form equation for predicting the hydraulic conductivity of unsaturated soils. Soil Sci. Soc. Am. J., 44: 892-898.

van Griensven, A., Meixner, T., Grunwald, S., Bishop, T., Diluzio, M., Srinivasan, R., 2006. A global sensitivity analysis tool for the parameters of multi-variable catchment models. Journal of Hydrology, 324(1-4): 10-23.

van Griensven, A., Meixner, T., 2007. A global and efficient multi-objective auto-calibration and uncertainty estimation method for water quality catchment models. Journal of Hydroinformatics, 9(4): 277.

van Griensven, A., Ndomba, P., Yalew, S., Kilonzo, F., 2012. Critical review of SWAT applications in the upper Nile basin countries. Hydrol. Earth Syst. Sci., 16(9).

Vandewiele, G.L., Elias, A., 1995. Monthly water balance of ungauged catchments obtained by geographical regionalization. Journal of Hydrology, 170(1-4): 277-291.

Vargas-Yáñez, M., Jesús García, M., Salat, J., García-Martínez, M.C., Pascual, J., Moya, F., 2008. Warming trends and decadal variability in the Western Mediterranean shelf. Global and Planetary Change, 63(2-3): 177-184.

Viola, F., Noto, L.V., Cannarozzo, M., La Loggia, G., 2009. Daily streamflow prediction with uncertainty in ephemeral catchments using the GLUE methodology. Physics and Chemistry of the Earth, Parts A/B/C, 34(10-12): 701-706.

Vogel, R.M., Fennessey, N.M., 1994. Flow-Duration Curves 2. New Interpretation and Confidence-Intervals. J. Water Resour. Plan. Manage., 120(4): 485-504.

Vogel, R.M., Fennessey, N.M., 1995. FLOW DURATION CURVES II: A REVIEW OF APPLICATIONS IN WATER RESOURCES PLANNING1. JAWRA Journal of the American Water Resources Association, 31(6): 1029-1039.

Vrugt, J.A., Diks, C.G.H., Gupta, H.V., Bouten, W., Verstraten, J.M., 2005. Improved treatment of uncertainty in hydrologic modelling: Combining the strengths of global optimization and data assimilation. Water Resources Research, 41(1): n/a-n/a.

Vrugt, J.A., Robinson, B.A., 2007. Treatment of uncertainty using ensemble methods: Comparison of sequential data assimilation and Bayesian model averaging. Water Resour. Res., 43(1): W01411.

Vrugt, J.A., ter Braak, C.J.F., Clark, M.P., Hyman, J.M., Robinson, B.A., 2008. Treatment of input uncertainty in hydrologic modelling: Doing hydrology backward with Markov chain Monte Carlo simulation. Water Resources Research, 44.

Wagener, T., Gupta, H.V., 2005. Model identification for hydrological forecasting under uncertainty. Stochastic Environmental Research and Risk Assessment, 19(6): 378-387.

Wagener, T., Sivapalan, M., Troch, P., Woods, R., 2007. Catchment Classification and Hydrologic Similarity. Geography Compass, 1(4): 901-931.

Wagener, T., Wheater, H.S., 2006. Parameter estimation and regionalization for continuous rainfall-runoff models including uncertainty. Journal of Hydrology, 320(1-2): 132-154.

Wagener, T., Wheater, H.S., Gupta, H.V., 2004. Rainfall-Runoff Modelling in Gauged and Ungauged Catchments. Imperial College Press, London: 300.

Wang, S., Fu, B.J., Gao, G.Y., Yao, X.L., Zhou, J., 2012. Soil moisture and evapotranspiration of different land cover types in the Loess Plateau, China. Hydrol. Earth Syst. Sci., 16(8): 2883-2892.

Wang, S., Kang, S., Zhang, L., Li, F., 2008. Modelling hydrological response to different land-use and climate change scenarios in the Zamu River basin of northwest China. Hydrological Processes, 22(14): 2502-2510.

Wang, W., Gelder, P.H.A.J.M.V., Vrijling, J.K., Ma, J., 2006. Forecasting daily streamflow using hybrid ANN models. Journal of Hydrology, 324(1–4): 383-399.

Wang, Y.-C., Yu, P.-S., Yang, T.-C., 2010. Comparison of genetic algorithms and shuffled complex evolution approach for calibrating distributed rainfall-runoff model. Hydrological Processes, 24(8): 1015-1026.

Wang, Y.-P., Trudinger, C.M., Enting, I.G., 2009. A review of applications of model–data fusion to studies of terrestrial carbon fluxes at different scales. Agricultural and Forest Meteorology, 149(11): 1829-1842.

White, M.J., Storm, D.E., Smolen, M.D., Zhang, H., 2009. Development of a Quantitative Pasture Phosphorus Management Tool Using the SWAT Model. JAWRA Journal of the American Water Resources Association, 45(2): 397-406.

Williams, J.R., 1995. The EPIC model. In: Water Resources Publications, Highland Ranch, CO. (ed.), Computer models of catchment hydrology, pp. 909-1000.

Xiong, L., O'Connor, K.M., 2008. An empirical method to improve the prediction limits of the GLUE methodology in rainfall-runoff modelling. Journal of Hydrology, 349(1-2): 115-124.

Yadav, M., Wagener, T., Gupta, H., 2007. Regionalization of constraints on expected catchment response behavior for improved predictions in ungauged basins. Advances in Water Resources, 30(8): 1756-1774.

Yang, J., Reichert, P., Abbaspour, K.C., Yang, H., 2007. Hydrological modelling of the Chaohe Basin in China: Statistical model formulation and Bayesian inference. Journal of Hydrology, 340(3-4): 167-182.

Yang, J., Reichert, P., Abbaspour, K.C., Xia, J., Yang, H., 2008. Comparing uncertainty analysis techniques for a SWAT application to the Chaohe Basin in China. Journal of Hydrology, 358(1-2): 1-23.

Yang, Q., Meng, F.-R., Zhao, Z., Chow, T.L., Benoy, G., Rees, H.W., Bourque, C.P.A., 2009. Assessing the impacts of flow diversion terraces on stream water and sediment yields at a watershed level using SWAT model. Agriculture, Ecosystems & Environment, 132(1-2): 23-31.

Yang, T., Zhang, Q., Chen, Y.D., Tao, X., Xu, C.-y., Chen, X., 2008b. A spatial assessment of hydrologic alteration caused by dam construction in the middle and lower Yellow River, China. Hydrological Processes, 22(18): 3829-3843.

Yang, Z., Yan, Y., Liu, Q., 2012. Assessment of the flow regime alterations in the Lower Yellow River, China. Ecological Informatics, 10: 56-64.

Zhang, X., Srinivasan, R., Van Liew, M., 2009a. Approximating SWAT Model Using Artificial Neural Network and Support Vector Machine. JAWRA Journal of the American Water Resources Association, 45(2): 460-474.

Zhang, X., Srinivasan, R., Zhao, K., Liew, M.V., 2009b. Evaluation of global optimization algorithms for parameter calibration of a computationally intensive hydrologic model. Hydrological Processes, 23(3): 430-441.